Laboratory Experiments on the Multi-phase Flow of

Organic Liquids in the Vadose and Saturated Zones

by

Stephen H. Conrad

Submitted in partial fulfillment for the Doctor of Philosophy degree in Hydrology
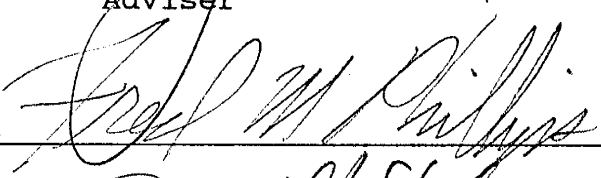
Department of Geoscience

New Mexico Institute of Mining and Technology

Socorro, New Mexico
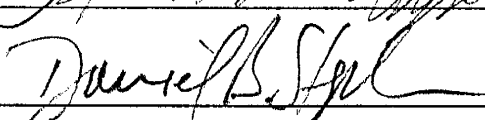
August 1990

This dissertation is accepted on behalf of the faculty
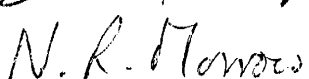of the Institute by the following committee:

_____ John L. Wilson _____
                      Adviser

___ Fred M. Phillips _____

___ Daniel B. Stephens _____

___ Norman Morrow _____

___ Jack C. Parker _____

_____ January 3, 1991 _____
                       Date

ABSTRACT

Organic liquids that are essentially immiscible with water migrate through the subsurface under the influence of capillary, viscous, and buoyancy forces. These liquids originate from the improper disposal of hazardous wastes, and the spills and leaks of petroleum hydrocarbons and solvents. The laboratory experiments described in this study examined this migration, with a primary focus on the behavior of the residual organic liquid saturation, referring to that portion of the organic liquid that is trapped by capillary forces in the soil matrix. The residual organic liquid saturation often constitutes the major volume of the organic liquid pollution, and acts as a continual source of dissolved or vapor phase organics.

Three experimental methods were employed. First, quantitative displacement experiments using short soil columns were performed to relate the magnitude of residual organic liquid saturation to fluid properties, the soil, and the number of fluid phases present. Second, pore and blob casts were produced by a technique in which an organic liquid was solidified in place within a soil column at the conclusion of a displacement experiment, allowing the distribution of fluid phases within the pore space to be observed. The columns were sectioned and examined under optical and scanning electron microscopes. Photomicrographs of these sections show the location of the organic phase within the porous soil matrix under a variety of conditions. And third, etched glass micromodels were used to visually observe dynamic multi-phase displacement processes in pore networks. Fluid movement was recorded on film and video tape. Many of the important issues in multi-phase flow were visited in this study, but none of these issues were explored as exhaustively as they might have been. Corresponding to this broad-brush approach, the focus of the experiments was on flow visualization of immiscible displacements in order to gain a fundamental understanding of the operative forces at work in controlling multi-phase flow.

From these experiments, it was found that the spatial distribution and saturation of organic liquid within the porous media depends on a variety of factors, including: (1) the soil structure and heterogeneity; (2) the number of fluid phases present; and (3) the fluid flow rates. Photomicrographs on a pore scale show that the residual organic liquid appears as blobs, films, rings, and wedges of microscopic size, depending on these factors. The size, shape, and spatial distribution of the residual organic liquid affects the dissolution of organic liquid into the water phase, volatilization into the air phase, and the adsorption and biodegradation of organic components. These four processes are of concern for the prediction of pollution migration and the design of aquifer remediation schemes.

Large amounts of residual organic liquid are trapped as isolated blobs in the saturated zone. Smaller amounts are retained as interconnected films, rings and wedges in the vadose zone. In the saturated zone, residual saturations are largely independent of fluid properties. Residual saturations are very sensitive to soil textural heterogeneities because of the interplay between capillarity and the heterogeneities. A mathematical model that used capillarity and flow velocities to predict two-phase flow through two media shows why this is so. Good qualitative agreement between the predictions of the mathematical model and experimental results was achieved.

Observations of two-phase displacements in micromodels showed that for typical aquifer flow velocities, the force exerted by capillarity was sufficient to cause by-passing of organic liquid in coarser regions even though these regions were more permeable.

The movement of organic liquid through the vadose zone is more complex than organic liquid movement in the saturated zone, especially because of the tendency for many organics to spread. The thin films formed between the the air and water phases appear to be an important mechanism of organic liquid advance. These films also maintain the continuity of the organic phase during drainage, explaining in part, the lower residual saturations found in the vadose zone. The presence of a third phase along with the comparatively larger buoyancy forces and smaller capillary forces found in the vadose zone also contribute to lower residual saturations. Finally, the formation of films exposes a large organic liquid surface area to the gas phase, making soil venting of organics in the vadose zone an attractive remediation strategy.

ACKNOWLEDGMENTS

NOTATION

Arabic:

A = area

a = normalized area

C = curvature of a fluid-fluid interface

d = diameter

g = acceleration of gravity

h = height of fluid in a buret

J = hydraulic gradient

K = hydraulic conductivity

k = intrinsic (absolute) permeability of soil

l = length

M = mass

N_B = Bond number

N_c = capillary number

n = porosity

P = pressure

Q = volumetric flow rate

q = flux rate

$\overline{q}$ = net flux rate

R = volumetric retention of residual organics in soils

r = radius

S = saturation; or,

= spreading coefficient

t = time

V = volume

V_p = pore volume

W = USBM wettability index

v = velocity

z = elevation above a datum

Greek:

α = T-test parameter for the probability of a false positive

δ = displacement ratio of the Amott test

Δ = change in a given parameter

γ = surface tension

ϱ = density

ϱ_b = soil bulk density

ϱ_s = particle density of a soil

σ = interfacial tension

θ = contact angle

μ = viscosity

Superscripts:

* = critical

Subscripts:

a = air phase

ao = air-organic

aw = air-water

c = capillary; or,

= curvature (when associated with a radius)

nw = non-wetting phase

o = organic phase

ow = organic-water

r = residual; or,

= relative (when associated with a permeability)

s = soil

t = pore throat; or,

= capillary tube

w = water phase; or,

= wetting phase

TABLE OF CONTENTS

LIST OF FIGURES

LIST OF TABLES

CHAPTER 1

INTRODUCTION

NATURE OF THE PROBLEM

Many hazardous waste sites, and most leaking underground storage tanks, involve non-aqueous phase organic liquids (e.g., Burmaster and Harris, 1982; EPA, 1980; Feenstra and Coburn, 1986; Jercinovic, 1984; Maugh, 1979). Usually released at or near the surface, these organic liquid contaminants move downward through the vadose zone toward the water table. Migrating as a liquid phase separate from the air and water already present in the vadose zone, some of the organic liquid is immobilized within the pore space by capillary forces. The remainder passes on, and if the volume of organic liquid is large enough it eventually reaches the water table. There the organic liquid spreads laterally along the water table if it is less dense than water. In instances involving an organic liquid more dense than water, it continues to move downward into the saturated zone. In both cases the organic liquid migrates down-gradient with the ambient groundwater flow. As it moves into the water saturated pores beneath the water table more organic liquid is immobilized by capillary forces (e.g., de Pastrovich et al., 1979; Schwille, 1967, 1988). In the saturated zone the immobilized organics remain as small, disconnected pockets of liquid, sometimes called 'blobs', no longer connected to the main body of organic liquid.

The immobilized volume is called the 'residual oil saturation' in petroleum reservoir engineering, and is measured as the volume of organic liquid trapped in the pores relative to the volume of the pores. Organic liquid at residual saturation can occupy from 15% to 50% of the pore space in petroleum reservoir rocks under conditions that are equivalent to those in the groundwater saturated zone (Melrose and Brandner, 1974). At a spill or hazardous waste site the entire volume of organic liquid can be exhausted by this immobilization, although if the volume of organic liquid is large enough, it continues to migrate down-gradient where it becomes a threat to the safety of drinking water or agricultural water supplies (Schwille,1967,1981; de Pastrovich et al., 1979).

The organic liquid phase is sometimes referred to as being immiscible with water and air. Although that expression is used here, it is important to realize that small concentrations of the various components of the organic phase volatilize into the air phase and dissolve into the water phase. A 'halo' of dissolved organic components precedes the immiscible phase in its migration. Even when the so-called immiscible organic liquid has been immobilized by capillary trapping, the passing groundwater dissolves some of the residual. In effect, the organic liquid phase acts as a continuing source of dissolved organic pollutants. Similarly, in the vadose zone, the residual organic liquid that volatilizes into the air phase migrates by gaseous diffusion and advection, becoming a source of organic components to air or water pollution, and perhaps a possible explosion hazard. In large spills and leaks it is apparent that most of the liquid organic remains as a liquid, some is volatilized and a little is dissolved. However small in volume, the

volatilized or dissolved components are usually the ones that cause problems. The liquid organic phase acts as a reservoir of additional contaminants to replenish the air and water phases with dangerous and/or toxic material. Clearly, the source of the dissolved or gaseous organic constituents — the liquid organic phase — must be removed or isolated in order to restore a polluted aquifer.

There is no wholly effective mechanism to remove the residual organic liquid. Waiting for the residual to dissolve could take several decades. In the vadose zone, induced volatilization may help reduce the residual volume for lighter organics, but is not effective for heavier ones (Burris et al., 1986). Engineered removal is usually attempted hydraulically, by sweeping the organic liquid out with water, or biologically, by encouraging the consumption of the organic constituents by the soil microbial community. This last process, biodegradation, is the focus of current research and several recent restoration efforts. It is seldom tried alone, for the microbes generally consume only the dissolved organics. Moreover, some organic chemicals are extremely resistant to biodegradation. PCBs, for example, biodegrade very slowly, or not at all in the subsurface (J.R.Roberts et al., 1982). Hydraulic sweeps remain a major component of any attempt to remove organic liquids although, commonly, hydraulic sweeps fail to remove all the liquid organic phase, often leaving a significant quantity of residual organic liquids behind (Wilson and Conrad, 1984). There is, of course, another removal option often used for small pollution events: excavate the site and dispose of or treat the contaminated soil. For large sites this alternative is unfeasible. Since there is no panacea for the removal of organic liquids, containment is often adopted as part of a restoration strategy. Hydraulic containment (e.g., Wilson, 1984), often in combination with structural barriers such as a slurry wall, is becoming standard practice.

SCOPE OF PREVIOUS WORK

Development of improved technologies to clean up organic pollutants depends in large part on developing an ability to understand and predict the migration of liquid, vapor, and dissolved organics. Liquid organics move through a water and sometimes air filled porous soil, as a separate phase, under the influence of viscous, gravity, and capillary forces. Dissolved organics move in the water phase and are subject to advection, dispersion, biodegradation, and adsorption onto soil particles. Organic vapors in the air phase are subject to similar mechanisms. A few of these major transport mechanisms are fairly well understood today, principally those associated with the behavior of dissolved organics. McCarty et al. (1981) and P. V. Roberts et al. (1982) have reviewed the progress of this research.

In contrast, the organic liquid phase transport mechanism has been virtually ignored by the research community in the United States, although it has been the subject of empirical studies in Europe (e.g., Schwille, 1967, 1981, 1984, and 1988; van Dam, 1967). Recently, however, American researchers have begun obtaining some laboratory results. Convery (1979) ran gravity drainage experiments on a long column to relate organic liquid retention in the vadose zone with grain size and sorting. Eames (1981) used a short soil core centrifuging method to measure residuals in the vadose zone. Eckberg and Sunada (1984), and Ferrand et al. (1986)

used gamma radiation attenuation and bulk soil electrical resistivity to measure three-phase fluid saturations at various times and at various elevations above a water table following a simulated petroleum spill. The experimental procedure allowed a petroleum 'spill' to be tracked as it moved through the vadose zone to the water table. Cary et al., (1989) performed experiments to test the ability of multi-phase flow theory to predict the infiltration and redistribution of wetting and non-wetting fluids. They met with limited success. Lenhard and Parker (1988c) used theoretical three-phase saturation-pressure relationships to estimate the volume of oil in soils given observed fluid levels in monitoring wells.

Some simple numerical simulations of multi-phase transport have been developed. These focus on immiscible transport of continuous phases. Residual organic liquids, trapped by capillary forces, are often ignored, although they are sometimes treated as a source of dissolved contamination. This research effort mirrors the state of the art of petroleum engineering's 'black oil' models. A few researchers (notably Baehr and Corapciaglu, 1984 and 1987; Corapciaglu and Baehr, 1987; Baehr, 1987; Abriola and Pinder, 1985a,b; and Pinder and Abriola, 1986) are looking into interphase transfer, including the volatilization and solution of organic components, using computer simulations. This again reflects the state of the art in petroleum engineering, where compositional models are used to examine enhanced recovery techniques.

Parker et al. (1987) have proposed a model to estimate the functional relationships between fluid pressures, saturations, and permeabilities of two- or three-phase porous media systems, and these functional relationships have been implemented in a multi-phase numerical flow model (Kuppusamy et al., 1987). The model has since been extended to include the effects of hysteresis and non-wetting phase trapping (Parker and Lenhard, 1987; and Lenhard and Parker, 1987a). The results of concurrent laboratory work were used to validate the model (Lenhard and Parker, 1987b,1988a,1989; and Lenhard et al., 1988).

Petroleum engineering's long history of research into improving recovery from petroleum reservoirs may be applied to rehabilitating fresh-water aquifers polluted by organic liquids. Through over forty years of experimentation, petroleum engineering has amassed considerable expertise in multi-phase transport and the mechanics of residual organic phase trapping and mobilization. To date, relatively little of this technology has been applied to recovering organic hazardous wastes and petroleum hydrocarbons released in the near-subsurface environment. Much of the petroleum literature on residual oil saturation is reviewed in a series of papers by Anderson (1986a,b;1987a,b).

MOTIVATION FOR THIS STUDY

This study focuses on the behavior of the residual organic liquid saturation, because it often constitutes the major volume of the organic pollution (Wilson and Conrad, 1984), and acts as a continual source of dissolved or vapor phase organics. In particular, there is a need to understand how the residual organic liquid is trapped and how it can be hydraulically mobilized or otherwise removed. As shown in the results chapters, the residual organic liquid appears to form

blobs, films, and rings of microscopic size, depending on the presence of other fluids, the pore geometry, the surface wetting of the solids, and soil heterogeneity. The size, shape, and spatial distribution of these blobs, films, and rings affect the dissolution of organic liquid into the water phase, volatilization into the air phase, and the adsorption and biodegradation of organic components. A paucity of experimental results regarding these issues makes site characterization conjectural, predictive modelling unreliable, and design of remediation programs for organic liquid contamination sites less effective than might be possible. This study contributes to understanding the nature of multi-phase flow in a near-subsurface environment through a series of related laboratory studies.

OBJECTIVES

The goal of this research has been to examine how organic liquids that are immiscible with water move in the subsurface. The overall objective has been to better understand the basic physical mechanisms controlling the movement of organic liquids in soils and groundwater. Emphasis was placed on relating the various mechanisms to the prediction of contaminant movement and to remediation. The magnitude and configuration of the residual saturation was of special interest because immobile organic liquids can act as a long-term source of contaminants to the groundwater. This broad goal was broken down into three categories of specific research objectives.

These three categories constitute the framework used for systematic study of multi-phase flow phenomena (Figure 1). The simplest category, *two-phase flow through homogeneous media*, formed the 'base case' of the study. More complex cases, *two-phase flow through heterogeneous media* and *three-phase flow through homogeneous media* were also studied allowing for direct comparison of heterogeneous versus homogeneous, and three-phase versus two-phase flow regimes. Incidentally, the three conceptual boxes shown in Figure 1 correspond to each of the three results chapters. Three-phase flow through heterogeneous media was not studied because of its extreme complexity, but study of that topic could serve as a logical extension of this work.

Operational Objectives

The specific research objectives are given first for some general objectives and then for the three main categories of research:

- Conduct experiments that quantify endpoint saturations in soils — especially residual organic liquid saturations;

- Conduct experiments that permit the visualization of multi-phase fluid flow and capillary trapping, and record the experiments on film and videotape; and,

- Use visualization experiments to observe multi-phase displacement behavior and the effect of this behavior on the magnitude and configuration of the endpoint saturations.

NUMBER OF PHASES

SOIL STRUCTURE

homogeneous   heterogeneous

2 phases
organic liquid and water
in the saturated zone

2-phase flow through homogeneous media: the base case

←→ compare →

2-phase flow through heterogeneous media

↕ compare

3 phases
air, organic liquid, and
water in the vadose zone

3-phase flow through homogeneous media

3-phase flow through heterogeneous media (not studied)
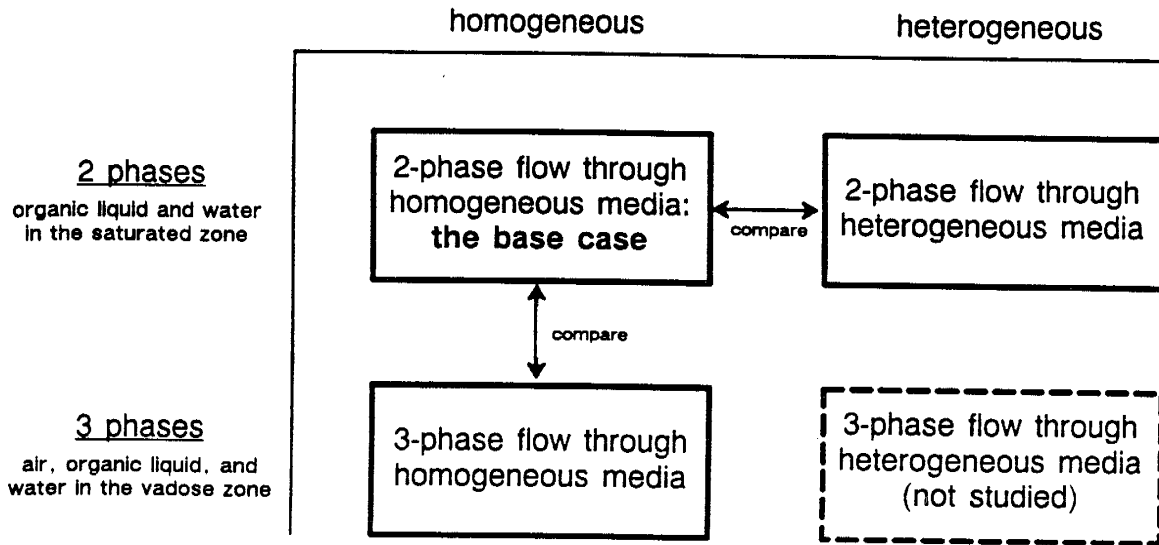
Figure 1.   The framework used in this study for the systematic study of multi-phase flow
phenomena.

Saturated Zone — Homogeneous

- Compare residual saturations for various organic liquids, testing the hypothesis that residual saturation is independent of organic liquid composition for expected conditions in hydrology;

- Compare residual saturations for various soils, testing the hypothesis that residual saturations should be similar in soils that have similar texture; and,

- Investigate how the rate of initial invasion of organic liquid may influence irreducible water saturations, and consequently, residual organic liquid saturations.

Saturated Zone — Heterogeneous

- Observe displacements through various types of heterogeneities and compare the results to one other and to base case to test the hypothesis that soil heterogeneity can dominate displacement and trapping mechanisms;

- Measure residual saturations in heterogeneous soils to test the hypothesis that the presence of heterogeneities can significantly alter the magnitude of the residual organic liquid saturation;

- Investigate the effect of flow rate on immiscible displacement behavior for heterogeneous media, and consequently, the impact of this displacement behavior on the residual organic liquid saturation; and,

- Develop a theoretical model of multi-phase flow and capillary trapping in heterogeneous media based on the interplay of viscous and capillary forces.

Vadose Zone

- Measure residual saturations in a soil and compare to the base case to test the hypothesis that residual organic liquid saturations are significantly lower in the vadose zone than they are in the saturated zone;

- Observe three-phase displacements and compare the results to those of the base case to test the assumption that the trapping mechanisms and the ultimate distribution of the residual organic liquid saturation in the vadose zone are profoundly different than those observed in the saturated zone; and,

- Compare the results of visualization experiments for spreading and non-spreading organic liquids to test the assumption that non-spreading organic liquids behave differently than spreading organic liquids.

EXPERIMENTAL APPROACH

The problem was approached experimentally, in three ways:

1. **Quantitative displacement experiments using short columns** were performed to relate the magnitude of residual organic liquid saturation to fluid and soil properties, and to the number of fluid phases present.

2. **Pore and blob casts** were produced for saturated zone conditions by a technique in which the organic liquid was solidified in place within a soil column at the conclusion of a displacement experiment, allowing the distribution of organic liquid to be observed. The polymerized organic phase was rigid and chemically resistant. Following polymerization, the water phase was removed and replaced by an epoxy resin. The solid core, composed of soil, solidified styrene (the organic phase), and epoxy resin (the water phase), was cut into sections to show the organic liquid phase in relation to the soil and the water phase. The sections were photographed under an optical microscope. Although polymerization only gave a 'snapshot' of the displacement process, it offered the advantage of seeing organic liquid in its 'natural habitat' (i.e. within a soil) as compared to that observed in etched glass micromodels. Sometimes, instead of replacing the water with epoxy resin, the solid matrix of the soil column was dissolved with hydrofluoric acid, leaving only the hardened organic liquid. The solidified organic phase was then observed under a scanning electron microscope (SEM) and photographed. For vadose zone conditions, styrene and epoxy liquids were sequentially applied, drained and hardened in an attempt to simulate

proper fluid distributions above the water table. The resulting pore casts were photographed under an optical microscope.

3. **Etched glass micromodels** were used to observe dynamic multi-phase displacement processes. Micromodels provide two-dimensional networks of three-dimensional pores. They offer the ability to actually see fluids displace one another in both a bulk sense and also within individual pores. Although displacements are known to be dependent upon a variety of factors, this study describes micromodel experiments that focused primarily on three: (1) the fluid flow rate, (2) the presence of heterogeneities and, (3) the number of fluid phases present. The experiments were photographed and videotaped.

Also, to interpret the experiments in heterogeneous material, a new but simple theoretical model of multi-phase flow and capillary trapping was developed. The model predicts trapping based on the interplay of viscous and capillary forces.

These experimental methods have been adapted from methods developed in the petroleum industry to study multi-phase flow phenomena. However, this study is distinguishable from a petroleum engineering study because in many cases the experiments were designed specifically to observe the flow behavior of organic liquids in groundwater aquifers. But this study is especially distinguishable from petroleum engineering studies because the results have been interpreted in terms of organic contaminant movement through groundwater aquifers.

This study could be characterized as rather 'broad brush'. With the exception of the wettability issue, many of the important issues in multi-phase flow were visited, but none of these issues were explored as exhaustively as they might have been. This was not intended to be a self-contained study of narrow focus, but more of a 'jumping off point' for further experimentation. Correspondingly, the focus of the experimental approach was on flow visualization — direct observation — of immiscible displacements in order to gain a fundamental understanding of the operative forces at work in controlling multi-phase flow. The flow visualization results have suggested lines of further inquiry, and many of these are presented as recommendations for future work.

This was a laboratory study. Of course the advantage of laboratory experimentation is that it offers good control (simplification) of the immiscible flow systems along with the ability to observe the displacements in sufficient detail to achieve an understanding of the operative mechanisms controlling flow. Since the ultimate interest is the prediction of organic contaminant migration, the challenge of this study has been to generalize or 'up-scale' the insights gained from laboratory experimentation to suggest implications for contaminant movement through groundwater aquifers.

ORGANIZATION OF THIS DISSERTATION

Chapter 2 provides some background in multi-phase and capillary trapping in porous media and helps to put the present study in context. Following this introductory chapter, are four chapters (3 through 6) that describe fluid and soil characterizations, and the experimental

methodology used for each of the three experimental approaches used in this study. These chapters contain the detailed information that is necessary to future investigators wishing to verify or extend the results of this investigation. The reader more concerned with results than methods can probably skip them. Experimental results and discussion are presented in Chapters 7 through 9. Chapters 7 and 8 describe experimental results for saturated zone conditions. In chapter 7, experimental results exploring the relatively simple case of two-phase (organic/water) flow through homogeneous porous media are presented. These results form the base against which other results are compared. Results from experiments designed to examine the somewhat more complex case of organic liquid movement through heterogeneous media is presented in Chapter 8. Chapter 9 describes experimental results examining organic liquid movement through the vadose zone. These three results chapters contain a large number of photomicrographs illustrating multi-phase flow and the eventual capillary trapping of organic-phase contaminants. The final chapter summarizes the conclusions of this study and gives recommendations for future work.

CHAPTER 2

BACKGROUND

This chapter deals with three topics — trapping, mobilization, and dissolution. These topics are all important in understanding the flow and transport of organic contaminants in the subsurface. The topics covered in this chapter form the foundation upon which the present study has been built. All the discussions and examples presented in this chapter deal with two-phase systems. Later, in the results chapters, the basic principles outlined here will be extrapolated to discuss implications to organic contaminant migration and remediation in groundwater aquifers, and to explain the more complex flow behavior of two-phase flow through heterogeneous media (Chapter 8), and three-phase flow (Chapter 9).

THE BASICS

To help provide a framework for the discussions on trapping and mobilization, it might be useful to briefly review the concepts of interfacial tension, wettability, and capillarity.

Interfacial Tension (Adamson, 1982)

In the interior of a homogeneous fluid, a molecule is surrounded on all sides by other like molecules exerting cohesive forces between one another. At the interface between two immiscible fluids however, there are few if any like molecules across the interface. A molecule at the interface is attracted to molecules of its own phase by a force greater than the force attracting it to molecules of the immiscible phase across the interface. The cohesive forces acting on a molecule inside a fluid phase, and on a molecule at the interface (liquid-gas or liquid-liquid) between fluid phases are illustrated in Figure 2. This unbalanced force draws molecules along the interface inward and results in the tendency for the fluid-fluid interface to contract. If the interface is stretched, it acts like an elastic membrane. The restoring force seeking to minimize the interfacial area between the two immiscible fluids, is called the interfacial tension, σ. When encountered between a liquid and a gaseous phase, this same force is called the surface tension, γ.

Wettability

Figure 3 illustrates a possible configuration of two immiscible fluid phases in contact with the solid phase (walls) of a cylindrical tube. At the line of contact where the two fluid phases meet the solid phase, both the cohesive forces within the fluids and the adhesive forces between the solid and each of the fluids are at work. Suppose that one of these fluid phases is water (fluid 1), and the other is an organic liquid (fluid 2). If the adhesive forces between the solid and the water phase are greater than the cohesive forces inside the water itself, and greater than the forces of attraction between the organic phase and the solid, then the solid-water contact angle, θ, will be
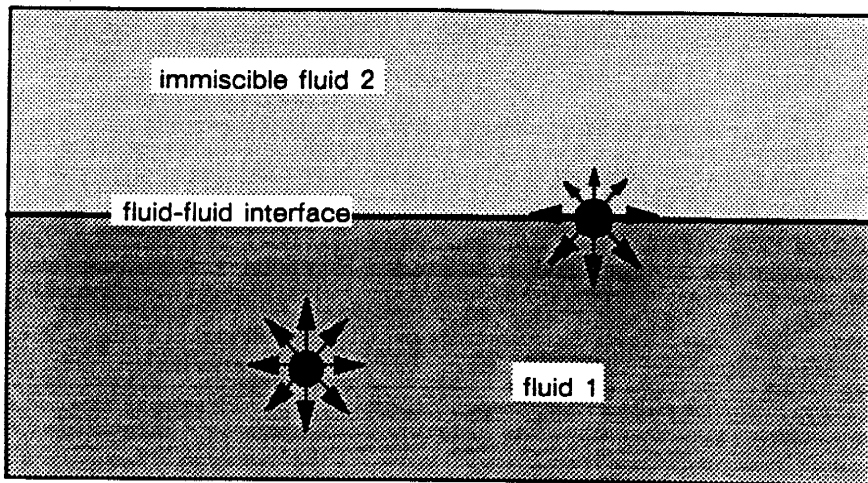
Figure 2.   Cohesive forces acting on a molecule inside a fluid and at its interface with another, immiscible fluid (after Hillel, 1980).
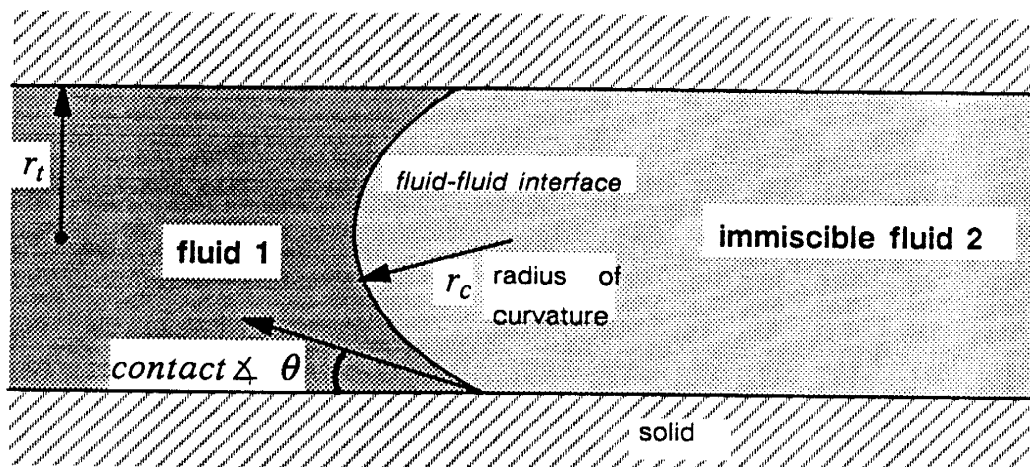
Figure 3.   Hydrostatic equilibrium of two fluid phases in contact with a solid phase (after Melrose and Brandner, 1974).

acute and the water will 'wet' the solid (Hillel, 1980, p.44). The contact angle provides the only direct measurement of wettability. As an example of a contact angle, on clean glass water forms an acute contact angle θ of about 25.5° in the presence of air. Water is a strong wetting fluid relative to air for this surface, but not necessarily for other surfaces, such as TFE (tetrafluoroethylene). Further discussion of wettability can be found in Chapter 3.

Capillarity

    As a result of the contact angle, a meniscus is formed between the fluid phases (Figure 3). The narrower the tube, the smaller the radius of curvature. Similar to the curvature produced by a pressure difference across a membrane, the presence of curvature implies a pressure
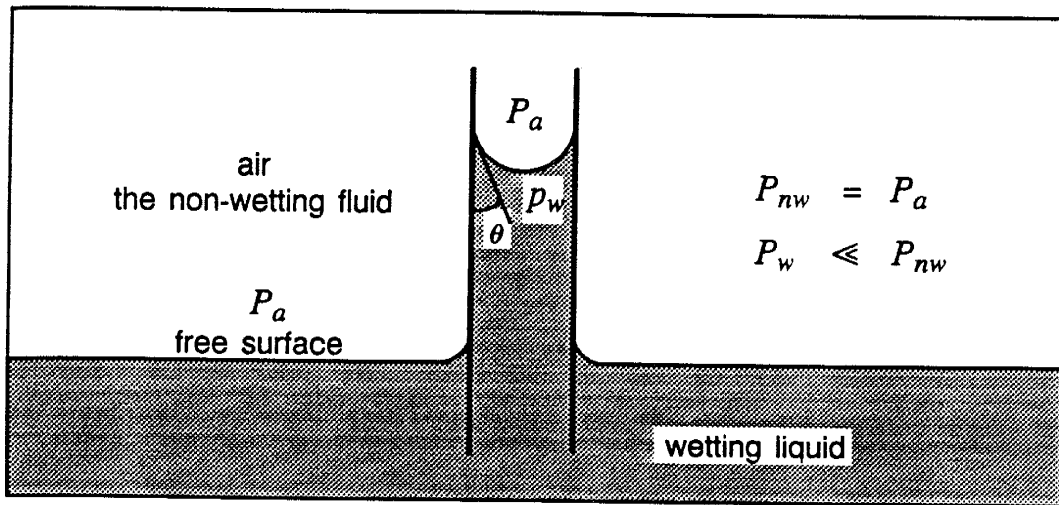
Figure 4. Capillary rise in a slim tube.

difference across the fluid-fluid interface. This pressure difference is called the capillary pressure:

$$P_c = P_{nw} - P_w = \sigma C = \frac{2\sigma}{r_c} = \frac{2\sigma \cos\theta}{r_t} \tag{1}$$

where: P_c = capillary pressure

P_w = pressure in the wetting phase (fluid 1 in the figure)

P_{nw} = pressure in the non-wetting phase (fluid 2 in the figure)

σ = fluid-fluid interfacial tension

C = curvature of the fluid-fluid interface

r_c = radius of curvature

θ = contact angle, measured through the wetting fluid

r_t = radius of capillary tube

The most common example given to illustrate capillarity is that of the capillary rise of water in a straight thin tube, or straw (see Figure 4). The pressure difference between the wetting and non-wetting fluid, at the interface inside the tube, causes the water to rise into the tube, above the level of the free surface.

These same forces operate on the pore scale for multi-phase flow in saturated, and unsaturated, porous media. The capillary fringe is a notable example. Also, the interplay of the various wettabilities and interfacial tensions of different fluids, and the capillary forces they give rise to, leads to trapping of fluids within pores, as the fluids migrate through, or drain out of, a system. These capillarity induced trapping mechanisms are discussed below.

11

TRAPPING MECHANISMS

Three major forces — capillary forces, viscous forces, and gravity or buoyancy forces — control the movement of organic liquids in the subsurface. Capillarity is the result of the interplay of cohesive forces within each fluid phase, and the adhesive forces between the solid phase and each of the fluids. The capillary force is proportional to the interfacial tension at the fluid-fluid interface and the strength of fluid wetting to the solid surface, and inversely proportional to the pore size. Viscous or dynamic forces are proportional to the permeability and to the pressure gradient, while buoyancy is a gravitational force proportional to the density difference between the fluids.

For two-phase fluid flow in an aquifer at typical aquifer flow rates, capillary forces often dominate over viscous and buoyancy forces. The dominance of capillarity results in the trapping of organic liquid blobs. Residual organic liquid appears to be trapped within a porous media by either or both of two major mechanisms: snap-off and by-passing (Mohanty et al., 1980; Chatzis et al., 1983; Wilson and Conrad, 1984).

Snap-off

Snap-off occurs as non-wetting fluid in a pore is displaced from a pore body into a pore throat. The mechanism strongly depends on wettability and aspect ratio — the ratio of pore-body diameter to pore-throat diameter (Wardlaw, 1982).

Consider the case of water displacing an organic liquid from a tube with a non-uniform pore diameter, as shown in Figures 5 and 6. The walls of the tube are smooth and strongly water wet. The water contact angle is acute, the water-organic liquid interface is curved, and the water phase 'wicks' along the pore wall. In high aspect ratio pores, the pore throats are much smaller than the pore bodies (Figure 5a and Figure 6). When the thin layer of water phase reaches the exit pore throat, a large blob of organic liquid still remains in the pore (Figure 6). Snap-off occurs as the water continues through the exit throat leaving behind the now disconnected singlet blob. In a sequence of high aspect ratio pores, a singlet blob is trapped by snap-off in each pore (Figure 5a). Pores in a pack of uniform sized glass beads have a high aspect ratio, explaining the prevalence for singlet blobs observed by Morrow and Chatzis (1982) and Chatzis et al. (1983). For low aspect ratio pores, in which the pore throats are almost as large as the pore bodies, the organic fluid can be completely displaced, as shown in Figure 5b.

Trapping is a function of wetting and contact angle as well as pore geometry. The combined effect of contact angle and pore geometry control the curvature of a fluid-fluid interface and determine the potential for snap-off (Wardlaw, 1982). Figure 7 depicts an interface with a 90 degree contact angle passing from a pore throat through a high aspect ratio pore body with smooth walls. The intermediate contact angle of 90° causes the curvature of the interface to remain relatively small. As the interface reaches the exit throat, little organic phase remains in the pore and no trapping occurs (Wardlaw, 1982). In rough walled pores, there is probably some trapping of the retreating phase in the asperities along the wall (see Figure 8).
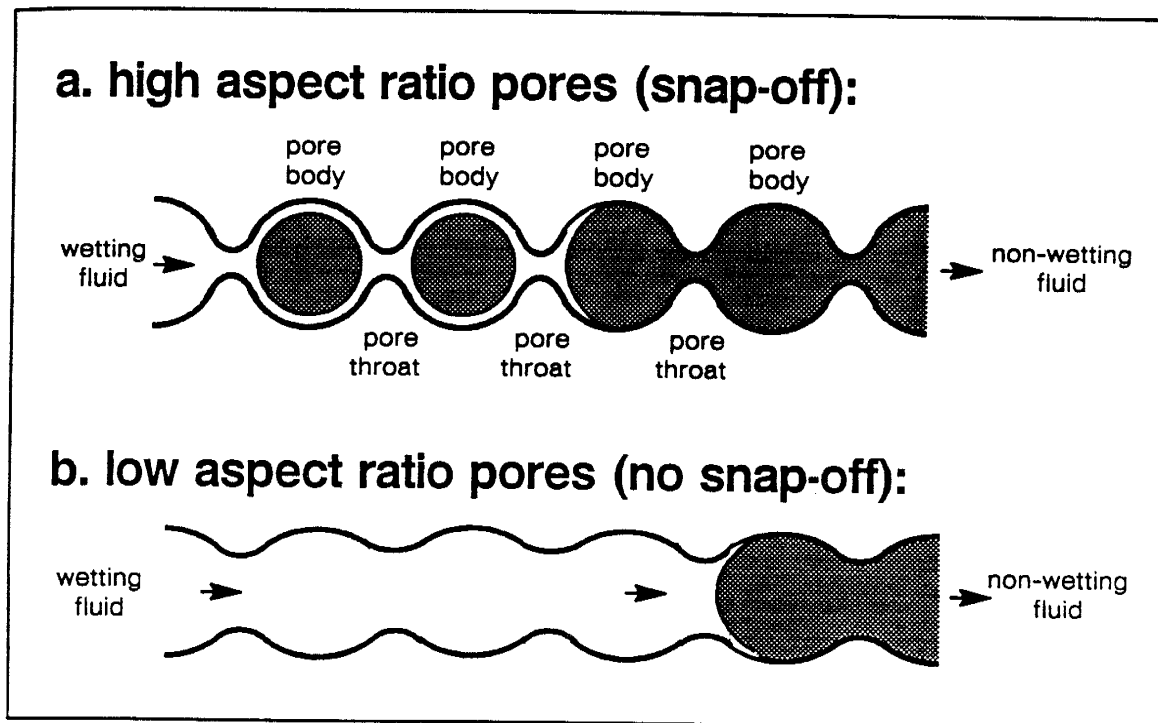
Figure 5. Effect of pore aspect ratio on organic liquid trapping in a tube of non-uniform diameter (after Chatzis et al., 1983).
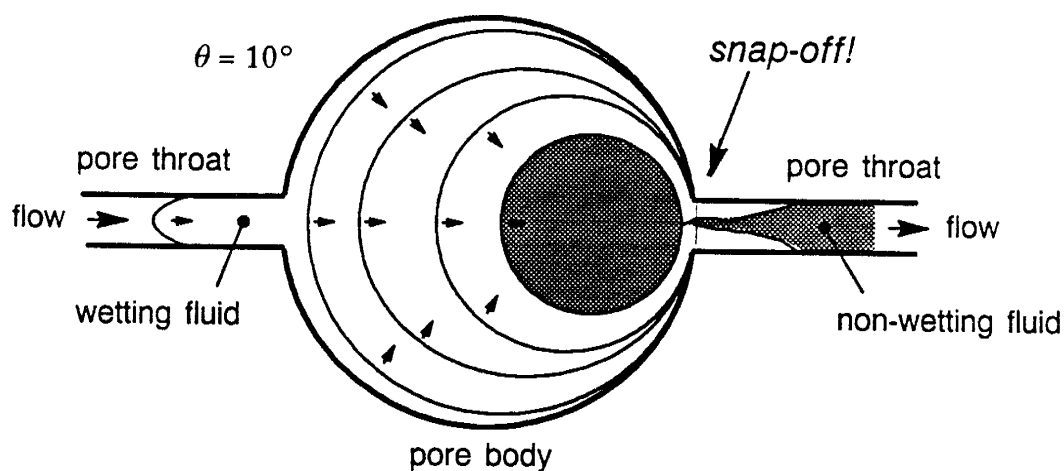
Figure 6. Wetting fluid displacing a non-wetting fluid from a circular, high aspect ratio pore under strongly wet conditions (after Wardlaw, 1982).

13
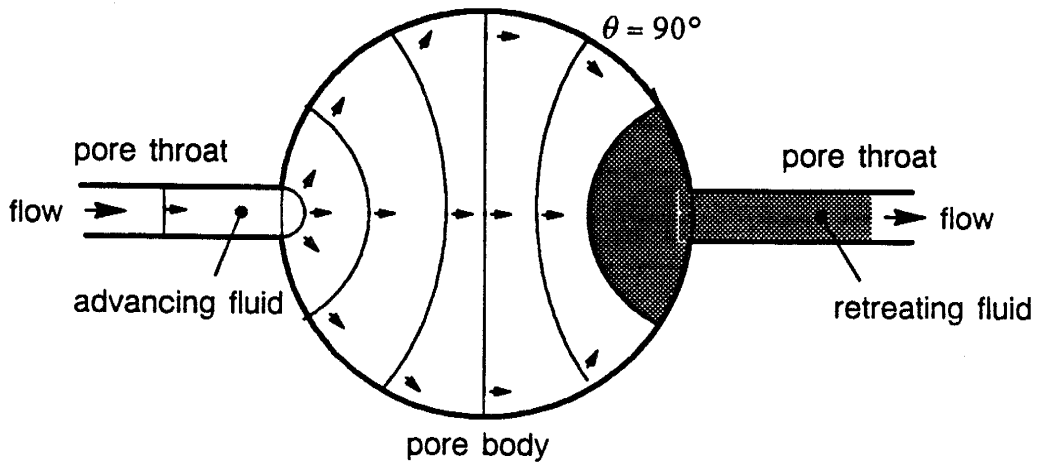
Figure 7. One fluid displacing another from a circular, high aspect ratio pore, under intermediate wetting conditions (after Wardlaw, 1982).
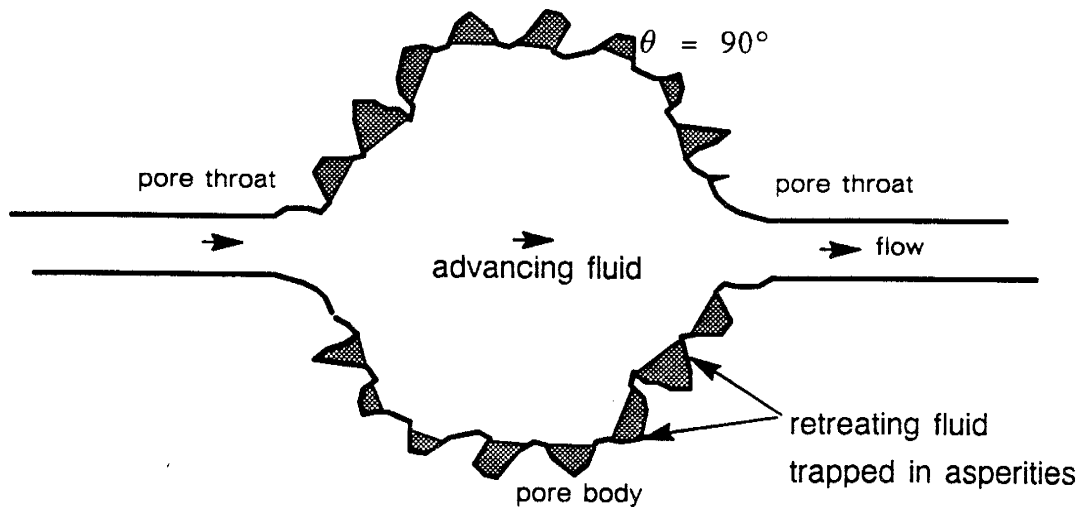
Figure 8. Final condition after an advancing fluid displaced a retreating fluid from a rough-walled pore under intermediate wetting conditions (after Wardlaw, 1982).

By-passing

The pore doublet model has been used to describe trapping mechanisms on a microscopic scale (Moore and Slobod, 1956; Chatzis and Dullien, 1983; and Chatzis et al., 1983). A pore doublet consists of a tube which splits into two pores, one generally narrower than the other, and then rejoins. The pore doublet concept is used here to describe organic phase trapping by the mechanism referred to as 'by-passing'.

Figure 9 depicts a wetting phase (water) displacing a non-wetting organic phase in a pore doublet under several different circumstances. The pore walls are smooth and strongly water
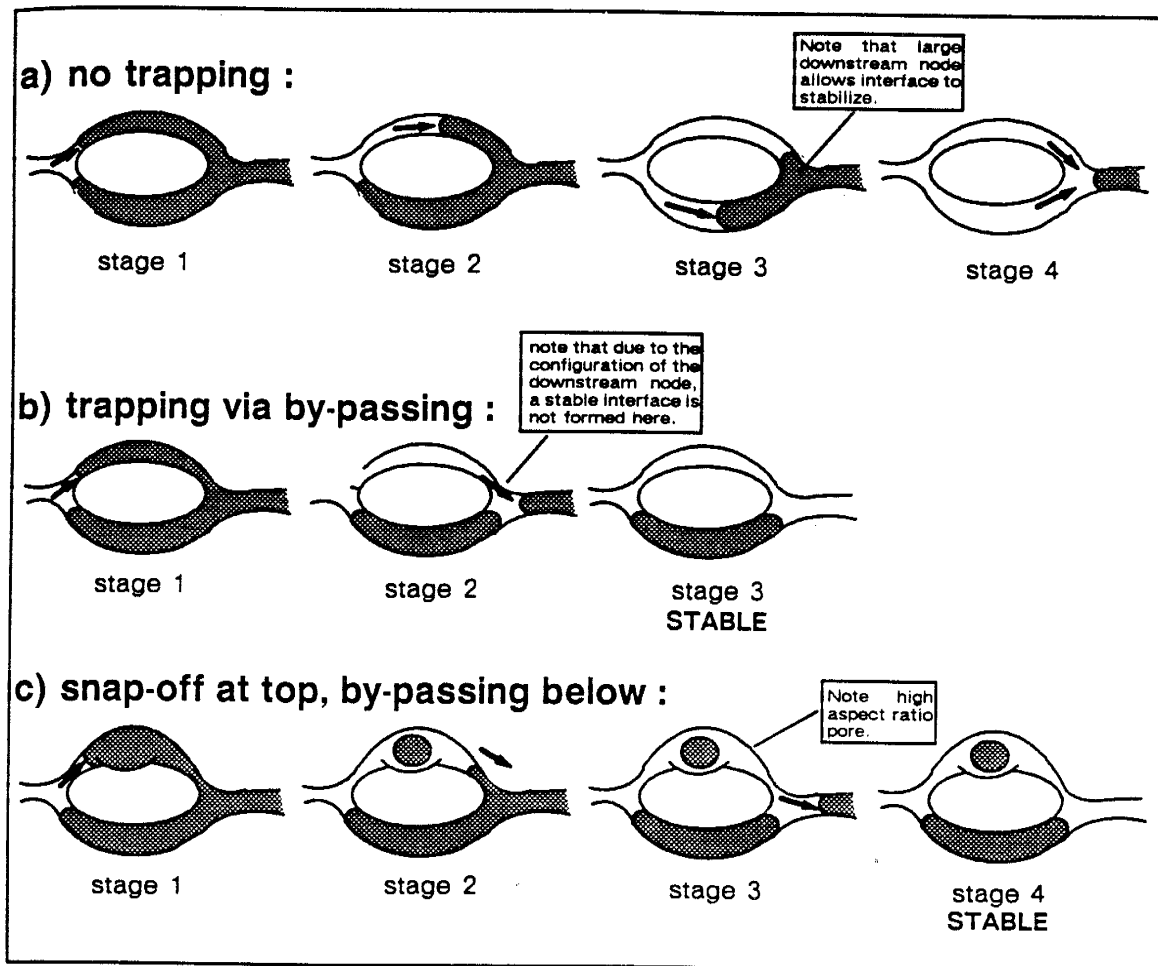
Figure 9. Sketches illustrating trapping mechanisms using the pore doublet model (after Chatzis et al., 1983)

wet. Figure 9a demonstrates circumstances under which no trapping occurs. The advancing water phase enters the narrower pore opening first (stage 1). In each pore, the total pressure drop driving flow is the sum of the capillary pressure and the dynamic pressure drop caused by flow (Moore and Slobod, 1956). For the pore doublet to have any physical meaning, the flow rates (and dynamic pressure drop) should be low enough to approximate aquifer conditions. On a pore scale, under such conditions, capillary forces are much larger than the dynamic viscous forces. Capillarity then controls advance of the wetting front causing water to fill the narrower pore (Chatzis and Dullien, 1983). The water-organic interface remains stable at the entrance to the wider pore (stage 2). When the water reaches the downstream node (where the pores rejoin), it forms a stable meniscus with the organic liquid because the cross-section at the downstream node is greater than at the entrance to the wider pore. In instances where a stable meniscus can be maintained at the downstream node, water can then push organic out of the wider pore (stage 3). The menisci rejoin at the downstream node (stage 4). In this case, the

15

water has displaced the organic liquid completely from the pore doublet and no trapping has occurred.

The displacement sequence for the pore doublet shown in Figure 9b illustrates the by-passing mechanism of trapping. As before, the water enters the narrower pore first. However, as water reaches the downstream node, it does not stop because no stable interface is formed (Figure 9b, stage 2). The organic liquid in the wider pore has become disconnected from the main body of organic liquid and is now unable to drain from the pore. This liquid has become 'by-passed' by the advancing water (stage 3).

Figure 9c uses a pore doublet model to demonstrate both snap-off and by-passing trapping mechanisms. Once again, water enters the narrower pore first (stage 1). Due to the high aspect ratio in the narrower pore, snap-off occurs (stage 2). Water continues to move through the narrower pore and through the downstream node. No stable meniscus is formed and organic liquid in the wider pore is by-passed (stages 3 and 4).

While the pore doublet model allows the organic liquid to be by-passed in at most one pore, in a porous medium the organic phase in several pores may be collectively by-passed leaving an organic blob which extends over the several pores. In contrast, blobs trapped by snap-off extend over one pore only. As pore aspect ratio decreases, the proportion of organic liquid trapped by by-passing, relative to snap-off, increases, and blobs become larger and more complex. Soil or rock heterogeneity also encourages trapping through by-passing, as is discussed in Chapter 8 (see also Chatzis et al., 1983). Wettability, pore aspect ratio, and soil (or rock) heterogeneity are important factors influencing trapping.

INFLUENCE OF WATER FLOW RATE ON RESIDUAL ORGANIC MOBILIZATION

Consider a homogeneous soil with a residual saturation of organic liquid. If the pressure gradient and Darcy velocity of the water phase are increased sufficiently, some of the trapped blobs begin to move because of an increase in the viscous force. This process is called mobilization. The pressure gradient must be sufficiently high to squeeze the blobs through pore throats. At the leading edge of the blob, organic liquid is displacing water (drainage), while at the trailing edge water is displacing organic liquid (imbibition). The dynamic pressure difference required to support mobilization is proportional to the difference in these drainage and imbibition capillary pressures (Melrose and Brandner, 1974).

A critical element in mobilization is the length of the blob in the direction of flow. For a fixed dynamic pressure gradient the longer blobs are easier to mobilize, because a greater pressure difference can be established across them. The amount of residual saturation reduction by hydraulic mobilization can strongly depend on how the trapped organics are distributed on a pore scale. If, for instance, many of the trapped blobs are relatively long and complex ganglia formed by by-passing, they can be more easily mobilized than if the majority of blobs are singlets resulting from snap-off. Once mobilized, blobs do not always maintain their size. The larger mobilized blobs can break up into smaller blobs, with a significant fraction being only temporarily mobilized (Chatzis et al., 1984). Also, as moving blobs collide with other blobs, the blobs may

coalesce (Ng et al., 1978). If substantial coalescence occurs, a bank of mobilized organic liquid may form. The factors controlling blob break-up and coalescence are not, as yet, well understood.

Mobilization can be aided by a difference in density between the water and the organic liquid. If the organic liquid is lighter than water, the blob will be buoyant and tend to rise vertically. If the blob is heavier than water it will tend to sink. The vertical migration of the blob due to the density difference is resisted by the capillary forces which trapped the blob in the first place. If the hydraulic gradient can be aligned so that viscous and buoyant forces reinforce each other, their combined force may be sufficient to induce mobilization.

There are many factors that influence this mobilization: the geometry of the pore network, fluid-fluid properties such as interfacial tension and density ratio, fluid-soil interfacial properties which determine wetting behavior, the applied water phase pressure gradient and its alignment with gravity (Morrow and Songkran, 1981). When only two fluid phases are present these factors can be incorporated into one of two dimensionless numbers. The ratio of viscous forces to capillary forces is known as the capillary number, N_c , while the ratio of gravity forces to capillary forces is the Bond number, N_B:

$$N_{c_1} = \frac{k \ \nabla P_w}{\sigma} \tag{2}$$

$$N_{B_1} = \frac{\Delta \varrho \ g \ r^2}{\sigma} \tag{3}$$

where: k = intrinsic (absolute) permeability of soil

   ∇P_w = water phase pressure gradient

   σ = interfacial tension between the fluids

   $\Delta \varrho$ = density difference between fluids

   g = acceleration of gravity

   r = representative grain radius

The subscript 1 in N_{c_1} refers to the version of the dimensionless number. This model of the capillary number assumes that the hydrostatic forces are negligible. The ratio of forces represented by the capillary number can also be given in terms of the Darcy velocity in the water phase (see, e.g., Taber, 1981):

$$N_{c_2} = \frac{q_w \ \mu_w}{\sigma} \tag{4}$$

where: q_w = specific discharge (darcy velocity) of the water phase

   μ_w = viscosity of water

This version of the capillary number inherently accounts for the gravitational (hydrostatic) portion of the driving force — the $\nabla(\varrho_w \ g \ z)$ term in the expansion of q_w:

$$q_w = \frac{k_{rw} \, k}{\mu_w} \, \nabla (P_w + \varrho_w \, g \, z) \tag{5}$$

where: k_{rw} = relative permeability for the water phase

         z = elevation of the point of interest above the datum

N_{c_2} can be obtained from N_{c_1} by adding in the gravity term and multiplying by the relative permeability of water. Wilson and Conrad (1984) defined a related capillary number for groundwater situations:

$$N_{c_3} = \frac{k \, \varrho_w \, g \, J_w}{\sigma} = \frac{K_w \, J_w \, \mu_w}{\sigma} \tag{6}$$

where: J_w = hydraulic gradient in the water phase, $\nabla \left(\dfrac{P_w}{\varrho_w \, g} + z \right)$

      K_w = water-saturated hydraulic conductivity of the soil, $\dfrac{k \, \varrho_w \, g}{\mu_w}$

This definition of the capillary number does not contain the relative permeability built into (4), but does contain the gravity term neglected in (2). When hydrostatics are negligible, (6) reduces to (2).

The Bond number also has at least one other version. It can be given in terms of intrinsic permeability instead of a characteristic grain size:

$$N_{B_2} = \frac{k \, \Delta \varrho \, g}{\sigma} \tag{7}$$

Morrow and Songkran (1981) used the Kozeny-Carman equation (Carman, 1937) to determine an approximate relation between the two forms of the Bond number for unconsolidated media of relatively uniform grain size. This second version of the Bond number may be more convenient to use for soils having a fairly wide grain size distribution — because the selection of a representative grain size in a poorly sorted soil for use in N_{B_1} may turn out to be rather arbitrary. Although buoyancy forces can aid mobilization, the following discussion will focus on viscous forces and the capillary number, referring the reader to work by Morrow[1] and to discussions in the results chapters (7, 8, and 9) concerning the effects of significant gravity forces.

Once the capillary number exceeds a critical value, the residual saturation decreases as the number is increased (see e.g., Figure 10). In the figure, the residual saturation is normalized by its initial value, S_{or}^*, which is the residual saturation measured under low capillary number flow conditions. Above the critical capillary number, N_c^*, viscous forces begin to overcome the

---

1. Morrow, 1979; Morrow and Songkran, 1981; and Hornof and Morrow, 1987.
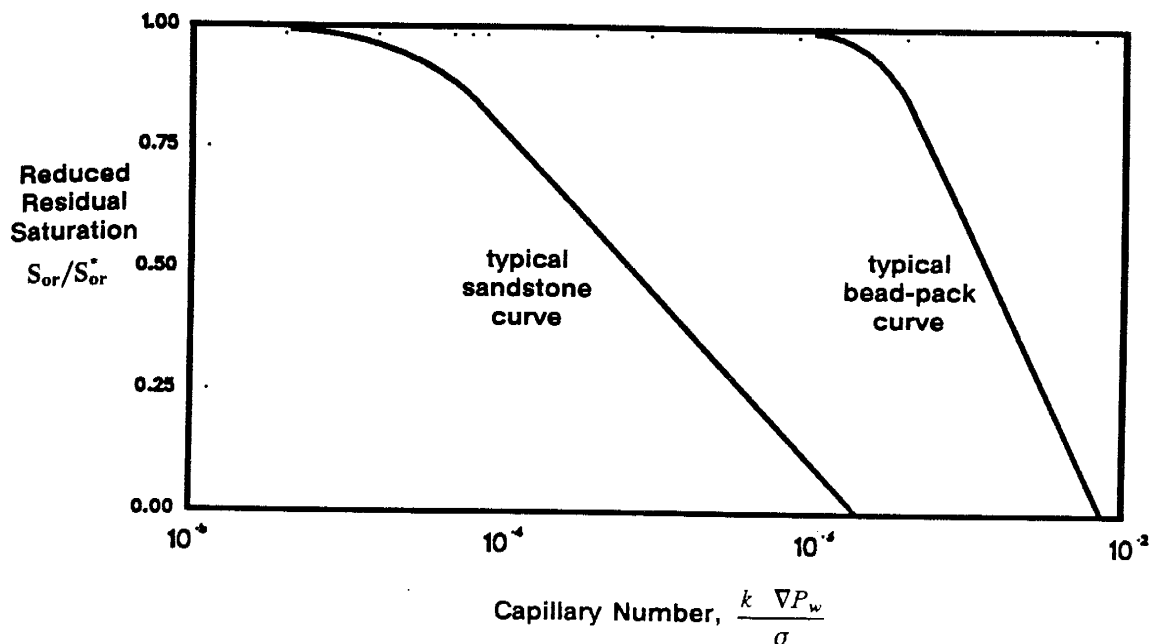
Figure 10. Relationship between residual saturation and capillary number for sandstones and glass beads. The sandstone curve is from Chatzis and Morrow (1984); the bead-pack curve is based on work reported in Morrow and Chatzis (1982).

The graph shows "Reduced Residual Saturation S_{or}/S_{or}^*" on the y-axis (0.00 to 1.00) and "Capillary Number, $\dfrac{k \; \nabla P_w}{\sigma}$" on the x-axis ($10^{-6}$ to 10^{-2}), with a "typical sandstone curve" and a "typical bead-pack curve".

capillary forces resulting in a reduction of the residual saturation. Chatzis and Morrow (1984) performed a large number of experiments using sandstone cores to explore this relationship between capillary number and organic liquid saturation. First a residual organic liquid saturation, S_{or}^* , was established in the cores under low Bond and capillary number conditions. Then the gradient across the core was increased in a stepwise manner, and at each step residual organic liquid production was observed. A typical curve for the sandstone is shown as the left-hand curve in Figure 10. The critical capillary number at which mobilization was initiated was typically $N_{c1}^* \approx 2 \times 10^{-5}$ for sandstones. N_c^{**} denotes the capillary number necessary to displace all of the blobs; $N_{c1}^{**} \approx 1.3 \times 10^{-3}$. Fifty percent of the residual organic liquid is removed when $N_{c1} \approx 3 \times 10^{-4}$. The relationship in Figure 10 holds for a wide variety of sandstones and organic fluids, provided that the organic liquid is the non-wetting fluid.

A similar set of experiments were performed for glass beads by Morrow and Chatzis (1982). Using a variety of sizes of uniform beads, and various organic liquids another correlation was obtained. It is shown as the right-hand curve in Figure 10, and looks nothing like the sandstone curve. A significantly larger capillary number (i.e. more gradient) is required to mobilize the blobs. This result is explained by the very large aspect ratio of the bead pack pores relative to sandstones, and the dominance of capillary trapping by snap-off. Sintering the beads (melting them together slightly) reduces the aspect ratio and produces a curve much closer to the sandstone curve (Morrow and Chatzis,1982). In a similar study Morrow and Songkran (1981)

found a that critical Bond number (N_{B1}) of about 0.005 was needed to reduce trapping in glass beads.

For natural soils, a correlation between the capillary number and the mobilization of residual organic liquid has yet to be determined. Determination of this relationship, which may well vary from soil to soil, is important to aquifer restoration. Understanding the dependence of organic liquid saturation upon capillary number (or hydraulic gradient) will help establish when it is possible to hydraulically mobilize trapped organic liquids — and when it is not possible. Understanding this relationship will also help prevent inadvertent mobilization of organic liquids during laboratory experiments.

Implications for Hydraulic Removal of Residual Saturation

Remediation schemes attempting to hydraulically remove capillary trapped residual by waterflooding can remove some of residual organic liquid when $N_c > N_c^*$. All of it will be removed when $N_c > N_c^{**}$. Figures 11a and 11b are plots of J versus k taken from Wilson and Conrad (1984) using the capillary number relationship of equation (6), and the sandstone value of the critical capillary number, N_c^*. Various organic-water interfacial tensions, σ, are shown. J is the hydraulic gradient in the water phase. The plots describe hydraulic gradients necessary to initiate blob mobilization.

For example, tetrachloroethylene (PCE) has a density of 1.62 g/cm, greater than that of water, and is likely to sink into the saturated zone. It has an interfacial tension of 47.5 dyne/cm. In a fine gravel, with $k = 10^{-5}$ cm^2, a gradient of $J = 0.1$ is necessary to start some of the blobs moving. This is a steep but not unreasonable gradient. In a medium sand with $k = 10^{-7}$ cm^2, the necessary gradient is a very steep $J = 10$.

Figure 12 is a plot of percentage residual organic liquid recovered as a function of gradient and soil permeability, for an interfacial tension of 10 dyne/cm. The top curve in Figure 11a is the 100% recovery curve for the same organic liquid using the sandstone value of N_c^{**}. Other organic liquids can be examined by simply multiplying these results by σ /10. For the fine gravel example, which required a gradient of only 0.1 to begin to mobilize PCE blobs, now requires a gradient of 1.0 to completely remove an organic liquid having an interfacial tension of 10 dyne/cm. For PCE, the necessary gradient is (47.5/10) = 4.75 times are large, or $J = 4.75$. It is improbable a gradient this large can be achieved at a spill site but is not an uncommon gradient for a laboratory experiment. In the medium sand (where k is 100 times smaller) it would take a gradient of $J = 100 \times 4.75 = 475$ to remove all of the residual PCE, clearly an impossible feat at a spill site.

In summary, residual organic liquid is easier to mobilize for lower interfacial tensions, higher permeability soils, and in the lab. It's harder to mobilize for higher interfacial tensions, lower permeabilities, and in the field where there are severe practical constraints on the hydraulic gradient. Although it may be possible in some instances to mobilize some of the residual, it is difficult to get it all.
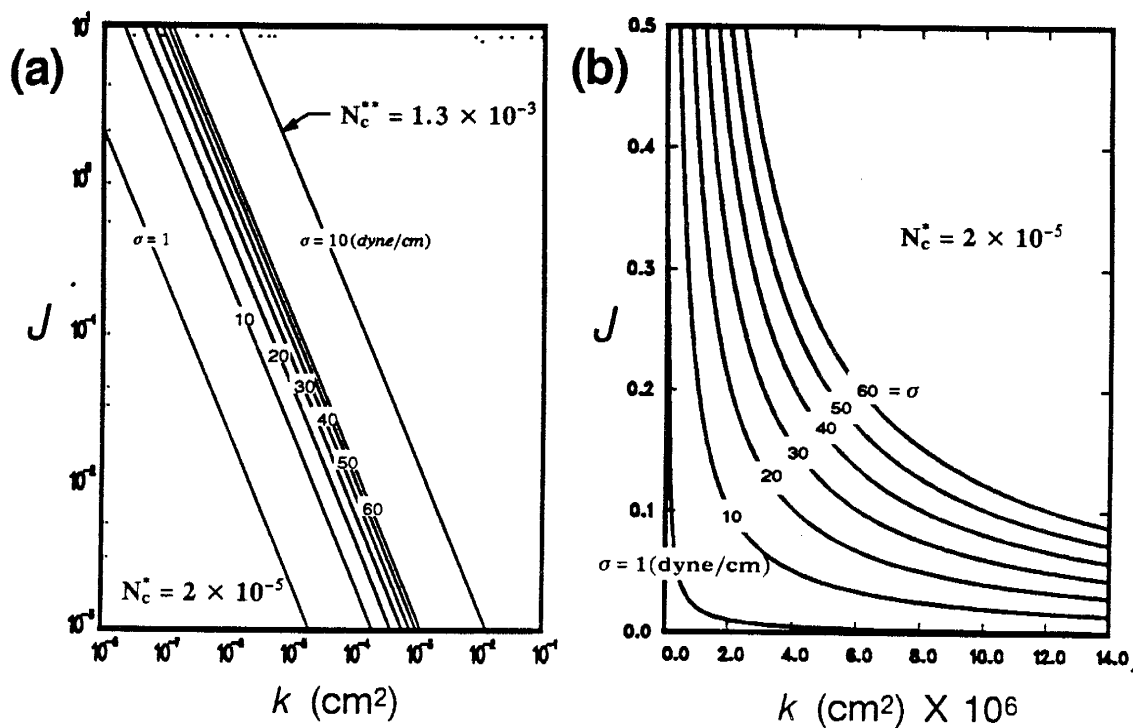
Figure 11. Hydraulic gradients required to initiate blob mobilization in porous media of various permeabilities, for organic liquids of various interfacial tensions. A critical capillary number of $N_c^* = 2 \times 10^{-5}$ was used. Plot (a) uses a log-log scale, while (b) is plotted using linear coordinates. The upper curve in (a) represents the gradient necessary for complete removal of all organic liquid with an interfacial tension of 10 dyne/cm. From Wilson and Conrad (1984).

Several schemes have been published in the literature and implemented in the field for hydraulically sweeping organic liquids from polluted aquifers. These schemes are presumably meant to sweep out the continuous organic liquid, knowingly leaving behind the residual. More often it seems that naivete prevails, and many designers assume that as long as ground water is flowing toward a collection system, eventually all of the organic liquid will make it. No matter how long one waits, unless gradients are increased above the critical level, none of the residual will be hydraulically removed (Wilson and Conrad, 1984).

DISSOLVING RESIDUAL ORGANICS

Dissolution is another process (in addition to hydraulic mobilization) in which the residual organic saturation can be reduced over time. Although dissolution of the organics is seldom used alone as a remediation scheme because complete removal of the organic phase by dissolution is often a very slow process, the advection of dissolved organic pollutants in the water phase is nonetheless an important transport mechanism.

First, let's consider the dissolution of a one-component residual organic liquid. Simple compositional models of interphase mass transfer usually assume that a local equilibrium is
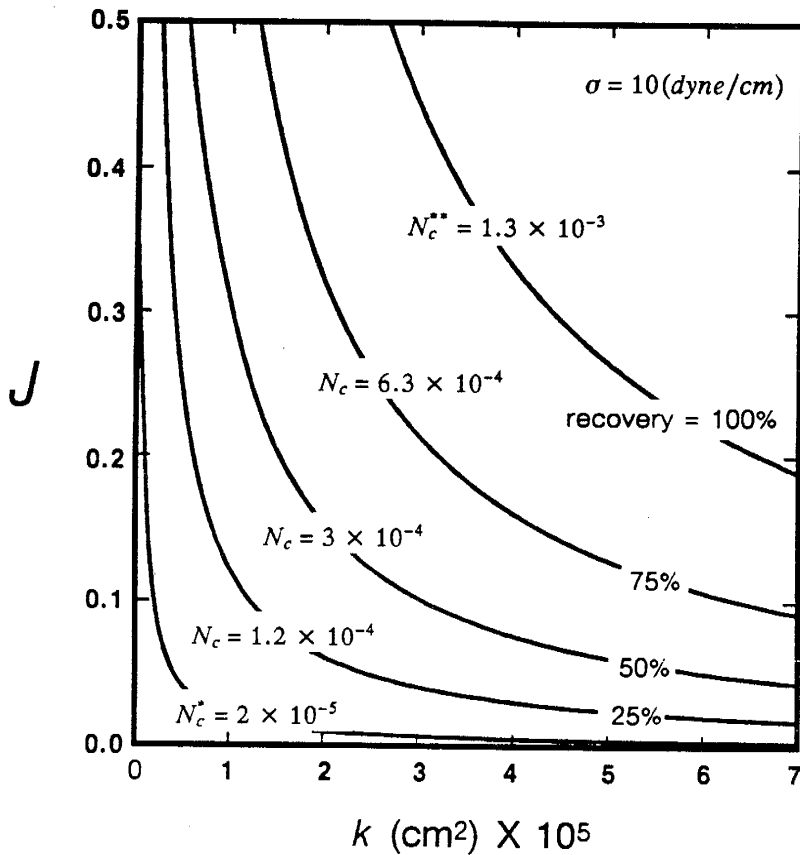
Figure 12. Recovery of residual saturation as a function of permeability and hydraulic gradient for an interfacial tension of 10 dyne/cm. From Wilson and Conrad (1984).

reached between the phases. As groundwater passes through the zone of residual saturation, trapped organic liquid is dissolved as water passes through. In the case where a local equilibrium is in fact reached, only blobs at the extreme upstream end are dissolved. By the local equilibrium assumption, as soon as water comes into contact with organic liquid the solubility limit of the water with respect to the organic is reached. With time, blobs at the upstream become dissolved and completely disappear. Blobs not at the upstream end are not dissolved at all because passing water has already been completely saturated with organic liquid. If we look spatially at this equilibrium dissolution process as a function of time, we see organic liquid saturation maintains a sharp front at the upstream end (Figure 13a), as does the dissolved concentration in the water phase (Figure 13b).

Often, when groundwater velocities are high enough or the dissolution kinetics are slow enough, the local equilibrium assumption no longer holds. In this case, the saturation distribution may look like that shown in Figure 14. A dispersed zone forms where traveling groundwater has not yet reached its solubility limit for the organic liquid. The dispersed zone is the region in which there is a reduced residual saturation ($0 < S_{or} < S_{or}^*$), and it looks like a backwards breakthrough

curve. Downstream of the dispersed zone, the water has reached its solubility limit and can no longer dissolve organic liquid. The higher the velocity and the lower the interphase mass transfer rate, the larger the dispersed zone will be. Powers et al. (1988) in a numerical modelling study, found the rate of mass transfer between phases can be strongly dependent upon the distribution of the residual saturation.

Dissolution from a multi-component organic phase is more complex. Many spilled organics — from gasoline and other fossil fuels, to transformer oils containing PCBs, to the mixed bag of organics that are sometimes found in industrial waste pits — are mixtures having many (sometimes hundreds of) organic components. The more soluble components of these mixtures can dissolve comparatively quickly, leaving behind the less soluble components to leach out

(a)

(b)
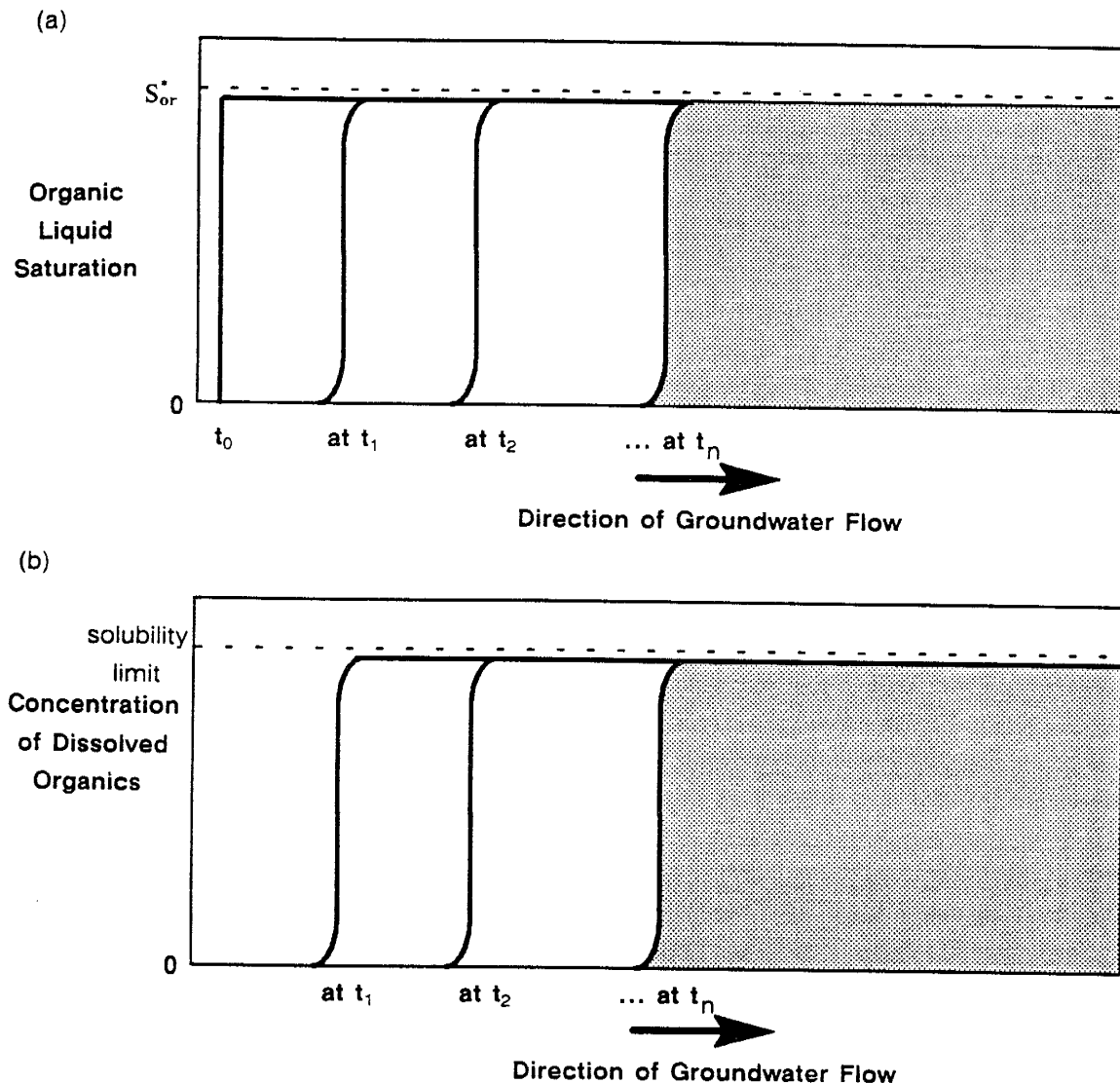
Figure 13.   The spatial distribution of a single-component residual organic liquid undergoing dissolution as a function of time when the local equilibrium assumption is invoked. Notice that a sharp front is maintained at the dissolution front for both the organic liquid saturation (a), and for the concentration of the organic dissolved in the water (b).
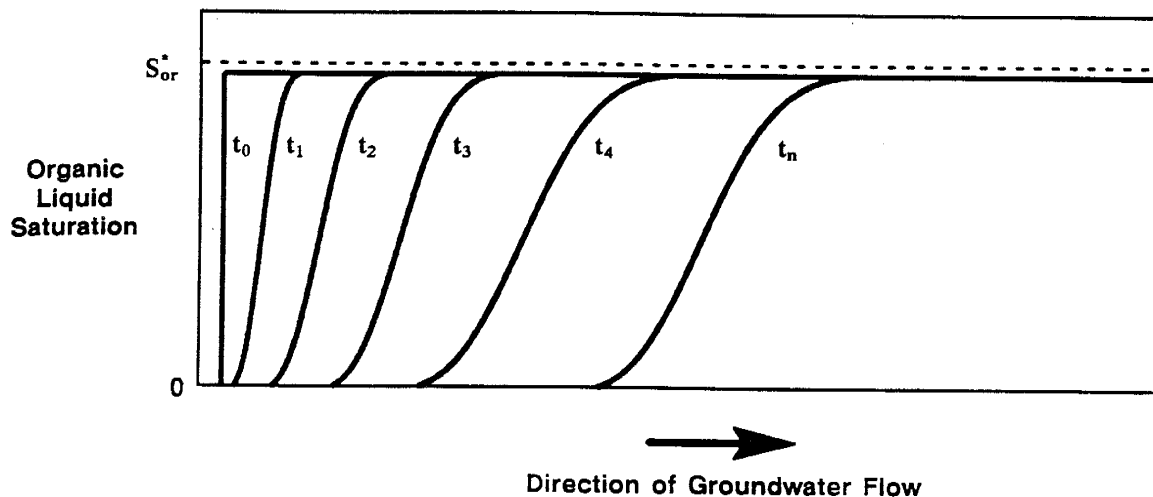
Figure 14. The spatial distribution of a single-component residual organic liquid undergoing dissolution as a function of time when a local equilibrium between the fluid phases is not reached. A dispersed zone forms and grows until a steady state is reached.

more slowly. There are also co-solvency effects to consider. Interaction between components can either enhance the solubility of a given component (co-solvency) or the interaction can reduce the solubility of that component (by a kind of salting-out process). With all these complicating factors, the saturation distribution of the residual organic phase becomes much more complex than the simple curves shown for dissolution of a single-component liquid.

Compositional models, numerical codes which simulate interphase transfer such as dissolution, are becoming more sophisticated as more of the complexities of the process are incorporated. Partitioning of organic chemicals between fluid phases is dependent, among other things, upon the pore-scale distribution of the residual saturation. This issue is discussed in all three of the results chapters. Particularly in Chapter 7, this issue is discussed at some length.

CHAPTER 3

CHARACTERIZING EXPERIMENTAL FLUIDS AND SOILS

In this chapter, characterization of the fluids and soils commonly used in several of the experiments is presented. Predictably, the chapter is divided into two main parts — fluids, and soils. Within each part, the methods used for characterization is described, followed by the characterization results themselves.

FLUID CHARACTERIZATION

Measurements of fluid properties such as viscosity, specific gravity, surface tension, and interfacial tension were performed following procedures outlined by the American Society for Testing and Materials (ASTM, 1986). Viscosity was measured with Cannon-Fenske routine viscometers according to ASTM methods D445-83 and D446-85a. Specific gravity measurements were made as described by ASTM method D1429-76 (pycnometer procedure). An adaptation of ASTM procedures D 1590-60 and D 971-82 were used to determine surface tension and aqueous-organic interfacial tensions, respectively, by the ring method with a Fisher Manual Model 20 tensiometer. The surface tension procedure was modified so that no centrifuging of the samples was done. The method of cleaning glassware and the platinum-iridium ring were also modified to follow that of the interfacial tension method.

Measured Fluid Properties

The measured properties of all fluids used in the laboratory experiments (except for styrene and the epoxies used in the blob and pore cast experiments) are shown in Table 1.

A 3000 ppm $CaCl_2$ solution was used as the aqueous phase in all column experiments. Distilled, de-ionized water was de-gassed by boiling. Enough calcium chloride dihydrate was added to the cooled water to bring the concentration to 3000 ppm. The solution was stored under a vacuum to keep it de-gassed. The properties of this aqueous phase are given in Table 1. The interfacial tensions of all the organic liquids were measured against this fluid.

Soltrol-130, a mixture of C_{10} to C_{13} isoparaffins, was the fluid most commonly used as the organic phase in these experiments. It is a colorless, combustible liquid having a mild odor and negligible solubility in water. A simple experiment was conducted to determine the relative volatility of Soltrol to water. Equal amounts of Soltrol and distilled water were placed side by side in identical graduated cylinders and periodically checked visually for liquid loss caused by evaporation. A plot of the results (Figure 15) demonstrates the much lower volatility of Soltrol. Other properties of Soltrol as measured in the laboratory are given Table 1.

SOIL CHARACTERIZATION

Quantitative descriptions of the soils were made, including particle density, particle size analysis, capillary pressure-saturation curves, and wettability. Soil particle densities were

liquid	density (g/cm³)	viscosity (cP)	interfacial tension with 0.3% $CaCl_2$ solution (dynes/cm)	surface tension (dynes/cm)
aqueous phase	1.000±0.002	0.98 ± 0.01	not applicable	72.0 ± 0.4
Soltrol-130	0.753 ± 0.002	1.45 ± 0.01	47.8 ± 1.2	19.1 ± 0.3
kerosene	0.807 ± 0.002	1.73 ± 0.01	38.6 ± 1.2	26.8 ± 0.4
gasoline	0.731 ± 0.005	0.48 ± 0.01	22.9 ± 0.3	20.5 ± 0.3
n-decane	0.727 ± 0.002 [21]	0.91 ± 0.01	44.5 ± 1.0	24.9 ± 0.3
benzene	0.877 [20] †	0.652 [20] †	not determined	28.9 [20] †
toluene	0.861±0.002	0.590 [20] †	not determined	28.5 ± 0.5
p-xylene	0.855 ± 0.005	0.60 ± 0.01	35.8 ± 0.8	28.4 [20] †
PCE	1.614 ± 0.005	0.87 ± 0.01	41.8 ± 0.7	31.7 [20] †
carbon tetrachloride	1.599 ± 0.002	1.05 ± 0.01 [21]	32.9 ± 0.8 [21]	28.2 ± 0.3 [21]

† Weast, 1986

Table 1. Measured properties of fluids used in experiments. All measurements were taken at temperatures between 22°C and 24°C except where noted.

determined using ASTM D584-83. Soil particle size distributions were measured using ASTM D422, and the saturated hydraulic conductivities were measured by ASTM D2434. Porosities and bulk densities of the soils were measured at the time of column packing and the methods used are described within the methods chapters for each experiment. Soil capillary pressure-saturation relationships were determined using equilibrium methods (Vomocil, 1965). Wettabilities of the soils to water and the organic liquid were by the Amott method (Amott, 1959) and the USBM method (Donaldson, 1969).
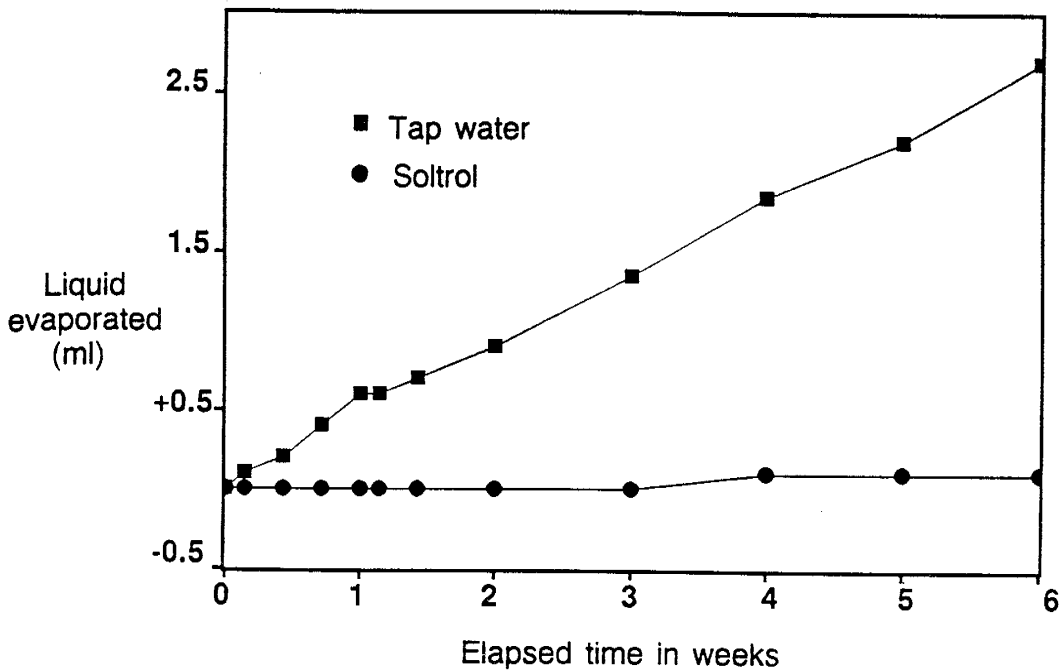
Figure 15. Qualitative comparison of Soltrol and water volatility.

Capillary Pressure-Saturation Test

Soil capillary pressure-saturation relationships were determined using equilibrium methods (Vomocil, 1965). Hanging column type equilibrium stepwise water-air, water-organic, and air-organic displacement experiments were performed under both drainage and imbibition conditions to determine the capillary pressure functions. The experiments were performed using prepared soil columns. The effective column length was kept short (5 cm) in order to keep fluid saturations relatively constant along the length of the column. Standard equilibrium procedures were altered for the water-organic liquid displacement experiments to accommodate conditions involving two liquid phases. Figure 16 shows this modified set up. Tubing was used to connect the tops of the burets to seal the system and reduce volatilization. The soil column was prepared as described later in Chapter 4 for a water saturated column. The soil column was attached to burets containing organic liquid (buret A) and water (buret B). The capillary pressure was increased stepwise. At each step the system was allowed to equilibrate (about 24 hours were required). The capillary pressure was measured as:

$$P_c = (\varrho_o \, h_1 + \varrho_w \, h_2) \, g \tag{8}$$

where: P_c = capillary pressure (dyne/cm^2)

h_1 = height of the organic liquid in buret A above the center of the column (cm)

h_2 = height of the water in buret B below the center of the column (cm)

ϱ_o = organic liquid density (g/cm³)

ϱ_w = aqueous fluid density (g/cm³)

g = acceleration of gravity (cm/s²)

Fluid saturations were measured both gravimetrically (by weighing the column after equilibration had been achieved in each step) and volumetrically (by measuring the volume change of the fluids in each buret). Gravimetrically, saturations were measured as :

$$S_w = S_{wp} + \frac{\Delta M}{\Delta \varrho \ V_p} \qquad (9)$$
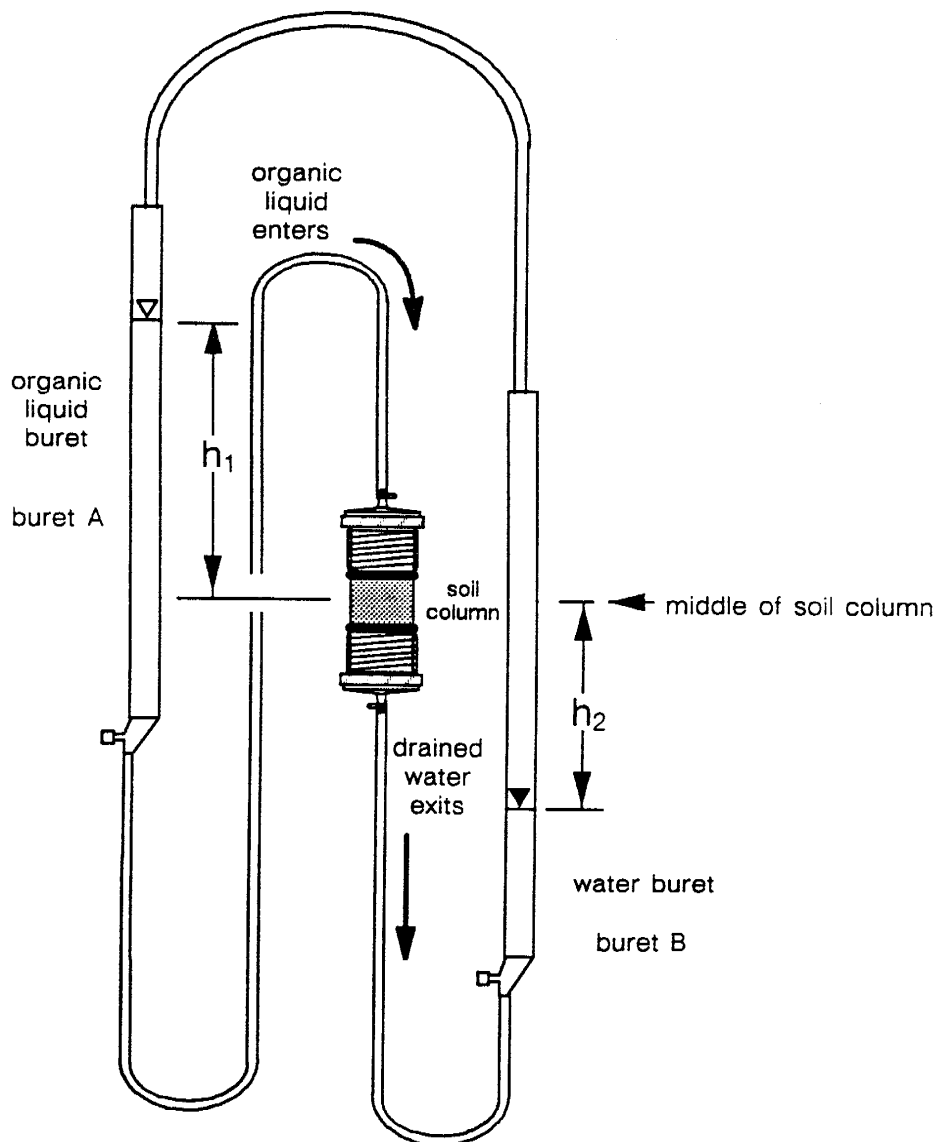
Figure 16. Setup for measuring organic/water capillary pressure-saturation relationships.

$$S_o = 1 - S_w \tag{10}$$

where: S_w = water saturation (–)

S_{wp} = water saturation at previous step (–)

ΔM = change in column mass from the previous step (g)

$\Delta \varrho$ = density difference between the fluids, $\varrho_w - \varrho_o$ (g/cm³)

V_p = pore volume of the column (cm³) (Chapter 4 describes how V_p was measured)

Volumetrically, the measurements were based on:

$$S_i = S_{ip} + \frac{\Delta V_i}{V_p} \tag{11}$$

where ΔV_i is the total change in volume of a fluid ($i = w$ or o) in the soil column as measured in the respective buret.

Wettability Measurements

Wettability refers to the relative affinity of the soil for the various fluids — water, air, and the organic phase. On a solid surface, exposed to two different fluids, it can be measured by contact angle (see Figure 17). Melrose and Brandner (1974) claim that contact angles are the only unambiguous measure of wettability. Several common methods for measuring contact angles are summarized by Adamson (1982); often a contact angle cell is used in petroleum engineering studies (Craig, 1971). The contact angle test is performed under brine. A drop of reservoir oil is placed between two polished crystals that are representative of the reservoir rock (usually quartz or calcite) and contact angles are measured. When surface active agents are present it may take up to hundreds of hours of interface aging time to reach equilibrium (Treiber et al., 1972). Hysteresis in contact angle measurements is common, so that both advancing and receding angles are often measured. There is some question as to how representative contact angle measurements are since they do not take into account the effect of surface roughness, heterogeneity, and pore geometry (Anderson, 1986b). Contact angle measurements were not used in this study. To measure the bulk wettability of the soils, adaptations of two methods commonly practiced on cores in petroleum engineering were employed: the Amott test and the USBM method. Both methods rely upon characteristics of organic/water capillary pressure-saturation curves to determine the wettability of the porous media.

The Amott (1959) test measures the wettability of soil as a function of the displacement properties of the soil-water-oil system. Four displacement operations are performed on the soil, and the ratio of spontaneous imbibition to forced displacement is determined for both the water and organic phases. The technique is similar to that required to determine capillary pressure-saturation relationships for two fluid phases. The four displacements are :

1) spontaneous displacement of organic liquid saturated core or column by water;

2) forced displacement of organic liquid saturated core or column by water;

3) spontaneous displacement of water saturated core or column by organic liquid; and,

4) forced displacement of water saturated core or column by organic liquid.

This test is based on the fact that the wetting fluid will spontaneously imbibe into the core, displacing the non-wetting phase. When the displacement-by-water ratio (δ_w) approaches one and the displacement-by-oil ratio (δ_o) is zero, the core is water-wet. If the opposite is true, the core would be oil-wet. The main problem with the Amott test is its insensitivity at near neutral wettability (Anderson, 1986b).

The USBM test compares the areas under two fluid phase capillary pressure-saturation curves as a measure of average wettability (Donaldson et al., 1969). When a soil is water-wet, the area under the organic-displacing-water capillary pressure curve (A_1) is larger than the water-displacing-organic curve (A_2). In fact, for a strongly water-wet system, most of the water will spontaneously imbibe into the soil, and the area under the water-displacing-organic curve will be very small. Since the work of fluid displacement is proportional to the areas under the capillary pressure curve (Morrow, 1970), the USBM wettability index in essence measures the
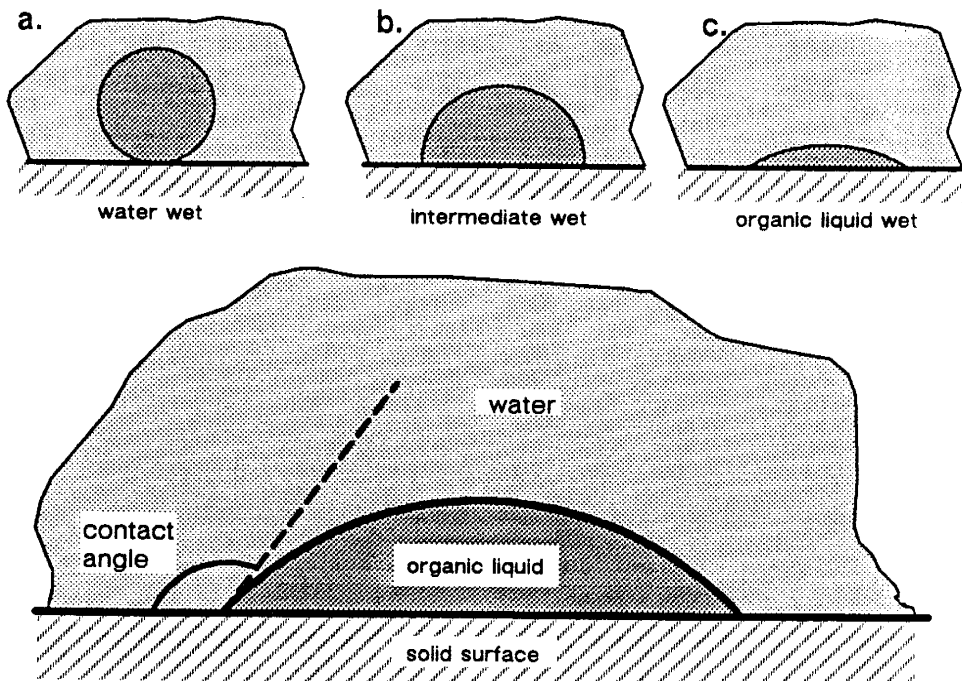
Figure 17.   Contact angle measurement on a clean, smooth solid surface.

WETTABILITY

	water-wet	intermediate-wet	organic-wet
contact angle			
minimum	0°	60° to 75°	105° to 120°
maximum	60° to 75°	105° to 120°	180°
Amott test			
displacement-by-water ratio (δ_w)	positive	zero	zero
displacement-by-oil ratio (δ_o)	zero	zero	positive
USBM wettability index, W	near 1	near 0	near -1

Table 2.　Relationship between wettability measurement methods (after Anderson, 1986b).

ratio of work needed for organic phase to displace water, to the work needed for the opposite displacement. The USBM wettability index, W, is given as:

$$W = \log \frac{A_1}{A_2} \tag{12}$$

Table 2 shows the wettability criteria for each of the three quantitative methods.

Sevilleta Soil

The Sevilleta dune sand was used in the majority of the experiments and hence, was the most extensively characterized soil. It is obtained locally and has been well studied by researchers at New Mexico Tech. The grains are sub-angular to sub-rounded. A mineral characterization of the sand indicates that it is composed mostly of quartz grains (72 ± 5% by number), with lesser amounts of feldspar(11 ± 2%) and lithic fragments (16 ± 3%). The lithics were generally much smaller in size than the other mineral grains; they compose about 5% of the sand by volume. An organic carbon analysis was conducted at North Carolina State University (courtesy of Dr. Cass Miller) and yielded an organic carbon content of 0.02%, an almost negligible amount.

The particle density of this sand was determined to be 2.65 ± 0.02 g/cm from five replicate measurements. Six sieve tests were conducted to measure the particle size distribution of the Sevilleta soil. There was excellent agreement between tests with all curves falling essentially on top of one another. The results of one test are presented in Figure 18. The particle size distribution classifies the soil is a uniform medium grained sand, with a median particle diameter of about 0.3 mm (300 microns) and a uniformity coefficient (d_{60}/d_{10}) of less than 2.
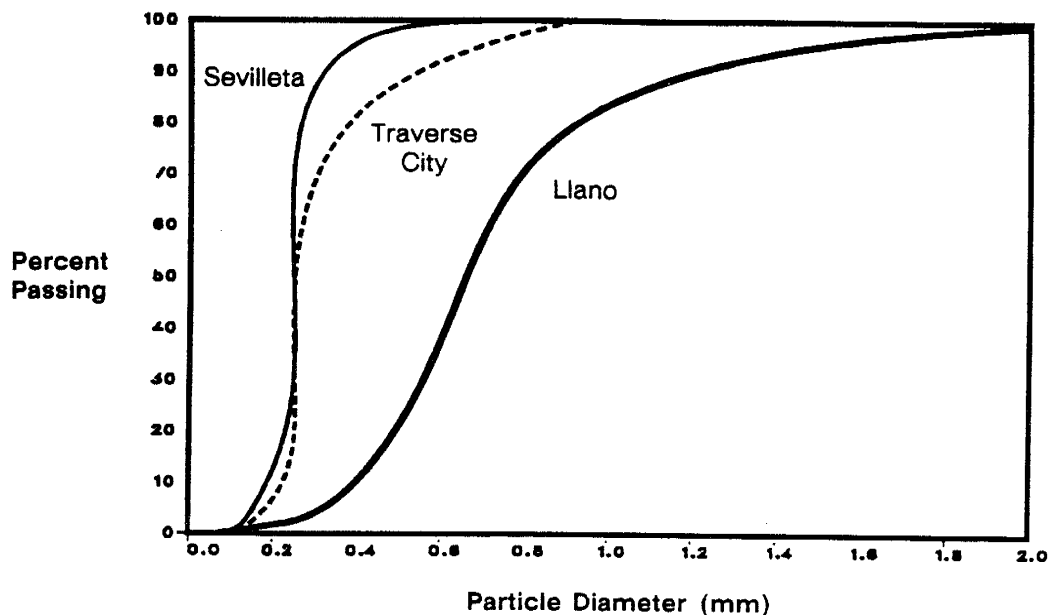
Figure 18. Particle size analysis for three of the soils used in this study.

Eleven replicate measurements of water-saturated hydraulic conductivity (K_w) and intrinsic permeability (k) were conducted in a constant head permeameter with the following results:

$$K_w = (1.03 \pm 0.20) \times 10^{-2} \text{ cm/sec}$$

$$k = 1.03 \times 10^{-7} \text{ cm}^2 = 104 \text{ darcys}$$

Capillary pressure-saturation curves for all fluid pair combinations (air-water, air-organic, and organic-water) were constructed with the Sevilleta soil. Soltrol-130 was used as the organic liquid phase in all trials. The soil capillary pressure-saturation plots from data acquired during 12 experimental trials include:

- **seven organic-water capillary pressure curves**, of which two curves have drainage, imbibition, and secondary drainage cycles, three curves have drainage and imbibition cycles, and two curves have the main drainage branch only;

- **two air-organic capillary pressure curves**, one curve with drainage, imbibition, and secondary drainage cycles, and one curve of the main drainage branch only; and,

- **three air-water capillary pressure curves**, of which two curves have the main drainage and imbibition cycles, and the third curve has the main drainage branch only.

For the air-organic trials, the soil column was packed under organic liquid. Examples of two of these 12 capillary pressure-saturation curves are shown in Figure 19. The remaining curves are presented in Appendix A.

Organic/water capillary pressure-saturation curves were used to determine the wettability of the Sevilleta soil. A typical Soltrol/water capillary pressure-saturation plot (shown in Figure 20)
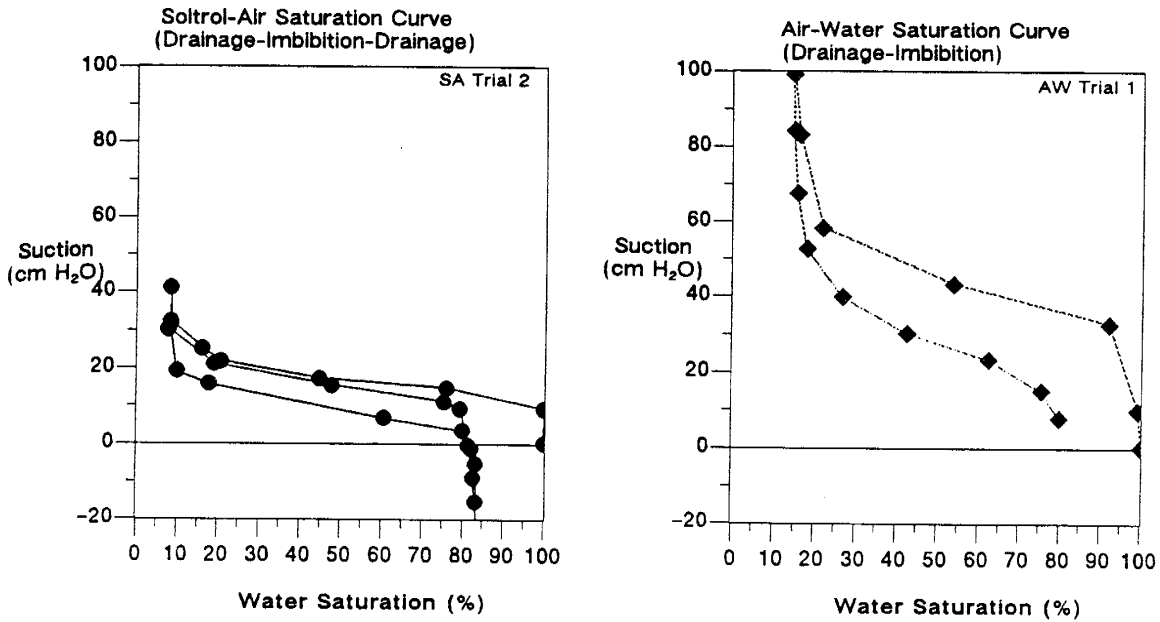
Figure 19.   Typical Sevilleta sand capillary pressure-saturation curves.
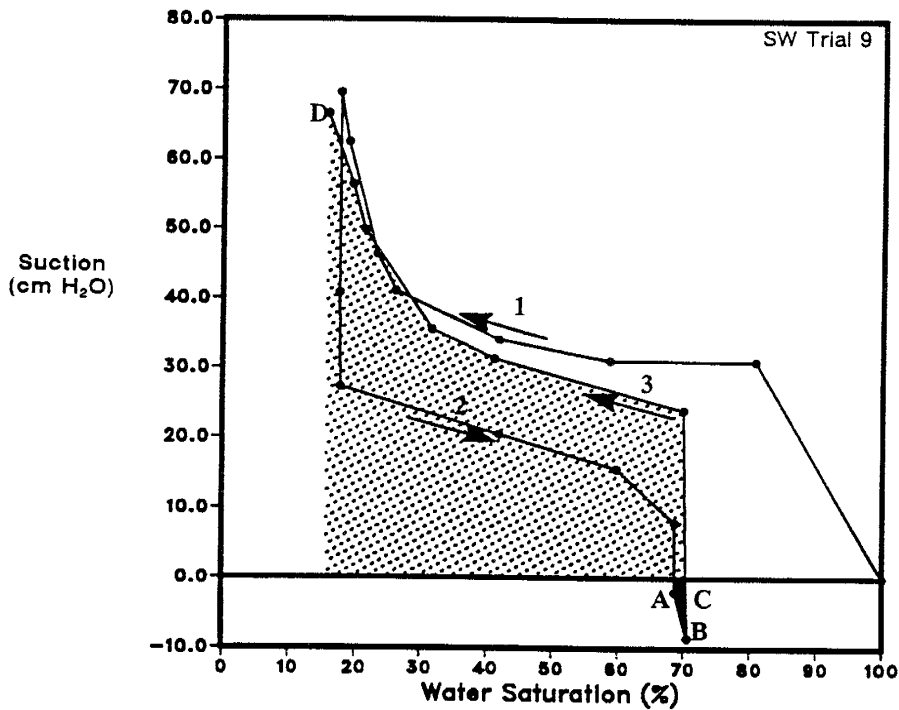
Figure 20.   A typical organic/water capillary pressure-saturation curve used to determine wettability, in this case for Soltrol-130 in Sevilleta sand.

was used in conjunction with the Amott and USBM methods to determine the wettability of the Sevilleta soil. The four displacement operations performed in the Amott test were:

1) spontaneous displacement of organic liquid by water (corresponding to a capillary pressure of zero on curve 2); point A;

2) forced displacement of organic liquid by water (corresponding to the residual organic liquid saturation); point B;

3) spontaneous displacement of water by organic liquid (corresponding to a capillary pressure of zero on curve 3); point C; and,

4) forced displacement of water by organic liquid (corresponding to residual wetting phase saturation); point D.

Preferentially water-wet soils have displacement ratios, $\delta_w = (S_{wA} - S_{wD})/(S_{wB} - S_{wD})$, approaching 1.0 and displacement-by-organic ratios, $\delta_o = (S_{wB} - S_{wC})/(S_{wB} - S_{wD})$, of zero. Organic liquid-wet soils give reverse results. The Sevilleta soil is strongly water-wet, not only to Soltrol, for which $\delta_w = 0.98$ and $\delta_o = 0.0$, but for all of the other organic liquids utilized.

The USBM test compares the areas under capillary pressure curves as a measure of wettability. When a soil is water-wet, the area under the organic-displacing-water capillary pressure curve (shaded) is larger than the area under the water-displacing-organic curve (black). In a strongly water-wet system, most of the water spontaneously imbibes into the soil, and the area under the water-displacing-organic curve is very small — as is the case for Soltrol in the Sevilleta soil as shown in Figure 20.

Palouse Loam

The Palouse loam soil, an agricultural soil from eastern Washington, was selected as an alternate soil for use in the saturated zone experiments. The Palouse soil provided a good contrast to the Sevilleta soil because of its much finer texture (15% sand, 80% silt, 5% clay) and its higher organic carbon content, 1.5% (Bowman et al., 1981). The water-saturated hydraulic conductivity of the soil was measured to be 5×10^{-6} cm/s using a falling head test, and the particle density was measured to be 2.67 ± 0.02 g/cm^3.

Due to the fine-grained nature of the soil, it was difficult to supply enough pressure to inject a non-wetting phase. Although it proved impossible to run capillary pressure curves for the Palouse loam, it can be surmised from the high non-wetting phase entry pressures that the soil is strongly water wet, and could serve as an effective barrier to movement of an organic phase.

Traverse City Soil

The Traverse City soil sample was obtained from a Superfund fuel spill site at a U. S. Coast Guard Air Station in Traverse City, Michigan. The soil is a clean, beach sand, composed primarily

of sub-rounded to rounded quartz grains, with some dolomite and igneous and metamorphic particles (Twenter et al., 1985). It has a particle density of 2.65 ± 0.01 g/cm³ and a saturated hydraulic conductivity of 1.0×10^{-2} cm/s. An organic carbon analysis conducted on soil samples from a nearby well indicated the soil had an organic carbon content of about 0.01% (Twenter et al., 1985). Sieve analysis of Traverse City soil is plotted in Figure 18. The Traverse City Soil is slightly coarser grained and more graded than the Sevilleta Sand.

Llano Soil

The Llano soil was a coarse sand obtained from the escarpment of the Llano de Albuquerque, remnants of a plain dissected by the Rio Grande and the Rio Puerco west of Belen, New Mexico. The soil sample is a clean, fluvial sand deposited by the ancestral Rio Grande or one of its tributaries. It has a particle density of 2.66 ± 0.01 g/cm³ and a saturated hydraulic conductivity of 1.6×10^{-1} cm/s. Sieve analysis of Llano soil is plotted in Figure 18. The Llano soil is more coarse grained and more graded than either the Sevilleta or Traverse City soils.

CHAPTER 4

SHORT COLUMN EXPERIMENTAL METHODS

Bench top short column experiments were performed to measure the residual organic liquid saturations of soils under either vadose zone or saturated zone conditions, providing a direct means to compare the amount of organic liquid trapped in the vadose zone to the amount trapped in the saturated zone. The complete set of results obtained using this technique was presented in Hagan et al. (1989). The soil used in most of the experiments was the Sevilleta dune sand, a uniform, medium-sized, quartz sand. Soltrol-130, a mixture of C_{10} to C_{13} isoparaffins with negligible solubility in water, most often served as the organic phase. The aqueous fluid used in the experiments was water with 3000 ppm calcium chloride added to prevent dispersion of clays. In other saturated-zone experiments, either kerosene, regular leaded gasoline, p-xylene, n-decane or tetrachloroethylene (PCE) was used as the organic phase to directly compare the differences in residual saturations to different classes of organic pollutants. Residual saturations were also measured in the other soils using Soltrol under saturated-zone conditions.

A short glass chromatographic column with threaded Teflon™ (tetrafluoroethylene) endcaps was used to contain the soil sample. The glass column had an inside diameter of 5 cm and an effective internal length of about 5 cm. The column was kept short so that — especially in the vadose zone case — saturations remained fairly constant over the length of the column. Semi-permeable membranes were used on the lower endcap to prevent capillary end effects. A paper filter placed on the upper endcap prevented clay-sized particles from leaving the column. Over the course of an experiment, the change in column mass was used, in conjunction with the known density difference between the fluids, to measure saturations. Soils and liquids were exposed only to glass, Teflon, and chemically resistant tubing during the experiments.

In the saturated zone experiments, organic liquid was introduced into an initially water-saturated soil sample until the water was reduced to its residual saturation. Water was then re-introduced into the soil displacing most of the organic liquid, but leaving behind some discontinuous blobs of organic liquid trapped by capillary forces. The fraction of the pore space occupied by these trapped blobs is the residual organic liquid saturation. The experiment represents a scenario in which organic liquid percolates into the saturated zone and is, in turn, displaced by ambient groundwater flow, leaving behind a residual organic liquid saturation.

In the vadose zone experiments, an initially water-saturated soil sample was drained with air under an applied suction until an equilibrium was reached. The drained soil represented vadose zone conditions in which the pore space is occupied by both air and water. As organic liquid was introduced (simulating a spill or leak), it displaced air and water as it percolated through the soil. Organic liquid was then drained from the soil under an applied suction, simulating the downward movement of organic liquid as it passes through the vadose zone toward the water table. Again, capillarity caused some organic liquid to become trapped in the pore space.

This chapter is begun by describing the fluids and soils used in these experiments and the rationale for those choices. (A detailed characterization of the fluids and soils used in the

experiments is presented in Chapter 3.) The short column apparatus is then described, followed by detailed procedures of how the apparatus was used to measure fluid saturations under two-phase (saturated zone) and three-phase (vadose zone) conditions. The conclusion of the chapter is spent discussing the limitations of the apparatus and possible errors that may occur when running these experiments.

FLUIDS AND SOILS

The aqueous fluid used in all experiments was distilled, de-ionized, de-aired water with 3000 ppm $CaCl_2$ added to prevent dispersion of clays.

Soltrol-130, a mixture of C_{10} to C_{13} isoparaffins produced by Phillips 66 Company was the organic liquid used to troubleshoot the apparatus and develop the experimental procedure. It is a colorless, combustible liquid having a mild odor and negligible solubility in water. Soltrol-130 proved to be the ideal fluid for debugging because of its relatively low solubility, volatility, and toxicity. For these desirable qualities and because of the need to hold all variables but the independent variable of interest constant, Soltrol-130 was used in all experiments comparing residual saturations in the saturated zone to those in the vadose zone, and for all comparisons of residual saturations between soils.

The other organic liquids selected for use in the experiments were chosen to be representative of several classes of organic liquid pollutants often present at landfills, hazardous waste sites, and accidental spills. Saturated zone residual organic liquid saturations were determined for six organic liquids; three of the liquids were mixtures (regular leaded gasoline, kerosene, and Soltrol-130), and three were single-component liquids. Of the single-component liquids, decane was chosen to represent straight-chain aliphatics, p-xylene was chosen to represent aromatics, and tetrachloroethylene (PCE) was chosen to represent halogenated hydrocarbons. Selection of a particular chemical to represent a given class of chemicals was based on the volatility and solubility of the organic liquid, and on the density difference between the organic liquid and water. Low volatility and solubility were desired to avoid competing physical processes. A large density difference between the organic liquid and water was desired because the soil columns were weighed — exploiting the density difference between the fluids — to measure the fluid saturations. Larger density differences between the fluids led to more accurate measurement of the saturations.

Gasoline leakage from thousands of storage tanks and spills, incurred during transportation and distribution of the fuel, are responsible for a large number of the groundwater contamination incidents reported today. Gasoline and its individual components (as represented by xylene for the lighter aromatic fraction and decane for the less volatile fraction) were considered for investigation because of gasoline's abundant use and its propensity to cause groundwater contamination problems.

Kerosene is very similar in composition to the aviation fuel used in all military aircraft and long-distance passenger-carrying aircraft. Groundwater contamination problems have occurred from spills of aviation fuel at airfields and military bases around the country.

PCE was one of two chemical carcinogens, TCE was the other, found most often in groundwater according to a report compiled in 1980 by the EPA Office of Drinking Water (Burmaster & Harris, 1982). PCE was also chosen because it represented the class of organic liquids that are denser than water.

Sevilleta dune sand was selected as the soil used to refine the test apparatus and procedure. Once again because of the need to hold all variables but the independent variable of interest constant, this soil was used in all experiments comparing residual saturations in the saturated zone to those in the vadose zone, and for all comparisons of residual saturations between organic liquids. The Sevilleta sand is a well sorted, medium aeolian sand, taken from a sand dune in the Sevilleta Wildlife Refuge, located 15 miles north of Socorro, New Mexico. This sand was chosen for three reasons:

1) It is a uniform, homogeneous soil with a fairly high hydraulic conductivity, a low percentage of fine particles, and a very low organic content. These properties made the Sevilleta sand easy to use during the testing of experimental technique.

2) The sand is easy to obtain. The Hydrology program maintains a field site at the location from which the soil is taken.

3) The Sevilleta sand has been used previously in several hydrologic studies here at Tech. This permitted a comparison of soil characterization results with those of previous studies.

The Traverse City soil, a sandy soil not unlike the Sevilleta sand, was used in several trials of the saturated zone experiment. This soil was supplied to us by the EPA's Kerr lab from their biodegradation field demonstration site in Traverse City, Michigan.

An attempt was made to use the Palouse loam, an agricultural soil from eastern Washington, as a third soil in the saturated zone experiments. The Palouse soil provided a good contrast to the Sevilleta and Traverse City soils because of its much finer texture (15% sand, 80% silt, 5% clay) and its higher organic carbon content of 1.5%. Unfortunately, the Palouse loam was found to be inappropriate for use in these experiments and pointed out some of the limitations of the apparatus. The fine-grained nature of the soil made it difficult to work with. The column had to be packed dry, because the Palouse loam became a gooey, unmanageable ooze when wet. Dry packing increased the length of time required to de-air the column by two to three weeks. Cracks in the soil, formed when the top endcap was tightened down, were a common problem, and, because of the small pores present in this fine-grained soil, it was difficult to supply sufficient pressure to force organic liquid into the soil. More about the problems encountered in using the Palouse loam can be found later in a discussion of the limitations of the apparatus.

EXPERIMENTAL APPARATUS

Each apparatus used in the experiments consisted of a short glass chromatographic column with Teflon endcaps (Figure 21), and associated plumbing. The glass column and Teflon endcaps were manufactured by Ace Glass, Inc. The glass column was specially fabricated to
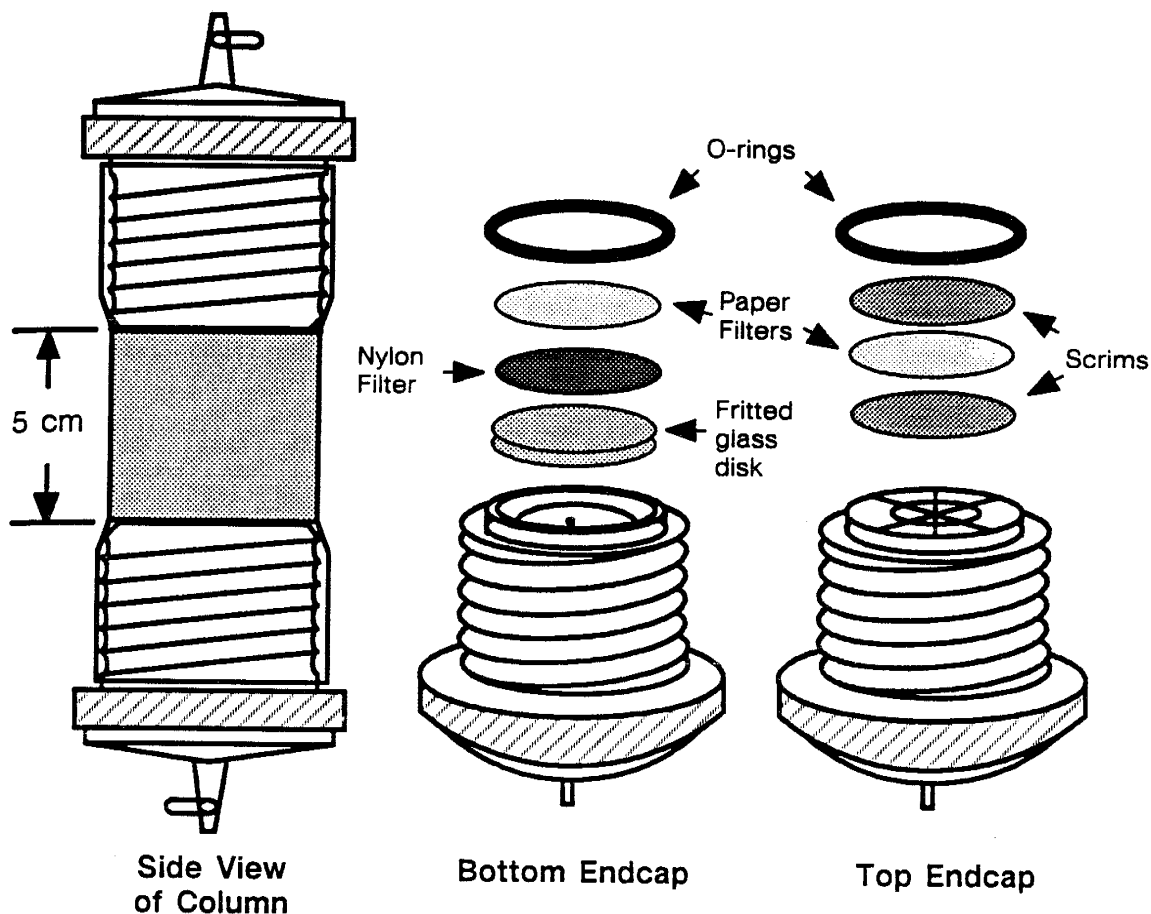
Figure 21. The short column apparatus, with blow-up views of the endcaps and filters.

specifications: 5 cm inside diameter and 5 cm effective internal length between Teflon endcaps. The effective column length was kept short in order to keep fluid saturations relatively constant along the length of the column. The endcaps were screwed into threaded ends on the glass column and sealed against the column with o-rings.

A 5 mm thick fritted-glass disk with a 20 micron average pore diameter was placed into the taper of the bottom endcap as a filter support. A water-wet nylon filter with a 0.22 micron pore diameter, designed to allow water, but prevent organic liquid from leaving the column, was glued along the edges to the fritted-glass disk. A paper filter was placed over the nylon filter to protect the nylon from abrasion by the soil.

A network of small channels, approximately 1 mm deep and 1.5 mm wide, were machined into the surface of the top endcap, in a pattern similar to that shown in Figure 21. The grooves allowed for a more uniform flow of fluids between the endcap and the soil. A paper filter was sandwiched in between two polypropylene scrims and glued to the endcap. The paper filter kept fine soil particles from leaving the column. The outer scrim kept the paper filter from tearing

against the soil when the endcap was screwed down against the soil. The inner scrim decreased clogging by preventing the paper filter from sagging back into the grooves.

In vadose zone experiments, endcaps with organic-wet filters were used as part of the experimental procedure (as described later in this chapter under 'vadose zone experiments'). Endcaps with organic-wet membranes, which allow organic liquid to pass through but not water or air, were constructed in one of two ways. By the first method, the endcaps were constructed identically to water-wet endcaps but an organic-wet, Teflon filter was glued in place instead of a water-wet nylon filter. The Teflon filters had an average pore diameter of 0.5 microns. By the second method, an organic-wet ceramic disk was simply glued into place in an endcap, in place of the fritted-glass disk, the membrane, and the paper filter. Before it was glued in place, an initially water-wet ceramic disk was treated with an organosilane compound to change its wetting to organic-wet. To change the wetting, the disks were first soaked in chlorotrimethylsilane for 2 hours, then immersed in toluene for 1/2 hour, and finally rinsed thoroughly in methanol for 1 hour. A similar procedure was used by Lenhard and Parker (1988a). The disks were one-half bar, high-flow ceramic disks. The ceramic disks were found to maintain their organic-wet properties much better if they were stored in wetting (organic) fluid when not in use. Because the experimental procedure called for these endcaps to be screwed into place against the soil, the Teflon membrane could become damaged by abrasion from the soil grains. Use of the much more rugged ceramic disks alleviated this problem, but since the disks offered a much higher resistance to flow, the experiments proceeded at a much slower pace.

Devcon 2-ton epoxy was used to glue filters and disks on all endcaps except those used in experiments employing PCE as the organic liquid. Since PCE dissolved the epoxy, silicon sealant was used to attach filters to the endcaps in any experiments involving the use of PCE.

Filter Testing

For the saturated and vadose zone experiments to run properly, it was essential that filters maintain their integrity. That is, the nylon filters must allow only water and not organic liquid or air to penetrate under experimental conditions; while the Teflon or treated ceramic filters must allow organic liquid to pass, but not water or air. Capillary forces held the wetting phase in the pores of the filter, allowing only that wetting phase to pass through. Non-wetting fluids could not pass through the filter, as long as the capillary pressures were maintained below the non-wetting phase entry pressure of the filter.

An air-entry test was used as a simple means to test the integrity of a filter and its glued seal to the endcap. The wetting fluid (water or organic liquid) was pulled through the filter and endcap under suction using a vacuum pump until the filter and any void space in the end reservoir behind the filter was completely saturated (see step 1 in Figure 22). The suction on the vacuum pump was set to a performance standard and run for a couple of minutes at that level. The endcap was removed from the wetting fluid with the vacuum suction continuing (see step 2 in Figure 22). If air breached the filter — seen as air bubbles in the tubing leading out of the endcap within 1 to 2 minutes — then the filter failed the air-entry test and was not used. Filters which allowed no air to penetrate them passed the air-entry test and were used in experiments.
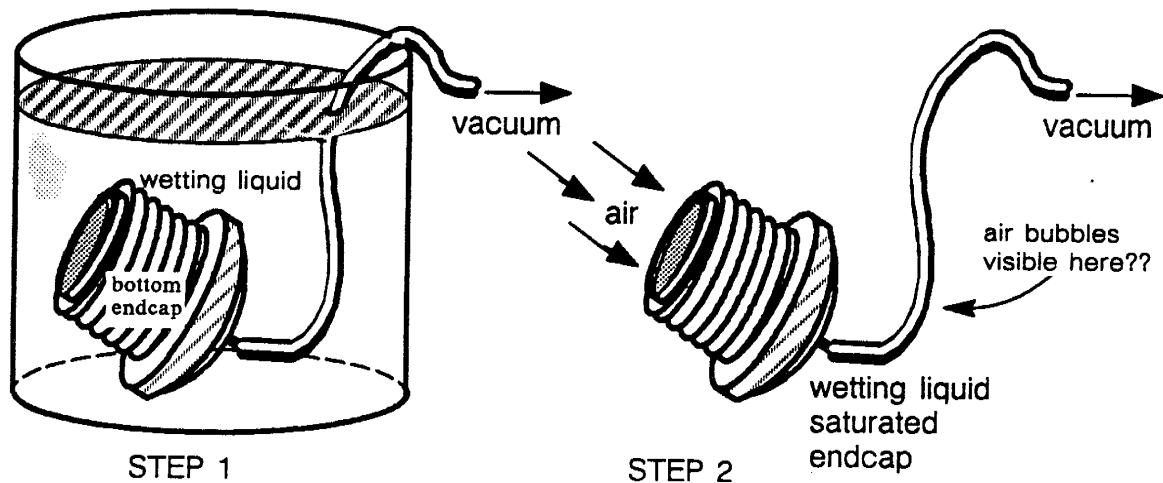
Figure 22.   Air entry test for bottom end cap filter and seal.

The performance standards were set with a margin of safety so that filters could be assured of maintaining integrity under experimental conditions for any combination of wetting and non-wetting fluids (water-air, organic liquid-air, water-organic liquid). For example, about 60 cm of water suction was needed to bring the Sevilleta sand close to residual water saturation. This suction was doubled to 120 cm (9 mm Hg) to ensure a margin of safety. To account for the fact that air was not always the non-wetting phase, the integrity test standard was corrected by the ratio of interfacial tensions. For Soltrol this correction was:

$$120 \; cm \; H_2O \; (water/soltrol) \times \frac{\sigma_{wa}}{\sigma_{wo}} \approx 185 \; cm \; H_2O \; (water/air) \approx 14 \; cm \; Hg \quad (13)$$

where: σ_{wa} = 73.6 dyne/cm = water/air interfacial tension = water surface tension
             σ_{wo} = 47.8 dyne/cm = water/Soltrol interfacial tension

The performance standard for this particular air-entry test of the water-wet membrane then, was set at 14 cm Hg.

Column Volume Measurement

Accurate measurement of the column volume was important because it was used in subsequent calculations of bulk density, porosity, pore volume, and fluid saturations. To measure the column volume, the column was weighed empty, filled with water, and weighed again. The difference between the two weights divided by the density of water yielded the column volume, V_c. Allowances were made for volume inside the column occupied by filters, the grooves in the top endcap, and how tightly the column was screwed together to give what is called the 'effective column volume' (V_{ce}), the volume occupied by soil and the fluids of

– 41 –

interest. What follows is a detailed description of the procedures used to measure the effective column volume.

The mass of the empty column (M_e) was determined by weighing the core body, endcaps with valves, and o-rings using a top-loading electronic balance with 0.01 g accuracy. The bottom endcap was weighed while still full of water from the filter test, and the top endcap was weighed before the filters were glued into place. The column was then assembled. The bottom endcap was screwed into the glass column and tightened in place using a bench vise. The top endcap was only hand tightened into the glass column. The top endcap and glass column were marked to show this reference alignment. The column was filled with water, and reweighed. The column volume was calculated as:

$$V_c = \frac{M_{w_1} - M_e}{\varrho_w}$$

(14)

where: M_{w_1} = mass of the water-filled column (g)

ϱ_w = density of water (g/cm³)

Packing a column with soil was an imprecise science. The column might have been slightly over-filled with soil one time, slightly under-filled the next. The top endcap could not be screwed down to the same degree in an over-filled column resulting in a slightly larger volume inside the column. Conversely, a slightly under-filled column might have been tightened down somewhat further than the reference, resulting in a slightly smaller column volume than the reference volume. To account for this variability in column volume from one packing to the next, a correction factor for endcap tightening was desired. To accomplish this, the valve on the top endcap was opened and the previously hand-tightened endcap was tightened in a bench vise. As the column volume was made smaller by the tightening, water squirted out through the opened valve. A new mark, aligned with the glass column mark, was made on the top endcap. The offset length between marks (l_c) was recorded, the column was reweighed, and the new mass (M_{w_2}) was recorded. The column tightening correction factor (C_t) was calculated as:

$$C_t = \frac{M_{w_1} - M_{w_2}}{l_c \ \varrho_w}$$

(15)

The volume of the top endcap (including the volume of the grooves, the connecting hole in the endcap, and the valve) was measured in a manner similar to the method used to measure the gross column volume. The endcap was weighed empty, the endcap was filled with a liquid of known density, and the column was reweighed. Similar to before, the mass of the full endcap minus the mass of the empty endcap divided by the liquid density provided a measure of volume which could be occupied by fluid in the endcap. Because the endcap was made of Teflon, an organic liquid did a much better job than water of wetting the surface and filling the grooves.

The volume of the filter, scrims, and glue on the top endcap reduced the volume of the column available to sand and fluids and also needed to be accounted for. The volume of the paper filter and the polypropylene scrims were calculated by simply multiplying the

cross-sectional area by the measured thickness. The endcap, filter, and scrims were weighed prior to gluing the filter and scrims onto the endcap. After the glue had hardened, the endcap was reweighed. The difference between the two weights was the weight of the glue, and when divided by the glue density yielded the glue volume. The density of hardened glue was determined using the ASTM D584-83.

The effective column volume was determined by accounting for the volume in the top endcap behind the filters (including grooves, connecting hole, and valve), the volume of the paper filter and scrims on the top endcap, the volume of glue on the top endcap, and the correction for how tightly the top endcap was screwed in place. The effective column volume was calculated as:

$$V_{ce} = V_c - V_{groove} - V_{filter} - V_{glue} - C_t \ l_s \tag{16}$$

where: V_{ce} = effective column volume (cm³)

V_c = original column volume (cm³)

V_{groove} = volume of the top endcap grooves (cm³)

V_{filter} = volume of the paper filter and polypropylene scrims (cm³)

V_{glue} = volume of the glue (cm³)

C_t = column tightening correction factor (cm²)

l_s = length shy of mark (cm)

Soil Packing

The glass column was packed by hand in small increments under about 1 cm of water. A previously determined mass of soil was gently poured into a vertically-oriented column. The water was controlled by a buret connected to the column through the bottom endcap. The soil was tamped into place using a modified metal spatula (bent flat and turned 90 degrees at one end). The column was packed to a depth of about 5 cm, reaching the top end, just at the base of the upper column threads. The soil was carefully leveled and the top endcap was screwed into place. If the top endcap alignment mark was offset from the mark on the glass column, the distance was measured as the length shy of mark (l_s). The effective column volume was calculated according to equation 16.

Occasionally, several attempts at sealing the top endcap needed to be made before the top endcap was successfully screwed into the column and the o-ring was seated properly. After the initial attempt, soil often had to be added or removed from the column before a tight o-ring seal was obtained and the endcap could be tightened in a vise. Any soil removed from the column was oven dried overnight and combined with the leftover soil. The mass of soil in the column, M_s, was simply the original mass of soil minus any leftover soil.

The mass of soil packed into the column was used in determining the bulk density, ϱ_b, the pore volume, V_p, and porosity, n, of the soil pack:

$$\varrho_b = \frac{M_s}{V_{ce}}$$ (17)

$$V_p = V_{ce} - \frac{M_s}{\varrho_s}$$ (18)

$$n = 1 - \frac{M_s}{\varrho_s \, V_{ce}}$$ (19)

where: M_s = mass of soil in the column (g)

ϱ_s = particle density of the soil (g/cm³)

Upon completion of packing, the column was reconnected to the buret tubing to test the top endcap's o-ring seal for water leakage. O-ring leakage was tested by closing the top endcap valve, opening the lower endcap valve and buret valve, and raising the input buret height, thus increasing the pressure on the o-ring seal. It was usually immediately apparent if the seal leaked, requiring the endcap to be refitted. A good o-ring seal was usually visually apparent, with the black o-ring appearing flat against the glass column wall. Only rarely did the seal leak when the top endcap was tightened down using a bench vise.

After the column had been tested for leakage, silicon sealant was placed on the outside of the glass column, between it and top endcap. This prevented any change in column mass due to evaporation of any water accidentally trapped in the threads between the glass column and top endcap.

In two experimental trials, the column was heterogeneously packed with coarse lenses within a finer matrix. The procedures used were identical to those used to to achieve heterogeneous packings in the pore cast experiments. A description of the procedures can be found in Chapter 5.

De-airing

. The column was flooded with 20 to 30 pore volumes of de-aired water in order to remove any gas bubbles trapped in the porous matrix or plumbing. Entrapped gas dissolved into the de-aired water and was carried out of the column. After every 100 ml of water added, the column was disassembled from its plumbing and weighed. The column gained mass as entrapped air was removed from the column and replaced by water. The column mass eventually stabilized as all entrapped air was removed. Operationally, three consecutive unchanging measurements of column mass were used to indicate the complete removal of entrapped air. The mass of the column at this point was called the initial column mass (M_1). The water-saturated column could now be used for capillary pressure-saturation tests (see Chapter 3), the saturated zone experiment, or the vadose zone experiment.

Saturated zone residual organic liquid saturation was determined by introducing organic liquid into a water saturated packed soil column (organic liquid flood), then displacing the organic liquid by water (waterflooding). These experiments simulated conditions beneath the water table.

Step 1: Organic Liquid Flooding

Once the column had been packed with soil and any entrapped air removed, organic liquid was flooded into the column simulating the movement of organic liquid into the saturated zone. To maintain a stable displacement front, the column was flooded from top to bottom for the case of an organic liquid lighter than water (Figure 23), or flooded from below when an organic heavier than water was used. The organic liquid was injected under sufficient head so that the water saturation was reduced to the residual water saturation, but the head was kept low enough to prevent organic liquid from breaking through the nylon filter on the bottom endcap.
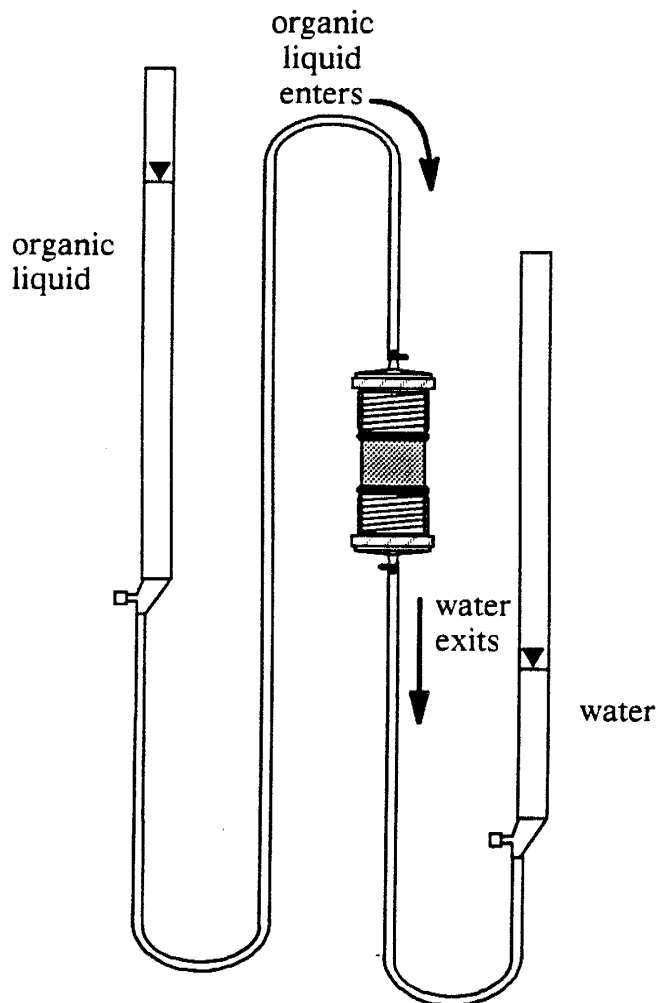
Figure 23.   Step 1: Organic liquid flood into a water saturated column.

All organic and aqueous liquids were loaded into the burets by a siphoning procedure to reduce aeration of the fluids. To avoid contact with hazardous vapors, p-xylene, tetrachloroethylene, and gasoline were siphoned into burets using a vacuum suction under a fume hood. The openings at the top of the burets were sealed to each other by a stopper and tubing arrangement (not shown in Figure 23) to close the system and limit emission of fumes.

The organic liquid flooding was continued for at least 24 hours or until the column weight stabilized, indicating that the fluid saturations had reached equilibrium. A stabilization of fluid levels in both the inflow and outflow burets also indicated that the system had reached equilibrium and fluid saturations had stabilized. Fluid production at the bottom endcap was observed to ensure that only water was produced (verifying that the nylon filter had maintained its integrity and no organic liquid had breached the filter). After stabilization, the column was detached from the burets and the column mass, M_2, was measured. The fluid saturations were determined employing the density difference between the organic liquid and water:

$$S_o = \frac{M_1 - M_2}{\Delta \varrho \; V_p} \qquad (20)$$

$$S_{wr} = 1 - S_o \qquad (21)$$

where: S_o = Organic liquid saturation (−)

$\Delta \varrho$ = Density difference between water, ϱ_w, and the organic liquid, ϱ_o, (g/cm³)

S_{wr} = Residual water saturation (−)

Modifications to the procedure were made in an attempt to introduce organic liquid (Soltrol) into the Palouse loam soil. Because the soil was fine-grained, compressed air was used to increase the pressure behind the Soltrol and force it into the water-saturated soil column. One tubing line was connected to an air compressor and split with a tee. One split line went to a mercury manometer board to record the pressure and the other line was connected to the buret containing Soltrol, through a stopper inserted on top of the buret. In this manner, a capillary pressure of about 500 cm of water was induced on the Palouse loam. Still, it was difficult pushing Soltrol into the soil.

Step 2: Waterflooding

Following the organic liquid flood, the column was slowly flooded with water at a rate of about 0.3 ml/min to displace the organic liquid. This displacement was intended to simulate the action of ambient groundwater displacing the organic liquid and leaving behind trapped organic liquid at residual saturation. As shown in Figure 24, the column was flooded from bottom to top to promote a stable displacement of the less dense organic liquid. When an organic liquid denser than water was used, the column was flooded from above, displacing the denser fluid out the bottom. A syringe pump, or a carefully controlled and monitored buret flow was used to push the water through the column at a low velocity to make sure the displacement proceeded under low Bond number and low capillary number conditions. (See Chapter 2 for definitions of Bond and
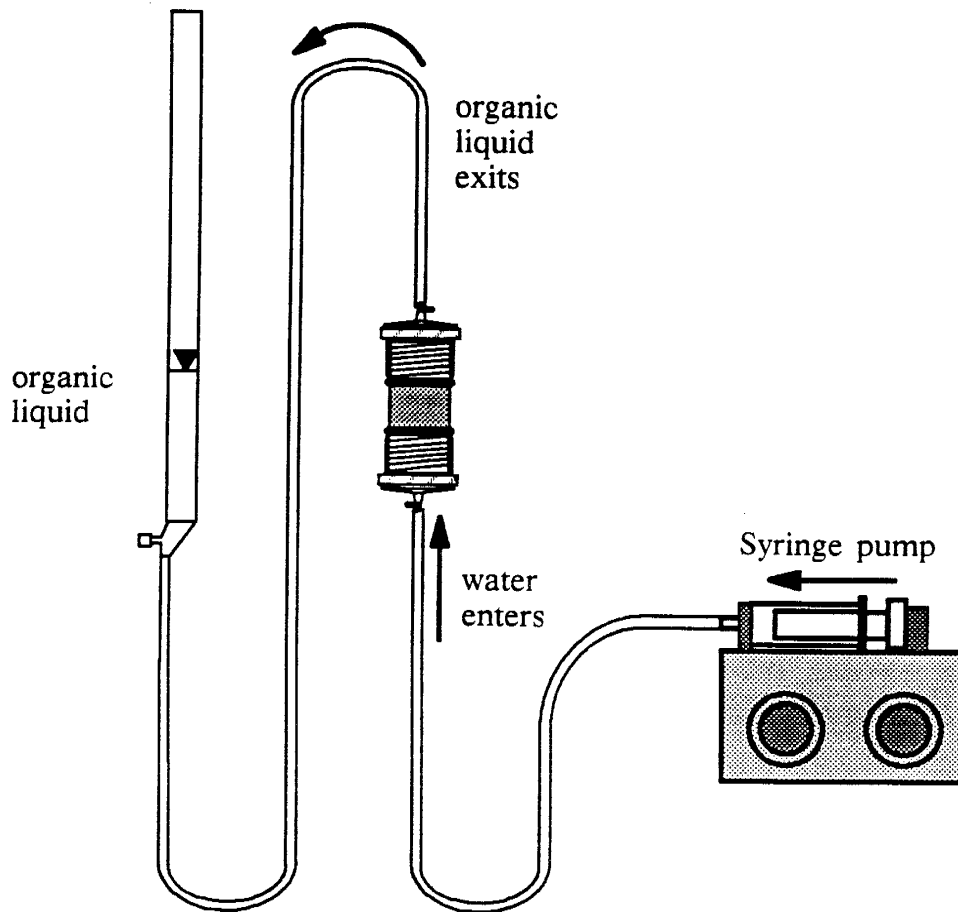
Figure 24. Step 2: Waterflooding at low velocity to reduce the organic liquid to its residual saturation.

capillary numbers.) The waterflood continued until no additional organic liquid was produced (as indicated visually through the transparent tubing and by an unchanging column mass). Introduction of about six pore volumes of water through the column was found to be sufficient to reach residual organic liquid saturation. Actually, the displacement must have proceeded as a fairly sharp front, since the organic liquid saturation was very nearly reduced to residual saturation before injection of the first pore volume had been completed. At the conclusion of the waterflood, the column was weighed, the mass (M_3) was recorded, and the residual organic liquid saturation was determined:

$$S_{or} = \frac{M_1 - M_3}{\Delta\varrho \ V_p} \tag{22}$$

$$S_w = 1 - S_{or} \tag{23}$$

where: S_{or} = Residual oil saturation (−)

S_w = Final water saturation (−)

The vadose zone experiments were designed to represent organic liquid trapping above the water table where air, water, and organic liquid are simultaneously present. The simulated residual water and organic liquid saturations were obtained under equilibrium conditions, at an equivalent height above the water table. To achieve these saturations, water was drained from an initially water saturated, de-aired soil column under an applied suction. Then organic liquid was introduced into the top of the column. Finally, the organic liquid was drained from the column under the same applied suction.

Step 1: Water Drainage

Beginning with a de-aired, entirely water-saturated column of known mass (M_1), a suction was placed on the column, draining water through the nylon filter and out the bottom endcap (see Figure 25). Air entered through the top endcap, replacing the drained water in the soil's pore space. The water-wet nylon filter allowed water, but not air to pass through the bottom of
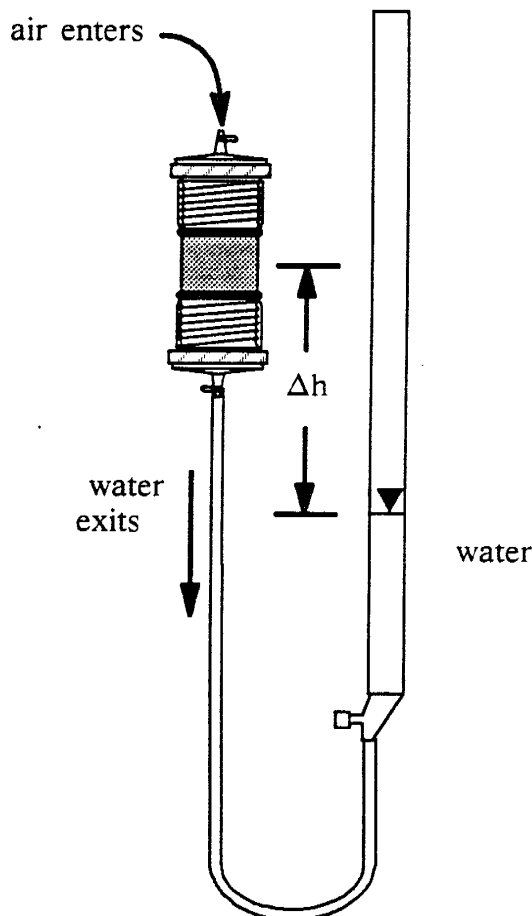
Figure 25. Step 1: Water being drained with air under an applied suction.

the column. The suction was applied by lowering the water level in the buret beneath the column in the same fashion as when determining water/air capillary pressure-saturation functions. Figure 25 shows the configuration used for applying a suction Δh to the column. The elevation difference Δh was measured from the middle of the soil column to the water level in the buret in centimeters of water. Equilibrium was reached when the water level in the buret stabilized and the column weight no longer changed.

Upon reaching equilibrium, the column was weighed and the mass (M_4) was recorded. Air saturation was a function of the suction applied and was measured at a particular equilibrium suction as :

$$S_{a,initial} = \frac{M_1 - M_4}{\varrho_w \ V_p} \tag{24}$$

$$S_{w,initial} = 1 - S_{a,initial} \tag{25}$$

where: $S_{a,initial}$ = air saturation following water drainage (-)

$S_{w,initial}$ = water saturation following water drainage (-)

The saturations found by this method were the fluid saturations for the soil under equilibrium conditions Δh centimeters above the water table.

Step 2: Organic Liquid Flooding

Once the water had been drained from the column, organic liquid was introduced to simulate the effect of organic liquid percolating through the vadose zone. Before proceeding with the organic liquid flood, the bottom endcap with the water-wet filter was removed from the column, and replaced with an identical endcap with an organic-wet Teflon filter or organic-wet ceramic disk in place of the nylon filter. The Teflon filter or ceramic disk was used as a vehicle through which to introduce the organic liquid into the column. In a later step it was used to pull organic liquid from the column under suction. To change endcaps, the column was inverted and the bottom endcap was unscrewed from the soil column. Any soil grains clinging to the paper filter on the bottom endcap were gently brushed back into the column. The replacement endcap with a Teflon or ceramic filter was screwed down tightly in place to ensure good contact with the soil. Prior to installation, the Teflon or ceramic filter was tested for integrity and the end reservoir behind the filter was saturated with organic liquid. The column was then reweighed (M_5) to account for any difference in the mass of the endcaps. Switching endcaps appeared to cause little disruption of the soil packing.

The column was once again attached to the burets (see Figure 26). Organic liquid was introduced through the organic-wet bottom endcap. Because water is more dense and air is less dense than the organic liquid used in the experiments, the column was turned horizontally to inhibit density instabilities that might occur in a vertical displacement. Organic liquid was pushed through the column under low capillary number conditions until no more water or air was

produced (verified by a stable column mass, M_6). This step usually required about 300 ml of organic liquid to be pushed through the soil column before the mass stabilized.

Once the fluid saturations had equilibrated, the volume of water produced from the soil pack was measured. The volume of water produced was measured by collecting the outflow (water and organic liquid) in a flask and withdrawing the water from the bottom of the flask with a syringe. A Teflon flask worked best because water would not adhere to the walls of a Teflon flask. The water was then injected into a graduated cylinder to determine the volume of the water produced (V_{wp}). The new water saturation was then calculated as:

$$S_w = S_{w,initial} - \frac{V_{wp}}{V_p} \tag{26}$$
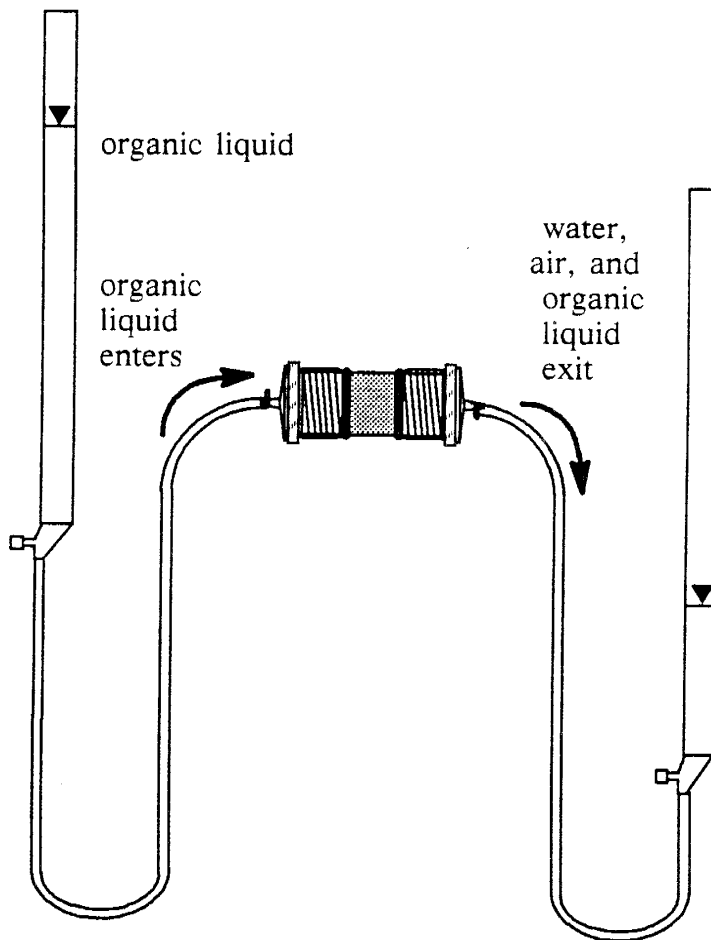
Figure 26. Step 2: Organic liquid flood in a column already drained by air.

With the water saturation known, the organic liquid saturation (S_o) and the air saturation (S_a) could be found using mass measurements of the column before (M_5) and after (M_6) the organic liquid flood:

$$S_o = \frac{M_6 - M_5 - \varrho_w \; V_{wp}}{\varrho_o \; V_p} \tag{27}$$

$$S_a = 1 - S_w - S_o \tag{28}$$

Step 3: Organic Liquid Drainage

In the final step of this process, organic liquid was drained from the column under an applied suction. The organic liquid saturation was reduced to an equilibrium saturation for a given height above the water table. For sufficiently large suctions, this represents the residual organic liquid saturation in the vadose zone. Figure 27 shows the set-up for organic liquid drainage. It was very
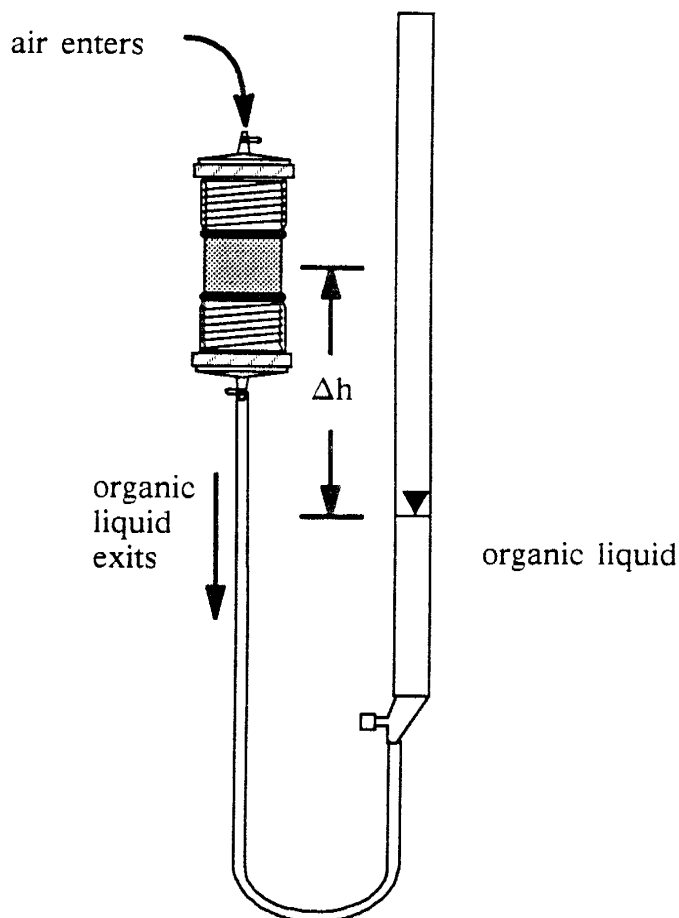
Figure 27.   Step 3: Organic liquid drained by air.

similar to the set-up used earlier in step 1, for draining water from the soil column (Figure 25). The drainage was a stable displacement, in which air entered from the top displacing organic liquid downward through the lower organic-wet filter. The elevation difference, Δh, for this step was equal to the Δh used in the previous water drainage step. For instance, if the suction used in the water drainage step was 70 cm of water, in the organic liquid drainage step the applied suction was 70 cm of organic liquid. Although in each case the fluid column in the buret was dropped the same distance beneath the soil column to induce suction, the capillary pressures induced in each of these steps was not the same. The difference in capillary pressures was scaled by the relative densities of the water and organic liquid phases.

The displacement proceeded until the organic liquid and air saturations equilibrated. (The water saturation remained unchanged during this step.) The equilibrated column was weighed (M_7) and the final organic liquid, water and air saturations were determined:

$$S_{or} = \frac{M_7 - M_5 - \varrho_w \ V_{wp}}{\varrho_o \ V_p}$$

(29)

$$S_a = 1 - S_w - S_{or}$$

(30)

POSSIBLE SOURCES OF ERROR

Several sources of experimental error were associated with performing multi-phase flow experiments to determine residual organic liquid saturations. Possible sources of error included:

- incomplete removal of entrapped gas,

- changes in fluid densities due to changes in laboratory temperature,

- lack or loss of filter integrity,

- faulty seals in the system leading to leakage or evaporative losses,

- trapping of fluids in the outflow end reservoir,

- packing variability (from one soil packing to the next), and

- error associated with the precision limits of the measuring devices.

What follows is a brief discussion of each of these sources of error.

Entrapped Gas

As soil was packed into a soil column, some gas was trapped in the pore space. For a water-wet system, trapped gas tends to reside in pores which would probably otherwise trap organic liquid (see for instance, Kyte et al., 1956). Residual saturations measured in the

presence of trapped gas would be expected to be lower than residuals measured under strictly two-phase conditions.

Entrapped gas presents other problems because its saturation may not remain constant over the duration of the experiment; some of it may dissolve into the liquid phases. When gravimetric measurements are used to determine fluid saturations, the loss of entrapped gas over the course of the experiment would indicate a lower residual saturation than is actually present (for an organic liquid less dense than water).

Entrapped gas was eliminated by flushing the column with several pore volumes of degassed water. As degassed water moved through the column, trapped gas dissolved into the water phase and was carried from the column prior to beginning the experiment. The column gained weight as the pore space previously occupied by gas was then occupied by water. All entrapped gas was assumed to be removed once the column weight stabilized.

Variable Laboratory Temperature

The worst and most persistent problem encountered during this project was the inability to control temperature variations in the laboratory. As the temperature in the laboratory fluctuated, so too did the densities of the fluids used in experiments, introducing error into gravimetric determinations of fluid saturations. In addition, fluctuations in column weight had been observed that were larger than could be accounted for by density effects alone. It is believed that as the temperature rose, dissolved gasses came out of solution and were trapped in the soil — this gas may have subsequently re-dissolved as the temperature fell. The appearance (and re-dissolution of) trapped gas introduced additional temperature-induced error to that caused by changes in density alone. This problem was especially acute when liquids containing volatile components, such as gasoline, were used.

Large temperature fluctuations in the laboratory over the course of an experiment led to poor reliability of the results. Residual saturations of Soltrol plotted against temperature variation (Figure 28) illustrate the large range in residual saturations that were measured when temperatures were not held constant over the course of an experiment. Results of experiments conducted with small temperature variations ($< 2\,^{\circ}C$) show much less scatter than experiments conducted under less controlled temperature conditions.

To remedy the problem of fluctuating temperatures during the experiments, a constant temperature cabinet was constructed. Experiments performed within the constant temperature cabinet displayed a noticeably smaller variation of residual saturations than experiments performed prior to completion of the cabinet.

Filter Integrity

Filters that allowed only the wetting phase to pass through were often used to reduce capillary end effects. If filter integrity was not maintained, end effects were not eliminated and the non-wetting fluid could have become trapped in the reservoir behind the filter. In the

column-flooding experiments, each filter was tested for integrity prior to use, and paper filters were glued above them to reduce abrasions from the soil which could have caused leakage. For experiments run at low flow rates, ceramic disks were sometimes used instead of filters because of their greater durability.

Leaking Seals

The endcaps were sealed to the column using o-rings. Each apparatus was pressure tested for leakage prior to use.

Outlet End Reservoir

In these experiments it was assumed that no organic liquid was trapped in the outlet end reservoir (top endcap), although this assumption was probably not entirely true. By keeping the outlet end reservoir small — less than 1% of the column pore volume — the effects of trapping within the reservoir were considered negligible.

Packing Variability

Variable soil packing from one experimental trial to the next could have lead to some variability in measured residual saturations. Determination of soil bulk density provided a good measure of the 'tightness' of each packing, but says little about the uniformity of a hand tamped column. Packing the columns in water undoubtedly produced some small-scale layering in the columns, but greatly reduced the amount of time needed to for de-airing.
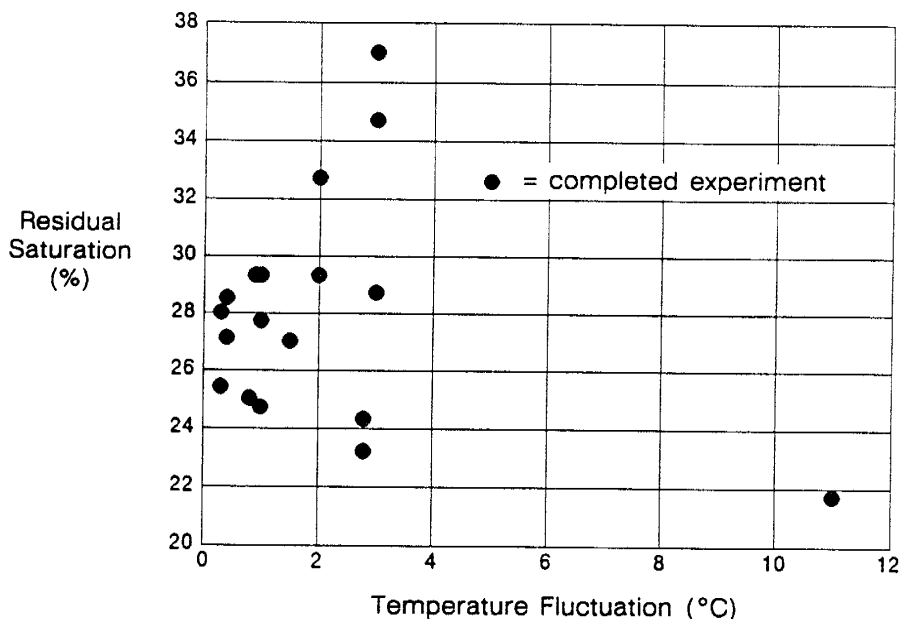
Figure 28.   Temperature range and its effect on the accuracy of results.

<u>Measurement Error</u>

Measurement error, due to the precision limits of measuring devices such as balances, were estimated and propagated through the sequence of calculations. For example, calculations of fluid saturations were dependent upon measures of fluid densities, soil particle density, total soil weight, total column volume, and measures of the column mass at several points in the progress of an experiment. All these measures have some error (or precision limit) associated with them and these errors were routinely propagated through the calculations used to determine fluid saturations. A worst case error approach (in which it was assumed all errors were additive) was used. Since some measurement errors would be expected to cancel each other out, this worst case approach was a conservative estimate of the total measurement error.

ADVANTAGES AND LIMITATIONS OF THE TECHNIQUE

The experimental apparatus and procedures used to measure residual saturations offered several advantages. First, gravimetric measurements (which exploit the density difference between the fluids to measure saturations) gave fairly precise measurements of residual organic liquid saturations. In the saturated zone, residual saturation measurements for most of the fluids were precise to within $\pm$ 2%. Measurements of residual saturation for Soltrol in the vadose zone were also precise to about $\pm$ 2%. Second, a short column with a semi-permeable membrane yields relatively constant saturations over the length of the column with no capillary end effect. These features are especially important for the vadose zone measurements, because measurements of organic liquid saturation in the vadose zone can be strongly biased by failure to account for capillary end effects. All in all, the short column method used relatively simple experimental procedures to provide fairly precise measurements of two- and three-phase fluid saturations in soils.

One limitation of the experimental technique was the inability to apply it to fine-grained soils, such as the Palouse loam. In the Palouse loam, the organic phase could not be injected with enough pressure — a pressure equivalent to more than seven meters of Soltrol was used — to overcome the entry pressure for a non-wetting phase. Even if it had been possible to inject the organic liquid with sufficient pressure, the entry pressure of the nylon filter on the bottom endcap might well have also been exceeded, resulting in failure of the filter. In order to accommodate fine-grained soils, the apparatus would have to be re-designed as a high-pressure system, including a high-pressure fluid delivery pump, a column built to withstand high pressures, and a bottom membrane with a very high non-wetting phase entry pressure.

The inability to inject an organic phase into the Palouse loam did however demonstrated that fine-grained, water-wet soils (which do not shrink in the presence of organics) can serve as an effective barrier to organic liquid movement in the subsurface.

Another limitation of the experimental technique occurred in the vadose zone experiments. Several trials of the vadose zone experiment were run using high applied suctions to measure the saturation of organics left behind a front of organics percolating through the vadose zone high above the water table. Additional vadose zone experiments were performed over a range of

applied suctions. These experiments were run to give an idea of the saturation distributions that can be expected in the transition zone between the saturated zone and the vadose zone.

Results from these transition zone experiments gave what is believed to be unreasonably high equilibrium organic liquid saturations. The limitation of the experimental procedure was that, during the organic liquid drainage step, water was unable to re-imbibe into the soil. Under low applied suctions representing the capillary fringe and just above, re-imbibing water would have displaced organic liquid resulting in lower organic saturations and higher water saturations than the values that were actually measured.

The largest change in forces acting on the organic liquid occurs in the capillary fringe and just above where the transition from the vadose zone to saturated zone conditions is most pronounced. Unfortunately, the experimental procedure used to measure three-phase saturations over this range was found to be inappropriate. This low suction range is important particularly for organic liquids lighter than water because it is the zone in which organic liquids spread, forming a lens on the water table.

CHAPTER 5

PORE AND BLOB CAST EXPERIMENTAL METHODS

Bench-top short column experiments were performed with polymers and epoxy resins to visualize non-aqueous phase organic liquid movement and capillary trapping in conditions simulating the saturated and vadose zones. Results obtained featuring this method were presented in Peplinski et al. (1989). A 3000 ppm $CaCl_2$ solution and styrene monomer modeled the water and organic fluid phases, respectively, in the saturated zone experiments. The styrene was then polymerized and, in some cases, the column was dissected for visual inspection of the organic liquid phase distribution with a scanning electron microscope. The polymerized organic phase was rigid and chemically resistant. At residual saturation the polymerized styrene was disconnected into individual ganglia or blobs. These hardened styrene objects were referred to as 'blob casts'. In other experiments, the water was replaced with dyed epoxy resin after the styrene had been polymerized. The column was cut then into sections and examined under an epifluorescent optical microscope. These sections were referred to as 'pore casts'. For vadose zone conditions, dyed styrene and two epoxy liquids were sequentially applied, drained, and hardened in an attempt to simulate fluid distributions of water, organic liquid, and air. The resulting pore casts were photographed under an epifluorescent optical microscope.

This chapter begins by describing the columns used in these experiments followed by some discussion about the fluids used. The experimental procedures for saturated zone conditions are then explained, including comments on pre-processing the styrene, packing the column, and dying and hardening the styrene and epoxy. A description of the experimental procedures used in the vadose zone experiments concludes the chapter.

COLUMN DESIGN

The columns used to hold the soil sample in the styrene/epoxy resin impregnation experiments were constructed from a 5 cm long Teflon cylinder (5 cm I.D., 6.5 cm O.D.), and two aluminum-Teflon endcaps with plug valves. A schematic of a column is shown in Figure 29. Teflon was chosen for the columns because of its non-reactivity and ease of machining. The endcaps were made of Teflon rod (7.6 cm in diameter, 3.8 cm long) with 0.6 cm thick aluminum plate screwed to the backs. An external groove was cut around the cylinder into which fit a 10 cm diameter aluminum split ring. Four threaded rods passed through the aluminum plates and split ring and provided a means of attaching the endcaps by bolting them on. Four o-rings, one on each end of the cylinder and one on each of the endcaps, securely sealed the column and created a purely mechanical method of holding filters in place.

The inner face of the endcaps had radial and concentric grooves machined into them to allow better fluid flow between the soil sample and the 1/16 inch endcap center hole. A fritted glass disc (50 mm diameter, 5 mm thick) was fitted on top of the groove pattern of the lower endcap as a support for filters. Plug valves were threaded through the aluminum plates and sealed against the Teflon rod with o-rings.
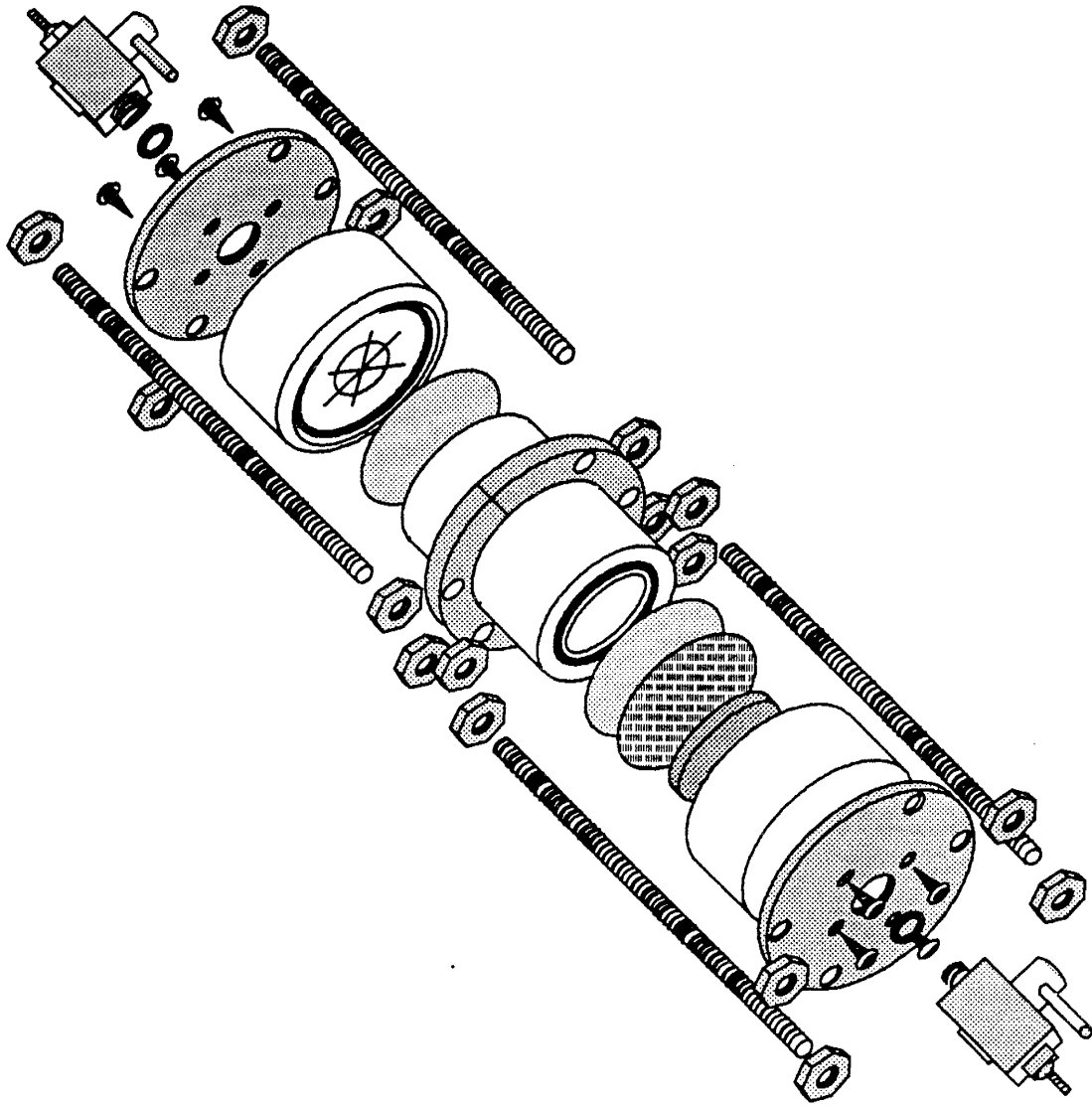
Figure 29.   Exploded view of the Teflon Short Column.

A nylon filter with pore diameters of .22 μm, held in place by an o-ring, was used on the bottom endcap. It acted as a semi-permeable membrane; the filter would allow water to pass but not a non-wetting phase, such as styrene. The nylon filter was covered with a paper filter to prevent abrasion against the sand. A paper filter alone was used on the upper endcap to prevent fine soil particles from leaving the column. In experiments which required epoxy drainage, polyvinylidene difluoride filters (0.2 μm pore size) were used in place of the water-wet nylon filters.

ABOUT THE FLUIDS USED

The technique of using styrene or epoxy to represent wetting or non-wetting fluids in indurated rock and bead packs has been used previously by petroleum engineers (Chatzis et al.,1983, 1984, 1988; Yadav et al, 1987; McKeller and Wardlaw, 1988), but so far little work has been done using this technique in unconsolidated soils. Styrene's immiscible behavior with water, its low viscosity, and its ability to harden while in contact with water make it ideal for simulating non-aqueous phase liquid movement through soils. Styrene however, does have several drawbacks; one of which was that although it initially has a low viscosity, once initiated, the viscosity increases over time. This viscosity increase indicates that polymerization begins as soon as initiator is added, albeit slowly(see Figure 30). Styrene also shrinks in volume by about 17% as it hardens (Boyer, 1970). The interfacial tension of the styrene with $CaCl_2$ solution was found to remain constant over time (35.3 dynes/cm) even when initiator was added.

Dyes were added to the styrene in order to improve its visibility, but they changed fluid properties. For example, 9,10-diphenylanthracene was added to styrene (0.6% by weight as recommended by McKeller and Wardlaw, 1988) causing the styrene to fluoresce blue under ultraviolet light. Addition of the dye caused the interfacial tension (IFT) with $CaCl_2$ solution to decrease from 35.3 ± 0.3 to 30.9 ± 3.0 dynes/cm, and also affected the change in viscosity over time, as shown in Figure 30.

Tracon's Tra-Bond® 2114 epoxy was also used in several experiments to represent a fluid phase. Rhodamine B, a red-orange fluorescent dye, was dissolved in benzyl alcohol and added to the Tra-Bond® 2114 epoxy. The addition of benzyl alcohol to this resin (40% by weight) caused
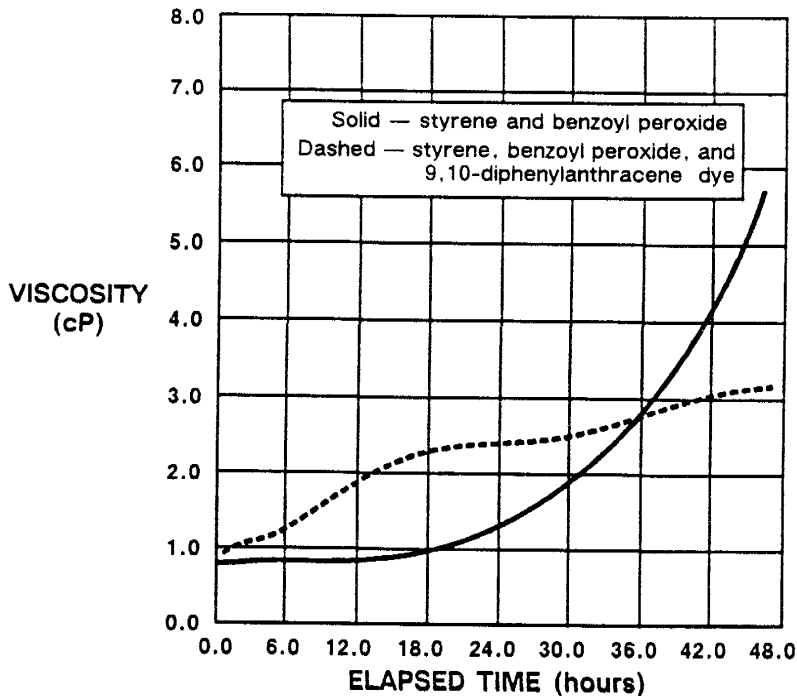
Figure 30.   Viscosity of initiated styrene versus time.

liquid	density (g/cm³)	viscosity (cP)	interfacial tension with 0.3% $CaCl_2$ solution (dynes/cm)	surface tension (dynes/cm)
aqueous phase	1.000 ± 0.002	0.98 ± 0.01	not applicable	72.0 ± 0.4
styrene	0.903 ± 0.002	0.81 ± 0.01	35.3 ± 0.3	31.9 ± 0.3
Tra-Bond® 2114	1.2 (factory)	597 (factory)	< 2	40.9 ± 0.5

Table 3.   Properties of fluids used in pore and blob cast visualization experiments. All measurements were taken at 23°C.

a dramatic decrease in the resin's viscosity but only a slight decrease in its surface tension. The addition of benzyl alcohol reduced the viscosity to about 50 cP and decreased the surface tension to 38 ± 1 dyne/cm.

A 3000 ppm $CaCl_2$ solution was used as the aqueous phase in all the saturated zone experiments. Properties of the fluids used are given in Table 3. Measurements of the fluid properties were performed following procedures outlined in Chapter 3. The Sevilleta sand was used in all the experiments. Its properties are also reported in Chapter 3.

SATURATED ZONE EXPERIMENTAL PROCEDURES

Packing and De-airing

Both homogeneous and heterogeneous sand-pack experiments were performed in the Teflon columns. The packing and de-airing procedures for the homogeneous case are reviewed first, followed by the heterogeneous case. Equations are then presented for calculating pore volume, bulk density, and bulk porosity of the packed sand.

Homogeneous packing

Before packing a column with soil to be used in a homogeneous saturated zone experiment, the lower endcap with filters was tightly bolted to the Teflon cylinder, and the cylinder and endcap were attached to an 18 cm Hg vacuum. Then the column was inverted and placed in a large beaker of $CaCl_2$ solution. Liquid was drawn through the filters, fritted glass disc, and associated plumbing to saturate them with water (see, e.g., Figure 22). When air bubbles were no longer observed, the column was removed from the vacuum and the filters checked visually for integrity. The water-wet filters should have prevented the flow of the non-wetting air phase. If the filters did not allow air to penetrate, the whole column was dried and weighed.

Next, the column was packed with soil using procedures similar to those presented in Chapter 4. Once the soil was packed to within about 2 cm from the top of the cylinder, capillary rise was used to saturate the soil to prevent the overflow of water and soil from the column (because the soil was packed flush with the top of the cylinder). The mass of soil in the column, M_s, was recorded. O-rings and a paper filter were placed on the cylinder and the upper endcap was lowered onto the column and bolted on. Entrapped air was removed from the column by flushing with de-aired $CaCl_2$ solution.

Heterogeneous packing

The heterogeneous sand pack column experiments were performed using the Sevilleta sand, split with a size 50 sieve into coarse and fine portions. The finer fraction was used as a matrix to surround 3 stringers or lenses, composed of the coarser fraction. The stringers were roughly circular in cross-section. The major difference in packing technique between the homogeneous and the heterogeneous cases was that the heterogeneous columns were packed dry. The Teflon cylinder and water saturated bottom endcap were assembled as described earlier, in the homogeneous packing procedures, but no $CaCl_2$ solution was allowed to flow into the column while it was being packed.

A 6 to 7 mm thick layer of the fine sand was placed on the bottom of the column assembly and three paper cylinders were pushed down into it. Then the fine sand fraction was carefully poured and packed around the paper forms, so as not to collapse them, until the level of the sand was 3/4's of the way to the top of the column. At that point the coarse sand was packed into the paper cylinders. They were filled to approximately 6 to 7mm from the top of the column. The rest of the matrix was then filled with the fine sand. The three paper forms were slowly pulled out of the column and any remaining volume was filled with the fine sand.

$CaCl_2$ solution was then pushed upwards, through the bottom endcap, wetting the sand. Settling of the sand was observed, and more fine sand as added to the top of the column. When the sand-pack was totally wetted, the upper endcap was attached and de-aired $CaCl_2$ solution was flooded through the column to remove entrapped air. These same methods were used for heterogeneous packings in the short column experiments described in Chapter 4.

Calculated quantities

At the conclusion of the de-airing procedure several useful quantities could be calculated. The pore volume of the column, V_p, the volume occupied by soil in the column, V_s, and the total column volume, V_t, were determined by:

$$V_p = \frac{M_1 - M_s - M_c}{\varrho_w} \tag{31}$$

$$V_s = \frac{M_s}{\varrho_s} \tag{32}$$

$$V_t = V_p + V_s \tag{33}$$

where: M_1 = total column mass at the conclusion of de-airing (g)

M_s = mass of soil (g)

M_c = apparent weight[2] of the empty column (g)

ϱ_w = density of the water phase (g/cm³)

ϱ_s = particle density of the soil (g/cm³)

The bulk density of the soil, ϱ_b, and the porosity, n, were determined from:

$$\varrho_b = \frac{M_s}{V_t}$$ (34)

$$n = \frac{V_p}{V_t}$$ (35)

Styrene Preprocessing

Styrene monomer is commonly sold containing an inhibitor to prevent polymerization during transport and storage. Inhibitor removal columns developed by Aldrich Chemical Company were used to remove 4-tert-butylcatechol inhibitor from the styrene.

Inhibited styrene, held in a separatory funnel, was slowly dripped into the column and then collected in a beaker or flask at the bottom of the column. Each inhibitor removal column has the capacity to remove inhibitor, at 15 ppm, from up to 4 liters of styrene. The uninhibited styrene was weighed and benzoyl peroxide, 1% by weight, was added as an initiator. Benzoyl peroxide was chosen as an initiator because it was found to preserve the water wetness of the soil sample (Chatzis and Morrow, 1984). Dyes were then added to the styrene.

Styrene Flooding

The initiated, dyed styrene was transferred from the flask to a 100 ml buret which was attached to the upper endcap of the de-aired column. To eliminate the possibility of air entering the column, the column was first inverted and the tubing attached while a slow stream of styrene flowed from the buret. The column was righted and the styrene elevated to a head of approximately 1 meter above the column. Valves on the water and styrene burets, and those on the column, were opened and styrene flowed into the column, as illustrated in Figure 31. During the flooding, the head on the column decreased as styrene left the buret. Water, displaced by the styrene, passed through the nylon filter and left the column via the lower endcap.

Experiments with Soltrol-130 have shown that the column-buret system actually required close to 48 hours before residual water saturation was reached. However because initiated

---

2. Apparent column weight is the weight of the column with only the main cavity of the column empty. To measure this weight, all component pieces of the column were weighed separately and summed to obtain a total weight. The endcaps were weighed when water filled.
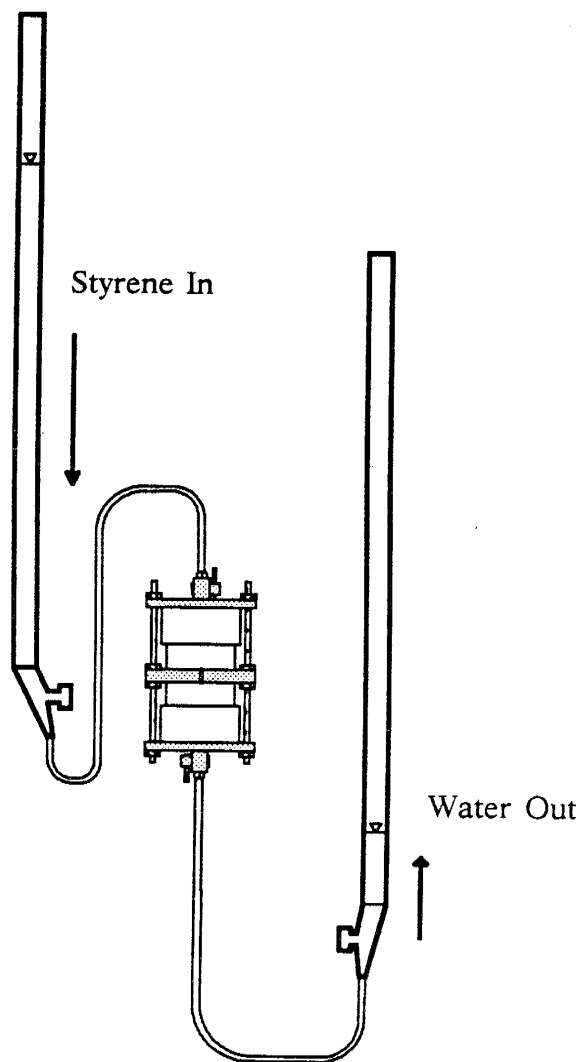
Figure 31. Experimental setup of a styrene flood.

styrene's viscosity increased with time, it seemed prudent to complete the entire experiment within 24 hours of initiation to avoid the possibility of inducing viscous fingering during the waterflooding step. Besides, many organic liquids of interest generally have viscosities close to that of water.

The styrene flood was continued for 18 hours. At the conclusion of this step, the outflow tubing and buret were checked to see that no styrene was produced. Styrene in the outflow line indicated a leak in the filter, invalidating the experiment. The Teflon column was weighed and the mass recorded as M_2. The fluid saturations were calculated from equations (20) and (21). It should be noted that these saturation measurements were not nearly as precise as those made in the short glass chromatographic columns (Chapter 4). Less precision was achieved because the density difference between styrene and water was not as large, and because the Teflon

column was heavier than the glass column and had to be weighed on a larger capacity (less precise) balance.

Organic saturations using styrene commonly reached values of 70 ± 6%. In experiments with Soltrol-130, S_o values were commonly around 85%. Clearly, the water had not yet been completely reduced to its residual saturation.

Water Flooding

Following the organic liquid flood, the column was flooded with water to displace the organic liquid. The water buret was raised to a head of approximately 1 meter and all the valves in the system were opened. The column was flooded from bottom to top to promote a stable displacement of the less dense organic liquid. A total of 6 to 7 pore volumes of $CaCl_2$ solution were flushed through the column in order to ensure that the styrene had been reduced to its residual saturation. At the conclusion of the waterflood, the column was weighed, the mass (M_3) was recorded, and the residual organic liquid saturation was determined from equation (22).

Observed residual styrene saturations for the Sevilleta sand, following this procedure, were generally 15 ± 7%. These values were significantly lower than those observed with Soltrol-130 (about 27%; see Chapter 7) and reflect, in part, procedural differences between the two sets of experiments. For a more complete discussion of the styrene two-phase residual saturation measurements see Appendix B.

Styrene Polymerization

The styrene residuals were hardened by placing the column in a pressure vessel, pressurizing it to 80 psig and then heating the vessel at 85 degrees centigrade for 40 hours.

About eight liters of de-aired $CaCl_2$ solution were poured into the pressure vessel. The column was placed into the pressure vessel with the valves on both ends open. Enough $CaCl_2$ solution was added to cover the column with liquid. The liquid acted to prevent air (especially oxygen) from entering the sand pack and interfering with the polymerization reaction.

After the lid of the pressure vessel was sealed, a 60 cm Hg vacuum was applied to the head space to evacuate as much atmosphere as possible. The vessel was then connected to a dry nitrogen source and pressurized to 80 psig. Following pressurization, the vessel was submerged under water to check for leaks in the seal. If no leaks were detected, the vessel was placed in a laboratory oven and heated to polymerize the styrene.

Observation of Styrene Residuals

To complete the saturated zone simulation, either the styrene blobs were removed from the sand matrix or the water phase was replaced by an epoxy. The first method produced individual styrene residual 'blob casts', whose shapes and sizes were viewed optically or with a scanning

electron microscope. The second method yielded polished epoxy slabs, the 'pore casts', in which the relationships between soil grains, the wetting phase, and the non-wetting phase were studied.

Blob casts

The styrene blob casts were removed from the matrix by dissolving the sand grains with acids. A small portion of the styrene-sand pack was carefully removed from the column with a spatula, placed in a Teflon beaker, and dried. The dry sample was covered with one of several concentrated acids and allowed to dissolve for several days after which the sample was filtered through a Teflon filter, washed with water, and covered with another acid. This process was repeated with concentrated hydrofluoric acid, sulfuric acid, nitric acid, hydrochloric acid, phosphoric acid, and chromic acid until essentially all of the matrix had been dissolved, leaving only the hardened styrene blobs along with some insoluble inorganic residue. Several styrene blob casts, as photographed with a scanning electron microscope, are shown in Chapter 7 (Figures 63 and 64).

Initially, it was hoped that a large number of the blob casts could be statistically analyzed to determine the size and shape distribution of the residual organic saturation. Although the styrene blob casts were chemically resistant, they were quite brittle. The transfer of a blob from filter paper to a microscope slide for observation often resulted in the breakage of the blob. It was not clear that the blob casts recovered from the acid bath were wholly unbroken. For this reason, it was decided not to conduct the statistical study.

Pore casts

To construct the pore casts, the column was taken out of the pressure vessel and the top endcap was removed. The column and endcap were placed back in the oven at 75-80 degrees centigrade and allowed to dry for 48 hours. The dried column was reassembled and attached to a pressure vessel filled with rhodamine B dyed Tra-Bond® 2114 epoxy resin. Resin was forced through the soil sample from the bottom of the column with air pressure. Four or five pore volumes of resin were forced through the column in order to remove as much air as possible. Time was of the essence, since the epoxy would generally harden within 1 hour. Twenty-four hours were allowed for the epoxy to properly set. The consolidated core was then removed from the column by cutting longitudinally through the teflon sleeve in two spots, and peeling the teflon away.

Rock saws were used to section the core. The face of a section to be analyzed was covered with a thin layer of undyed epoxy to fill in holes left by plucked grains, and to create a solid surface for polishing. To remove air bubbles from the still-wet epoxy, the section of core was placed in a vacuum dessicator for 5 minutes under a 60 cm Hg vacuum. Once the epoxy layer dried, lap wheels were used to grind the epoxy layer down to a flat surface. Smaller sections of the core were easier to polish and hence provided better optical surfaces. 220 and 400 grit powders were used to remove the majority of the epoxy coating, and 10 minutes of polishing with 14.5 μm and 9.5 μm grit provided the final surface.

Photomicrography was performed using either a Zeiss SR stereoscope or a Nikon Opti-Phot epifluorescent microscope system. Examples of these photomicrographs are shown in Chapter 7 (see for instance Figures 61 and 62).

VADOSE ZONE EXPERIMENTAL PROCEDURES

Attempting to simulate organic liquid transport in the vadose zone using styrene and epoxies presented several difficulties. In the vadose zone, there are three fluid phases: water, air, and the organic liquid. In these visualization experiments, all three phases obviously could not be fluid simultaneously since most epoxies and styrene monomer are miscible. It was decided to simulate the three fluid phases by a sequence of two phase experiments in which the wetting phase of each experiment would be hardened. Styrene was used as the wetting phase (representing water), and nitrogen was used to drain the styrene to a residual saturation. The styrene was then hardened. An epoxy was then flooded into the column and drained with gas to simulate the advance and subsequent drainage an organic contaminant moving through the vadose zone. And finally, the remaining gas-filled void space was filled with a second epoxy so that it too would show up in the photographs.

This approach raised a question about surface energies. In this experiment, styrene (acting as a wetting phase) was drained to some residual saturation and hardened. As the epoxy (representing the organic phase) moved through the column, it interacted with this (extremely) immobile 'wetting phase'. So the question is this: How much difference is there between the real system (a liquid-liquid interaction between an intermediate-wetting phase and a liquid but stationary wetting phase) and an approximation to that system (a liquid-solid interaction between an intermediate-wetting phase and a now solid styrene)? In each case the intermediate-wetting phase would be more wetting than the air phase and tend to spread on the surface in order to decrease the surface energy of the system. This second phase would tend to spread over the surface of the 'wetting phase' whether the surface is a solid or a liquid. A wetting phase at residual saturation may not be as immobile as a solid, yet simple wetting experiments have shown that a less-wetting liquid will not completely displace a wetting liquid from a surface; rather, a film of the wetting phase will continue to exist between the solid surface and the less-wetting phase. So in this sense, a solidified wetting phase may be a reasonable approximation of a fluid wetting phase, as long as flow in the wetting phase is not significant (Amaufule and Handy, 1982). Granted, there are differences between a liquid propagating over a solid surface versus a liquid surface, but it is believed that there is a similarity between the final distribution of the fluids in the real system and the approximation to that system.

Wetting Phase

Styrene was used to represent the wetting (aqueous) phase in these three-phase polymerization experiments. But because oxygen interferes with styrene polymerization, the column was packed under styrene inside a glove bag containing a nitrogen atmosphere. The glove bag was connected to a tank of dry nitrogen, inflated, and purged to remove any air. The

dyed and initiated styrene, the sand, the pressure vessel, and the column were put into the bag and the bag was purged twice more. A vacuum line and a line of tubing attached to a buret were punched through the side of the bag. With these lines, styrene could be removed from, or introduced into, the bag.

Using the vacuum line, styrene was pulled through the bottom endcap of the column to purge gas from behind the nylon filter. Styrene, which had passed from the column, through the vacuum line to a reservoir outside the glove bag, was transferred to the buret, which in turn was attached to the lower endcap of the column. The styrene in the buret was used to pack the column in a method similar to that described earlier, for the saturated zone column.

After column packing was completed, a paper filter was placed over the sand and the upper endcap was bolted on. Approximately five pore volumes of styrene were pushed from the buret upward through the column and out to the reservoir on the vacuum line. Nitrogen trapped in the sand pack was removed in this manner. After the styrene flooding, the column was considered saturated.

Draining styrene from the column to a residual wetting phase saturation was achieved by simply lowering the styrene buret beneath the column to apply a suction. Styrene drained through the nylon filter to the buret while nitrogen entered the column through the upper endcap. Initially, the styrene level in the buret was lowered to 50 cm below the column. After 1 hour, the buret was lowered another 25 cm and the column was allowed to drain for for 2 more hours.

The residual styrene was polymerized by heating as in the saturated zone experiment. The column was placed into the pressure vessel while still within the glovebag, so that the nitrogen atmosphere was maintained. Once the pressure vessel was sealed, it was removed from the glove bag, pressurized, and heated in an oven as before.

Intermediate Wetting Phase

After the styrene had been polymerized, the Teflon column was disassembled and cleaned. Hardened styrene clogged the fritted glass disc, froze the plug valves, and filled the grooves in the endcaps. Soaking the valves and endcaps in toluene dissolved the styrene. The fritted glass disc was discarded. A new fritted glass disc and new filters were used to reassemble the column. A 0.2 μm polyvinylidene difluoride filter was used in place of a nylon filter in this step because it was found that the Tra-Bond® 2114 resin used to represent the organic phase wetted the polyvinylidene difluoride filter better, and therefore better drainage of the resin could be attained.

The resin (containing rhodamine B dye, 0.5% by weight, and benzyl alcohol, 40% by weight) was pulled under a vacuum into a small stainless steel pressure cylinder. The upper end of the cylinder was removed from the vacuum and reattached to a source of dry air with a pressure of 40 psig. The lower end of the pressure cylinder was connected with tubing to the bottom end of the reassembled column, as shown in Figure 32. A short length of tubing led from the upper endcap of the column to a drainage beaker. The applied air pressure forced resin upwards through the lower endcap displacing air. Approximately one pore volume of the moderately viscous resin could be forced through the column in a 45 minute period.

Dry Air

To Drain

▽
Pressure
Vessel

Epoxy
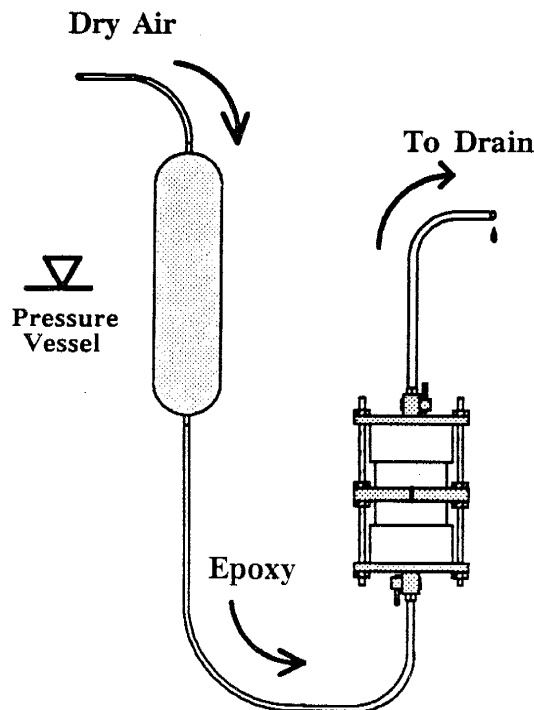
Figure 32. Intermediate-wetting phase flood.

The column was drained by turning off the air source, removing the upper drain tubing, and attaching a vacuum line to to pressure cylinder. Thirty cm Hg of suction were applied to the column. The column was drained until excess resin in the drainage beaker showed signs of hardening (about 1 hour after the hardener was added to the resin). At that time, the valves on the column were closed and the pressure cylinder was disconnected from the system.

The epoxy was allowed to cure for 24 hours, after which the column was disassembled and cleaned. Benzyl alcohol was used to flush epoxy from the pressure bottle and to dissolve epoxy from within the endcaps.

Non-Wetting Phase

The third fluid phase to be added to the column represented the non-wetting air phase. Again Tra-Bond epoxy was used, but this time it was dyed with coumarin 6. Preliminary experiments indicated that the epoxy resin's liquid phase would not react with its solid phase.

This step was the easiest of all. The dyed epoxy was pulled into the stainless steel pressure cylinder, as described earlier, and flooded into the column through the bottom endcap until it was produced from the top.

Once the core had cured sufficiently, the teflon cylinder was cut away and the core was prepared for observation as 'pore casts', as described previously for the saturated zone experiments.

ADVANTAGES AND LIMITATIONS OF THE TECHNIQUE

The advantage of this technique is that it is possible to observe the distribution of the different fluid phases within the pore space. Like with the micromodels discussed in the next chapter, the fluid distributions may be observed in both a bulk sense and within individual pores. Because the fluids eventually become solidified, one can only see a 'snapshot' of the flow behavior using this polymerization technique. However, the advantage over micromodels (in which the the actual displacement process can be observed as it is unfolding) is that here the fluid distributions can be observed in a real soil. Such a soil has three-dimensional pore interconnections, irregularly shaped pores, and rough surfaces which are not found in micromodels.

Without access to image analysis equipment, these blob polymerization techniques are only marginally quantitative. The precision for residual organic liquid saturation measurements were commonly in excess of $\pm 6\%$.

As discussed in Chapter 9, difficulties in attaining complete drainage of the organic liquid surrogate in the three-phase experiment presented a problem. And as was pointed out in the vadose zone experimental procedures for this technique, there is some question as to whether solidifying the wetting phase prior to introduction of the intermediate-wetting phase gives realistic fluid distributions.

Still, the pore and blob casts give important information about the distribution of residual organic liquids within the pore space. And as is discussed in Chapters 7 and 9, the distribution of fluids within the pore space has implications to dissolution, volatilization, and biodegradation of residual organic liquid contaminants.

CHAPTER 6

MICROMODEL EXPERIMENTAL METHODS

Micromodels are physical models of a pore space network, created by etching a pattern onto two glass plates which are then fused together. The pores have complex three dimensional structure, although the network is only two dimensional. The advantage of performing multiphase flow experiments using micromodels is that they give us the ability to actually see fluids displace one another both in a bulk sense and in individual pores. Photographs of the entire model allow examination of the bulk displacement processes, while photomicrographs taken through an optical microscope permit observation of details on a pore level. Etched glass micromodels provide an excellent method with which to study the mechanisms controlling the transport and capillary trapping of organic liquids because the structure of the pore network and the wettability of the system can be closely controlled (see e.g. Chatzis et al., 1983; Wardlaw, 1982). The complete set of results obtained using this method was presented in Mason et al. (1989b).

This chapter is begun by describing the micromodel fabrication process. The experimental procedures for saturated zone conditions are then explained, followed by a description of the experimental procedures used in the three-phase experiments.

MICROMODEL CONSTRUCTION

A glass mirror, stripped of its protective enamel backing to reveal a copper layer, was coated with a photosensitive resin. A transparency of a desired pore-network pattern was placed on the coated mirror surface and was exposed with ultraviolet light. The unexposed resin beneath the opaque portions of the pattern was removed with xylene. The copper beneath the pattern was removed with nitric acid, and the glass beneath the copper was etched with hydrofluoric acid (HF). A mirror-image pattern was etched on another piece of mirror, and the two etched halves were fused together in a muffle furnace to form the completed micromodel. The micromodel construction procedures described in this report were modifications of those methods developed by Eastman Kodak (1975, 1979).

Pattern Preparation

Pore-network patterns were created by modifying commercially available drafting pattern films with drafting pens. A local photographer reduced each pattern to a standard size and transferred it and a mirror image onto plastic transparencies. The emulsion side of each transparency contacted the coated glass plates; transparencies laid emulsion-side up on a plate allowed too much light to leak under the pattern during exposure to UV light. The patterns included 'reservoirs' at each end of the network through which fluids were added and removed in the completed micromodel. An example of a pore-network pattern is shown in Figure 33.
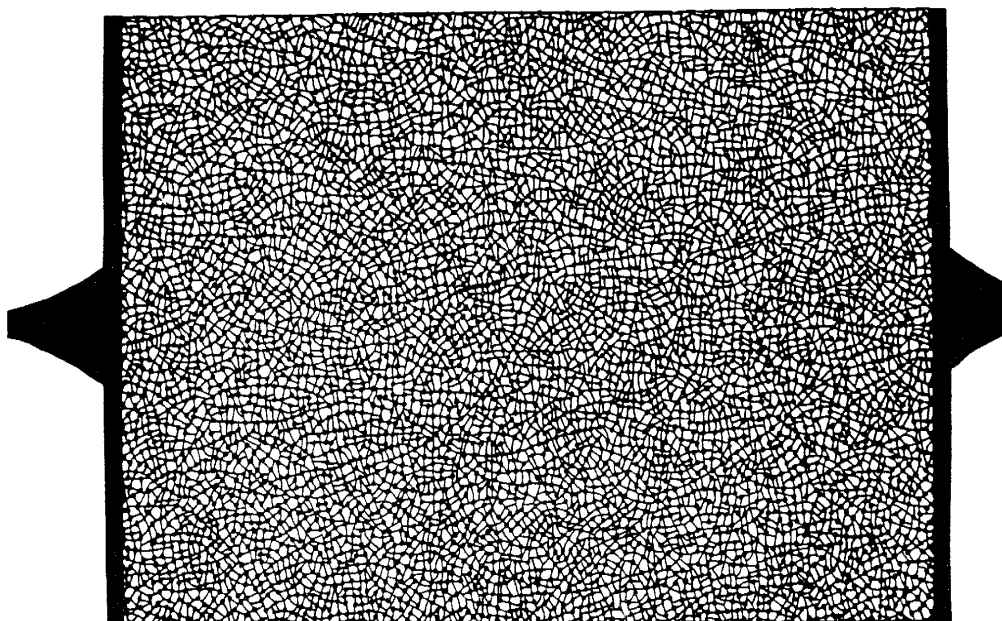
Figure 33. Pore-network pattern for the homogeneous model.

Mirror Preparation

Ordinary mirrors are manufactured by coating a piece of glass first with a silver layer, then a copper layer, and finally a protective enamel backing (see Figure 34). Mirrors were used in micromodel construction as a matter of convenience: the copper layer provided a binding surface for the photosensitive resin described in the next portion of this chapter, and the enamel backing served to protect the copper during transport and storage.

A 5 X 8 inch piece of mirror glass was prepared for coating with resin by first placing it, enamel side up, in a hot 50% by weight solution of NaOH to remove the protective backing. The solution was kept as hot as possible without actually boiling (approximately 90°C). During the next 5-10 minutes, the integrity of the enamel was tested by gentle scraping with teflon tongs. When the backing scratched easily, the mirror was taken from solution and the enamel was removed from the plate by gentle rubbing with a gloved hand under a stream of hot tap water. If the plate was left for greater times in solution, the backing slid off easily with no rubbing necessary; however, for these longer soaking times, the NaOH slightly corroded the copper beneath the enamel layer. If any enamel was left on the plate after the rinse, the affected portion was reinserted into the solution for a short time and then re-rinsed. Some experimentation was necessary to find a brand of mirror with enamel that could be removed completely and easily. (The backing can be easily stripped from Willard mirror glass, for instance.) After the backing was removed, the plate was rinsed with distilled water and dried in an 80°C oven (Figure 35).
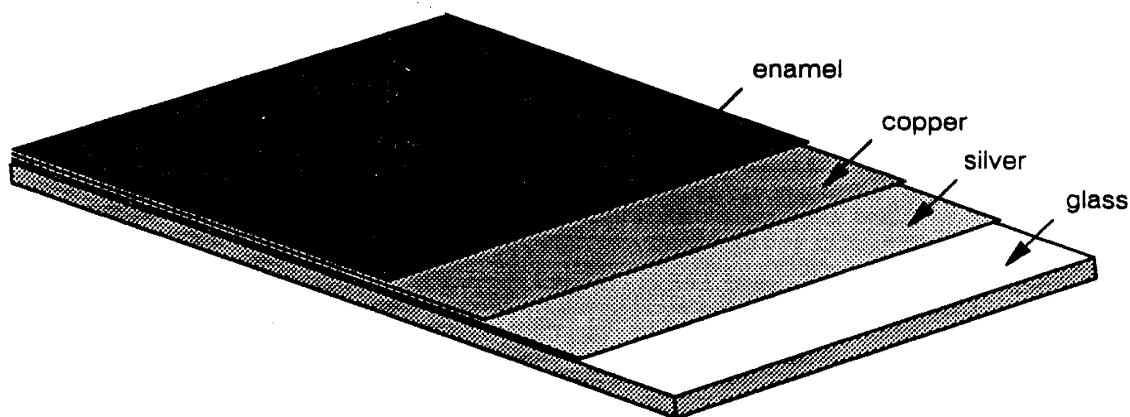
Figure 34.   Mirror construction.
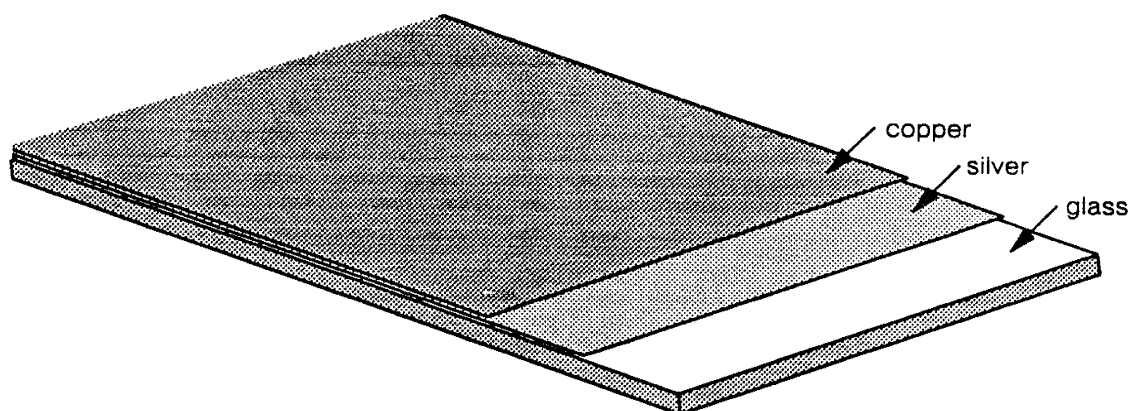
Figure 35.   Mirror with enamel removed to reveal copper surface.

<u>Pattern Exposure</u>

Kodak Thin Film Resist (KTFR), an ultraviolet-sensitive resin, was used to transfer the pore-network pattern to the mirror surface. In a darkened room, 1 part KTFR by volume to 2 parts xylenes were mixed. A mirror plate stripped of its protective backing was held horizontally, copper side up, and coated with approximately 10 ml of resist mixture. The plate was tipped in various directions to evenly distribute the resin over the copper surface in a layer of uniform thickness (see Figure 36). The plate was tilted vertically and allowed to air dry until the coating was no longer sticky to the touch (generally 20-30 minutes). If long HF etching times were expected, the plate was baked in an 80°C oven for 10 minutes to help the resin adhere to the copper surface. The disadvantage of baking was that the resin was difficult to remove in later steps. Unused coated plates were stored in a dark place.

After the coating was dry, the patterned transparency was placed emulsion-side down on the coated mirror surface, covered with a clear piece of glass to ensure good contact between the
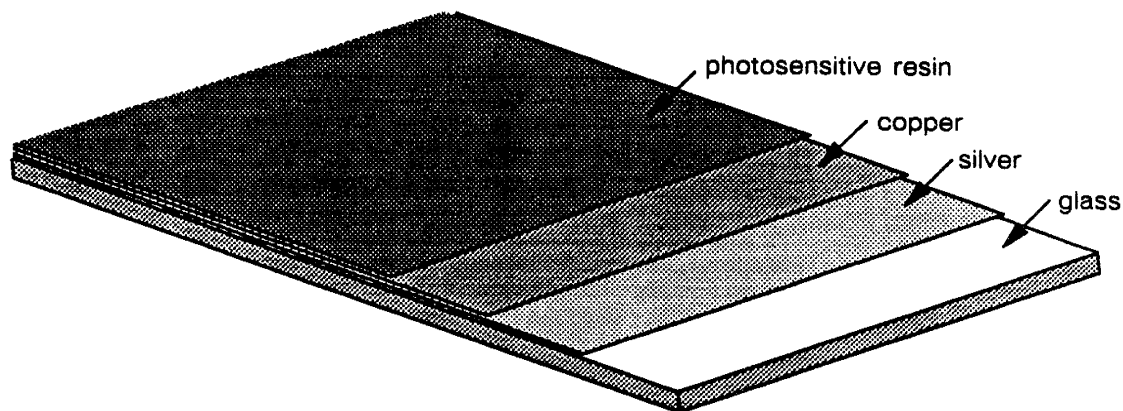
Figure 36. Copper surface coated with Kodak Thin Film Resist (KTFR).

pattern and the surface, and placed under a 1600 microwatt per centimeter long-wave ultraviolet light source at a distance of 25 cm. The assembly was exposed to the UV source for approximately 12 minutes as illustrated in Figure 37.

Exposure times were found to be a function of the thickness of the resin coating, the intensity of the light source, and the distance of the light source from the plate. A thick coating (an undiluted KTFR mixture) better protected the non-pore areas from HF during the etching step but required greater exposure times than for a thin coating. However, thin coatings made by diluting KTFR with xylene reproduced fine details more faithfully and required smaller exposure times than for thick resist layers. It was also found that exposure time decreased with a shortened distance between the light source and the model, and with increased intensity of the light source.
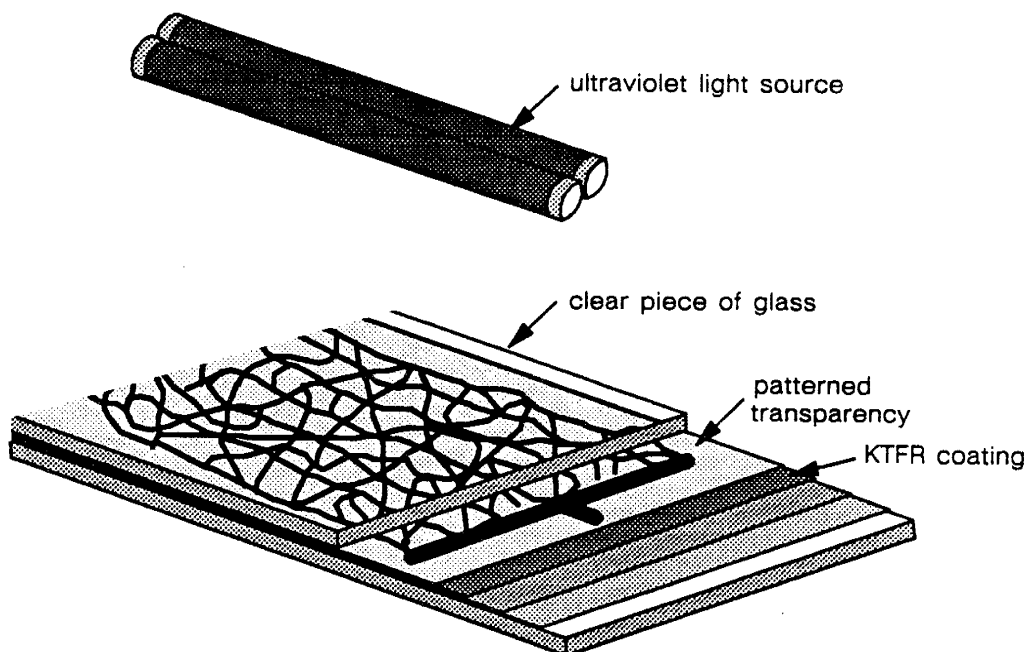
Figure 37. Pore-network pattern exposed with UV light onto coated copper surface.
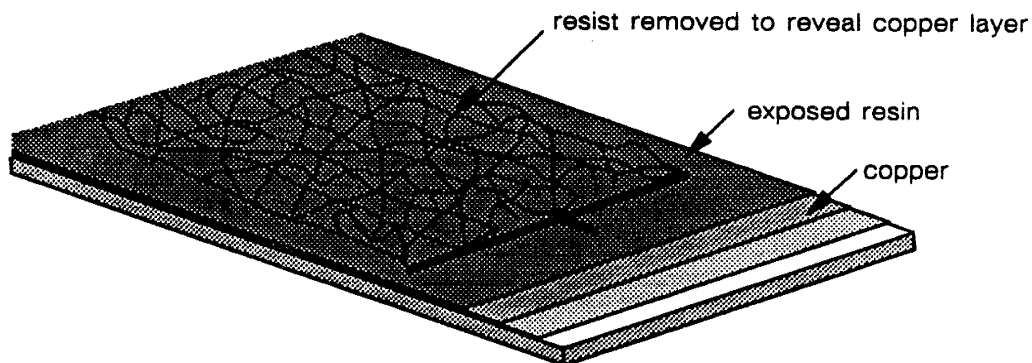
Figure 38.   Pore-network pattern exposed on the resin coating.

Exposure times were also affected by the age of the resin — the older the resin, the longer the exposure times needed.

When the exposure was complete and while the room lights were still dim, the plate was removed from under the UV light and the surface was sprayed with xylene. The plate was tipped back and forth for about 1 minute to wash away the undeveloped resist representing the pore-network pattern (see Figure 38). The plate was rinsed with warm tap water, then distilled water, after which the normal room lighting was restored. If the pattern was not visible, more xylene was applied, and the plate was rinsed again. The plate was shaken to remove excess water droplets and was placed in an 80°C oven for 10 minutes. The plate was removed from the oven and cooled before the next step.

Etching the Copper

The cooled model was placed in a 50% by weight solution of HNO_3 for approximately 10 seconds, or until the copper and silver layers unprotected by resist (the pore-network pattern) had dissolved to reveal the underlying glass surface, as illustrated in Figure 39. The plate was rinsed quickly with cold tap water and then with distilled water. After the plate had been dried in an 80°C oven, the pattern was examined under a microscope for imperfections. Small undissolved portions of the network were removed carefully with a dental tool or scriber. If necessary, the plate was re-dipped in the HNO_3, then re-rinsed, to remove copper and silver left in the network after the first acid dip.

Etching the Pattern in the Glass

All areas of glass that were to remain un-etched, such as the model edges and back, were coated with excess resist mixture and allowed to dry. The model was placed pattern-side up in a tray of concentrated HF for about 15 minutes. Longer etching times were used for models requiring deeper pores. When the model was removed from solution, it was promptly rinsed in cold water, and the network was scrubbed with a wire brush to remove siliceous deposits formed during etching. The resist was removed with a razor blade, the copper and silver with HNO_3, and the model was washed with detergent, rinsed with distilled water, and allowed to dry.

copper and silver layers removed
to reveal glass beneath network

exposed resin
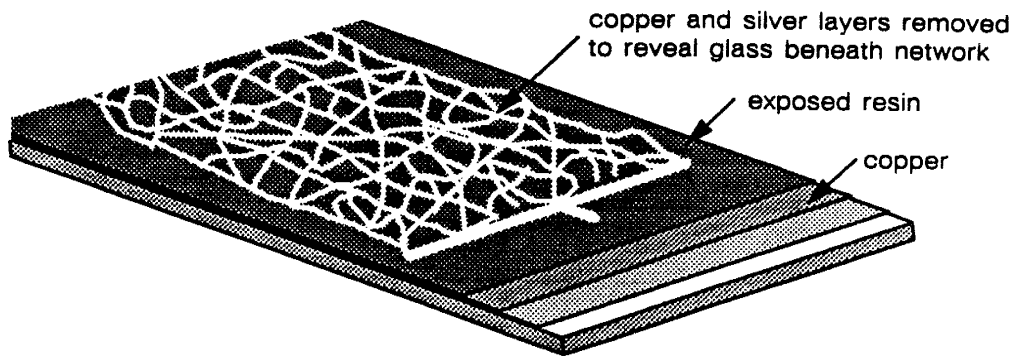
copper

Figure 39. Copper and silvers layers under the pore network pattern removed to reveal the underlying glass plate.

Model Assembly

. A mirror-image micromodel half was produced by the above methods using a mirror-image transparency. Inlet and outlet ports were drilled with a diamond drill bit in the reservoir areas of one of the plates. The two halves were aligned under a microscope, and cyanoacrylate glue was wicked in between the plates from the edges to temporarily hold them together. The model was placed in a muffle furnace and fused at 720°C for 15 minutes. Longer fusing times resulted in smoother, smaller pores; however, if a model was left too long in the furnace, some of the pores closed and the network became disconnected.

A completed micromodel has pores that are rather eye-shaped (Figure 40). During multi-phase displacements, the most wetting phase tends to preferentially fill the wedges on either side of a pore — in a sense mimicking behavior in natural soils in which the wetting phase tends to remain as pendular rings at grain-to-grain contacts.

MICROMODEL EXPERIMENTAL PROCEDURE

In the two-phase micromodel experiments, an initially water-saturated micromodel was flooded with Soltrol at a prescribed rate to simulate the movement of an organic liquid into the saturated zone. After the fluid saturations stabilized, the model was flooded with water at low velocity. The organic liquid still in the model after water injection remained as residual saturation. The two-phase experiments represented a scenario in which an organic liquid percolated into the saturated zone, then was displaced by ambient groundwater flow, and finally was left behind as residual organic liquid saturation.

In the three-phase experiments, an initially water-saturated micromodel was drained with air under an applied suction. The magnitude of the applied suction determined the water saturation remaining in the model. Organic liquid was then injected into the column under low-flow conditions, simulating the infiltration of organic pollutants into the vadose zone. After equilibrium conditions were reached, the organic liquid was again drained with air. The three-phase
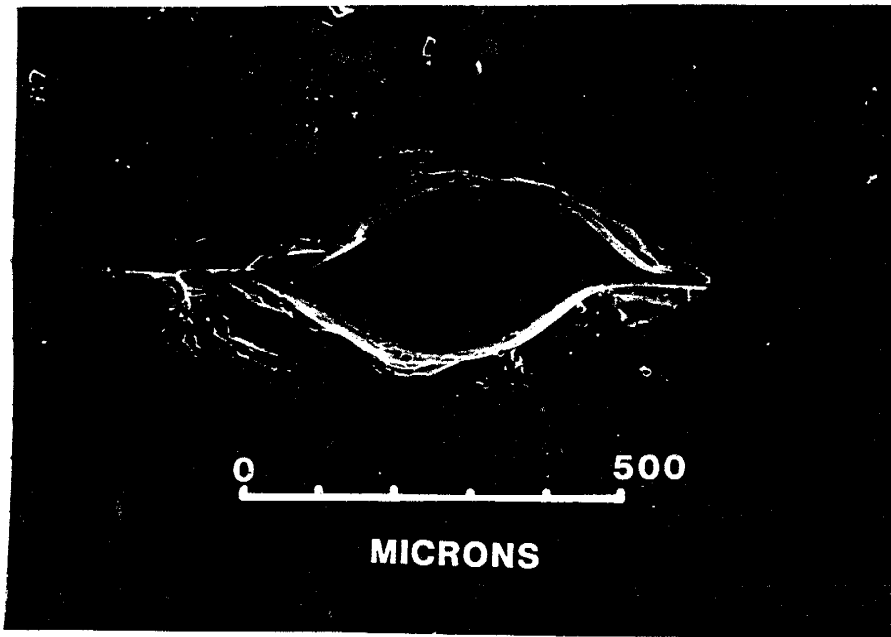
Figure 40. SEM photomicrograph cross-section of a typical pore in a micromodel.

experiments represented a scenario where an organic liquid percolated through the vadose zone to the water table, leaving behind trapped organic liquid.

During displacements, a capillary end effect was sometimes observed at the outflow end of the model (see Figure 55a, for example). A cure to this end effect problem was developed rather late in this study. The pore-network pattern was altered so that it included a series of small pores in one of the end reservoirs (Figure 41). These small pores which served as a capillary barrier would be similar in function to the capillary barriers described in Chapters 4 and 5. Only the three-phase experiments have been run in a micromodel having such a capillary barrier.

Fluid Preparation

The fluids used in the micromodel experiments were air, water, and Soltrol-130. The aqueous phase was prepared by combining 10 milliliters of blue food color with one liter of distilled water. The organic phase was prepared by combining 0.90 grams Oil Red O with one liter of Soltrol-130 and then by straining the mixture through a coarse paper filter. The micromodels were cleaned with chromic acid, thoroughly rinsed with distilled water, and were saturated with the aqueous phase prior to the experiments.

Two-Phase Experimental Procedure

The micromodels were initially saturated with water by connecting each one to a circulating pump and a reservoir of the aqueous phase as shown in Figure 42a. Water was then flushed
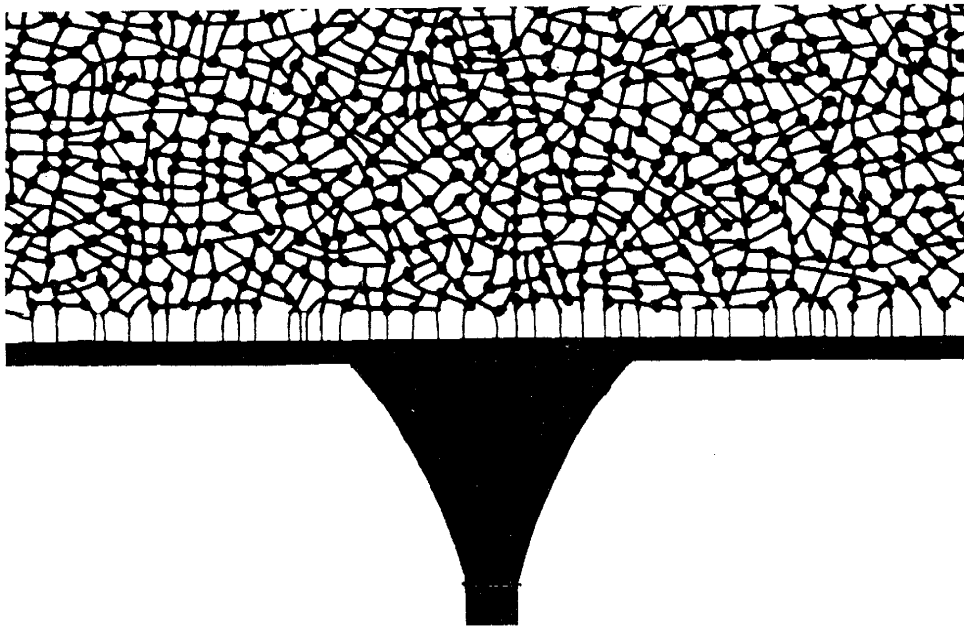
Figure 41.   Photograph of a capillary barrier built into one end of a micromodel.

through the model until all entrapped air was removed. Then, Soltrol was injected at a prescribed rate into each model using a syringe pump. After the fluid saturations stabilized, the syringe pump flow direction was reversed and the model was flooded with water. Capillary forces trapped the some of the organic liquid as immobile, disconnected blobs.

Micromodels were oriented either vertically or horizontally during the two-phase experiments. For vertically-positioned micromodel experiments, the syringe pump was connected to the top fitting of the model and was flooded with Soltrol from the top to the bottom (Figure 42b). In the horizontally-oriented experiments, the syringe pump was arbitrarily connected to the left fitting and Soltrol was flooded into the model from left to right (Figure 42c). The pore networks shown in Figures 33, 43, and 44 were run vertically. The network in Figure 45 was run in both the horizontal and vertical positions.

Three-Phase Experimental Procedure

As in the two-phase experiments, the micromodels in the three-phase experiments were de-aired with a circulating pump. With the model positioned vertically, the micromodel was drained with air into a buret. The fluid level in the buret was positioned such that sufficient suction was applied to drain the model but not so much so that air was able to penetrate the capillary barrier at the bottom of the model (Figure 46a). In the next step, the syringe pump was attached to the model's top fitting and organic liquid was introduced into the top of the model to simulate the infiltration of an organic liquid into the unsaturated zone (Figure 46b). As organic liquid was
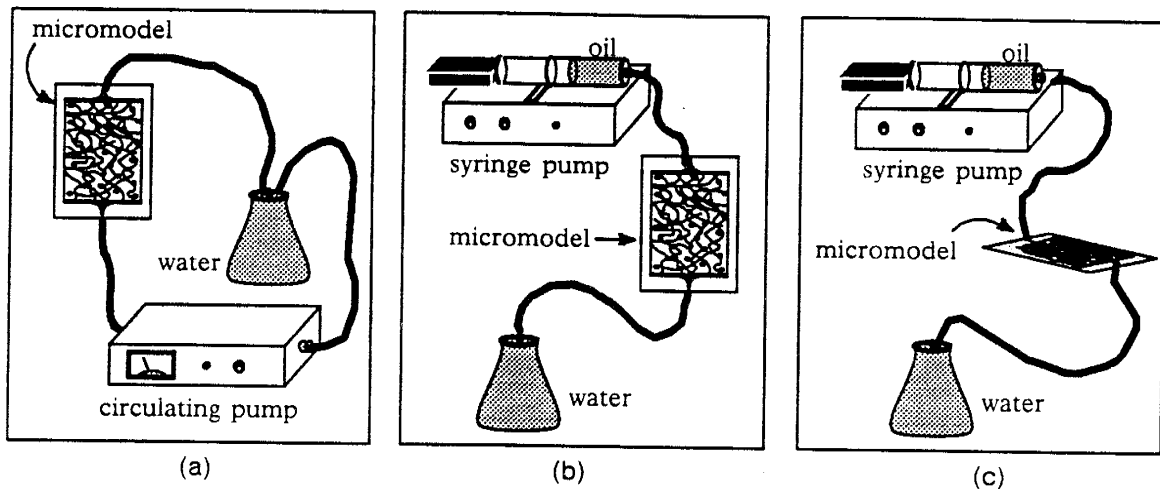
Figure 42.   Two-phase micromodel experimental set-up.
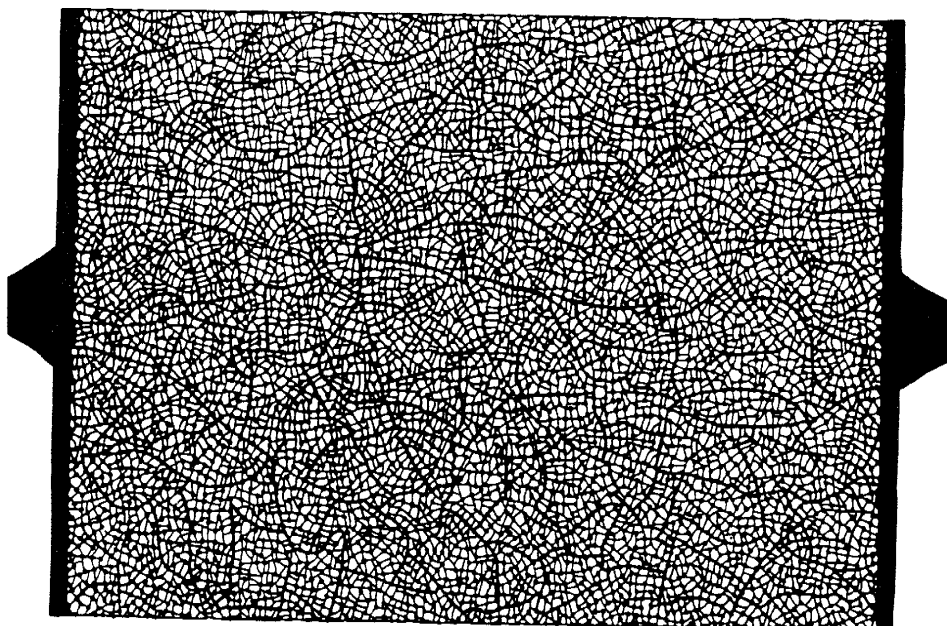
Figure 43.   Pore-network pattern for the 'aggregated' model.

injected, sufficient pressure was generated to force air through the capillary barrier and out of the model. After the fluid saturations stabilized, the syringe pump was disconnected and the buret reconnected. In the final step, hydraulic connection between the capillary barrier was re-established and the micromodel was once again drained with air.
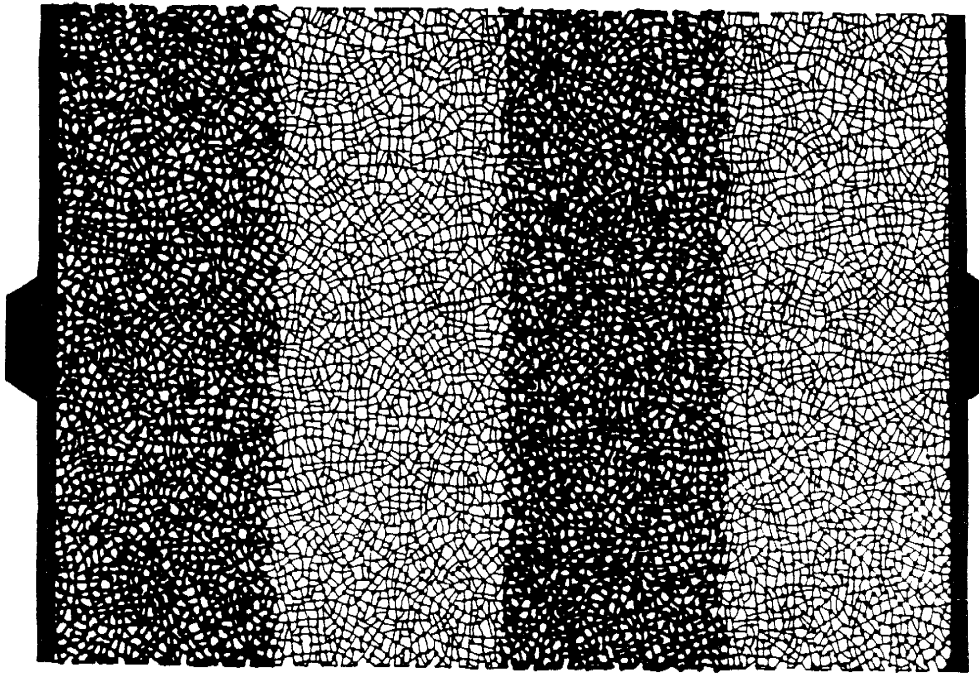
Figure 44.   Pore-network pattern for the 'layered' model.
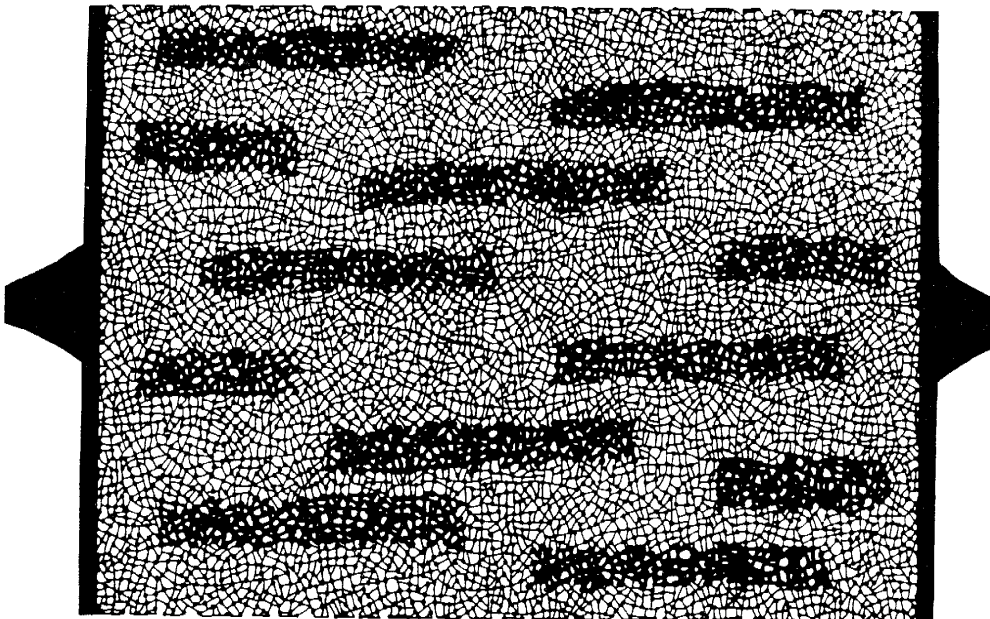
Figure 45.   Pore-network pattern for the 'lens' model.

(a)   (b)
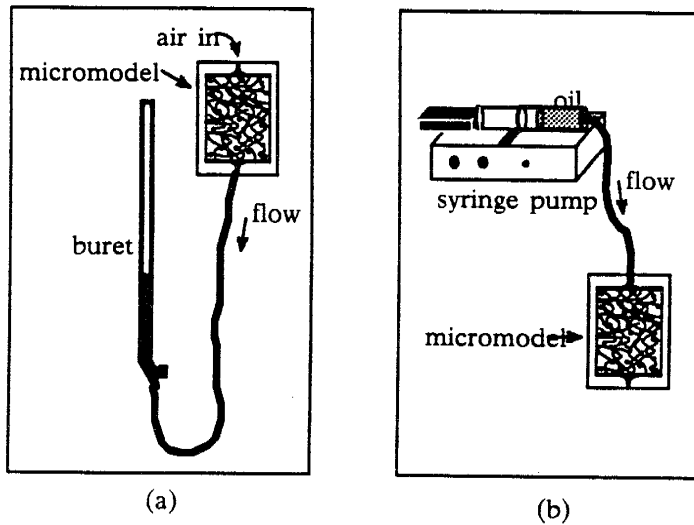
Figure 46.   Three-phase micromodel experimental set-up.

ADVANTAGES AND LIMITATIONS OF THE TECHNIQUE

The attractiveness of performing multi-phase flow experiments in glass micromodels is that we can actually see the fluids displace one another. Micromodels provide an excellent method with which to study multi-phase flow behavior because the structure of the pore network and the wettability of the system can be closely controlled.

The biggest limitation of using micromodels is the lack of quantitativeness. Fluid saturations cannot be accurately measured without image analysis capabilities. Further, it is difficult to measure media properties such as hydraulic conductivities, characteristic curves, or on a smaller scale, the dimensions of individual pores. And of course, the micromodels suffer from having regularly shaped pores and two-dimensional interconnections between pores.

CHAPTER 7

SATURATED ZONE RESULTS IN HOMOGENEOUS MEDIA

Figure 47 depicts the portion of the aquifer that includes residual saturation in the saturated zone. For an organic liquid more dense than water (left below), the slug of organic liquid leaves behind a trail of capillary trapped residual as it makes its way downward toward the bottom of the aquifer, and then laterally along that barrier. Within and below the capillary fringe the trapped organic liquid shares the pore space only with water. When an organic liquid less dense than water reaches the water table, the weight of the organic phase can depress the water table (right below). Later, as the organic phase redistributes laterally and the water table rebounds, trapped organics are left behind within the saturated zone. During this redistribution, laterally moving organic liquid can be trapped within the capillary fringe. A rising water table can also lead to this same type of organic liquid trapping of a 'floater' in the saturated zone.

Organic liquid movement and capillary trapping in the saturated zone is presented over two chapters. This chapter deals with homogeneous media, while Chapter 8 deals with
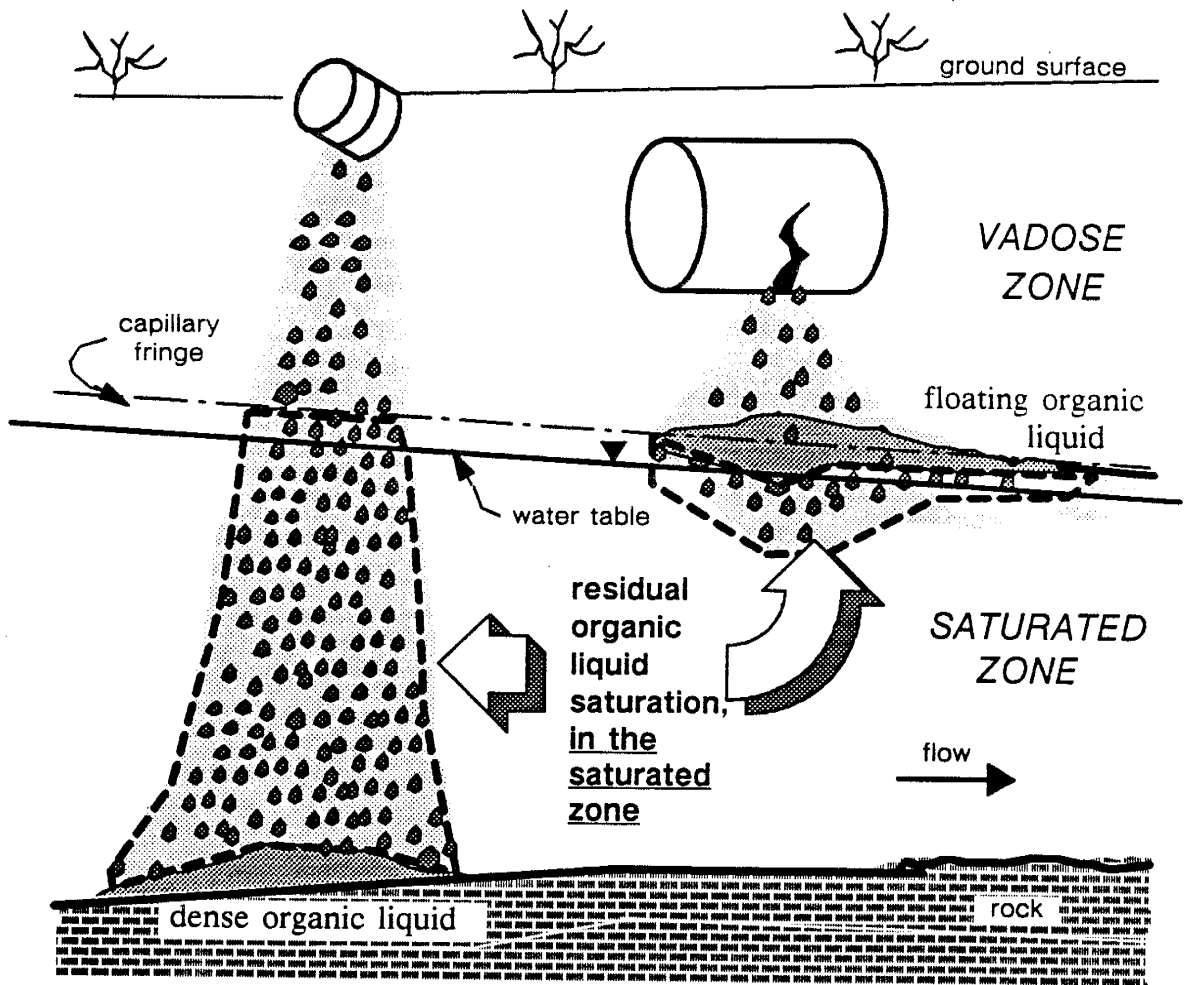
Figure 47.   Schematic of residual organic liquid trapped in the saturated zone.

heterogeneous media. This chapter begins by presenting measurements of residual saturations from the short column experiments. In this series of experiments, residual saturations were measured for several soils and over a range of organic-phase fluid properties.

Following the presentation of these quantitative results, the results of several flow visualization experiments are presented. The micromodel experiments allow us to look more carefully at the actual displacement process leading up to capillary trapping of organic liquid contaminants. The similarity of pore cast and blob cast results to those of the micromodel experiments gives confidence that immiscible displacements in micromodels are reasonable representations of how these displacements occur in actual soils.

In both sections of this chapter, the results are related to theoretical explanations of trapping mechanisms at work on a pore scale. Throughout the chapter the implications of the results for contaminant transport and the cleanup of organic pollutants in the saturated zone are discussed.

QUANTITATIVE MEASUREMENTS OF RESIDUAL SATURATION IN SOIL COLUMNS

Quantitative measurements of residual saturation were made in short soil columns, as described in Chapter 4. Briefly, in each experiment an initially water saturated soil column was first flooded with an organic liquid to simulate the movement of an organic liquid into the saturated zone. The injection pressure was held low enough to prevent the organic liquid from passing through a water-wet filter at the lower endcap of the column. As can be seen later, this boundary condition, which reduces the possibility of capillary end effects, is different than that used in the micromodel experiment. After the fluid saturations stabilized, the column was flooded with water at a low velocity. Six pore volumes of water were found to be more than sufficient to reach a stable organic liquid residual saturation. As documented in Chapter 4, fluid saturations were determined gravimetrically using the density difference between the fluids.

Organic liquid saturation is measured as the volume of organic liquid per unit void volume, measured over a representative elementary volume of the porous media:

$$S_o = \frac{V_{organic\ liquid}}{V_{voids}} \tag{36}$$

where the "o" indicates the organic liquid. The residual saturation at which the organic liquid becomes discontinuous is defined by:

$$S_{or} = \frac{V_{discontinuous\ organic\ liquid}}{V_{voids}} \tag{37}$$

where the "r" indicates residual. In the saturated zone the water saturation is given by:

$$S_w = 1.0 - S_o \tag{38}$$

Another measure of residual saturation often used in organic liquid pollution studies is the volumetric retention (e.g., de Pastrovich, 1979; Schwille, 1967):

$$R = \frac{liters\ of\ residual\ organic\ liquid}{cubic\ meters\ of\ soil} = S_{or} \times n \times 10^3 \qquad (39)$$

where n is the soil porosity.

Residual saturation results were obtained for several organic liquids using the same soil (Sevilleta dune sand) to test the effect of varying fluid properties on the residual saturation. Additional residual saturation measurements were taken using different soils while holding the organic liquid constant (Soltrol). These results were also reported in Hagan et al. (1989).

The Base Case: Soltrol in Sevilleta Sand

In this study, measurements of the residual saturation of Soltrol in Sevilleta sand form the base case against which many other experimental results were compared. Soltrol and Sevilleta sand were the common denominators for experiments in which residual saturations were measured for several different organic liquids, and in several different soils. These same results will also be used later to examine the effects of heterogeneities on residual saturation (Chapter 8), and to compare S_{or} in the saturated zone to those measured in the vadose zone (Chapter 9).

Tables 4 and 5 summarize the experimental results for Soltrol in Sevilleta sand. These tables also include the maximum organic liquid saturation measured when water was at (or near) the residual saturation, S_{wr}. Water saturations and organic retention can be calculated from equations (38) and (39). Included in the tables are measured values of sample porosity and bulk density. These measurements provide information for ancillary calculations, and their variability is a measure of experimental control over the packing.

	porosity (%)	bulk density (g/cm³)	maximum organic liquid saturation (%)	residual organic liquid saturation (%)
all 22 experiments	34.3 ± 1.2	1.741 ± 0.033	84.7 ± 3.4	28.0 ± 3.8
good temp. 13 experiments	33.9 ± 0.6	1.752 ± 0.016	85.1 ± 2.8	27.1 ± 1.7
poor temp. 9 experiments	34.9 ± 1.7	1.724 ± 0.044	84.0 ± 4.1	29.3 ± 5.4

Table 4.   Soltrol residual saturation and other measurements in Sevilleta sand, for three temperature dependent categories (sample mean ± sample standard deviation).

Many of the earlier Soltrol experiments were run without the benefit of a constant temperature cabinet. This is noted in the second column of Table 5, and the difference between maximum and minimum temperatures during the course of the experiment is given in the last column. As discussed in Chapter 4, those experiments with large temperature fluctuations provided less reliable results. In particular, it can be seen from the Table 5 that the two

trial	in box ?	porosity (%)	error (%)	bulk density (g/cm³)	error (g/cm³)	organic liquid saturation (%)				temp. range (°C)
						maximum	error	residual	error	
1	no	33.8	0.6	1.754	0.008	84.6	3.5	29.3	1.7	1.0
2	no	36.5	0.5	1.683	0.007	82.2	3.0	32.5	1.5	5.0
3	no	34.0	0.5	1.750	0.007	77.5	3.1	24.6	1.4	1.0
4	no	34.1	0.5	1.747	0.008	85.7	3.5	29.3	1.7	1.0
5	no	33.2	0.6	1.769	0.008	92.7	3.9	34.7	2.0	3.0
6	no	34.8	0.5	1.729	0.007	84.1	3.2	32.7	1.6	2.0
7	no	38.6	0.9	1.626	0.017	78.6	3.7	21.6	1.5	11.0
8	no	34.6	0.5	1.732	0.007	80.2	3.0	37.0	1.7	3.0
9	no	34.6	0.5	1.733	0.008	84.7	3.5	29.3	1.7	2.0
10	no	34.3	0.5	1.741	0.008	87.5	3.6	28.6	1.8	3.0
11	no	34.1	0.6	1.747	0.009	87.0	3.9	26.9	1.8	1.5
12	no	34.1	0.6	1.746	0.009	82.6	3.6	24.3	1.6	2.8
13	no	33.7	0.5	1.756	0.008	83.5	3.3	23.1	1.4	2.8
14	yes	34.9	0.5	1.726	0.007	87.0	3.4	27.9	1.6	0.3
15	yes	34.2	0.6	1.745	0.010	85.8	3.9	25.0	1.7	0.8
16	yes	34.7	0.6	1.730	0.010	88.2	3.9	28.5	1.8	0.4
17	yes	33.7	0.5	1.758	0.006	83.8	3.2	25.4	1.4	0.3
18	yes	34.1	0.6	1.747	0.009	85.6	3.7	27.1	1.7	0.4
19	yes	34.1	0.6	1.746	0.011	86.0	4.0	29.2	1.9	0.9
20	yes	32.8	0.6	1.781	0.010	88.3	4.1	27.6	1.9	1.0
21	yes	33.1	0.6	1.774	0.009	83.0	3.7	24.6	1.7	1.0
22	yes	33.2	0.5	1.771	0.007	84.1	3.4	26.6	1.7	1.1

Table 5.   Summary of Soltrol / Sevilleta sand saturated zone results.

experiments with the largest temperature fluctuations also had the largest estimated porosity and extreme estimates of residual saturation. Sample statistics for the twenty-two experiments are presented in Table 4, with data divided into three categories: a) all experiments; b) thirteen experiments conducted with good temperature control ($\Delta t < 2°C$); and c) nine experiments conducted with poor temperature control ($\Delta t > 2°C$). Error measurements, using a worst case error approach in which all errors were assumed additive and propagated through the calculations, are given in Table 5. Comparing these estimates to the sample standard deviations suggests that the thirteen temperature controlled experiments account for the known and tractable experimental errors. Thus the estimate of residual saturation, $S_{or} = 27.1 \pm 1.7\%$, taken from these 13 experiments is appropriate. This is slightly lower than earlier published estimates (Wilson et al., 1988b), which were biased by the temperature fluctuations of the first experiments.

Twenty-seven percent of the Sevilleta sand pore space is occupied by immobile, discontinuous, blobs of Soltrol. If this estimate is typical for most organic liquids and sandy soils there is a tremendous storage capacity of organic liquid pollutants in the saturated zone. Expressed in terms of volumetric retention (equation 39), the Sevilleta sand has the capacity to store over 90 liters of Soltrol per cubic meter of soil. For example, a single 10,000 gallon spill of an organic liquid could be contained in about 420 m³ of saturated soil. This volume corresponds to a cube of soil with sides only 7.5 meters in length. If for example we suppose that these 10,000 gallons of organic liquid were benzene (with a solubility in water of about 1780 mg/l), the benzene would have the potential to contaminate at least 4.5 million gallons of groundwater as it dissolves. And of course with the help of dispersive mixing, the benzene would likely contaminate a significantly larger volume of groundwater than that.

The earlier discussion on mechanisms focused on capillary trapping as a function of pore structure among other factors. Each experiment recorded in Table 5 included measurements of porosity and bulk density. Presumably, these measurements allow some inference about the pore structure as controlled by the density of soil packing. A tendency for increased trapping with decreased porosity has been reported in the petroleum literature (Morrow et al., 1988). This tendency is believed to be related to the fact that for more heavily cemented petroleum reservoir rocks, the pore throats (from which organic liquid is easily displaced by water) make up a smaller percentage of the total pore volume (Chatzis et al., 1983). Lower pore connectivity, another attribute of low porosity (heavily cemented) media, is also suspected of contributing to increased trapping (Pathak et al., 1982). Although only unconsolidated soils have been used in this study, there was some concern that some systematic change might be seen in residual saturations with change in porosity from one packing to the next. Figure 48 presents a plot of maximum organic liquid saturation and residual saturations for the 13 best samples in Table 5. In these results, there appears to be no discernible correlation between porosity and either the residual or maximum organic liquid saturations. Although the porosities varied somewhat, this variation did not seem to affect the measurements of saturation in any systematic way. The lack of correlation between S_{or} and n is probably due to the small range over which the porosities varied.
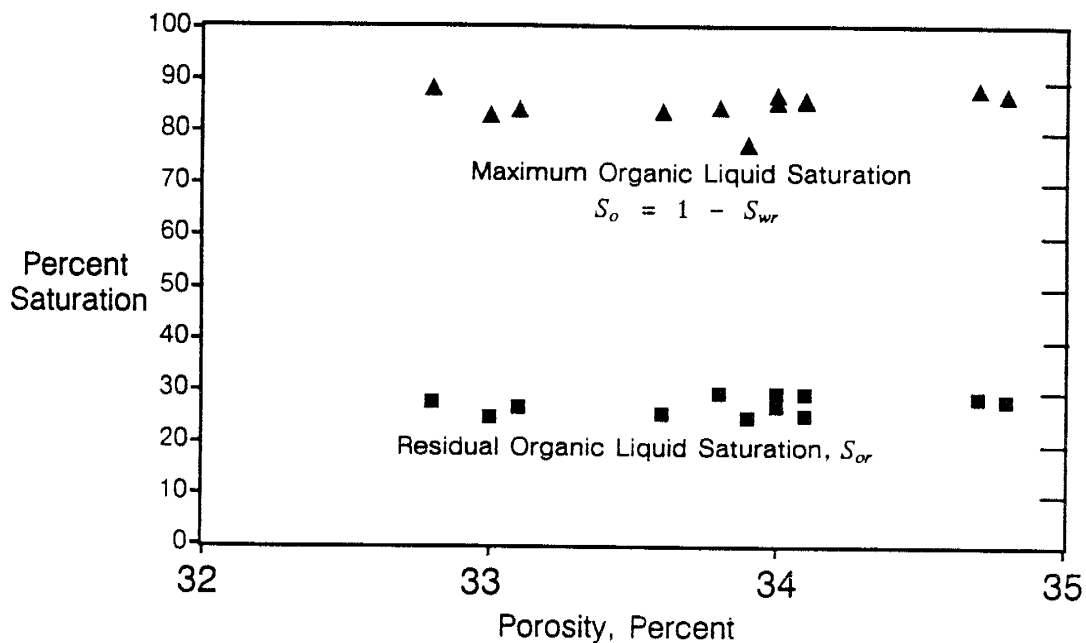
Figure 48.   Correlation of maximum Soltrol saturation (triangles), and residual Soltrol saturation (squares), to porosity in the Sevilleta dune sand.

Other Fluids

It was hypothesized that for commonly spilled organics, residual saturations would be independent of fluids or fluid properties. Since capillary forces so thoroughly dominate the movement and trapping of organic liquids in porous materials, it was believed that variability in fluid properties over the range encountered for commonly spilled organic pollutants would be insufficient to affect the balance of forces controlling trapping mechanisms. To test this hypothesis, a series of short column experiments were run in the Sevilleta sand using a variety of fluids — kerosene, gasoline, p-xylene, PCE, and n-decane.

The kerosene experiments presented in Table 6 were run early in the project without the benefit of a constant temperature cabinet. The n-decane experiments presented in Table 7 and the gasoline experiments presented in Table 8 were conducted under good temperature control. The six p-xylene tests summarized in Table 9 were conducted under a fume hood, but the temperature was fairly well controlled. Although the smaller density difference between water and the p-xylene resulted in greater error propagation for organic liquid saturations, the actual sample standard deviation was relatively small in comparison. The PCE tests described in Table 10 were also conducted under a fume hood with relatively good temperature control.

A summary of all the tests is given in Table 11. From this table it is apparent that the soil packing was very consistent from the tests of one liquid to those of another. The soil dependent properties, porosity and bulk density, remained nearly constant over the most of the experiments. The porosities for the PCE experiments, however, were slightly but consistently

lower than all the other experiments because the operator of these experiments screwed down the top endcap on the column a little tighter as an added precaution against leakage. This slightly lower soil porosity appeared to have no influence on the results.

Trial	porosity (%)	error (%)	bulk density (g/cm³)	error (g/cm³)	Organic liquid saturation (%)				Temp. range (°C)
					maximum	error	residual	error	
1	33.1	0.4	1.765	0.002	73.3	2.0	28.1	0.9	5.0
2	33.0	0.4	1.769	0.003	52.8	1.6	28.3	0.9	4.0
3	33.7	0.4	1.751	0.003	78.9	1.6	27.3	0.9	3.0
4	33.2	0.5	1.765	0.003	70.1	2.0	25.3	0.8	3.0
5	33.8	0.5	1.747	0.003	73.8	2.1	23.8	0.8	3.0
6	33.7	0.4	1.750	0.002	73.1	2.0	23.3	3.2	5.0
7	33.3	0.3	1.760	0.001	80.1	2.1	25.4	0.8	2.0
8	35.0	0.5	1.721	0.008	80.9	2.8	29.0	1.5	7.0
Avg.[*]	33.6	0.6[*]	1.754	0.014[*]	72.9	9.0[*]	26.3	2.1[*]	——

[*] Average = sample mean ±standard deviation

Table 6.   Summary of kerosene / Sevilleta sand saturated zone results.

Trial	porosity (%)	error (%)	bulk density (g/cm³)	error (g/cm³)	Organic liquid saturation (%)				Temp. Range (°C)
					maximum	error	residual	error	
1	34.7	0.6	1.732	0.010	77.0	3.6	28.6	1.8	2.6
2	33.2	0.6	1.776	0.010	72.3	3.6	24.6	1.8	1.1
3	34.2	0.6	1.743	0.010	78.8	3.9	25.1	1.9	1.5
4	32.2	0.6	1.797	0.010	82.4	4.1	26.7	1.8	2.1
5	33.5	0.6	1.763	0.010	82.5	3.9	24.6	1.6	2.0
Avg.[*]	33.6	1.0[*]	1.762	0.026[*]	78.6	4.2[*]	25.9	1.7[*]	---

[*] Average = sample mean ±standard deviation

Table 7.   Summary of n-decane / Sevilleta sand saturated zone results.

There was also some concern over the high variability in the maximum organic saturations, and whether this variability would substantially affect the residual saturation results. In running the experiments, there was some trepidation in applying high suctions for fear of exceeding the breakthrough pressure of the bottom, semi-permeable membrane. As a consequence, it was not always certain that the water had been completely reduced to its so-called residual saturation and that the maximum organic saturation possible had been achieved. A plot of

Trial	porosity (%)	error (%)	bulk density (g/cm³)	error (g/cm³)	Organic liquid saturation (%)				Temp. range (°C)
					maximum	error	residual	error	
1	34.3	0.7	1.742	0.011	75.2	6.0	26.9	2.6	0.8
2	33.1	0.6	1.772	0.008	80.9	6.2	29.3	2.8	1.3
3	32.6	0.6	1.786	0.008	83.1	6.3	31.0	2.9	0.6
4	32.1	0.6	1.799	0.009	84.5	6.5	26.9	2.6	1.1
5	33.5	0.6	1.762	0.009	81.2	6.2	28.8	2.7	0.4
Avg.*	33.1	0.8*	1.772	0.022*	81.0	3.6*	28.5	1.7*	----

* Average = sample mean ±standard deviation

Table 8. Summary of gasoline / Sevilleta sand saturated zone results.

Trial	porosity (%)	error (%)	bulk density (g/cm³)	error (g/cm³)	Organic liquid saturation (%)				Temp. Range (°C)
					maximum	error	residual	error	
1	34.1	0.6	1.747	0.009	62.8	8.1	24.3	4.0	2.6
2	33.8	0.6	1.755	0.011	79.6	11.1	25.7	5.2	1.1
3	32.8	0.6	1.781	0.009	75.4	9.8	21.3	3.9	1.5
4	32.6	0.6	1.786	0.009	78.2	10.0	20.1	3.6	2.1
5	34.0	0.5	1.748	0.008	78.2	9.7	26.5	4.2	1.3
6	33.8	0.5	1.754	0.008	78.6	9.7	21.9	3.7	0.6
Avg.*	33.5	0.6*	1.762	0.017*	75.5	6.4*	23.3	2.6*	---

* Average = sample mean ±standard deviation

Table 9. Summary of p-xylene / Sevilleta sand saturated zone results.

Trial	porosity (%)	error (%)	bulk density (g/cm³)	error (g/cm³)	Organic liquid saturation (%)				Temp. range (°C)
					maximum	error	residual	error	
1	32.5	0.6	1.788	0.008	69.5	3.1	27.5	1.4	0.5
2	33.0	0.6	1.776	0.009	85.0	3.9	25.7	1.4	1.7
3	32.2	0.6	1.796	0.010	78.9	3.8	26.1	1.5	0.9
4	32.4	0.6	1.791	0.010	86.2	4.2	28.8	1.6	1.3
Avg.*	32.5	0.3*	1.788	0.009*	79.9	7.6*	27.0	1.4*	---

*Average = sample mean ±standard deviation

Table 10.   Summary of PCE / Sevilleta sand saturated zone results.

Fluid	porosity (%)	bulk density (g/cm³)	maximum organic liquid saturation (%)	residual organic liquid saturation (%)
Soltrol (13 trials)	33.9 ± 0.6	1.752 ± 0.016	85.1 ± 2.8	27.1 ± 1.7
kerosene (8 trials)	33.6 ± 0.6	1.754 ± 0.014	72.9 ± 9.0	26.3 ± 2.2
gasoline (5 trials)	33.1 ± 0.8	1.772 ± 0.022	81.0 ± 3.6	28.5 ± 1.7
p-xylene (6 trials)	33.5 ± 0.6	1.762 ± 0.017	75.5 ± 6.4	23.3 ± 2.6
PCE (4 trials)	32.5 ± 0.3	1.788 ± 0.009	79.9 ± 7.6	27.0 ± 1.4
n-decane (5 trials)	33.6 ± 1.0	1.762 ± 0.026	78.6 ± 4.2	25.9 ± 1.7
all liquids	33.5 ± 0.8	1.761 ± 0.020	79.5 ± 7.1	26.4 ± 2.4

Average = sample mean ±standard deviation

Table 11.   Average values for different organic liquids in the Sevilleta sand saturated zone experiments.

Figure 49. Residual organic liquid saturation as a function of the maximum organic liquid saturation.

Figure 50. Residual organic saturation for tested organic liquids in the Sevilleta sand.

maximum organic liquid saturation versus residual organic liquid saturation for all the experiments is shown in Figure 49. Visual inspection of the scatter plot does not reveal much correlation between maximum organic saturation and residual saturation, but least-squares regression analysis revealed a slight positive correlation.

The relationship between residual saturation and the type of organic liquid is displayed in Figure 50. The average residual organic liquid saturation, S_{or} , was relatively uniform, varying from a low value of 23.3% for p-xylene to a high value of 28.5% for gasoline. The average residual saturation over all the fluids was 26.5%. All the fluids were tested against one another for a statistically significant difference in the sample means using the student's t-test. Although the differences in residual saturations between the fluids appear to be small, the p-xylene results

Figure 51. Residual organic saturation as a function of interfacial tension (IFT). The error bars represent the sample standard deviations taken from Table 11.

were found to be statistically different from each of the other fluids at the 97.5% confidence interval ($\alpha = 0.025$). P-xylene was the most soluble of the organic liquids tested (about 0.20 g/l). In each experiment at least 6 pore volumes, or about 250 ml of water, was flushed through the column to reach residual saturation. If it is assumed that the water was flooded slowly enough so that the effluent water had reached equilibrium with the xylene, then as much as 0.05 g of xylene could have been removed from the column by dissolution, resulting in an underestimation of the residual saturation by as much as 1.0%. The reduction of xylene's residual saturation by dissolution may account for the significant difference in residual saturation between it and the other fluids tested. None of the remaining combinations showed significant differences in residual saturations between fluids at the 97.5% confidence interval, although both kerosene and n-decane were found to have sample means statistically different from gasoline at the 95% confidence interval.

Effect of interfacial tension

These same residual saturation results are again plotted in Figure 51, as a function of the interfacial tension (IFT) between water and the organic liquid. There appears to be no discernible correlation between IFT and S_{or} — and none was expected. The capillary forces (proportional to the IFT) so outweigh the other forces which may act to reduce trapping (buoyancy and viscous forces) that halving the interfacial tension — from an IFT of 47.8 for Soltrol to only 22.9 for gasoline — has no effect on the amount of organic liquid trapped. Indeed, at typical aquifer flow

rates IFTs may have to be reduced by at least an order of magnitude or more before any reduction in trapping occurs, as can be illustrated in the following analysis.

Consider again the pore scale trapping mechanisms discussed in Chapter 2. If we look at these mechanisms in a quantitative way, using as an example the flow rates of these experiments together with some observed characteristics of the Sevilleta sand, we can attempt some prediction of the reduction of interfacial tensions required to begin to lower residual organic saturations.

Consider the snap-off mechanism first. Wardlaw (1982) performed flow visualization experiments in glass micromodels using a single pore and pore throat to examine snap-off as a function of several properties including interfacial tension. An illustration of the pore and pore throat pair used in Wardlaw's experiments is given in Figure 6. For strongly water-wet systems, snap-off occurred for all fluid pairs studied even though the interfacial tensions ranged from 480 dyne/cm down to 0.1 dyne/cm. Trapping by snap-off was found to be insensitive to IFT down to 0.1 dyne/cm and it is expected that IFTs would have to be reduced still much further to avert the Haine's jump instability that leads to snap-off.

Although it appears that snap-off cannot be averted, perhaps for low enough IFTs the blob could become mobilized immediately after the Haine's jump caused its formation. Oh and Slattery (1979) in a theoretical study looked at the pressures required to mobilize blobs in a periodically constricting tube (similar to that shown in Figure 5). The critical dimensionless pressure needed for mobilization in a strongly water-wet pore with an aspect ratio of about 4 was:

$$\frac{\Delta P \ r_t}{2 \ \sigma} \ = \ 1.03 \qquad\qquad (40)$$

where: ΔP = Pressure drop across the blob

   r_t = Radius of the pore throat

   σ = Interfacial tension

As an example, the interfacial tension needed to mobilize the blob trapped in the Sevilleta sand, pictured in Figure 61, was considered. With a flux rate in the column experiments of about 2.5×10^{-4} cm/s, the pressure drop across the blob was estimated to have been about 3.7 dyne/cm^2. The pore throat radius was estimated to be about 50 microns and the aspect ratio to be 4. Using these estimates, the interfacial tension would need to be less than 0.01 dyne/cm to induce mobilization of the blob.

A similar analysis can be performed using data taken directly from these Sevilleta sand column experiments. Wilson et al. (1989) found the critical capillary number ($N_{c_2}^* = q\mu/\sigma$) for blob mobilization in the Sevilleta sand to be in the range of 10^{-4}. Using values from the column experiments ($q = 2.5 \times 10^{-4}$ cm/s and μ =1cP), the interfacial tension would need to be less than 0.025 dyne/cm to induce mobilization of the blob.

Next consider the by-passing mechanism. To prevent trapping in a pore doublet like the one shown in Figure 9b, the velocities of the interfaces traveling through each pore would have to be

about equal. That is, either the flow rate needs be increased, or the capillary forces reduced (by reducing σ) so that the water does not preferentially travel through the smaller pore of the doublet. To evaluate this, an equation presented by Moore and Slobod (1956) for computing competing velocities in a pore doublet was used:

$$\frac{v_1}{v_2} = \frac{\frac{4lQ\mu}{\pi r_2^2} + r_2^2\left(\frac{1}{r_1}-\frac{1}{r_2}\right)\sigma\cos\theta}{\frac{4lQ\mu}{\pi r_1^2} - r_1^2\left(\frac{1}{r_1}-\frac{1}{r_2}\right)\sigma\cos\theta} \tag{41}$$

where:
v_i = Velocity through pore i

l = Length of the pores

Q = Total flow rate through the doublet, $\dfrac{q\pi(r_1^2 + r_2^2)}{n}$

q = Flux rate

n = Porosity

μ = Viscosity

r_i = Radius of pore i

σ = Interfacial tension

θ = Contact angle

The ratio of the velocities was set equal to one and then σ was solved for using reasonable values from experiments in the Sevilleta sand: r_1 =100μm; r_2 =75μm; l=400μm; $\mu_o=\mu_w$=1cP; the average flux rate, q= 2.5 × 10^{-4} cm/s; the porosity, n=0.33, and the contact angle, θ=0°. Under these circumstances, σ would have to be less than 2 dyne/cm to avert trapping by by-passing.

By looking at the pore scale mechanisms that cause trapping, and by relating these mechanisms to this particular experimental system, it has been shown why S_{or} appears to be independent of IFT in these experiments — and why S_{or} would be expected to be independent of IFT for many commonly spilled organic pollutants (see Table 12 for some representative IFTs).

Effect of viscosity

Figure 52 relates observed residual saturations to non-wetting phase viscosity. Residual saturations would be expected to be independent of viscosity over the range of viscosities encountered, and the results match expectations. Some variability in S_{or} might have been possible had fingering occurred during the displacements, but since low flow rates were used and since the displacements were stable with respect to density, no viscous instabilities developed.

Effect of density

A plot of observed residual saturation versus non-wetting phase density is shown in Figure 53. There appears to be no overall correlation between density and S_{or} and none was expected. However, fluids having a larger density difference with water tend to give more

PRIORITY POLLUTANT	INTERFACIAL TENSION (dyne/cm)
carbon tetrachloride	45.0
PCE	47.5
benzene	35.0
chlorobenzene	37.4
ethylbenzene	38.4
toluene	36.1
phenol	39.3[A] (40°C)
o-chlorophenol	42.25[B]
naphthalene	28.8[B]

A — Lyman et al., 1982
B — Weast, 1986

Table 12.   The interfacial tension of some priority pollutants with water at 20°C. The data were obtained from Girifalco and Good (1957) unless otherwise noted.

accurate results due to the gravimetric method of measuring saturations. A larger density difference increases the buoyancy forces, but in this case they are well below the threshold for gravity induced reduction of trapping. However, had a very coarse soil been tested — a gravely soil perhaps — buoyancy effects might not have been negligible.

For those organics lighter than water, there appears to be a decrease in S_{or} as the density of the fluids approach one (as the density difference between the organic and water approaches zero). Such results are the opposite of what one would expect had buoyancy played a role. These results are probably a coincidental effect of the reduced measurement accuracy as ϱ_o approaches ϱ_w.

PCE was the only organic liquid tested having a density greater than water. Although the PCE experiments were run with the column upside-down to prevent any density induced instabilities, it is important to realize that on an aquifer scale as a dense organic liquid percolates downward through the saturated zone, density induced fingering may well develop. For more about density induced instabilities, please refer to the discussion in Chapter 8 on the interaction between density induced instabilities and layering.
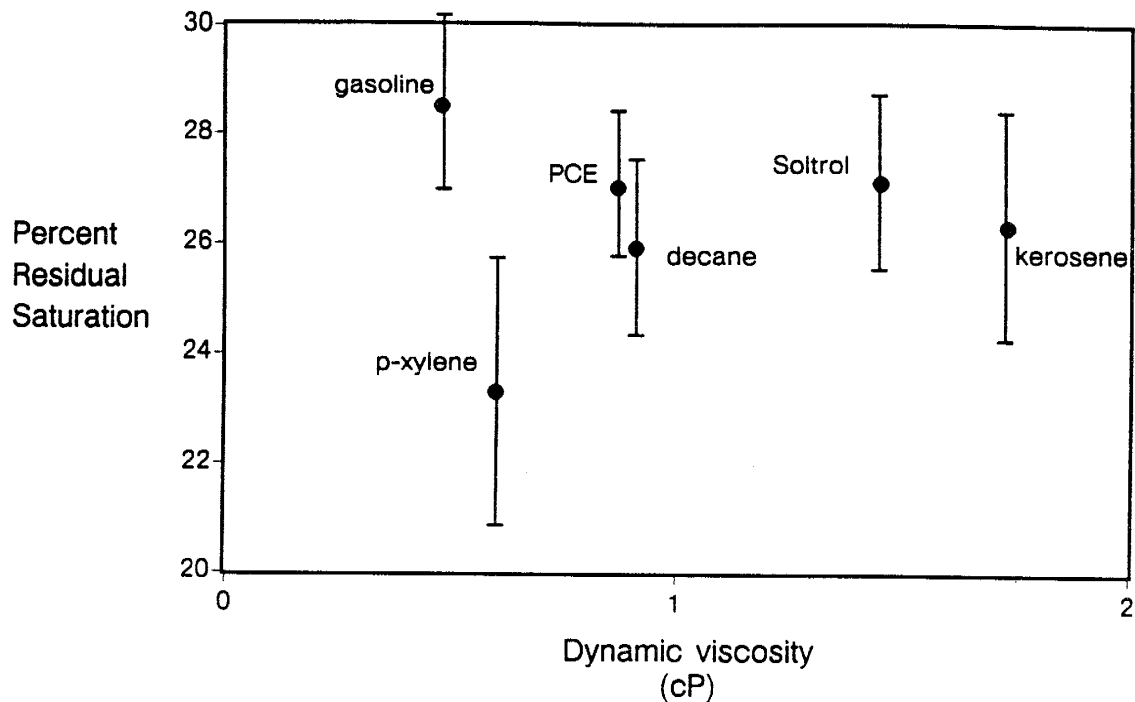
Figure 52. Residual organic saturation as a function of non-wetting phase viscosity. The error bars represent the sample standard deviations taken from Table 11.

Summary

In summary, residual saturation has been shown to be invariant with respect to fluid properties, at least over the range of fluid properties for common organic pollutants used in these experiments. So although it seems reasonable to directly measure residual saturations of whatever organic liquid was spilled at a particular contamination site, it might be better to chose an ideal fluid with which to run residual saturation experiments. Unless some odd wetting behavior is anticipated, or unless some interaction between fluids or between fluids and the solid is expected, it is probably preferable to chose a fluid which has low solubility, low volatility, low toxicity, and a sufficient density difference with water.

Other Soils

Palouse loam

Two quantitative experiments were run with Soltrol and the Palouse Loam soil. In the first trial no Soltrol could be forced into the column even though a head of almost 500 cm H_2O was placed on the column. In the second trial the maximum Soltrol saturation reached was 11.7%, with a corresponding water saturation of 88.3% (Figure 54). Great difficulty was encountered in injecting organic liquid into this soil. The inability to inject an organic phase into the Palouse loam did however demonstrate that fine-grained, water-wet soils (which do not shrink in the presence of organics) can serve as an effective barrier to organic liquid movement in the subsurface.
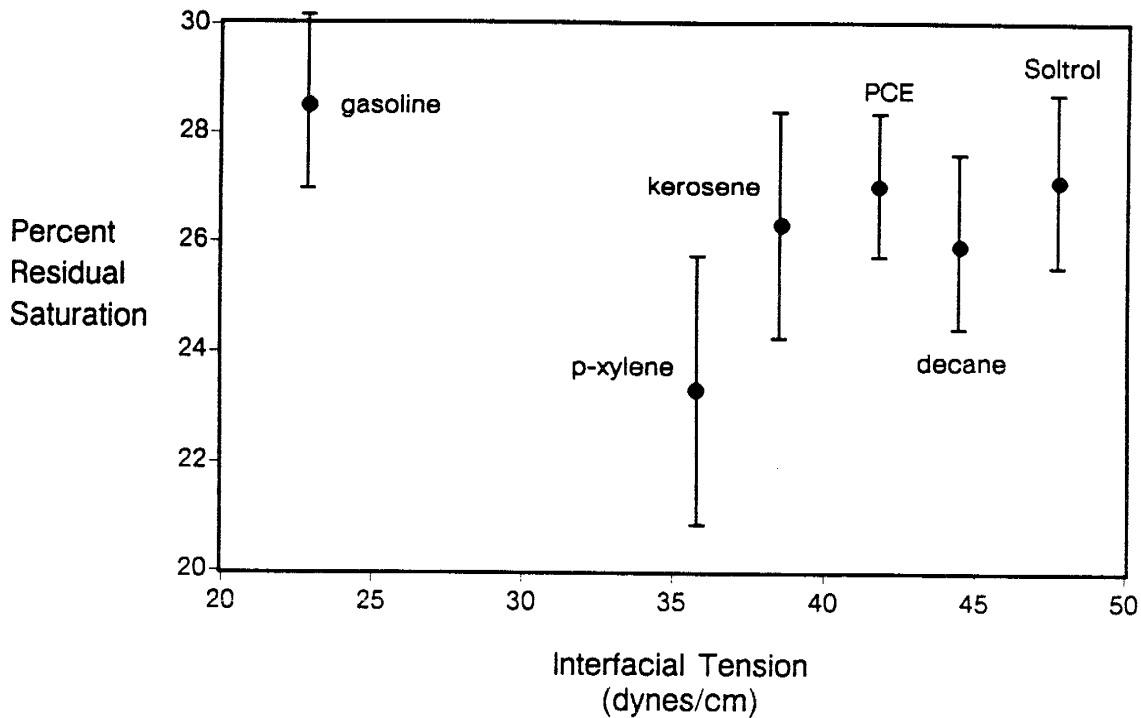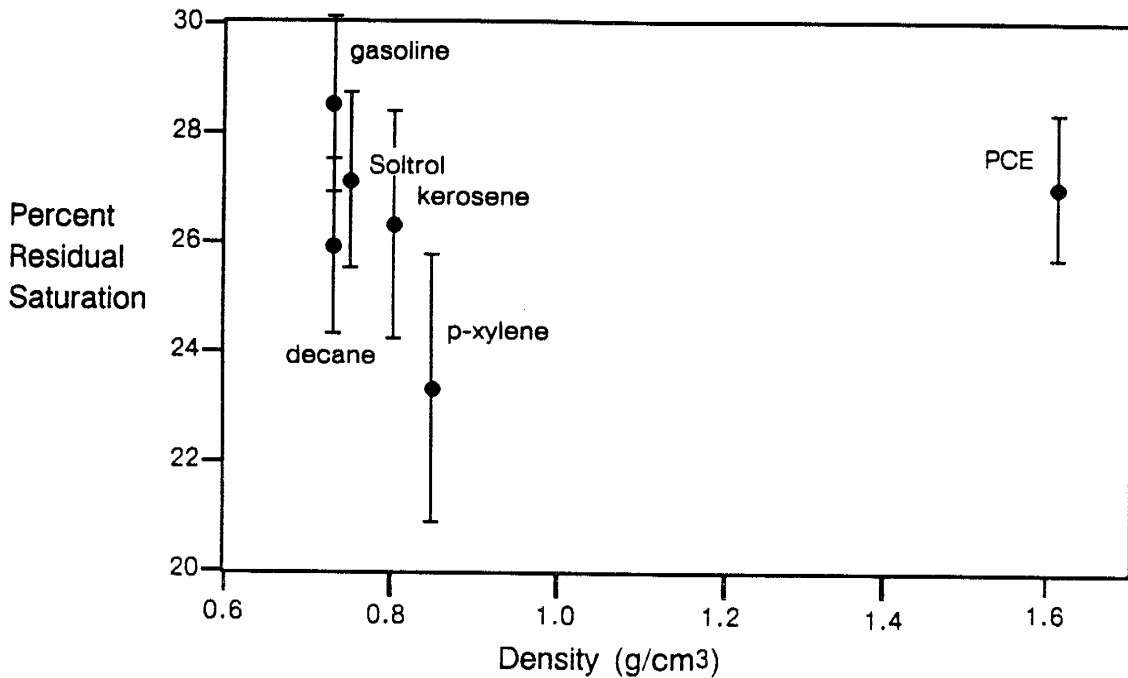
Figure 53. Residual organic saturation as a function of non-wetting phase density. The error bars represent the sample standard deviations taken from Table 11.

Llano coarse sand

Results from a series of related experiments yielded a residual saturation measurement of 17.2% for Soltrol in the Llano soil (Wilson et al., 1989). This residual saturation is similar to values reported for glass beads (about 15%, Morrow et al., 1988), and is much lower than the S_{or} measured for the Sevilleta sand (27.1%).

Traverse City sand

The results of four experiments conducted with Traverse City soil and Soltrol are shown in Table 13. All experiments were conducted under good temperature control conditions. The average residual saturation of Soltrol in the Traverse City soil was 17.6%. Surprisingly, this saturation was almost 10% lower than the residual saturation found in the Sevilleta soil, even though these two soils have very similar texture (see Figure 18). In fact, the average S_{or} measured in the Traverse City sand was almost identical to the S_{or} measurement in the Llano soil, and therefore also similar to residual saturations reported for glass beads.

Effect of soil texture

Perhaps it is appropriate to ask, *Why are residuals in the Sevilleta sand so high?* After all, one would expect a uniform, unstructured, coarse soil to behave in a manner similar to glass beads — as the Traverse City and Llano sands presumably did.

In packing soil under water into the columns, undoubtedly some small-scale layering developed. Perhaps significantly, the Sevilleta sand contains a small but not negligible fine fraction not present in either the Traverse City or Llano sands which may play an important role in
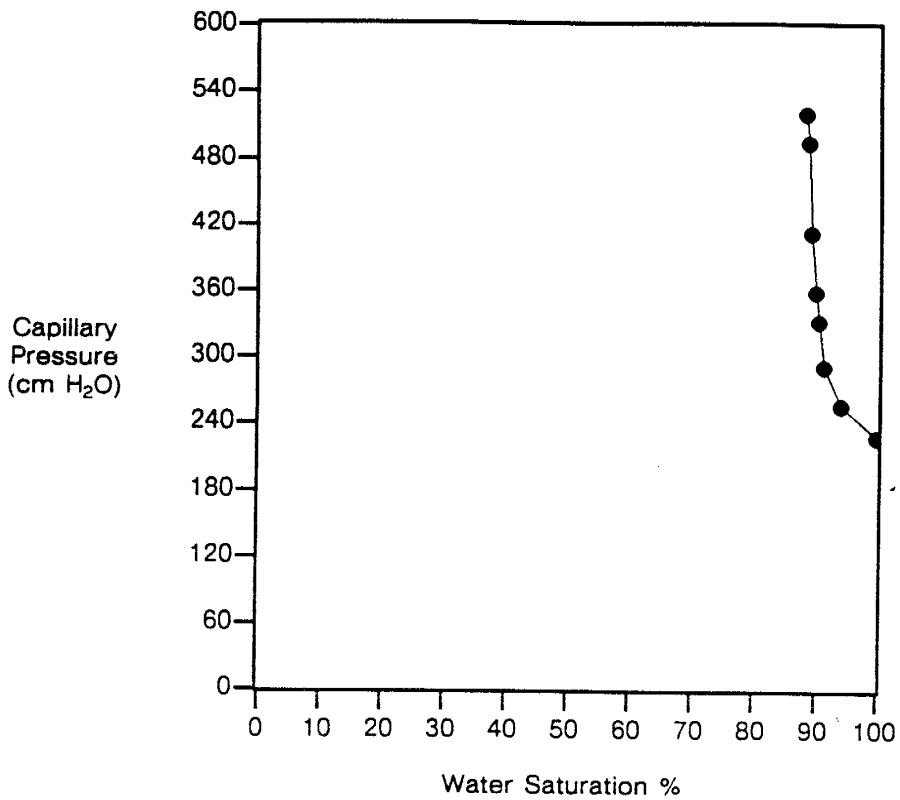
Figure 54. Organic/water saturation versus capillary pressure for Soltrol in the Palouse loam.

| Trial | porosity (%) | error (%) | bulk density (g/cm³) | error (g/cm³) | Organic liquid saturation (%) | | | | Temp. range (°C) |
					maximum	error	residual	error	
1	34.4	0.6	1.738	0.009	85.1	7.3	17.0	2.4	0.7
2	35.7	0.6	1.705	0.010	84.6	6.8	15.8	1.9	1.9
3	36.0	0.6	1.696	0.009	86.6	6.9	19.3	2.2	1.7
4	33.9	0.6	1.753	0.010	88.0	7.2	18.4	2.1	1.1
Avg.*	35.0	1.0*	1.723	0.027*	86.1	1.5*	17.6	1.5*	----

* Average = sample mean ±standard deviation

Table 13. Summary of Soltrol / Traverse City soil saturated zone results.

the formation of layers in the column. Due to differential settling (Stoke's law), any soil containing some fines can be expected to develop micro-scale layering as it is packed under water.

As a matter of fact, drainage of water-filled Sevilleta sand by air (in step one of the three-phase experiments) showed that small-scale layering was present in Sevilleta sand columns packed under water. Through the glass walls of the column, air could be observed entering the column as drainage commenced. As the pressure drop propagated through the column, at a certain pressure slightly coarser micro-layers drained while finer micro-layers remained water filled. As the pressure continued to drop, the finer layers then drained as well. The layers were observed to be on the order of 1-3 mm thick. The difference in air-entry pressure heads between the coarse and fine micro-layers was on the order of about 1 or 2 cm H_2O. As an aside, McCord et al. (1988b) found micro-scale layering in the natural (wind blown) deposition of the Sevilleta dune sand as evidenced by the state-dependent anisotropy of the sand.

As an offshoot of this study, Wilson and Mace (1989) removed the fine fraction from the Sevilleta sand and measured residual saturations. They reported an average residual saturation of 16.9% from 10 trials, a residual saturation much lower than that found for the unadulterated Sevilleta sand, but similar to those measured for the Llano coarse sand, the Traverse City sand, and glass beads. The dramatic reduction in residual saturation consequent with removal of the fines from the Sevilleta sand suggests that the formation micro-layers can have a dramatic impact on the residual saturation.

The effect of heterogeneities on multi-phase flow are explored in detail in the next chapter. At the conclusion of that chapter, after some observations on how heterogeneities affect multi-phase flow have been presented, the case of the Sevilleta sand is revisited and a hypothesis offered for why residual saturations were so high. In the meanwhile, I'll leave one final question for the reader: *In measuring S_{or} in the laboratory, should great pains be made to eliminate heterogeneities from the soil packings even though similar micro-scale heterogeneities are produced by natural depositional processes in so-called homogeneous soils?*

FLOW VISUALIZATION

Flow visualization techniques are ideal for illustrating the process of organic liquid advance in the saturated zone and subsequent displacement by flowing groundwater. Later, results from these homogeneous experiments are compared to the organic migration in the vadose zone, and migration of organics through heterogeneous media in the saturated zone. The following two micromodel sections are an expansion of discussions first presented in Wilson et al. (1988b).

Organic Liquid Advance in a Homogeneous Micromodel

A water-wet etched glass micromodel experiment (Figures 33 & 55) serves as good example of the displacement process of organic liquid movement into a water-saturated homogeneous

a)

top

flow →

b)

top

flow ←
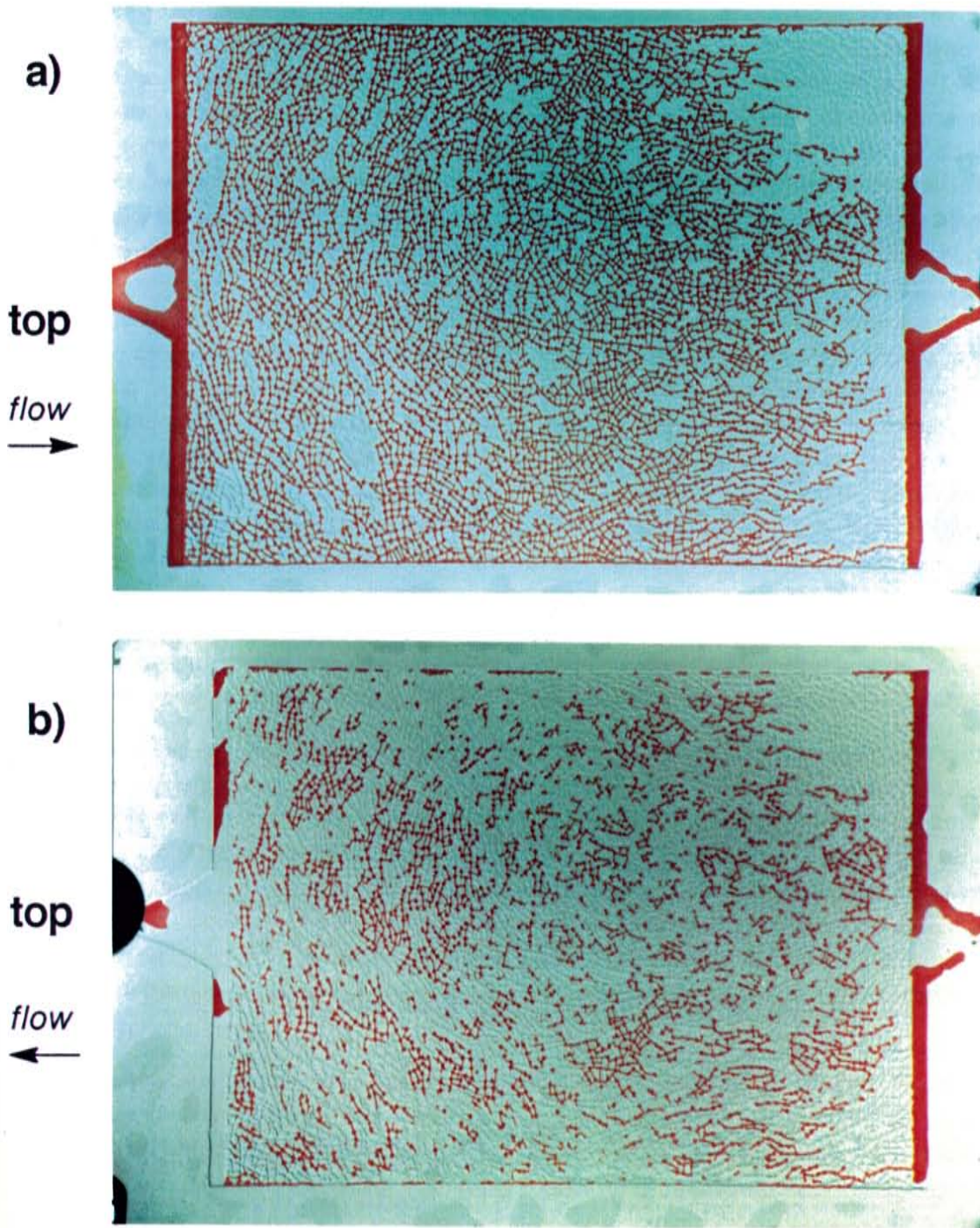
Figure 55. In the upper photo (a) Soltrol displaced water from the left (the top of the model) to the right (the bottom of the model), yielding a residual (irreducible) wetting phase saturation. In the lower photo (b) Soltrol was displaced by water from the right (the bottom of the model) to the left (the top) yielding a residual non–wetting residual saturation. Soltrol was dyed red; the water was not dyed. The photos record steady state flow conditions at the end of the displacements.

soil. The water-saturated micromodel was oriented vertically, and flooded from the top with red-dyed Soltrol at a relatively slow rate of 0.096 ml/min using the techniques described in Chapter 6. These displacements were captured on videotape (Mason et al., 1988). The equilibrium condition, at the end of the organic liquid advancement, is shown in the top photographs of Figures 55 through 57. Figure 55a shows the entire model at equilibrium saturation, while Figures 56a and 57a show close-ups from this displacement. Figure 56 is from an area located very near the top of the model, and slightly to the right of center. Figure 57 shows an area located just below the very center of the model. Overall the displacement of water was fairly efficient, except at the bottom of the model where a capillary end effect came into play (see Figure 55a). The residual water saturation occupied several by-passed pockets of the pore network, as well as films, rings and wedges in individual pores. The term 'film' refers to the film of wetting fluid covering all glass surfaces; 'ring' refers to the pendular rings of wetting fluid found in many of the pore throats; and 'wedge' refers to the wetting fluid in the narrow crevices of the the pores, where the glass plates meet. (These films, rings,and wedges are similar to those that are observed in natural porous media — natural pores are not circular, nor are micromodel pores.) The capillary end effect is similar to what one would find in a fine sand layer overlying a coarse sand or gravel layer. The micromodel pore network represents the upper fine sand layer. The bottom model reservoir mimics the lower gravel layer. The organic liquid breaks though to the lower layer along one, or perhaps two flow paths. The continuing flow of organic liquid takes place through the one or two connected flow paths, which offer less resistance than displacing water from the many remaining water-saturated pores (Mason et al., 1988).

Had a capillary barrier been used at the bottom boundary, it is believed that the residual water saturation would have been somewhat smaller. Not only would there have been no capillary end effect, but slowly moving water in pockets and the wedges would have been more likely to drain. This assertion is supported by evidence from a study by Dullien et al.(1986) who build a heterogeneous model with a checkered pattern of coarse and fine pore zones. They embedded the outlets in two of the fine zones, in effect simulating a capillary barrier at the outlet of the model. Their micromodel experiments, and related sandstone core experiments, appear to confirm the hypothesis that residual wetting phase saturation depends on the outlet boundary condition.

These micromodel experiments were reproducible. An example is shown in Figure 58. The photograph in this figure can be compared to Figure 55a, and depicts the results of an identical experiment, where Soltrol has advanced into the micromodel, displacing water. The character of the saturation pattern is similar for both experiments, only the details vary. The two-phase flow field appears to be a stochastic process, with the same mean behavior, but a different detailed realization for each experimental replication.

Displacement of Organic Liquid by Water in a Homogeneous Micromodel

In the next step, water was displaced upward through the micromodel at the same rate, pushing much of the Soltrol out, but leaving behind a capillary-trapped, residual Soltrol saturation. When the model reached a new equilibrium, additional photos were taken. The bottom photos of Figures 55 through 57 depict the residual organic liquid left behind. As seen in

a)

top

flow →

b)

top

flow ←
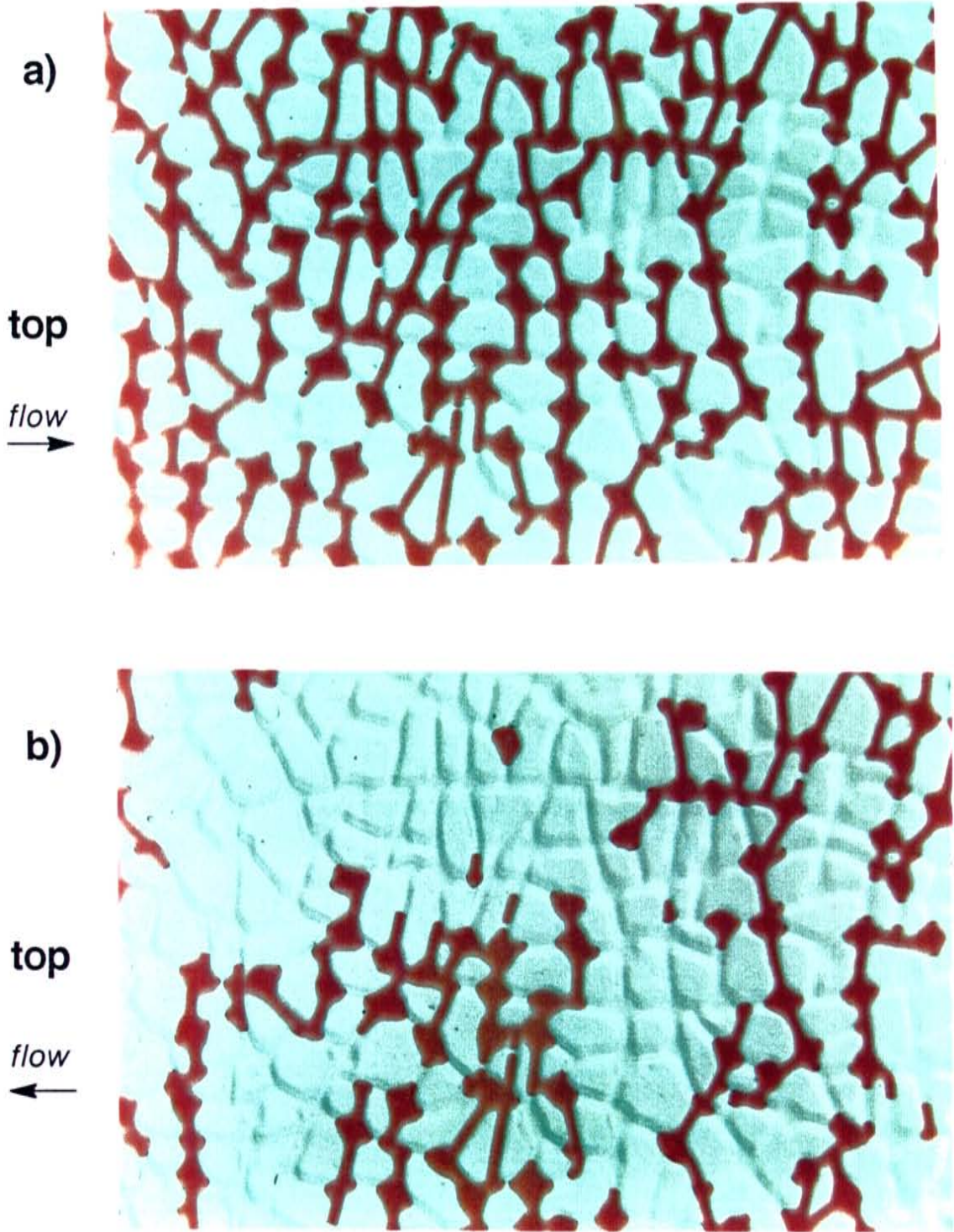
Figure 56   Detail from Figure 55 showing conditions following the displacement of the water by Soltrol (a), and at residual non-wetting phase saturation (b). The area is located near the top of the model, just to the right of the centerline.

a)

top

flow →

b)

top

flow ←
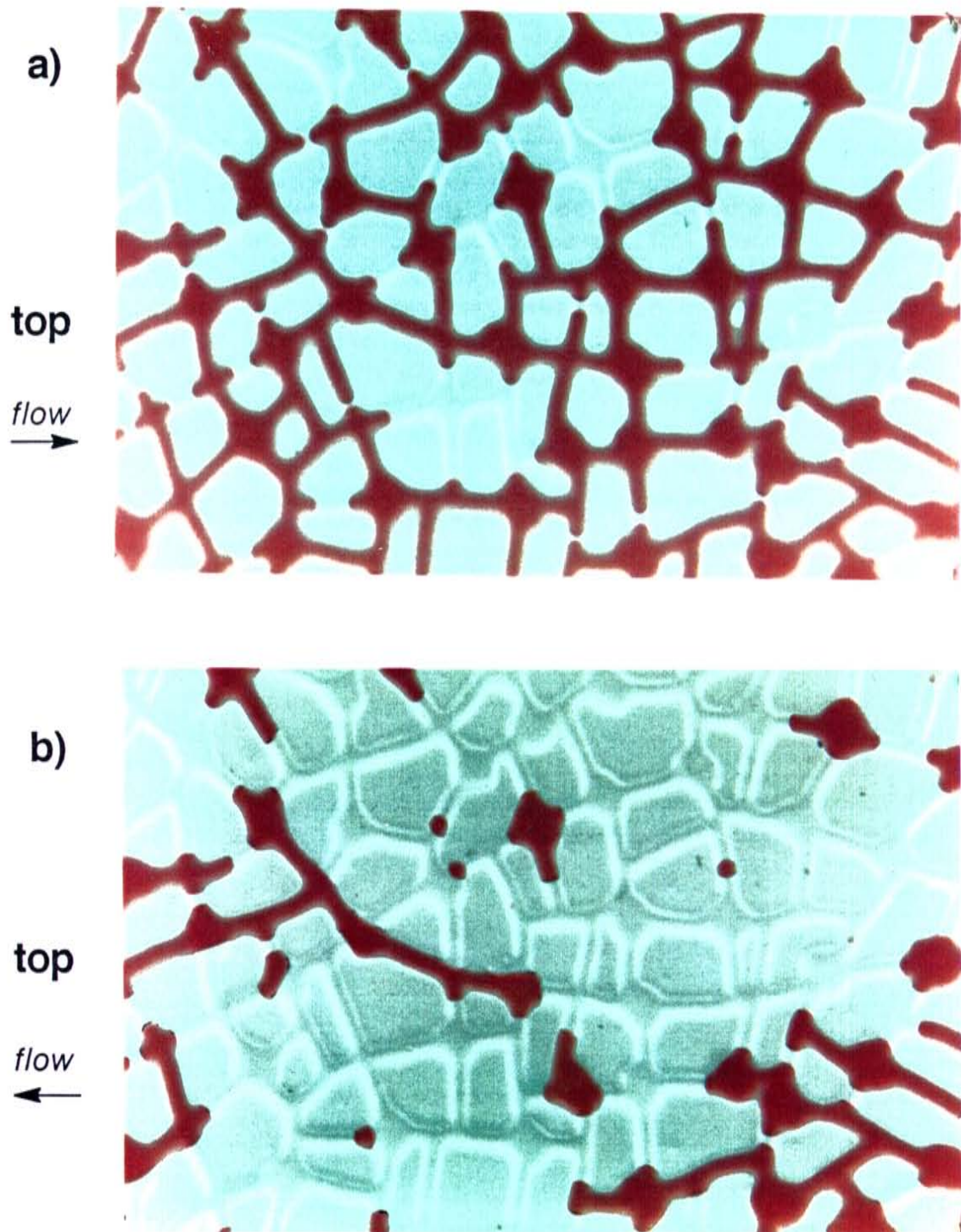
Figure 57   Another detail from Figure 55 showing conditions following the displacement
of the water by Soltrol (a), and at residual non-wetting phase saturation (b).
The area is located just below the very center of the model.

these photos, the residual organic liquid saturation in these strongly water-wet models is composed of disconnected blobs and ganglia which are fairly evenly distributed throughout the model and appear to occupy up to 30% of the pore space .

Microscopic Inspection of Blob Size and Shape in Micromodels, Pore Casts, and Blob Casts

Figures 59 and 60 present 'pore scale' close-ups of typical blobs taken from similar experiments conducted in the same micromodel (Conrad et al., 1989; Mason et al., 1989b). The top photo of Figure 59 shows a blob trapped in a pore body. This blob is referred to as a 'singlet'. The surrounding pore throats are filled with water, the wetting fluid. The trapped singlet is roughly the size of the pore body. The bottom photo of Figure 59 depicts a 'doublet', a blob occupying two pore bodies and the pore throat between. Although many blobs have shapes like this singlet and doublet, some are more complex and extend over a number of pores bodies and the connecting pore throats, such as the micromodel blobs shown in Figure 60. Other examples of
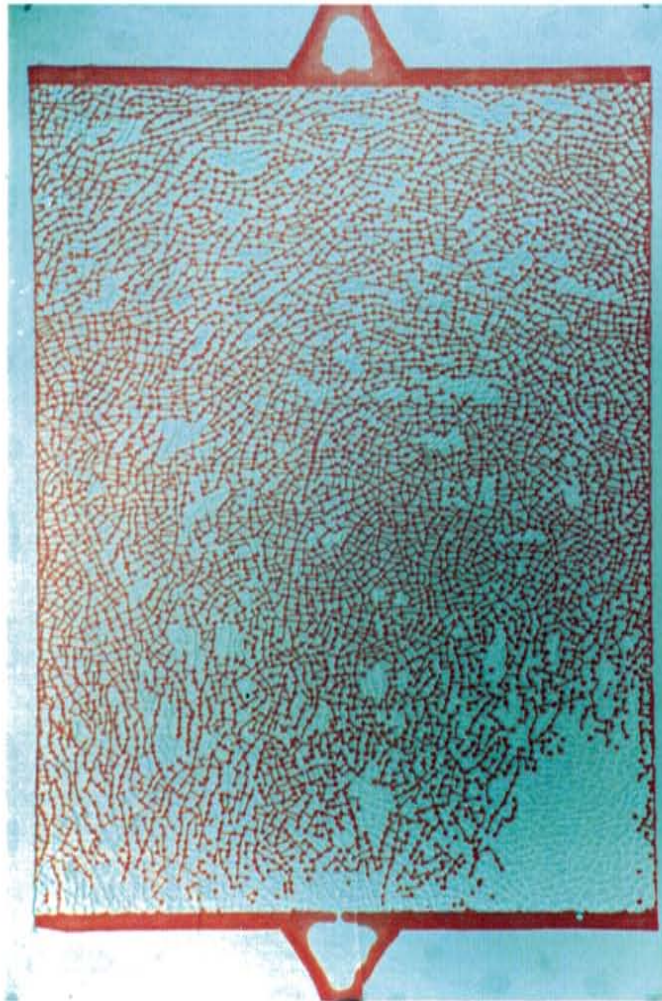
Figure 58.   A second experiment in the homogeneous micromodel, depicting conditions at the end of the organic liquid advance. Compare to Figure 55a .
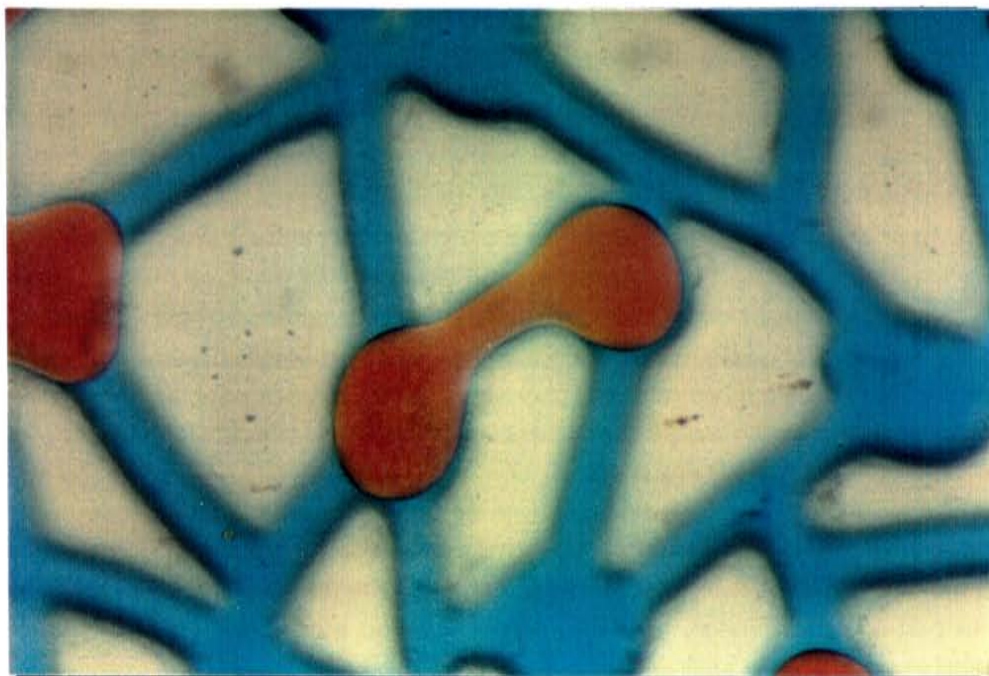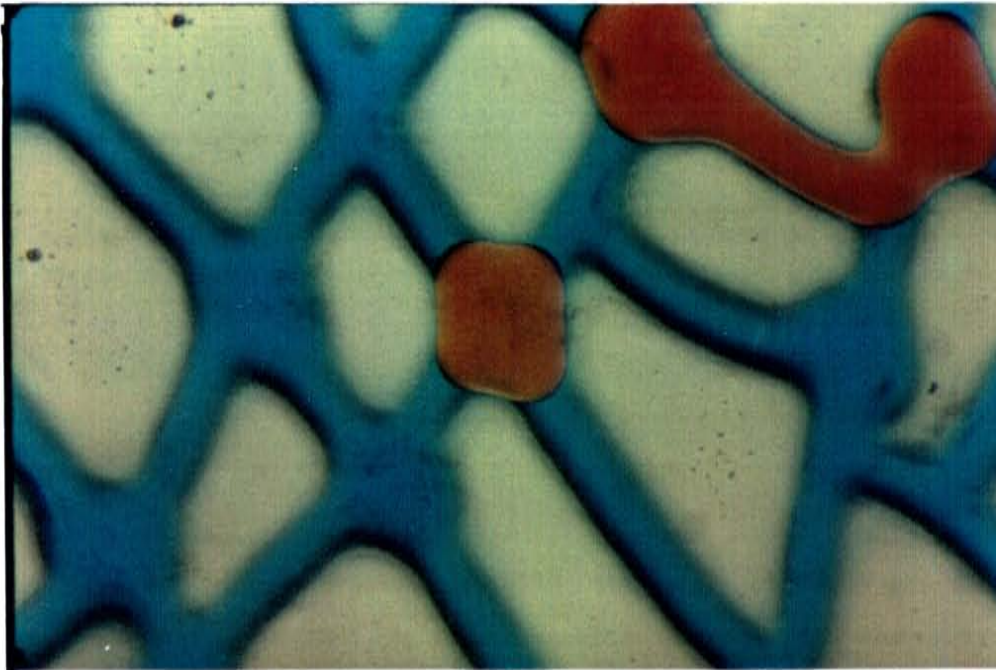
Figure 59. Photomicrograph of a singlet blob (above) and a doublet blob (below) as observed in the micromodel.

Figure 60.   Photomicrograph of a complex blob observed in the micromodel.

both simple and complex blob shapes can be seen in the right-hand photos of Figures 55 through 57. These more complex shapes include branched blobs with more than two 'heads'.

The same features were observed in the soil columns. Photomicrographs of polymerized blobs embedded in epoxied pore casts are shown in Figures 61 and 62. These pore casts were constructed in short TFE columns of Sevilleta soil using the techniques described in Chapter 5. Compare the singlet and doublets shown in Figure 61 from the soil column (Wilson et al., 1988b; Conrad et al., 1989), to those in Figure 59, from the micromodel. The similarity between blob shapes in the two different media gives confidence that micromodels can reasonably be used to simulate the immiscible displacements taking place in the subsurface. Figure 62 shows a variety of more complex blobs found in the same pore cast. The pore casts also reveal the position of the blobs within the pore space, and their position relative to the sand grains. In the pore throats, there appears to be only a thin film of water between the blob and the sand grain 'pore wall'. The micromodel mimics this behavior (Figures 59 and 60). There is, however, a difference in the observed behavior. Micromodel blobs appear to occupy most of each pore body they are found in, again leaving only a film of water between the blob and the pore wall. Blobs in the Sevilleta pore casts indicate a greater pore body saturation with water, perhaps due in part to greater surface roughness and irregularities in the pore walls of the Sevilleta sand, but more likely due to shrinkage of the styrene blobs as they polymerize.

SEM photomicrographs providing a three-dimensional view of polymerized blob casts from another Sevilleta soil column are shown in Figure 63 (Wilson et al., 1988b; Peplinski et al., 1989). The rough spots on the surface of these blobs is probably due to the SEM coating process. Once
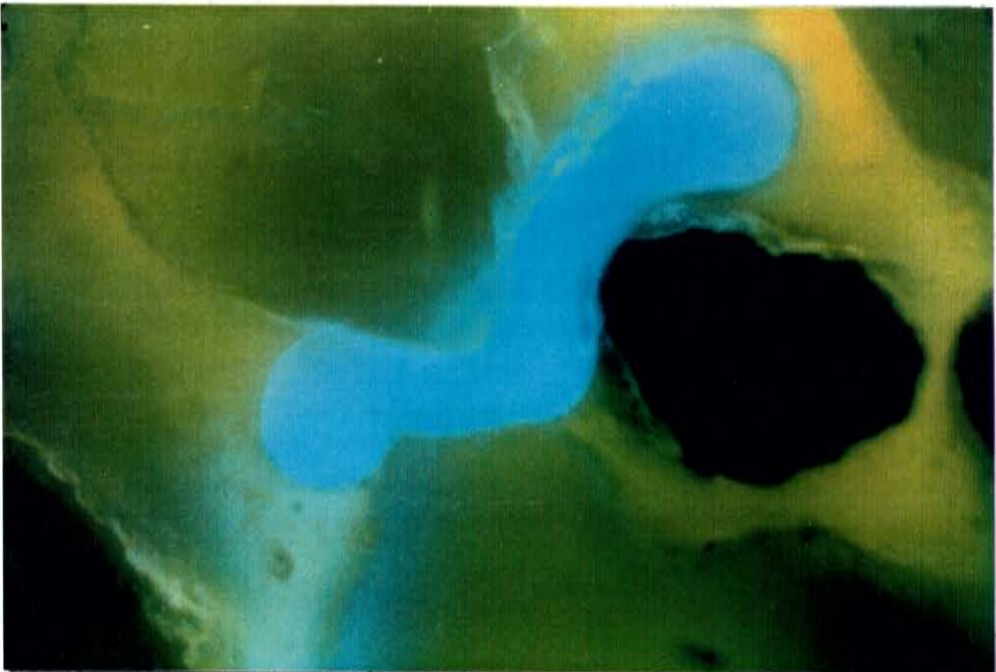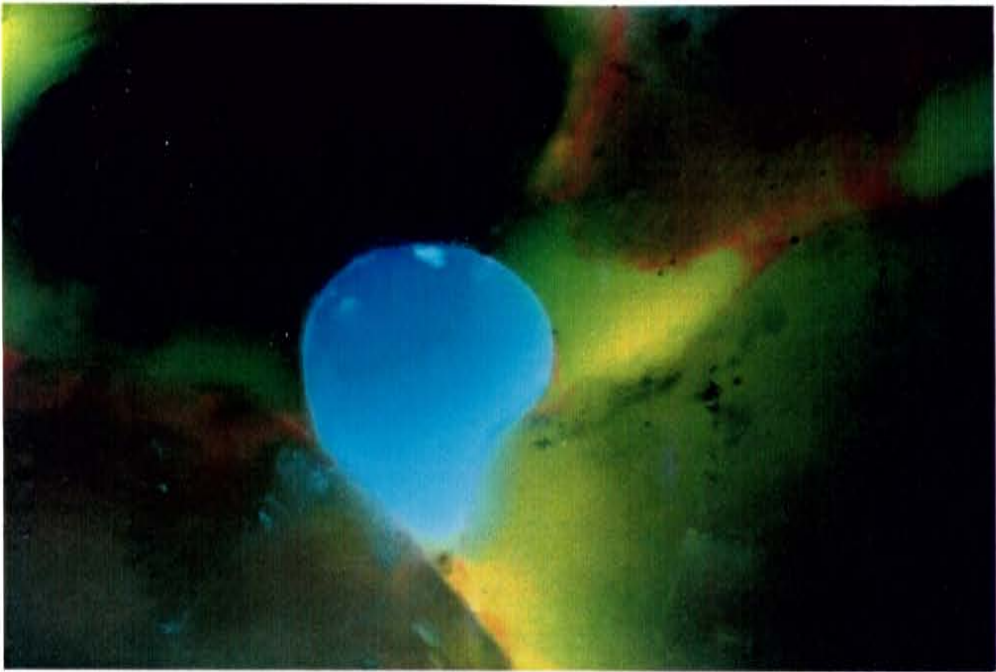
Figure 61. Photomicrograph of a singlet blob (above) and a doublet blob (below) as observed in a pore cast.
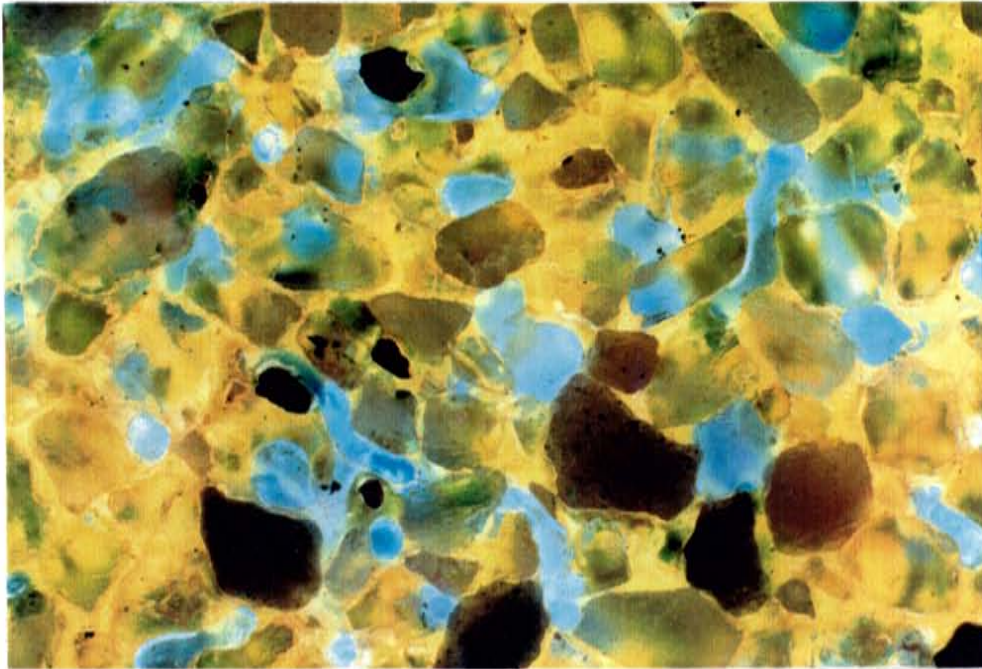
Figure 62. Photomicrograph of complex blobs as observed in a pore cast.

again there is a typical singlet (upper left), and a doublet (lower left). The singlet is almost spheroidal, with a length of 200 microns and a diameter of 100 or more microns. The doublet includes one pore body of roughly 100 microns in diameter, and another that appears to be almost 200 microns in diameter. At the pore throat, the doublet is only 20 microns in diameter. The two more complex shapes involve four (upper right) and six (lower right) pore bodies. The pore bodies of these more complex blob shapes appear to have a diameter of roughly 100 microns, while the typical throat diameter is less than 50 microns. Contrast these diameters with the grain size distribution of the very uniform Sevilleta soil, as given in Figure 18. The mean grain diameter is about 200 microns. Few grains are larger than 400 microns, or smaller than 100 microns. Typical pore body blob diameters tended to be about 100 microns and were sometimes as large as 200 microns. They tended to be somewhat smaller than the mean grain size. The blob lengths depend on the number of pore bodies involved. The singlet in Figure 63 is 200 microns long, the doublet bends through a length of 400 microns, the quadruplet is 800 microns long, and the contorted sextuplet is at least 800 microns long (part of the sextuplet is sticking up into the photo, and thus its entire length is not readily apparent). Several more complex blob casts, taken from the same column, are shown in Figure 64. Here are large, branched blobs occupying 10 or more pore bodies.

At the beginning of this project, it was anticipated that a size and shape analysis would be performed on the pore casts. Such analyses have been conducted on blob casts taken from oil reservoir sandstone cores and glass bead packs by colleagues here at New Mexico Tech's
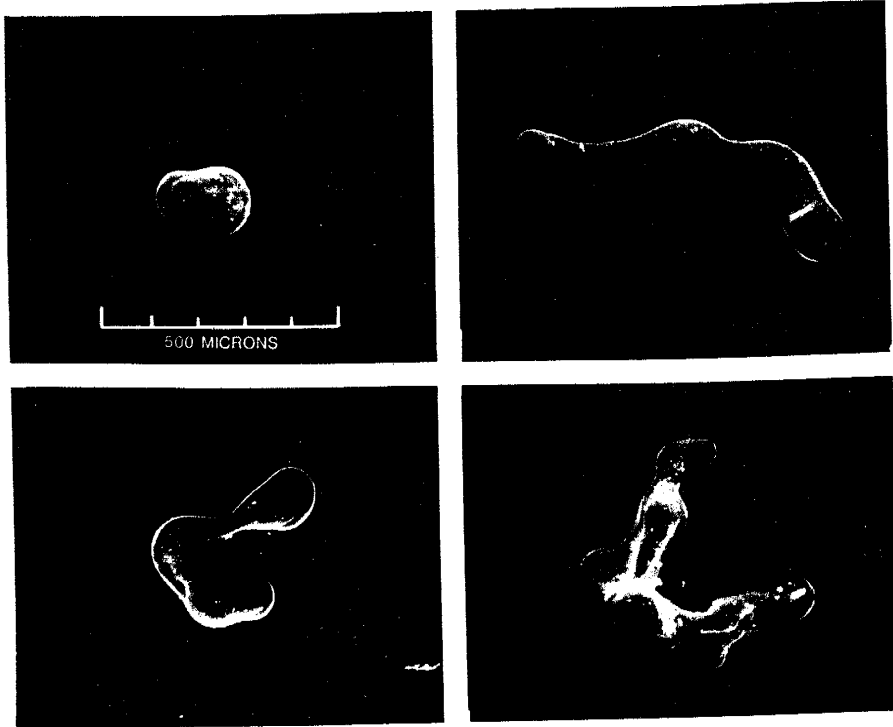
Figure 63.   SEM photomicrographs of blob casts from Sevilleta sand column.

Figure 64.   SEM photomicrographs of branched blob casts from Sevilleta sand column.

Petroleum Recovery Research Center (Morrow and Chatzis, 1982; Chatzis et al., 1983; and Chatzis et al., 1988). As discussed in Chapter 5, the pore casts taken from the Sevilleta soil columns were too fragile for quantitative analysis using a Coulter Counter or even an image analyzer. Many of the larger casts broke into several pieces when handled. The right end of the blob cast depicted in the lower right photo of Figure 64 is broken. This complex blob of roughly 15 pore bodies was even bigger before it broke. The branched blob in the lower left also appears to have broken ends. Breakage of this kind would have severely biased a size analysis. It is possible that the PRRC samples also suffered from the same problem, and their results may be so biased. A second approach would be to use image analysis on the sectioned epoxied pore casts. This approach proved to be beyond the resources of this project, but is strongly recommended in future research efforts.

In strongly water-wet Berea sandstones, Chatzis et al. (1988) found that the majority of blobs were singlets or doublets. The largest, more complex blobs which were often branched, tended to be no larger than 10 pore bodies in size. Fifty percent of their blobs had an 'equivalent diameter' in the range of 30 to 130 microns, consistent with measured pore sizes in Berea sandstone (Wardlaw and Taylor, 1976). In water-wet, uniformly-sized glass beads, Morrow and Chatzis (1982) and Chatzis et al. (1983) found that most of the blobs were trapped as singlets (58%), much more so than in sandstone. Once again the largest blobs measured on the order of 10 pore bodies long. Although by number there were more singlets than any other blob size, they held less than 15% of the volume of the residual saturation. Blobs spanning five or more pore bodies held at least 50% of the residual, even though they constituted less than 24% of the blob numerical population.

Figure 65 is a photomicrograph of a Sevilleta sand pore cast, showing many blobs. Figure 66 is optical photomicrograph of a random sample of Sevilleta blob casts. These photographs indicate that most of the Sevilleta blobs are larger than a singlet or doublet. Upon closer inspection of the pore cast, with a stereoscope, it is seen that most of the blobs, which appear on the surface to occupy only one or two pores, actually extend down into the sample (Peplinski et al., 1989). Blobs commonly wind down and around into the pore network forming 'ghosts' at depth when viewed through the relatively transparent quartz sand. Figure 66 may be somewhat misleading in reference to the size of the blobs since some of the blob casts in the photomicrograph are broken.

Implications for phase partitioning

Blob size and shape influence the partitioning of organic liquid components to the aqueous phase. Mass transfer coefficients used in the mathematical models of this partitioning often employ the analogy of an equivalent spherical blob (e.g., Pfannkuch, 1984). Certainly singlets can be represented by a spherical model, but it is less clear that this model works for the multiple pore-body elongated blobs of Figure 63, or branched blobs of Figure 64. These large complex blobs may be fewer in number than the simple shapes, but they hold the majority of the liquid organic volume. Their surface area to volume ratio is also greater. For multi-component organic liquids it may be easier for these more complex shapes to 'leach out' a lighter organic component than for a spherical blob of equal volume (this equivalent sphere may be much larger than a real pore). But break these complex shapes into many 'model' spherical singlets of
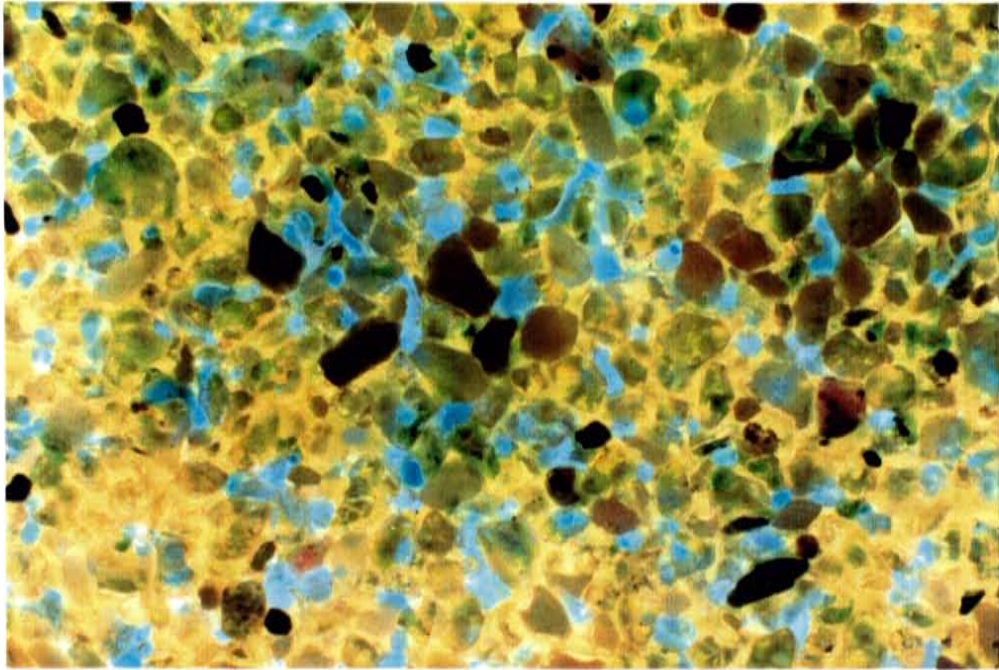
Figure 65.   Photomicrograph of Sevilleta sand pore cast covering many pores.
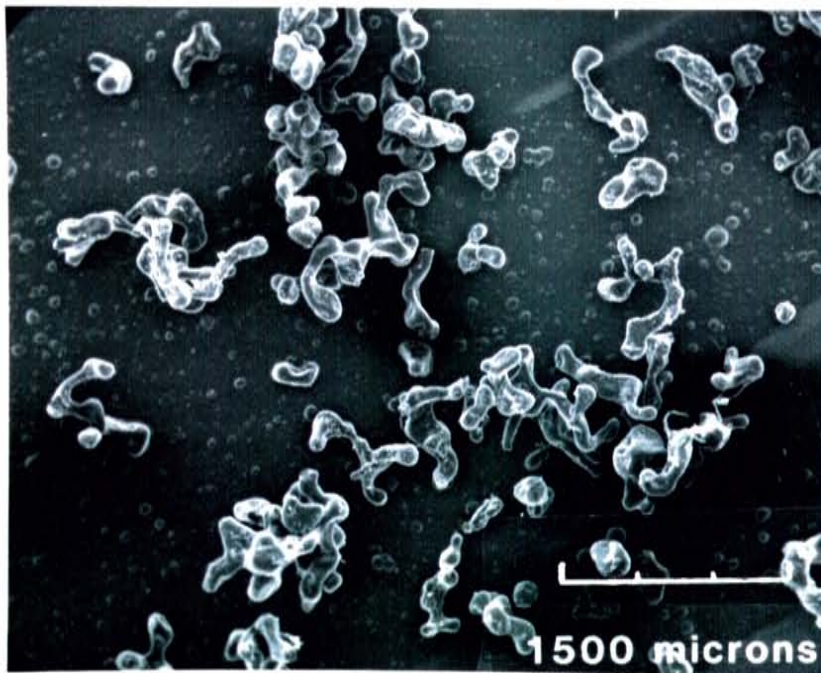
1500 microns

Figure 66.   Optical photomicrograph of many blob casts from the Sevilleta sand.

realistic size, say 100 microns diameter for the Sevilleta sand, and the model leach rate increases dramatically. Coupled with this issue is the fact that there is a distribution of blob sizes and shapes in any sample (see Figures 55b, 65 and 66). An appropriate definition of equivalent sphere size has yet to be proposed, although work is progressing in that direction (Powers et al., 1988).

Particularly for large, branched blobs (such as those shown in Figures 60 and 64) a large portion of the blob surface can be in contact with only a thin film of water along the pore walls. In such cases, the interphase transfer rate may be limited by advection or diffusion through these films of water. Preliminary observations in micromodels indicate that the flowing water tends to move preferentially around the blobs, through completely water-filled pores with relatively little water movement through the films to help advect organic components away (Mason et al., 1988). This initial observation requires additional experimental confirmation, but suggests that diffusion through water films to the main body of passing groundwater may sometimes be the rate-limiting step for organic constituents dissolving into the water phase. Alternatively, it is possible that the majority of organic constituents may enter the water through the ends or 'heads' of the branched blobs, since it is likely that these 'heads' are the only part of the blobs exposed to flowing groundwater. Under such a scenario, the rate-limiting factor could be either the dissolution kinetics across the organic/water interface in the heads, or the diffusion rate of organic constituents to the heads from within the blob itself.

Implications for biotransformation

There are several implications of these observations on the study and practice of biotransformation of organic components. Microorganisms attached to the pore wall, at the water-solid interface, experience an environment that depends on their location. In blob-filled pore throats, the organisms have ready access to organic components that partition into the aqueous phase from the nearby blob surface. However, these organisms may not have a ready supply of other substrates such as oxygen, which can only diffuse (or flow) slowly through the thin water film. In blob-filled pore bodies that have a surrounding water film, the same situation applies, as it does for microorganisms attached to the blob surface in these regions of thin aqueous films. In the other pores, occupied by flowing water, wall-attached microorganisms are readily exposed to available dissolved substrates, subject only to upstream substrate re-supply and biological consumption.

Migration of microorganisms is also probably influenced by the spatial distribution of blobs. It should be difficult for a seed population to find its way into regions with thin aqueous films because of their low flow rates and tortuous diffusion paths. In any event, most organisms would probably not thrive in these stagnant regions because of the substrate re-supply problem and the possibility of toxicity due to locally high concentrations of dissolved organics.

Where exactly within the pore space the growth of microorganisms occurs is important because the growth of microbial colonies will certainly influence the flow field. If, in fact, microbial colonies tend not to develop immediately at the water/organic interface but some distance away where both oxygen and organic substrates are more readily available, then it is possible that the microbes could clog previously water-filled pores resulting in appreciably more

water flowing directly past the blobs and greater dissolution of organic components. On the other hand, one could argue that the growth of microbial colonies would further reduce the permeability to water through the entire region of trapped organics resulting in less flow and less dissolution of organic components.

Glass micromodels would provide an ideal medium in which to study the growth of microbes within a two-phase (organic/water) flow field.

Influence of Displacement Rate

The homogeneous micromodel was rerun at a 'fast' flow rate of 1.5 ml/min, approximately 15 times higher than before (Wilson et al, 1988b; Mason et al., 1989b). The equilibrium saturation following organic liquid advance is shown in Figure 67a. The organic liquid displacement of water was found to be more efficient than before (compare to Figure 55a). The faster flow rate in this displacement generated viscous forces large enough to partially overcome capillary forces resulting in fewer by-passed pockets of water, and possibly less water held in wedges. The capillary end effects were also largely overcome.

This experiment illustrates the misleading nature of the term 'irreducible water saturation' often used to represent the wetting phase residual saturation. Even at residual saturation the wetting phase is continuous, and is composed of an interconnected network of films, rings and wedges (see, e.g., Amaefule and Handy, 1982; Dullien, et al., 1986; Chatzis, et al., 1988) This situation is considerably different than the discontinuous 'blobs' found for a non-wetting phase residual. The wetting phase liquid can move through its interconnected network, draining the films and rings, and reducing the residual wetting phase saturation. Several experiments provide some idea of the correlation between non-wetting phase flow rate and wetting phase 'residual' saturations. The wetting phase residual appears to be a function of non-wetting phase flow rate, although the flow rate must vary over orders of magnitude before the change in residual is significant (Amaefule and Handy, 1982). This correlation and the micromodel experiments shown here and in Dullien et al. (1986) provide ample evidence that an increase of the non-wetting phase flow rate leads to a decrease of the wetting phase residual. In some cases it may be important to account for flow rate when measuring and modeling the residual water saturation.

The bottom photo (Figure 67b) depicts the residual organic liquid saturation at the completion of a upward displacement by water at the same 'fast' rate of 1.5 ml/min. The residual organic saturation looks similar to that observed after the slow experiment (Figure 55b). Having similar residual saturations for the 'fast' and 'slow' experiments is in accordance with capillary number theory which predicts the same degree of residual saturation until the critical capillary number (or in this specific case, critical velocity) is exceeded. Apparently, that critical velocity was not exceeded in this experiment.

Despite the larger amount of organic liquid in storage before the water displacement in the 'fast' experiment (compare Figure 67a to 55a), the residual saturations between the two experimental trials were similar. One possible explanation for the improved organic displacement

a)

top

flow
→

b)

top

flow
←
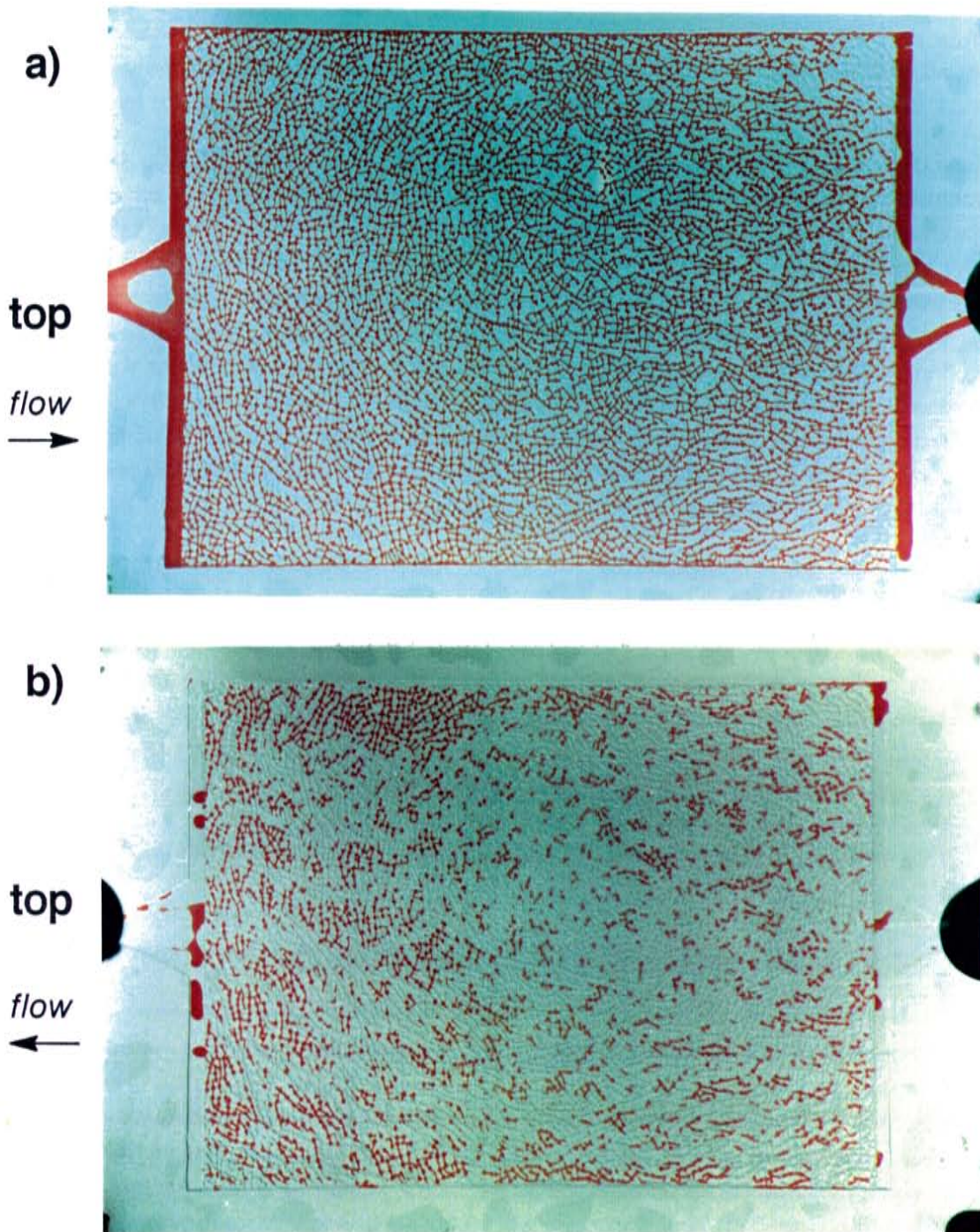
Figure 67. Homogeneous model. In the upper photo (a) Soltrol displaced water from the left (the top of the model) to the right (the bottom of the model), at 1.5 ml/min yielding a residual (irreducible) wetting phase saturation. In the lower photo (b) Soltrol was displaced by water from the right (the bottom of the model) to the left (the top), also at 1.5 ml/min, yielding a residual non-wetting residual saturation. Soltrol was dyed red; the water was not dyed. The photos record steady state flow conditions at the end of the displacements.

efficiency compared to the 'slow' trial is that in the 'slow' trial the relatively large by-passed water zones remaining after organic liquid advance (see Figure 55a) provided pathways for the upwardly advancing water to by-pass organic liquid. In any event, these results are in agreement with the short column experiments in which the residual saturation was found to be relatively insensitive to the maximum organic liquid saturation attained.

Although there appeared to be little difference in the magnitude of the residual saturations between the 'fast' and 'slow' experiments, there was some difference in the configuration of the residual saturations. In the 'fast' experiment, a greater proportion of the residual saturation was left as singlets, doublets, and other small blobs. This finding corroborates evidence presented by Chatzis et al. (1988) that at higher flow rates, proportionally more of the residual becomes trapped as singlets (even though the residual saturation has still not been reduced). These changes in the blob size distribution occur before critical capillary number is reached, but reflect changes in the ratio between viscous to capillary forces. Since changes in blob sizes can affect the partitioning rates, it might be interesting to use micromodels in conjunction with image analysis to look more explicitly at changes in blob size distribution over the progression from low flow rates to the critical flow rate needed for reduction of residual saturation and beyond.

Implications for organic liquid recovery

For homogeneous media, the recovery of organic liquids in the saturated zone would be expected to be independent of pumping rate. Again, this observation is in accordance with capillary number theory (presented in detail in Chapter 2). It should be remembered, however, that natural soils are seldom homogeneous. We'll see in the next chapter that, depending on the type of heterogeneity, organic liquid recovery may in fact be dependent on the pumping rate.

CHAPTER SUMMARY

The experimental results presented in this chapter have examined two-phase (organic/water) movement and capillary trapping in homogeneous porous media.

First, measurements of residual Soltrol saturations in the Sevilleta dune sand were presented. It was found that temperature control was important for obtaining consistent results. The measured residual saturations were independent of the variability in packing from one experimental trial to the next and relatively insensitive to the maximum organic liquid saturation attained. The average residual saturation measured in the Sevilleta sand was 27.1%. If this result is at all typical, it says something about the success to be expected when trying to recover organics spilled into aquifers. Even under optimal conditions, hydraulic removal of organic liquids will leave behind a substantial portion of the total spilled volume. Any unrecovered organics constitute a continuous source of contamination to the aquifer as constituents of the organic phase slowly dissolve into the water phase.

Next, residual saturations were measured in the Sevilleta sand for a suite of organic liquids. The fluids were selected as examples of (or surrogates for) commonly spilled organics, and to cover a fairly wide range of fluid properties between them. As expected, residual saturations

were independent of fluid properties (namely interfacial tension, density, and viscosity) over the range of properties tested. Residual saturations measured for xylene were anomalously low, but these low residuals were probably due to dissolution of the xylene into the water over the course of the experiment. Since residual saturation has been shown to be independent of fluid properties, it is probably best to chose an ideal organic liquid when measuring residual saturations in the lab. Such a surrogate for the organic liquid of interest would have the following attributes: low solubility in water, low volatility, low toxicity, and (for gravimetric measurement of saturations) a sufficient density difference with water.

Residual saturations were also measured over several soils. The difficulty in injecting organic liquid into the Palouse loam demonstrated that the high entry pressures required to introduce organic liquid into fine-grained water-wet soils makes them an effective barrier to organic liquid migration. Two sandy soils, the Llano coarse sand and the Traverse City sand yielded residual saturations of 17.2% and 17.6% respectively. These residual saturations were much closer to results reported for glass beads than to the Sevilleta sand results. It is believed that the fine fraction present in the Sevilleta sand but not the other two soils contributed to the formation of small-scale packing heterogeneities and that the presence of those heterogeneities resulted in elevated residual saturations. Similar small-scale heterogeneities have been reported for naturally-deposited Sevilleta dune sand.

Two types of flow visualization experiments — micromodels and organic-phase polymerization — permitted the observation of the pore-scale distribution of organic liquid and water resulting from immiscible displacements. Photographs of pore-scale fluid distributions following organic liquid advance into a previously water-filled micromodel show the residual wetting-phase saturation located in by-passed pores and pore clusters and as films, rings, and wedges within individual pores. In contrast, photographs of trapped organic liquid in micromodels, pore casts, and blob casts show that this residual saturation existed as disconnected blobs of varying size and shape. Although no quantitative analysis was performed on the distribution of blob sizes, direct observations of the residual organic saturation from both the micromodel and the blob polymerization experiments corroborates earlier studies which showed that even in homogeneous media, the majority of the residual saturation is held in large, branched blobs.

As discussed in this chapter, the pore-scale distribution of the residual organic phase may have important implications for dissolution and biodegradation. It was pointed out that because the bulk of trapped organic liquid is liable to be held in branched blobs, the dissolution rates may depend as much upon diffusion and advection of organic constituents through thin water films as upon organic-to-water partition kinetics. Not only might the pore-scale distribution of organics affect the rate of biodegradation, but microbial growth may in turn affect how water flows through the blob-filled pore network.

Finally in this chapter, micromodel experiments were used to examine the influence of flow rate on organic/water displacements. The residual water saturation was observed to be dependent upon flow rate. Higher flow velocities of organic liquid displacing water resulted in reduced residual water saturations. In contrast, the residual organic liquid saturation was independent of flow rate. In these micromodel experiments as in the column experiments, the

residual saturation was shown to be insensitive to the maximum organic saturation attained in during organic liquid advance. Under the higher flow rate, however, a greater proportion of the residual saturation was contained in small blobs — singlets and doublets. The results from these micromodel and column experiments suggest that for the pumping rates attainable in homogeneous aquifers, a higher pumping rate will not result in increased recovery of free product, but it may change the pore-scale distribution of the residual organics. While it has been suggested that the pore-scale configuration of the trapped organic phase has an effect on dissolution and biodegradation, research has not progressed to the point where it is possible determine its relative importance in predicting the transport and fate of organic contaminants.

CHAPTER 8

SATURATED ZONE RESULTS IN HETEROGENEOUS MEDIA

No soil is truly homogeneous. Soils exhibit spatially variable properties that are a result of their original deposition and subsequent diagenesis. The importance of this variability on the flow of fluids and the transport of contaminants has only recently begun to be addressed by most groundwater hydrologists. Gelhar (1986) and Dagan (1986) have reviewed the literature on this topic; conspicuously absent is any discussion of multiphase flow, other than water percolation in a soil with air at a uniform pressure (the Richard's equation approach to two phase flow). Following this approach Yeh et al. (1985a,b,c), Mantoglou and Gelhar (1987), and Ababou et al.(1988) have developed geostatistical theoretical and computer simulation models that demonstrate the importance of soil stratification on moisture movement in the vadose zone. At high capillary pressures, the finer textured layers and lenses of soil absorb water through capillary forces while the coarse layers remain relatively dry and impervious. The net result is a hypothesis that the anisotropy of water permeability is a function of saturation. At low water saturations the fine material is more permeable to water than the coarse material, and water has a preference for horizontal flow along the beds due to capillary forces. At high saturations the coarse material has the greater water permeability, and gravity forces tend to cause vertical flow. This hypothesis has been verified in the field and the laboratory by Stephens and Heermann (1988), Mattson et al. (1988) McCord et al. (1988a,b) and others. A similar observation was made by Schwille (1988) using a hydrocarbon as the wetting phase. Petroleum reservoir engineers have largely ignored spatial variability, although that has started to change. The 1989 SPE Reservoir Simulation Conference had several sessions devoted to the topic, which reservoir engineers refer to as 'reservoir heterogeneity' (Lake and Carroll, 1986; also Moissis et al., 1989; Ewing et al., 1989). Most of this petroleum related work is focused on miscible displacement, involving the advection and dispersion of chemical components in a single non-homogeneous fluid phase. Earlier, Chatzis et al. (1983) briefly examined the effect of reservoir heterogeneity on immiscible displacement, at the pore network level, using heterogeneous glass bead packs. They observed that during water floods the spatial variation of capillary properties can lead to large scale by-passing of oil-filled, coarse bead zones. This observation is consistent with the vadose zone water infiltration studies showing air by-passed in the coarse lenses and layers.

There are conceivably many different types of heterogeneity that may occur in a soil or rock. This research has focused on three simple types. The first is classified as an 'aggregated soil', with strings of interconnected macropores penetrating a homogeneous matrix of micropores. The macropores can also be viewed conceptually as fractures through a consolidated porous rock. The micropores represent the porous matrix of that rock. Figure 43 is an illustration of the micromodel pattern used to represent an aggregated soil. The pore network was identical to that of the homogeneous model presented earlier(Figure 33), with the pores and pore throats selected to be macropores simply enlarged in size. The second type of heterogeneity investigated was lenses of coarse porous material embedded in a matrix of fine porous material. An example of this heterogeneity is gravel lenses buried in a sand matrix. Figure 45 is an illustration of the micromodel pattern used to represent this type of variability. The third type of

heterogeneity was a layered micromodel, illustrated in Figure 44. In all three cases, the pore network was identical to the homogeneous model, but the pores in the coarse zones were enlarged in size. All three types of heterogeneous micromodels could be said to have bi-modal pore size distributions, with one peak associated with the coarse lenses or macropores, and the second peak associated with the fine matrix or micropores. Both the aggregated micromodel and the coarse lens micromodel were run under two flow rates in order to examine the dependence of trapping on flow rate. The recovery of organic phase from the coarse lens micromodel was found to be strongly dependent upon the rate of displacement. These results are predicted by a theoretical model. This model, based on the interplay between viscous and capillary forces, explains why capillary trapping is strongly dependent on fluid flow rate when discontinuous lenses or similar heterogeneities are present.

The coarse lens micromodel experiments were duplicated in short column studies to yield: 1) pore casts of trapped organic liquid in a heterogeneously packed sand column and, 2) quantitative measurements of increased trapping under this type of heterogeneity. There were no short column experiments undertaken per se for either the aggregated or the layered systems. But as for the effect of layering, the 'homogeneous' Sevilleta sand short column experiments are revisited in an attempt to explain the anomalously high residual saturations as a result of layering in the soil column.

In each laboratory experiment, the heterogeneous sample was first saturated with water and then subjected to flooding with the organic liquid (Soltrol or styrene). After the fluid saturations stabilized, the organic liquid was displaced by water, resulting in a residual organic liquid saturation that depended on the type of heterogeneity present and the fluid flow rates.

AGGREGATED MEDIA

Micromodel experiments were conducted to examine the effect of an aggregated structure on the advance and subsequent displacement of immiscible organics (first published in Wilson et al., 1988b). When the experiments were repeated at a higher flow rate, the effect of increased flow on the displacements was observed — but this effect was relatively inconsequential compared to the tremendous impact that the aggregated structure imparted on the movement of the fluids.

Organic Liquid Advance into an Aggregated Pore Micromodel

Soltrol was advanced vertically downward into the aggregated micromodel at a 'slow rate' of 0.075 ml/min. The experiment was then repeated with a 'fast rate' of 1.5 ml/min. The model was strongly water wet. Figures 68a, 69a, and 70a depict the equilibrium conditions in the model at the end of the organic liquid advancement at the slow rate. The close-ups are focused on the same area depicted earlier for the homogeneous model (Figures 56 and 57). The equilibrium condition for the fast displacement is shown in Figure 71a. These experiments have also been recorded on videotape (Mason, et al., 1988).
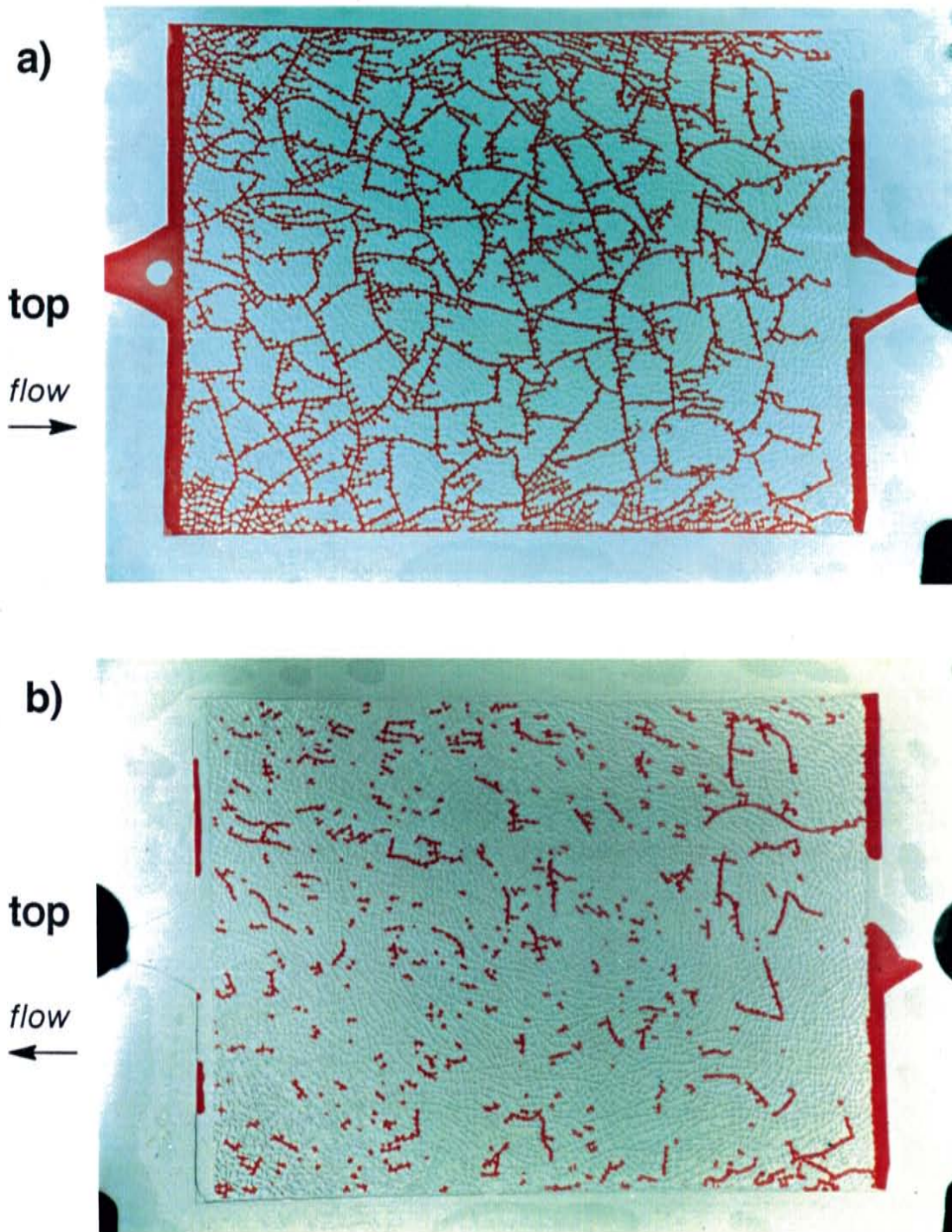
Figure 68. Aggregated model. In the upper photo (a) Soltrol displaced water at a rate of 0.075 ml/min, from the left (the top of the model) to the right (the bottom of the model), yielding a residual (irreducible) wetting phase saturation. In the lower photo (b) Soltrol was displaced by water at the same rate, from the right (the bottom of the model) to the left (the top), yielding a residual non-wetting residual saturation. Soltrol was dyed red; the water was not dyed. The photos record steady state flow conditions at the end of the displacements.

a)

top

flow →

b)

top

flow ←
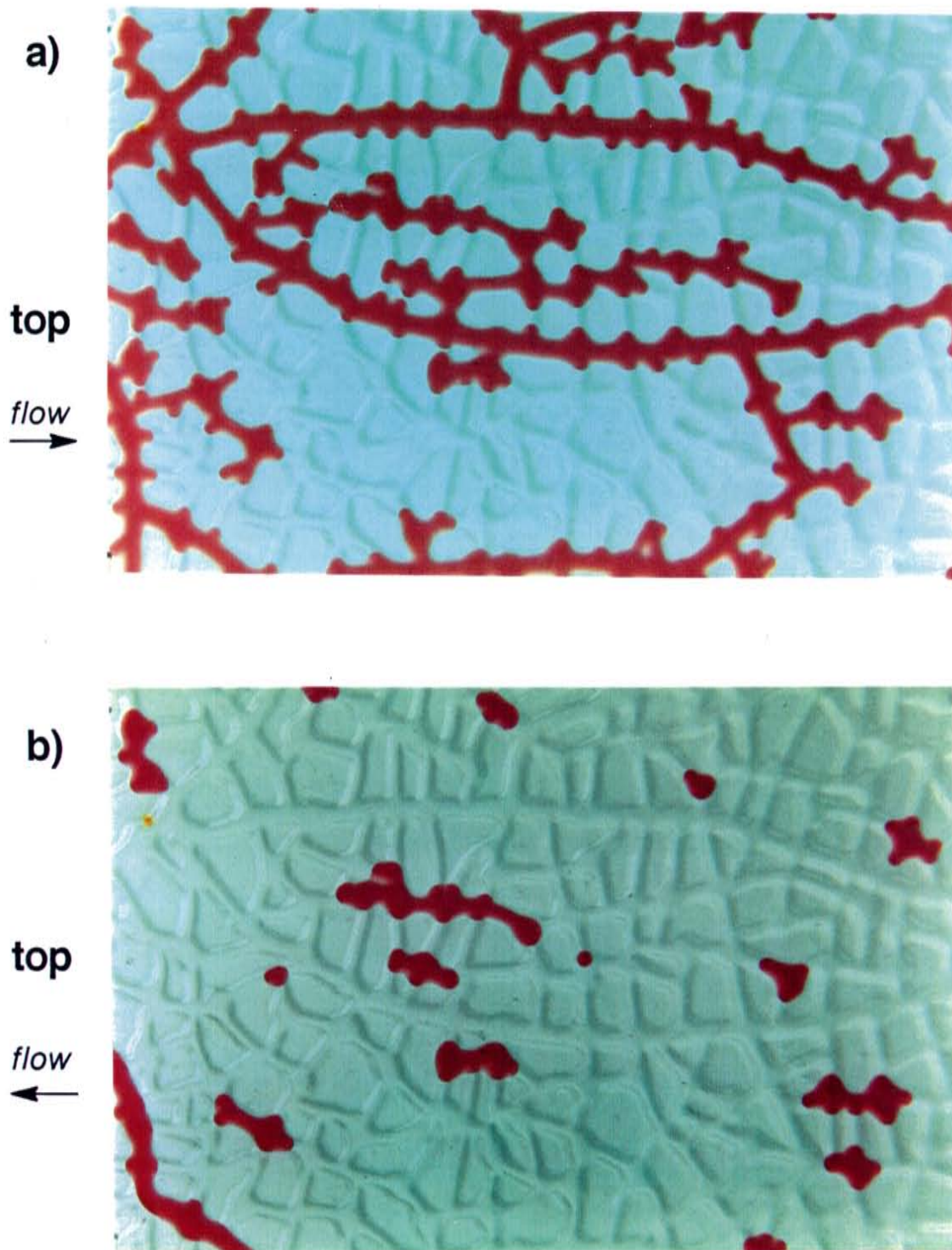
Figure 69.   Aggregated model detail from Figure 68, showing conditions following the displacement of the water by Soltrol (a), and at residual non-wetting phase saturation (b). The area is located near the top of the model, just to the right of the centerline.

120
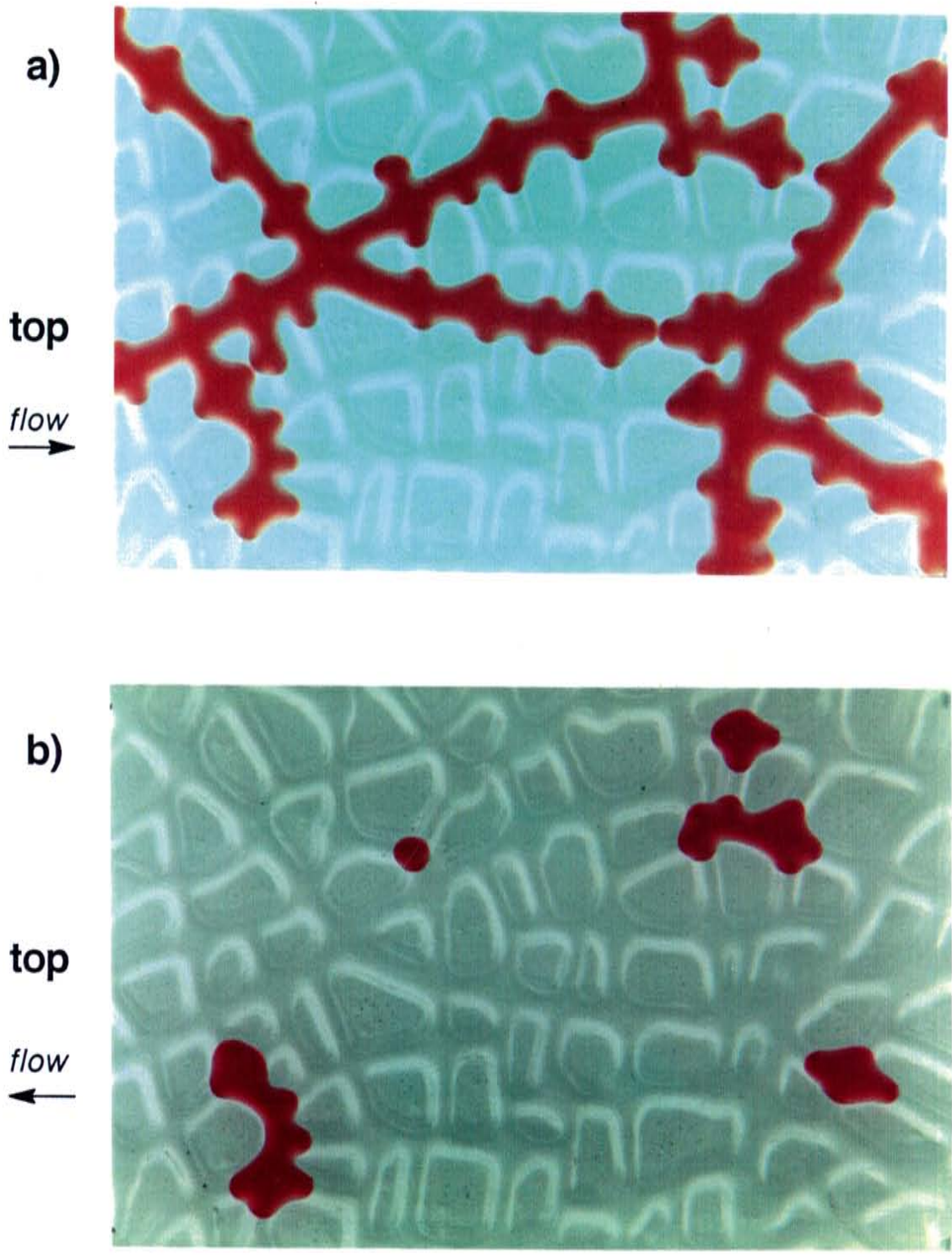
Figure 70. Another aggregated model detail from Figure 68, showing conditions following the displacement of the water by Soltrol (a), and at residual non-wetting phase saturation (b). The area is located just below the very center of the model.
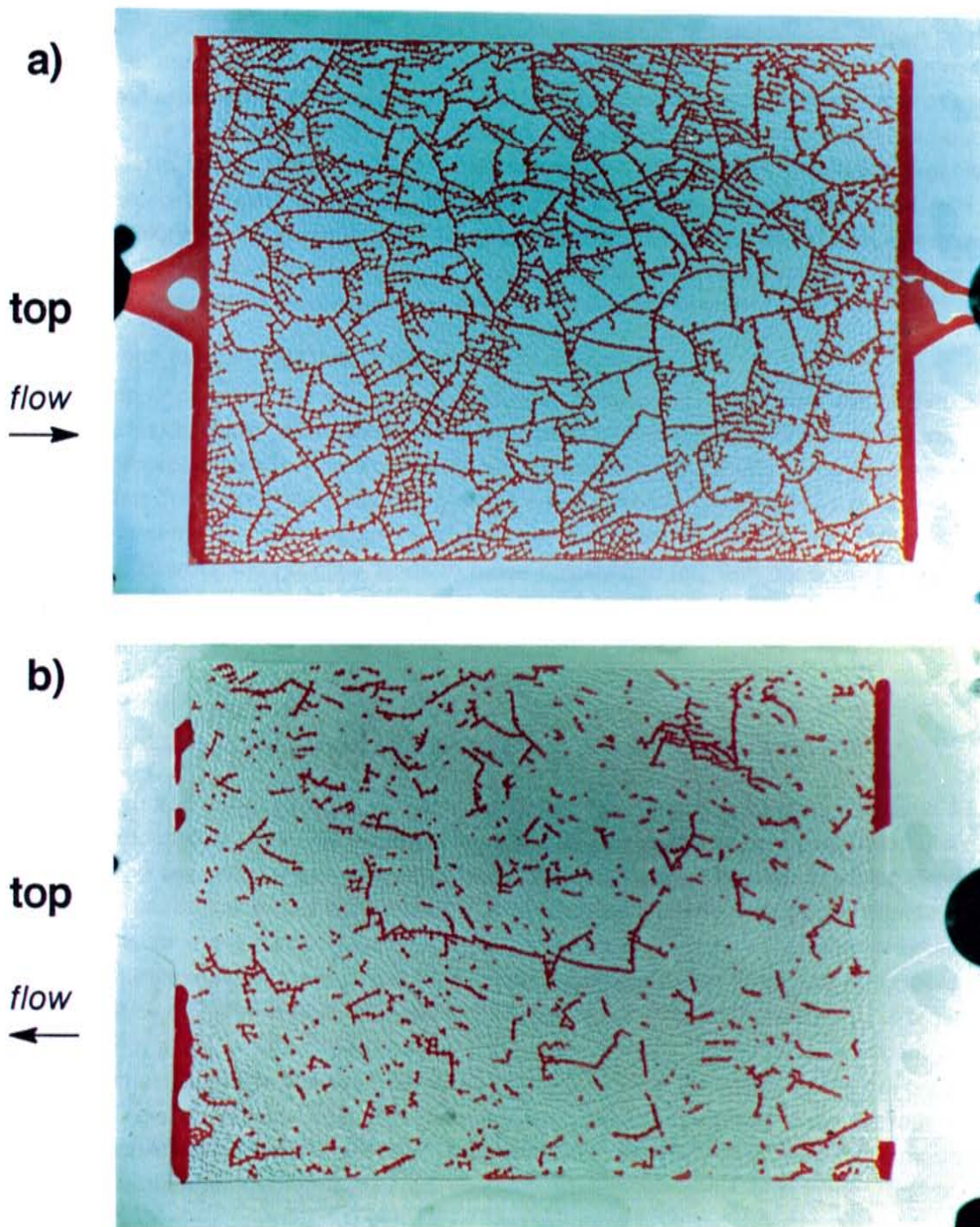
Figure 71. Aggregated model. In the upper photo (a) Soltrol displaced water from the left (the top of the model) to the right (the bottom of the model), at 1.5 ml/min yielding a residual (irreducible) wetting phase saturation. In the lower photo (b) Soltrol was displaced by water from the right (the bottom of the model) to the left (the top), also at 1.5 ml/min, yielding a residual non–wetting residual saturation. Soltrol was dyed red; the water was not dyed. The photos record steady state flow conditions at the end of the displacements.

The equilibrium saturations are similar in character for both rates. Capillary forces caused the organic liquid to preferentially travel through the strings of macropores, almost completely by-passing the water-filled micropores. Because very little organic liquid entered the micropore matrix, the organic liquid traveled across the model much more quickly than it did for the same injection rate in the homogeneous model. This by-passing of the water within the aggregates resulted in a much higher residual water saturation, and a lower maximum organic liquid saturation. Under 'slow' conditions essentially all of the micropores are by-passed, while 'fast' flow conditions permit some organic liquid penetration of the micropores due to the pressure generated by significantly larger viscous forces. The 'fast' flow rate's larger viscous forces also account for reduction in capillary end effects at the lower end of the model.

Implications for spill migration rates and travel distances

In many parts of the country, groundwater consultants commonly distinguish between gasoline leaking from underground tanks in unconsolidated deposits and leaks bedrock. In the unconsolidated deposits, anecdotal evidence suggests that the much of the gasoline is trapped by capillary forces with slow migration of the liquid gasoline. The gasoline tends to appear in nearby streams not as a separate phase, but dissolved in the groundwater discharge. In fractured bedrock the gasoline tends to move quickly and far, with observable liquid gasoline discharges to nearby streams. The aggregated micromodel appears to provide a good analogue to this fractured bedrock situation in which the matrix porosity of the bedrock is by-passed, and rapid migration of the gasoline occurs through fractures.

Displacement of Organic Liquid by Water in an Aggregated Pore Micromodel

The photos in Figures 68b to 70b, and Figure 71b, depict the residual organic liquid left behind after 'slow' and 'fast' upward waterfloods, respectively. In each case, the residual non-wetting saturation largely consisted of by-passed strings of organic liquid left behind in the macropores. Because very little organic liquid initially penetrated into the aggregates, very little organic liquid was subsequently trapped in them, resulting in much smaller residual organic liquid saturations than were found in the homogeneous model. Perhaps coincidentally, the sweep efficiency (the amount of organic liquid recovered divided by the amount of organic liquid originally in place) was actually about the same for the two models. Displacement of organic liquid from the aggregated micromodel was no more efficient than displacement of organic liquid from the homogeneous model, but the observed residual saturations in the aggregated model were much lower because the amount of organic liquid originally emplaced in this model was so much less than for the homogeneous model.

Increasing the flow rate had a relatively minor effect on the residual saturations, yet there was some difference observed between the two experiments run in the aggregated micromodel. The 'fast' experiment led to a slightly higher residual, with more trapping within the aggregates. When the organic liquid advanced into the model at a 'fast' rate it was able to penetrate into a portion of the some of the aggregates. Later, during the water flood, some of this organic was left behind, even though the water flood occurred under high flow rate conditions with significant viscous forces. The low flow rate waterflood led to slightly lower residual organic saturations, not because it was more efficient, but because there was less organic liquid to be removed.

Implications for aquifer remediation

Two-phase flow experiments conducted in an aggregated micromodel demonstrate that the saturation and spatial distribution of organic liquid found behind an advancing front of free product depends on the combined effects of soil heterogeneity and capillarity. The amount of organic liquid that is ultimately trapped within a unit volume of aquifer is strongly dependent on how much organic liquid was originally emplaced within that volume.

Spilled organics can be expected to move quickly through aquifers which have interconnected macropores or fractures. The organic phase travels preferentially through large pores and fractures by-passing smaller pores in the matrix of these dual-porosity systems. The residual saturations left behind following the recovery of free product tend to be comparatively low, but can be expected to extend over a much larger portion of the aquifer.

In this aggregated micromodel, most of the residual organic liquid was trapped as by-passed strings in the macropores. For field sites involving aggregated or cracked soils or fractured rock, the implications are that it will be difficult to hydraulically remove all of the organic liquid from the cracks and fractures. Since real fractures tend to be planar features, rather than the simple linear cracks shown in this micromodel, multiphase flow in the field is considerably more complex than in laboratory micromodel experiments (see, e.g., the videotape on multiphase flow in a single fracture by Wilson et al., 1988a).

MEDIA CONTAINING COARSE LENSES

In a sense, the 'coarse lenses' model serves as the opposite case to the aggregated type of heterogeneity in that the larger pores are discontinuous within a matrix of finer pores while in the aggregated model the larger pores were continuous and the finer pores were discontinuous.

Of the three types of heterogeneity, the 'coarse lens' type was the most extensively investigated. Four complimentary activities were undertaken to examine two-phase displacements through media containing discrete coarse lenses in an otherwise fine matrix: (1) micromodels were run horizontally and vertically, and under two different flow rates allowing visual observation of the displacements under a variety of conditions, (2) pore casts were created in a soil column (qualitatively substantiating the micromodel results), (3) experiments measuring the residual saturations in soil columns were performed (quantitatively substantiating the results of the other experiments), and (4) a predictive model was developed to explain the experimental results. Piecemeal or otherwise less complete versions of these results have been previously presented in Conrad et al. (1988), Mason et al. (1989b), and Peplinski et al. (1989).

In terms of scientific rigor it might be better to present the theoretical model first and support it with the experimental results. But since it may not be intuitively obvious that the presence of discontinuous coarse lenses can lead to large-scale by-passing of the organic phase, the flow visualization experiments are presented first, allowing the reader to develop a feel for the displacement processes at work. After the flow visualization and quantitative experimental results are presented, the development of the mathematical model is given. The flow behavior predicted by the model is explained and related back to the experimental observations.

Organic liquid advance

Soltrol was advanced into a horizontally-held micromodel containing a number of coarse lenses (Conrad et al., 1988; Mason et al., 1989b). The lenses were oriented parallel to the flow direction. The Soltrol injection was relatively slow, at 0.096 ml/min. Figure 72 illustrates the process. During the experiment, the front of organic liquid advanced in the finer pore matrix until it encountered a lens, then slowed while most of the incoming organic liquid preferentially traveled through that lens because capillary forces resisting organic liquid entry were lower in the larger pores of the lens (see top photo in Figure 72). When the lens was full, the front in the fine pores picked up speed again until another lens was encountered. If the front encountered more than one lens at a time it fed both of them until the one was full, and then fed only the second. The front in the fine pore matrix always advanced from the rear; although a full lens might serve as a source for a new front in the fine pores, movement always proceeded slower than movement of the front through fine pores further behind. Favorable mobility (a more viscous fluid displacing a less viscous one) played a stabilizing role in this displacement. Had the coarse lenses extended across the length of the model, the fine regions would have been almost entirely by-passed, similar to the displacement behavior seen in the aggregated model. Due to the presence of the discontinuous lenses, progress of the advancement was very unsteady, with the fine matrix front decelerating and accelerating as lenses were encountered. Consider this unsteady flow to be a macroscopic analogy to the Haines' jumps seen on a pore level during the advancement. (Haines' jumps on a pore scale are graphically recorded on the videotape by Mason et al.,1988.) The final or equilibrium fluid distribution is shown in the bottom photo in Figure 72. Wetting phase residual saturation is found in both the coarse and fine pore regions. Because of the role of the lenses in the advancement, there are zones of fine material, located between closely spaced coarse lenses, where the water was largely by-passed, leaving behind a large residual wetting phase saturation in those locations.

The horizontal experiment was repeated in the same heterogeneous model but at a faster flow rate of 1 ml/min. As above, the front of organic liquid advanced in the finer-pore matrix until it encountered a lens, then slowed. Even though there was a slight difference in the way the model filled with organic liquid, it did not make much difference in the residual water saturations behind the front in each model. The only difference was that at the faster rate, there was less of a capillary end effect.

Organic liquid selectively travels through the coarser portions of heterogeneous aquifers. Lenses of coarse material embedded in a matrix of fine material (e.g. gravel in sand; sand in silt) will influence the rate and direction of movement of an organic liquid, and create a 'fingering' or 'dispersion' of the location of the immiscible displacement front, provided that the lenses are oriented in parallel to the flow direction. The front will 'finger' because of the heterogeneity, and the competition between viscous and capillary forces. This fingering is a function of the length and width of the lenses, and their pore-size contrast with the matrix.

For media with continuously varying properties that can be represented geostatistically, the lens length would correspond to a correlation length. It is currently a controversial issue to
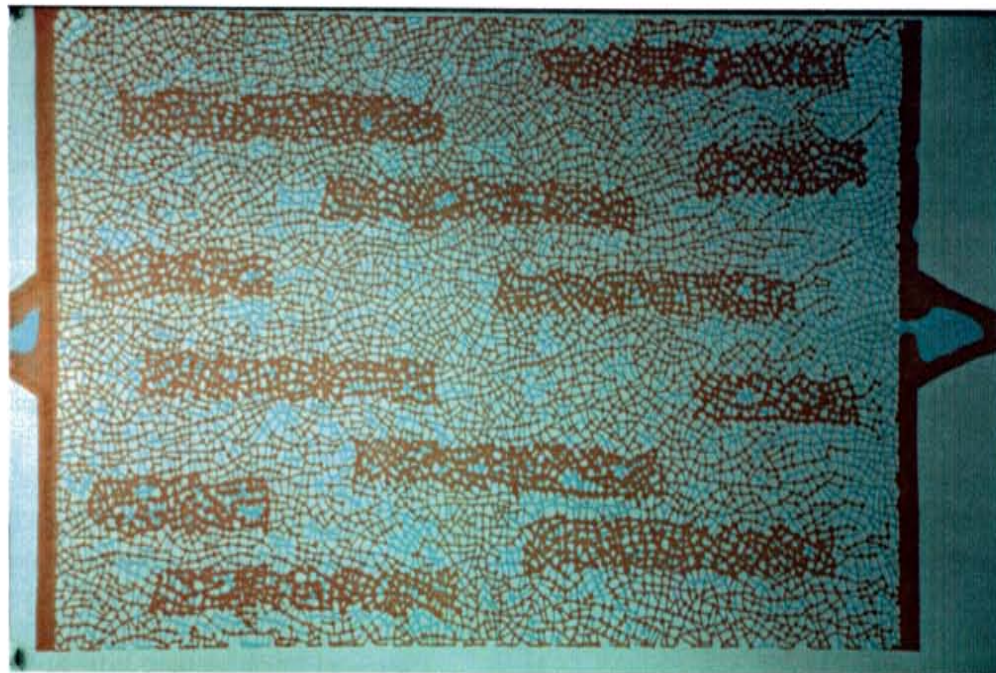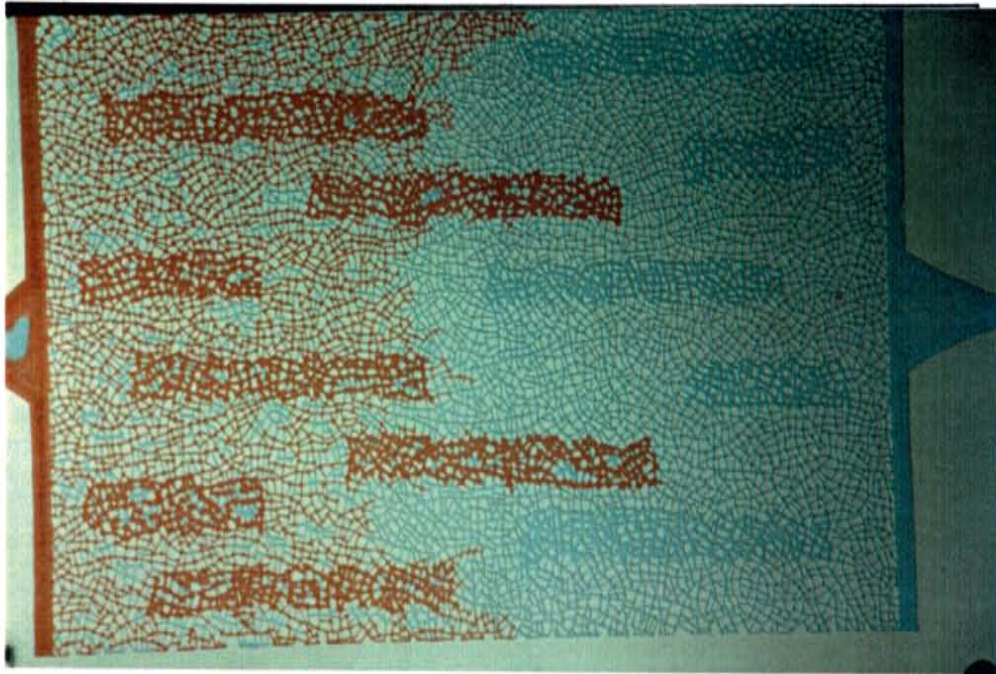
Figure 72. Organic liquid advance into the horizontally-aligned 'coarse lens' micromodel. The photos show fluid distributions as the organic liquid was part way through the model (top), and once the organic liquid had advanced completely through the model (bottom).
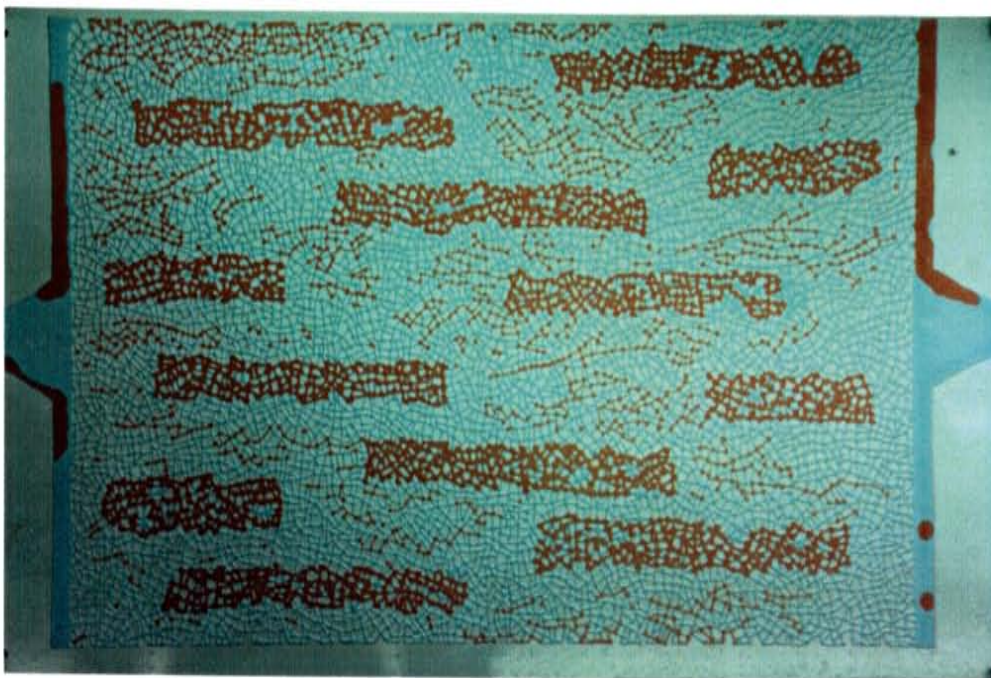
Figure 73.   Lens model, run at slow rate, at residual saturation.

determine when 'fingering' due to heterogeneity, sometimes considered to be a form of 'macrodispersion', dominates over fingering due to viscous or density instabilities caused by a contrast in viscosity or density across the immiscible interface. Most of the recent work on this topic has focused on miscible displacement (Moissis et al., 1989; Ewing et al., 1989; Welty and Gelhar, 1987,1989; Araktingi et al., 1988). The effect of capillarity in immiscible displacement has been considered by some to be similar to local hydrodynamic dispersion operating during miscible displacement, the reasoning being that transverse mixing caused by either processes tends to limit viscous or gravity instabilities or 'macrodispersion' induced by heterogeneities aligned with the direction of flow. While this notion may hold true for advance of a wetting phase, the opposite appears to be true for advance of a non-wetting phase. During any drainage process (non-wetting fluid displacing a wetting fluid), capillarity effectively limits transverse mixing and enhances the growth of fingers. As we have seen for both the aggregated and coarse lense micromodels, the advancing organic liquid has been constrained by capillarity to traveling preferentially through coarse regions, and that this 'macrodispersion' was not mitigated by any transverse capillary mixing process.

Displacement of organic liquid by water

Figure 73 shows the displacement of the organic liquid by water for the model depicted in Figure 72. The water was injected at a rate of 0.096 ml/min (from the right of the photo). As water advanced, the front moved in the fine pore matrix, splitting as it migrated around each of the coarse lenses filled with organic liquid. At this slow rate, capillary forces dominated over viscous forces to the extent that water was preferentially imbibed into the fine pore matrix even

127

Figure 74. Lens model, run at fast rate, at residual saturation.

though it was of lower permeability. When the front reached the downstream end of a lens it closed back together and trapped the non-wetting fluid in the lens via by-passing. Very little, if any, non-wetting organic liquid was displaced from the coarse lenses. Typical pore-level capillary trapping of blobs in the fine matrix occurred, but it was of much smaller scale, typical of the results seen in the homogeneous model (Figure 55b). Figure 73 shows the equilibrium condition at the end of the displacement. The residual organic liquid saturation was significantly higher for this heterogeneous model, than it was for the homogeneous model, due to large-scale by-passing of the organic liquid in the coarse lenses.

Figure 74 shows the model after organic liquid had been displaced by water at a fast rate of 1 ml/min. In contrast to the slow rate displacement, a significant amount of organic liquid has been swept from the coarse lenses. The organic liquid remaining in the lenses was trapped on the downstream end of the lenses. Sufficient viscous forces were generated by the fast flow rate to partially overcome the capillary forces which held organic liquid in the lenses at the slow rate. The effect of flow rate upon displacement was much more dramatic for this model than for either the homogeneous model or the aggregated model in which only a modest rate effect was observed. Since the viscosity of water is lower than that of Soltrol, this displacement was somewhat unstable, and some viscous fingering was observed as water moved through the model. The fingering resulted in some by-passing in both the fine and coarse zones. However, many common organic pollutants are less viscous than water. For these fluids, the viscous instability experienced in this experiment run under high flow rates would not be expected.

128

At typical aquifer flow velocities, capillary forces can relegate the flow of water to finer-grained regions, by-passing the coarser organic-filled regions. The result can be poor recovery of organic liquids, as high residual organic liquid saturations are left behind.

Conventional wisdom in the aquifer remediation business has it that free-phase organics should be recovered using a low pumping rate in order to reduce the cone of depression and avoid 'smearing' the organics over a larger vertical extent in the aquifer. While not disputing the fact that increased smearing may result from applying high pumping rates, it is believed that in many instances the prospects of dramatically increased recovery may make the application of high pumping rates worthwhile.

Buoyancy effects: displacements in a vertically-held micromodel

In a variation of the 'coarse lens' micromodel experiment, Soltrol was advanced downward into the vertically-held micromodel (Mason et al., 1989b). The Soltrol injection rate, as before, was relatively slow at 0.096 ml/min. The organic liquid advance was virtually identical to that in the horizontally-held case, except that buoyancy forces played a role in stabilizing the displacement front by acting in the direction opposite to flow.

Organic liquid was displaced by water from bottom to top in the vertically-oriented model at a rate of 0.096 ml/min, and the end result is depicted in Figure 75. Notice that a significant amount of organic liquid was displaced from the coarse lenses even though the flow rate was low. In the absence of sufficient viscous forces, buoyancy forces (generated by injecting the more dense water phase from below) partially overcame the capillary forces which had previously held organic liquid in the lenses.

Capillary trapping is a function of both buoyancy and viscous forces. Whenever possible remediation schemes should be designed so that buoyancy forces operate in favor of maximum displacement.

Column Results

This 'coarse lens' experiment was repeated in several short TFE columns using styrene as the organic liquid phase (Conrad et al., 1988, 1989; Peplinski et al., 1989). Three cylindrical lenses were created by splitting the Sevilleta sand into two fractions with a size 50 sieve. The fine fraction was used to pack the major portion of the column, with the coarse fraction used to construct the three lenses, roughly 3.5 cm long and about 2 cm in diameter. The column was held vertically, and styrene was advanced downward slowly. Later, water was injected from the bottom and displaced styrene upward at a relatively slow rate. The residual saturation of styrene was hardened at the end of the water displacement, and pore casts were constructed by replacing the water phase with epoxy. A longitudinal section of the column through one of the lenses is shown in Figure 76. The coarse lenses contained a much greater saturation of styrene than the surrounding fine matrix, validating the micromodel results. The residual saturation trapped in the fine matrix was observed to be the same or perhaps even less than that observed in the earlier homogeneous experiments. Even though this column was oriented vertically, buoyancy forces were small and had little effect on the results. The greater density of styrene

Figure 75.   Lens model, vertically held run at slow rate at residual saturation.

along with much smaller pore sizes in the sand pack resulted in a much smaller ratio of buoyancy forces to capillary forces than was encountered in the vertically-oriented micromodel.

Another experimental trial was conducted in a similar column, but this time the column was oriented horizontally during the organic displacement step, and the displacement was conducted at a much faster rate. A longitudinal section of this column through a lense is shown in Figure 77. Notice that some organic liquid was displaced from the coarse lenses, again corroborating the results from the corresponding micromodel experiment. By-passed styrene still remained in the down-gradient end of the stringer but the residual saturation in the up-gradient end was reduced to small disconnected blobs similar to that found in the matrix of finer pores.

Two vertical glass short column experiments were also run with coarse lenses, and quantitative measurements were made of final Soltrol residual saturation (Conrad et al., 1988). The columns were packed with three lenses, similar to the heterogeneous pore cast
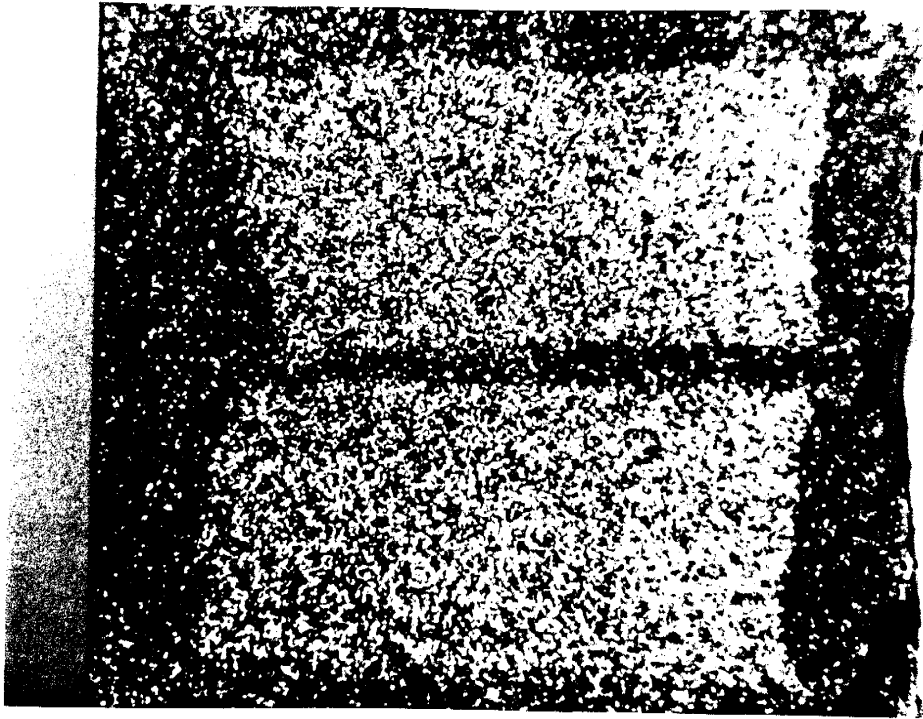
Figure 76.   Photograph of residual organic liquid saturation (shaded light) in a heterogeneous sand pack. Water was flooded from left to right at a low rate. Notice the high organic liquid saturation in the coarse lenses. The core is 5 cm long.
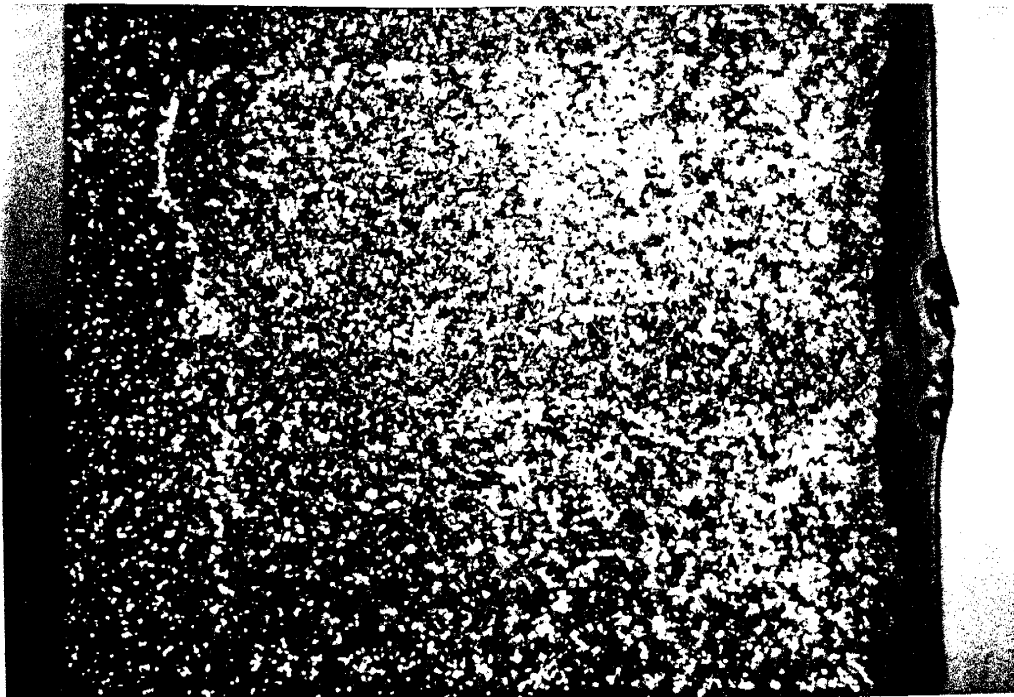
Figure 77.   Photograph of residual organic liquid saturation (shaded light) in another heterogeneous sand pack. Water was flooded from left to right. A high rate of flow produced sufficient force to displace some organic liquid from the coarse lenses. This core is 5.8 cm long.

sample	porosity * (%)	volumetric percent coarse/fine	bulk maximum organic liquid saturation * (%)	bulk residual organic liquid saturation * (%)
1	38.2± 0.4	29 / 71	85.1± 2.5	31.0± 1.4
2	37.6± 0.4	31 / 69	85.4 ± 2.4	31.2± 1.5

* measured value ± propagated error

Table 14. **Measurements of bulk residual organic saturations in two heterogeneous packings of the Sevilleta sand. The sand was divided into a coarse and a fine fraction, and the coarse fraction was packed into the column as cylindrical lenses within a matrix of the fine fraction.**

experiments. The results of these experiments are given in Table 14. The observed 'bulk' maximum and 'bulk' residual Soltrol saturations represent volumetric averages over the entire column pore space. The observed 'bulk' maximum Soltrol saturation is consistent with that observed in the homogeneously packed Sevilleta soil columns. If both the coarse and fine zones had the same maximum organic saturation, and if no water imbibed into the coarse lenses during the upward water displacement, then the residual Soltrol saturation in the lenses should not have changed from this value of roughly 85%. In the fine matrix surrounding the lenses, the Soltrol saturation was presumably reduced to something like 17%, less than the residual saturation reported for 'homogeneous' packings of the Sevilleta sand but close to the S_{or} values measured in the less structured packings of the Traverse City sand and the Llano coarse sand. A low residual saturation would be expected for the matrix because no layering would be expected to develop since it was not packed under water. Accounting for the relative volume of each soil fraction, an estimate for the expected bulk residual Soltrol saturation can be made. If one assumes that little to no drainage of styrene occurred in the stringers, the measured 'bulk' residual saturation can be compared with a theoretical value:

estimated bulk residual saturation

$$= (normalized\ lens\ volume) \times S_o + (normalized\ matrix\ volume) \times S_{or} \tag{42}$$

$$= 0.3 \times 0.85 + 0.7 \times 0.17$$

$$= 0.38$$

The actual bulk residual Soltrol saturation was only 31%, much greater than the 17% expected for homogeneous soil packings and greater than the 27% found in 'micro-layered' Sevilleta sand columns, but also lower than the expected value of 38%. Perhaps the coarse lenses actually occupied less volume than calculated. It is likely that some mixing occurred between the coarse lenses and the fine matrix when the packing forms used to make the lenses were removed from the column thereby reducing the effective volume of the coarse lenses.
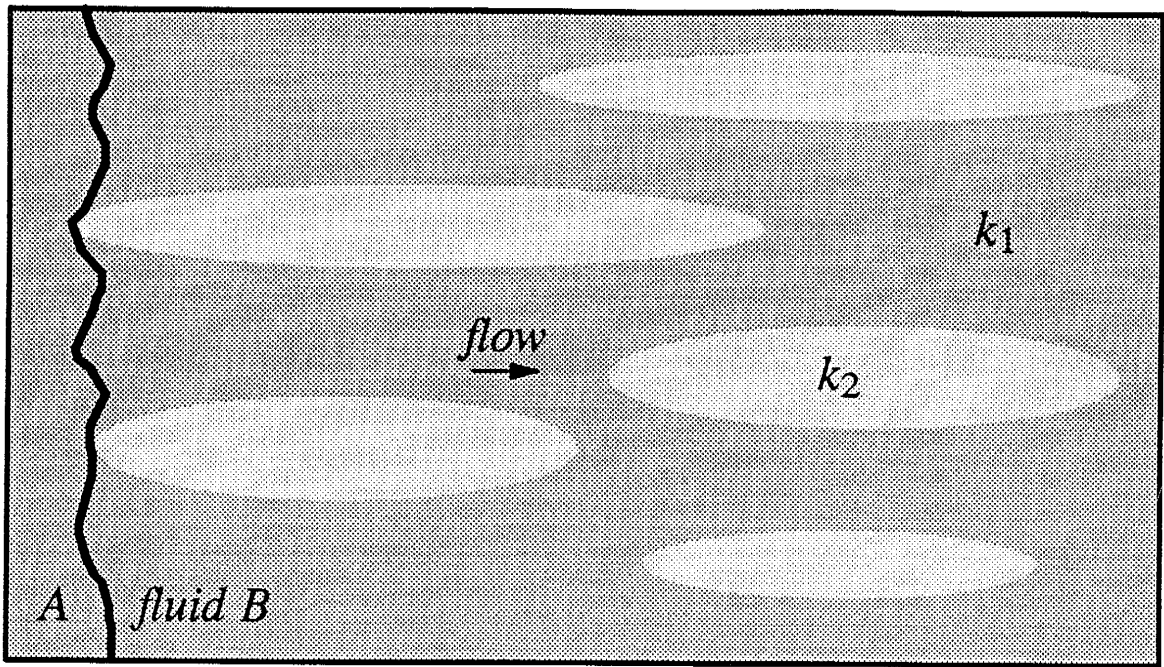
Figure 78 Random lenses of permeability k_2 in a matrix of permeability k_1.

Secondly, unlike the lenses in the micromodel experiment which had uniformly larger pores than the matrix, the random arrangement of the coarse soil grains in the lenses would result in some proportion of small pores within the lenses. And presuming some degree of connection between these pores, it would be expected that some of these pores would imbibe water during the waterflood, reducing the saturation in the lenses somewhat from the maximum saturation of 85% — and thereby reducing the overall saturation as well.

These quantitative results are somewhat inconclusive. On one hand, residual saturations were increased by the presence of coarse lenses, in agreement with both the micromodel and pore cast results, but the observed residual saturations were somewhat less than the theoretically predicted value.

A Mechanism for Trapping in Heterogeneous Porous Media: a Simple Dual-Media Model

The basic mechanism for capillary trapping via by-passing on a pore scale has been recognized in both the petroleum and hydrologic literature, as has been reviewed earlier in Chapter 2. On a larger scale, the displacing wetting fluid can migrate around clusters or lenses of coarser pores which are preferentially occupied by the non-wetting fluid. Although this basic mechanism is recognized, there appears to be no literature that looks at the conditions under which displacement of non-wetting fluid from these lenses, may be achieved. A preliminary version of the following discussion was presented by Conrad et al. (1988).

Model development

To better understand the mechanisms, consider a simple conceptual model of the aquifer with porous lenses of intrinsic permeability k_2 embedded in a matrix of permeability k_1 as

133

illustrated in Figure 78. The pore space of this binary media is initially filled by fluid B, one of two immiscible fluid phases. The other fluid is designated fluid A. Fluid A is injected at a known flow rate $\bar{q}$ on the left, and displaces fluid B from the pore space. The micromodel and column experiments were run under similar constant flux conditions. There may also be some ambient pore level residual saturation of fluid A. The pore space may be strongly wet by either of the two fluids, or it may be neutrally wet. For example, Soltrol would be represented by fluid A, as it advances into a glass micromodel saturated with water, fluid B. When water displaced Soltrol, fluid A would be the water and fluid B the Soltrol. The capillary properties of the matrix and lenses are assumed to be correlated with their permeability. The spatial pattern and efficiency of the displacement depends on the spatial statistics of the lenses (size, shape, frequency), wetting, permeabilities, capillary properties, and the flow rate.

For this simple mathematical analysis a greatly simplified geometrical and fluid mechanical conceptual model is adopted, as shown in Figure 79. The lenses are assumed to be roughly rectangular in shape, with length l . Over the cross-section taken normal to the flow, relative areas of each flow zone can be calculated. The relative area of the lenses is a_2, while the relative area of the matrix is a_1, such that:

$$a_1 + a_2 = 1 \tag{43}$$
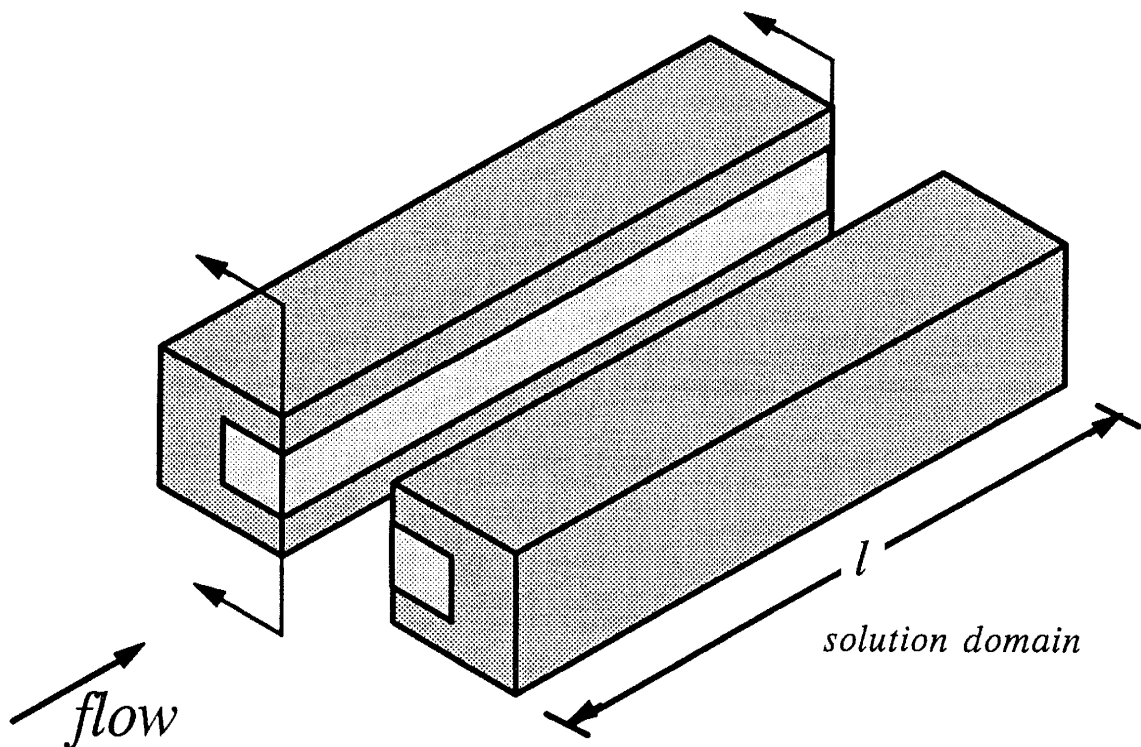
Figure 79.   A uniform, parallel lens of permeability k_2 in a matrix of permeability k_1.

When the front hits the lenses the total flux will be divided into flow around the lenses, q_1, over the area a_1, and flow through the lenses, q_2, over area a_2. The net flux $\overline{q}$ is related to the individual fluxes by:

$$\overline{q} = a_1 q_1 + a_2 q_2 \tag{44}$$

Note that if the total cross-sectional flow area is A, then the flow areas of k_1 and k_2, are A_1 and A_2, respectively. That is $A = A_1 + A_2 = a_1 A + a_2 A$, and the total flux over area A is given by $\overline{q} A = q_1 A_1 + q_2 A_2$.

The model is based on the premise that displacement occurs as a sharp front. On each side of the front only one of the two fluids is at greater than residual saturation. To the right this would be fluid B, while to the left it would be fluid A. Then the flux rates are given by Darcy's law, which for flux in area a_i (= 1,2) is:

$$q_i = \frac{k_i k_r}{\mu} \frac{\Delta P_{\mu_i}}{l} \tag{45}$$

where q_i is the flux over the solution domain, l, in material i, which has intrinsic permeability k_i. The relative permeability for each fluid is k_r, and the viscous pressure drop is ΔP_{μ_i} (as distinguished from the total pressure drop, ΔP, or the capillary pressure, P_c).

For the sake of simplicity, two assumptions are made:

● uniform viscosity, $(\mu_A = \mu_B)$; and,

● each fluid has the same relative permeability and that permeability is uniform within each fluid, $(k_{rA} = k_{rB} = constant)$.

These assumptions are easily relaxed for a more sophisticated analysis.

From these assumptions it follows that within each material the pressure gradient across the domain will be constant except for a pressure jump at the immiscible front caused by capillary forces. For the case of a wetting fluid displacing a non-wetting fluid, the pressure profile in each material is assumed to look something like that shown in Figure 80. Note that the total pressure drop across the domain must be the same for both materials (ie, $\Delta P_1 = \Delta P_2$), from which it follows that:

$$\Delta P_{\mu_1} - P_{c_1} = \Delta P_{\mu_2} - P_{c_2} \tag{46}$$

By rearranging (46) in terms of ΔP_{μ_1}, substituting the result into (45), and solving in terms of q_1, we get:

$$q_1 = \frac{k_1 k_r \ (\Delta P_{\mu_2} + P_{c_1} - P_{c_2})}{\mu \ l} \tag{47}$$
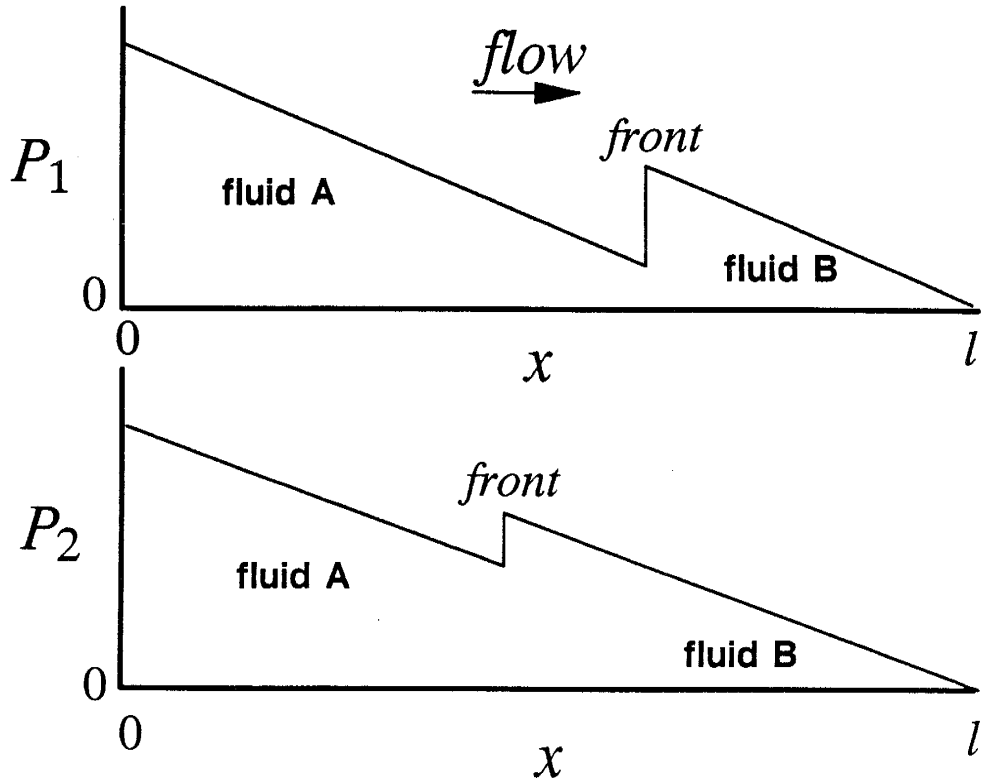
Figure 80. Pressure profiles for fluid A as the wetting fluid for the fine matrix(top) and the more coarse lens (bottom).

Now, solving (45) in terms of ΔP_{μ_2} and substituting the result into (47):

$$q_1 \;=\; \frac{k_1 k_r}{\mu l}\left(\frac{q_2 \mu l}{k_2 k_r} + P_{c_1} - P_{c_2}\right) \tag{48}$$

By rearranging (44) in terms of q_2, substituting the result into (48) and solving for q_1 we get:

$$q_1 \;=\; \frac{\dfrac{\overline{q}\mu l}{k_2 k_r a_2} + P_{c_1} - P_{c_2}}{a_1 \mu l\left(\dfrac{1}{k_1 k_r a_1} + \dfrac{1}{k_2 k_r a_2}\right)} \tag{49}$$

And, by analogy,

$$q_2 \;=\; \frac{\dfrac{\overline{q}\mu l}{k_1 k_r a_1} + P_{c_2} - P_{c_1}}{a_2 \mu l\left(\dfrac{1}{k_2 k_r a_2} + \dfrac{1}{k_1 k_r a_1}\right)} \tag{50}$$

136

Within each material, the capillary pressures can be related to the permeabilities in a gross sense by way of the Kozeny-Carman equation (Carman, 1937). First, note that for a single pore or capillary:

$$P_{c_i} = \frac{2\sigma \cos\theta}{r_i} \tag{51}$$

where r_i is the radius of the capillary. By the Kozeny-Carman equation, $R_i \approx 18\sqrt{k_i}$ for random packings of equal spheres (where R_i is the sphere radius). If a medium of well-sorted spheres is assumed where r is of the same order as R:

$$P_{c_i} = \frac{2\sigma \cos\theta}{r_i} = \frac{2\sigma \cos\theta}{R_i} = \frac{\sigma \cos\theta}{9\sqrt{k_i}} \tag{52}$$

Finally, by substituting this relation into equations (49) and (50) and by merging these equations into ratio form we get:

$$\frac{q_2}{q_1} = \frac{\frac{\overline{q}\mu l}{k_1 k_r} + \frac{a_1\sigma\cos\theta}{9}\left(\frac{1}{\sqrt{k_2}} - \frac{1}{\sqrt{k_1}}\right)}{\frac{\overline{q}\mu l}{k_2 k_r} + \frac{a_2\sigma\cos\theta}{9}\left(\frac{1}{\sqrt{k_1}} - \frac{1}{\sqrt{k_2}}\right)} \tag{53}$$

Using the dual-media model to analyze the displacement process

According to equation (53), the displacement process changes depending on the ratio of the flux rates, $\frac{q_2}{q_1}$. The ratio of the flux rates can be divided into three regions of interest: $\frac{q_2}{q_1} < 0$, $0 < \frac{q_2}{q_1} < 1$, and $\frac{q_2}{q_1} > 1$; and two boundaries between these regions: $\frac{q_2}{q_1} = 0$ and $\frac{q_2}{q_1} = 1$. The displacement behavior within each of these regions will be examined for the case of a wetting fluid (water) displacing a non-wetting fluid (organic liquid).

The first region, when $\frac{q_2}{q_1} < 0$, suggests counter-current flow. That is, for a wetting fluid displacing a non-wetting one, q_2 must be negative — indicating that the flow direction in the lenses is opposite to that in the matrix. Since the initial conditions of this model have been set up such that counter-current flow is not possible, $\frac{q_2}{q_1} < 0$ actually means that no flow occurs through medium 2, the coarse lenses. Under such conditions, the advancing wetting fluid flows entirely through the matrix, completely by-passing the non-wetting phase in the lenses. Just such a displacement process was observed for low flow rate displacements in both the micromodels and the column experiments (refer back to Figures 73 and 76). In both

137

experiments, the organic phase in the coarse lenses was completely by-passed resulting in a high residual saturation.

When $\frac{q_2}{q_1}$ becomes positive, flow through both media is achieved. To find the critical flux, $\vec{q}^*$, needed to initiate the flow of water into the coarse lenses, equation (53) is set equal to zero $\left(\frac{q_2}{q_1} = 0\right)$ and solved in terms of $\bar{q}$:

$$\vec{q}^* = \frac{\sigma \cos\theta \; k_1 \; k_r \; (1 - a_2)}{9 \; \mu \; l} \left(\frac{1}{\sqrt{k_1}} - \frac{1}{\sqrt{k_2}}\right) \tag{54}$$

From equation (54), one can see that the critical flux needed to initiate displacement of organic liquid from coarse lenses is inversely proportional to the length of the lens, l, and the relative area occupied by the lenses, a_2, but is directly proportional to the capillary force, $\sigma \cos\theta$. As the length of the lenses is increased, the effect of capillarity relative to viscous forces becomes proportionally less important and $\vec{q}^*$ becomes smaller. So too, as the portion of the cross-sectional area occupied by lenses is increased, proportionally less matrix is available for flow and it becomes easier to initiate flow into the lenses. And as expected, as the capillary force is increased, it becomes more difficult to initiate flow into the lenses.

Figure 81 shows the relationship between the critical flux and the permeabilities. When $k_1 = k_2$, the system is homogeneous and the critical flux is zero. As k_2 is increased, the critical flux increases toward an asymptotic value. The fine matrix, k_1, can vary between zero and k_2. Toward either of these end points, the critical flux approaches zero, in one instance as k_1 becomes impermeable, and in the other instance as the system approaches homogeneity. In between these extremes the critical flux reaches a maximum in which displacing organic liquid from the coarse lenses becomes most difficult. At this point there is both sufficient permeability in the matrix and a sufficient contrast in capillarity between the matrix and lenses to make displacing organic liquid from the coarse lenses most difficult. For this particular formulation, $\vec{q}^*$ reaches a maximum when $k_1 = k_2/4$.

If some reasonable values are selected for the parameters in equation (54) ($\sigma = 35$ dyne/cm, $\theta = 0°$, $k_1 = 5 \times 10^{-8}$ cm^2, $k_2 = 10^{-7}$ cm^2, $k_r = 0.5$, $a_2 = 0.25$, $l = 100$ cm, $\mu = 1$ cP), an average flux rate of 9.6×10^{-5} cm/s is obtained, which translates to a gradient of 0.05. While it is important to realize that natural depositional processes create lenses of varying lengths and permeabilities, the results of this sample calculation demonstrate that recovery efficiency can quite often be a function of pumping rate within the range of achievable field pumping rates.
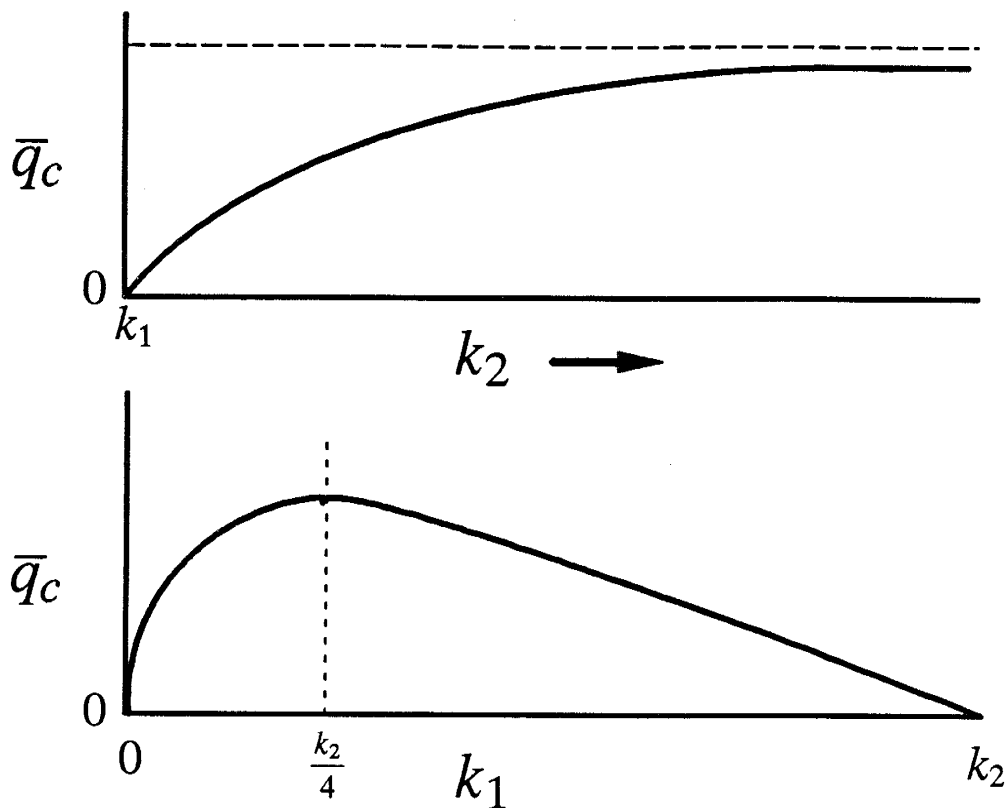
Figure 81. Critical flow rates needed to displace organic liquid from coarse lenses as a function of permeability in the coarse lens (top), and in the fine matrix (bottom).

For the case when $0 < \frac{q_2}{q_1} < 1$, flow occurs through both the fine matrix and the coarse lenses, but the flux rate through the matrix is greater. If it is assumed that the porosities for each medium are the same, then the ratio of the velocities is equivalent to the ratio of the fluxes $\left(\frac{v_2}{v_1} = \frac{q_2}{q_1} \right)$. The ratio of the velocities directly corresponds to the proportion of non-wetting phase displaced from the lenses by the time water moving through the matrix has reached the downstream end of the lens and by-passed any organic phase still remaining in the lens. For example if $\frac{q_2}{q_1} = 0.25$, then the displacement front would be moving four times as fast through the matrix as through a lens. Under such a scenario, only one fourth of the lens will have been drained by water by the time water travelling through the matrix has reached the downstream end of the lens. Three-fourths of the lens would still be filled with organic liquid when the lens became cut off from the main body of organic liquid and by-passing occurred. Again, experimental observations were in agreement with this model of displacement behavior. In both

the micromodel and column experiments, at higher flow rates some organic liquid was displaced from the coarse lenses (refer back to Figures 74 and 77).

As $\frac{q_2}{q_1} \to 1$, proportionally less organic liquid becomes by-passed in the lenses. When $\frac{q_2}{q_1} = 1$, the flux rates (and the velocities) are equivalent and no large-scale by-passing occurs.

When $\frac{q_2}{q_1} = 1$, The critical flux, $\overline{q}^{**}$, for equal velocities of flow in the matrix and the lenses is given by:

$$\overline{q}^{**} = \frac{\sigma \cos\theta \; k_1 \; k_2 \; k_r}{9\mu \; l \; (k_2 - k_1)} \left(\frac{1}{\sqrt{k_1}} - \frac{1}{\sqrt{k_2}} \right) \tag{55}$$

Note that unlike the previous case (when $\frac{q_2}{q_1} = 0$, equation 54), the average flux rate is no longer dependent on the proportion of cross-sectional area occupied by the lenses, a_2. Since the velocities — and hence the net resistance to flow — are now equivalent, the proportion of area occupied by lenses is becomes unimportant.

Using the same parameter values as before ($\sigma = 35$ dyne/cm, $\theta = 0°$, $k_1 = 5 \times 10^{-8}$ cm2, $k_2 = 10^{-7}$ cm2, $k_r = 0.5$, $l = 100$ cm, $\mu = 1$ cP) an average flux rate of 2.5×10^{-4} cm/s is obtained, which translates to a gradient of 0.08. Again, the sample calculation demonstrates that substantially improved recovery can often be achieved within the realm of practicable field pumping rates.

As a practical matter, in cases where the organic phase is more viscous than water, increases in pumping rate may induce viscous fingering. In such cases, by-passing as a result of viscous fingering can offset any gains in recovery efficiency due to the avoidance of by-passing in the coarse lenses. Equations for predicting the onset of frontal instabilities have long been available (e.g., Chouke et al., 1959). However, many commonly spilled organic liquids are actually less viscous than water. In such cases, viscous instabilities would not present a problem.

When $\frac{q_2}{q_1} > 1$, the advancing water front moves more quickly through the coarse lenses.

When water is the more viscous fluid, it would be expected that even though the flow velocities are not equal, the displacement efficiency would be high. Just as had been seen earlier for organic liquid displacing water in the micromodel experiment, favorable mobility would be expected to play a stabilizing role in the displacement. However when water is the less viscous fluid, any fingers formed due to higher water-front velocities in the lenses would be expected to

continue to grow out of the downstream ends of the lenses resulting in by-passing of organic liquid in the matrix and a reduction in displacement efficiency.

Applications of the dual-media model

This simple analytical model is useful in that it provides a conceptual framework to demonstrate the range of displacement processes for this type of heterogeneity. It highlights important parameters and their effect on the displacement process. It is also useful because it works; it qualitatively reproduces the experimental results.

Because of the simplifying assumptions used in the development of the model, however, it is not well suited for quantitative predictive modelling of laboratory experiments or aquifer remediation operations. For such purposes, it is recommended that a multi-phase flow model (e.g. Kuppusamy et al., 1987) be used — with the heterogeneities explicitly included in the representation of the flow domain. The dual-media model developed as part of this study is best used to explain on a continuum scale the physics of fluid entrapment in discontinuous lenses, and predict the conditions under which such trapping may be averted.

LAYERED MEDIA

The effect of layering perpendicular to flow on organic/water displacements were explored in three ways. First, a layered micromodel was used to demonstrate that the capillary end effect is not only an experimental artifact to be minimized, but a process which repeats as displacements advance over repeating sequences of coarser and finer layers. The capillary end effect has important implications for multi-phase flow in layered systems. Second, the insights gained from the layered micromodels are used to revisit the Sevilleta sand column experiments. Evidence is presented suggesting that the 'homogeneous' Sevilleta sand columns inadvertently contained small-scale layering, and that the layering resulted in anomalously high residual saturations. Finally, an additional layered micromodel experiment is presented in which it is shown that layering perpendicular to flow retards the growth of fingers, particularly for dense organics which are especially prone to fingering.

Micromodels

Figure 82 is a close-up of a layered micromodel at the juncture between a coarse layer (below) and a fine layer following the displacement of organic liquid by water. In this experiment, an initially water-saturated micromodel (shown in Figure 44) was injected with Soltrol from top to bottom, and then the Soltrol was displaced by water from bottom to top. In a process analogous to that shown earlier in Figure 55a that produced a capillary end effect, water was displacing Soltrol from the coarse layer until the water broke through to the fine layer along one or perhaps two flow paths. The continuing flow of water takes place through the one or two connected flow paths, as capillary forces preferentially draw the water into the fine layer, by-passing the Soltrol remaining in the coarse layer. As you might imagine, such by-passing could lead to significantly higher residual saturations — especially if the layers were not very thick. In such a case,
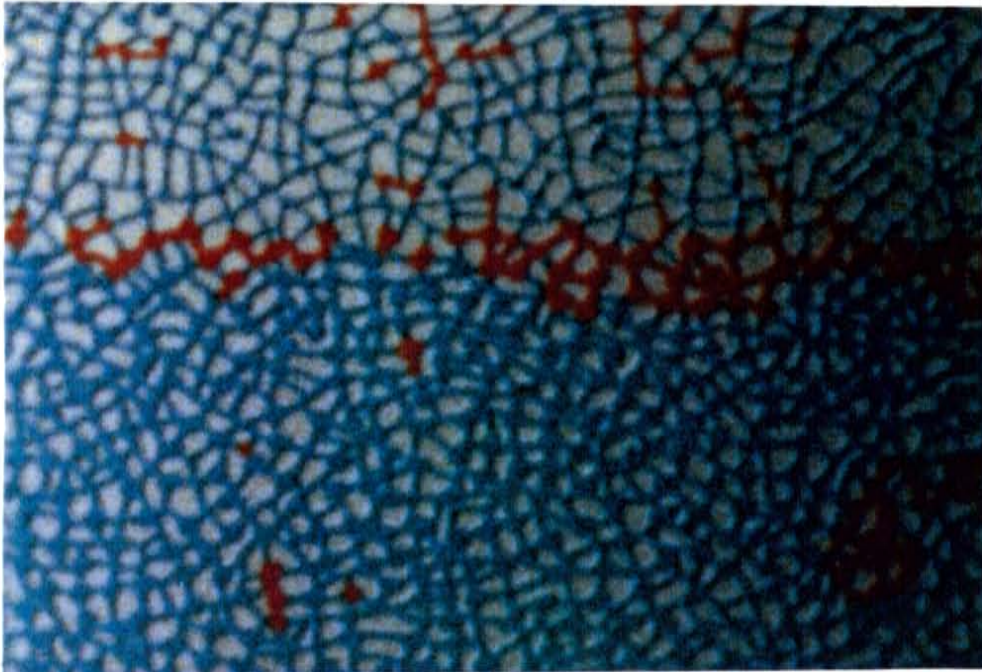
Figure 82. Close-up of organic liquid trapped as a result of a capillary end effect. Water (blue) displaced organic liquid (red) from bottom to top.

displacement in the fine layers might be fairly efficient, but the majority of the organic liquid in the coarse layers would be by-passed. Almost as soon as water began displacing organic liquid from a coarse layer, a finger of water would break through to the next fine layer resulting in by-passing.

'Homogeneous' Sevilleta Sand Short Columns Revisited

Evidence for layering in column packings of the Sevilleta dune sand was related in the previous chapter. Based on that layering and on the demonstration of by-passing seen in the layered micromodel, it is hypothesized that for water displacing organic liquid, water preferentially imbibes into the finer micro-layers. Since the organic phase was the non-wetting fluid in both the column and the micromodel experiments and far less likely to maintain continuity, some of the organic liquid in the coarser layers was completely by-passed as the water leapfrogged from fine layer to fine layer resulting in a relatively high residual saturation.

In a perfectly homogeneous porous media, the trapped blobs tend to be aligned with the flow of water. That is, trapped blobs of organic liquid tend to be longer in the direction of water flow than transverse to that direction. It is suspected, but unfortunately cannot yet be tested with the data presently available that the blobs trapped in the Sevilleta sand were preferentially oriented with the layering instead of with the direction of water flow.

For homogeneous media, it is known that chlorinated organic solvents have a tendency to finger upon reaching the saturated zone. These solvents often are more dense and less viscous than water and non-wetting relative to water, all of which promotes flow instabilities. Table 15 gives the density and viscosity of some common chlorinated solvents. Schwille (1988) presented flow visualization experiments which demonstrated the fingering of a dense organic liquid (PCE) as it migrated downward through a glass bead pack.

Even though it has been shown that fingering of dense, low viscosity organics occurs in the saturated zone, the displacement behavior of these fluids is much different in layered media. Figure 83 serves to illustrate this point. An experiment was performed in a vertically aligned micromodel with coarse lenses aligned perpendicular to flow. In actuality, Soltrol (less dense than water) was flooded upward into the initially water-saturated micromodel, but the photograph is presented up-side down because the instabilities caused by the upward migration of a light organic liquid is directly analogous to dense organic moving downward. However, since Soltrol is more viscous than water while chlorinated solvents can commonly be less viscous than water, this experimental displacement was believed to be somewhat more stable than the displacement it was intended to represent. The experiment could easily have been performed using a chlorinated solvent, but it was preferable from a health and safety standpoint to run the experiment using relatively innocuous Soltrol rather than a toxic chlorinated solvent such as TCE or PCE.

Figure 83 shows the distribution of the organic and water phases after the organic liquid has progressed all the way through the micromodel, but from this image it is easy to relate the 'story' of how the displacement progressed. As organic liquid entered the model, it uniformly filled the end reservoir but immediately formed several fingers upon entering the pore network. Each finger continued to grow until it encountered a coarse lens. Once a finger encountered a lens, the finger ceased growing vertically as organic liquid from the finger tip flowed into the lens until it was filled. The effect of capillarity resulted in preferentially restricting the flow of the non-wetting phase to coarser regions. And when the coarser regions form lenses or layers perpendicular to

chlorinated solvent	density (g/cm^3)	viscosity (cP)
tetrachloroethene (PCE)	1.62	0.89
trichloroethene (TCE)	1.46	0.58
1,1,1-trichloroethane (TCA)	1.34	1.18
1,1,2,2-tetrachloroethane	1.60	1.84
carbon tetrachloride	1.59	0.97

Table 15. Density and viscosity of some common chlorinated solvents at 4°C. (from Byer et al., 1981).

flow, there exists a lateral component to flow sufficient to outweigh the forces causing the growth of fingers.

Once the lenses filled, organic liquid again began flowing 'downward' and again immediately became unstable as fingers formed off the downstream edge of the lenses. Fingers continued to grow until yet another lens was encountered. This scenario repeated itself over and over as the organic liquid progressed through the micromodel. Again, Figure 83 shows the final disposition of the displacement. The coarse lenses were filled with organic liquid and fingers of organic liquid interconnected the lenses. The presence of the lenses served to inhibit the growth of fingers, which would have progressed unchecked in a homogeneous micromodel.

Implications for the migration of dense organics

In truly homogeneous media, dense organic liquids would tend to form fingers upon reaching the saturated zone, just as has been seen in this micromodel experiment. Such fingering would allow the dense organic phase to migrate downward through the aquifer quite rapidly — at a rate
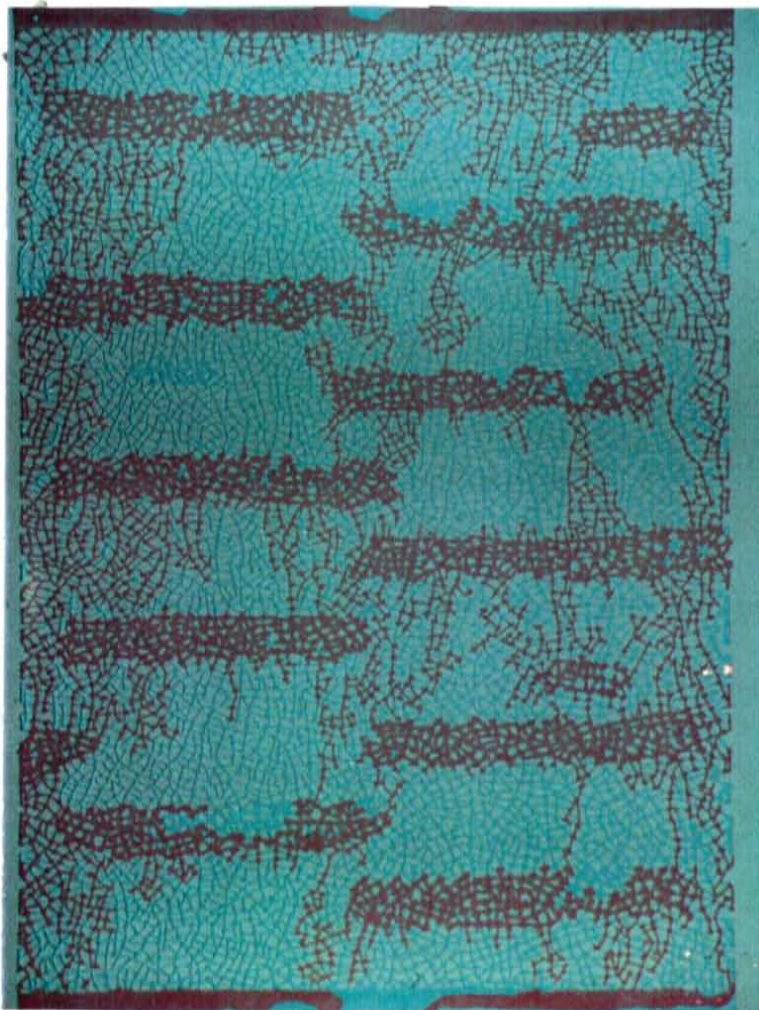
Figure 83. The final distribution of fluids from a micromodel experiment representing the percolation of dense organics through the saturated zone. The organic phase was dyed red; the water was undyed. This experiment demonstrated the effect of layering perpendicular to flow in impeding the growth of fingers.

144

much faster than predicted by presently available numerical models which presume stable displacements. These experimental results have also shown that layering can impede the growth of fingers and make the migration of dense organic 'sinkers' behave more stably. However for aquifers in which the heterogeneities are not well characterized, the presence of lenses and layering can cause the organics to travel in unforeseen and unpredictable directions while diverting it from its density-driven destination with the bottom of the aquifer.

Now consider again the case of micro-layered media, such as has been seen in the Sevilleta sand columns. Almost invariably, any so-called homogeneous geologic media actually has micro-scale heterogeneities imparted by deposition and diagenesis. For the specific case of dense organics migrating beneath the water table in such media, it is certain the micro-layering normal to the downward flow direction would inhibit the growth of fingers and stabilize the displacement. As a matter of fact, Schwille's (1988) experiments using sand instead of glass beads showed stable migration of dense organics in the saturated zone. In many of his photographs, it is also possible to see the small-scale layering in so-called homogeneous packings as made evident by the displacement process itself. It is not yet known however, the conditions under which a dense organic liquid would finger as it moved downward beneath the water table. For micro-layered 'homogeneous' media, the onset of fingering would be a function of the fluid (the organic phase's density, viscosity, its wettability relative to water) and of the media (the soil's texture and especially the magnitude of the capillary contrast between micro-layers). Clearly, theoretical work and systematic experimentation need to be performed to address this important flow phenomenon. In the meanwhile, use extreme caution in attempting to predict the downward migration of dense organics with any of the currently available multi-phase flow models (e.g. Faust, 1985; Pinder and Abriola, 1986; Osborne and Sykes, 1986; Kuppusamy et al., 1987; Corapcioglu and Hossain, 1990).

CHAPTER SUMMARY AND SOME CONCLUDING COMMENTS

The experimental results presented in this chapter have examined two-phase (organic/water) displacements and capillary trapping in a variety of heterogeneous porous media. The effect of heterogeneities on fluid flow and transport is currently a hot topic in hydrology, but the vast majority of this work has been related to either scale-dependent dispersion of a solute in the saturated zone (single-phase flow and transport) or, state-dependent anisotropy in the vadose zone (two-phase flow of water and air). In contrast, relatively little experimental work has been performed to look at the effect of heterogeneity on the two-phase flow of an organic phase through the saturated zone.

Three types of heterogeneities were studied. In the aggregated system, strings of interconnected macropores separated clumps of micropores. This dual-porosity arrangement served as an analog to fractured media. In the coarse lenses system, coarse lenses were imbedded into a finer matrix. In the layered system, coarser and finer layers were arranged perpendicular to flow. Each of the three types of heterogeneity were formed from a bi-modal distribution of pore sizes. In each case the coarser regions contained pores having larger pore bodies and pore throats, and consequently a larger intrinsic permeability than the finer regions.

Aggregated Media

In organic/water displacements conducted in the aggregated micromodel, the organic phase moved quickly through the interconnected coarse macropores, largely by-passing the aggregates of micropores. The residual organic liquid saturation remaining following the waterflood was much lower than that remaining in the homogeneous micromodel. These experimental results suggest that spilled organics can be expected to move quickly through aquifers which have interconnected macropores or fractures. The organic phase would be expected to travel preferentially through large pores and fractures, by-passing smaller pores in the matrix of dual-porosity media. The residual saturations left behind following the recovery of free product would tend to be comparatively low, but would be expected to extend over a much larger portion of the aquifer.

Media Containing Coarse Lenses

Of the three types of heterogeneities examined, the 'coarse lenses' heterogeneity was the most extensively studied. Flow visualization displacements were conducted in both micromodels and sand columns. Residual saturation measurements were obtained from additional sand column experiments.

In addition, a mathematical model that used capillarity and average flux to predict two-phase flow through two media aligned in parallel was developed. Although the model was demonstrated for the case of water displacing organic liquid from coarse lenses, it could just as easily been applied to the aggregated model to predict the flux rate at which organic liquid would penetrate into the aggregates. The model could also be applied to the case (not covered here) of continuous layering parallel to flow.

For the case presented, the model showed that the force exerted by capillarity was sufficient to cause by-passing of organic liquid in the coarse lenses even though these lenses were more permeable. At higher flow rates water can be forced into the coarse lenses, resulting in displacement of additional organic liquid and improved recovery. The critical flow rate at which water enters the coarse lenses is a function of: the permeabilities of each of the media, the proportion of cross-sectional area occupied by the lenses, the length of the flow domain (for this example, the length of the lenses), and the interfacial tension and the relative wetting of the fluids.

The capillarity of the system does not change with flux rate. At still higher flux rates, capillarity becomes relatively unimportant and the flow regime approximates a single-phase system in which water preferentially flows through coarser (higher permeability) regions. At high average flux rates, the flux rates between regions approach the ratio of the permeabilities — just as would be the case for one-phase flow.

In the absence of mobility-induced fingering, improved recovery of organic liquid is attained when the ratio of fluxes through coarse and fine regions becomes greater than zero, and maximum recovery is attained when the ratio of fluxes approaches unity. Or in other words,

increasing the average flux rate beyond a critical value results in improved recovery. Using a hypothetical example, it was shown that improved recovery can be achieved within the realm of attainable field pumping rates.

Laboratory experiments conducted in micromodels and in Sevilleta sand columns showed identical flow behavior to that predicted by the dual-media model. At low flux rates the organic liquid in the lenses was completely by-passed. At higher rates, some displacement of the organic liquid in the lenses was attained, resulting in improved recovery and a reduced residual saturation. These results of these experiments are comparable with the results obtained from similar types of experiments undertaken to demonstrate state-dependent anisotropy (e.g. Stephens and Heermann, 1988; McCord et al., 1988a,b).

Layered Media

The layered media experiments were conducted in micromodels. Observations of water displacing organic liquid from a layered micromodel showed by-passing of the organic phase as the water front progressed from a coarse layer to a fine layer. This particular form of the by-passing mechanism, which coincidentally is identical to the capillary end effect observed in two-phase laboratory experiments, can result in significantly higher residual saturations — especially if the layers are not thick and the process repeats often.

It is speculated that anomalously high residual saturations measured in the Sevilleta sand were caused by micro-layering developed during packing. These results are significant because sedimentary geologic media commonly contains micro-scale bedding imparted by depositional processes.

The presence of layering may be fortuitous in the case of dense organics such as halogenated hydrocarbons migrating downward through the saturated zone. These solvents may finger as they move downward through the saturated zone because they tend to be more dense, less viscous, and non-wetting relative to water. In layered media, the tendency for a non-wetting phase to migrate into coarser layers results in a lateral component to the flow which slows the growth of fingers. The presence of layering means: the dense organic liquid flows downward in a more stable manner, the downward flow is much slower, and this movement can be adequately predicted using presently available multi-phase flow models.

One Final Comment

In addition to whatever these experiments have illustrated about the nature of immiscible flow of organic liquid and water in heterogeneous media, they also make excellent tests against which to attempt to validate flow models. From a survey of the literature it appears that, aside from Osborne and Sykes (1986), nobody has attempted to model the immiscible flow of organic pollutants in anything but homogeneous media. It would be interesting to test the currently available numerical models to see which ones could reproduce the flow behavior seen in these experiments. It would also be interesting and appropriate to use these experimental results to attempt to validate 'pseudo-function' models (e.g. Saez et al., 1989). These models attempt to represent heterogeneous multi-phase flow behavior with an effective homogeneous medium.

CHAPTER 9

VADOSE ZONE RESULTS

Figure 84 depicts the portion of the aquifer that includes residual saturation in the vadose zone. Whether an organic liquid is more dense than water (left below) or less dense than water (right below), it leaves behind a trail of capillary trapped residual in the vadose zone as it makes its way downward toward the capillary fringe. Above the capillary fringe the trapped organic shares the pore space with air and water.

The movement of organic liquid through the vadose zone is more complicated (especially on a pore scale) than in the saturated zone. In the vadose zone, a downward percolating organic phase encounters a partly air-filled, partly water-filled pore network. The organic liquid is generally of intermediate wettability — that is, non-wetting relative to water, but wetting relative to air. The organic phase, depending on whether it encounters air or water, can display either
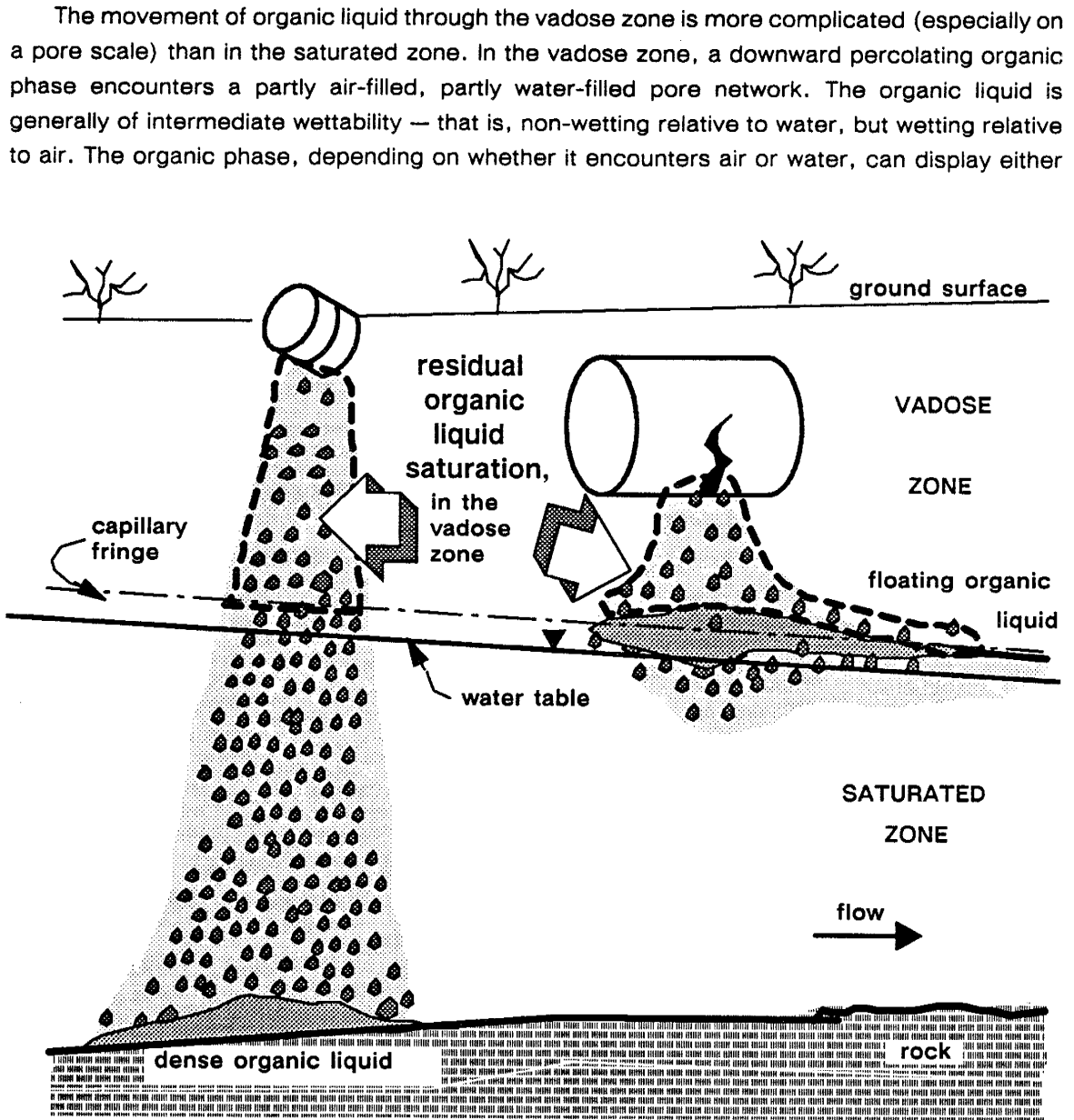
Figure 84.   Schematic of residual organic liquid trapped in the vadose zone.

wetting or non-wetting behavior. And because of its intermediate wettability, the organic phase tends to be found in between the water phase which preferentially occupies the smallest pores and the air which preferentially fills the largest pores. In fact, many organics have low internal cohesion and will spread, forming thin films between the water and air phases. For these reasons, the distribution of residual organic in the vadose zone is much more diverse and complex than in the saturated zone. A dropping or fluctuating water table can further complicate the behavior of organic liquids in the vadose zone.

This chapter on organic liquid movement and capillary trapping in the vadose zone begins by presenting the quantitative measurements of residual saturations from the short column experiments. The implications of these results are discussed and theoretical considerations are presented, including a comparison to saturated zone conditions. Qualitative results of several micromodel flow visualization experiments, as well as results from pore cast experiments are then presented and these results are also related to saturated zone conditions.

RESIDUAL SATURATION MEASUREMENTS IN SOIL COLUMNS

Quantitative measurements of residual saturation were made in short soil columns, as described in Chapter 4. Ten trials of the column experiments were successfully completed to determine residual saturations in the vadose zone, representing conditions far above the water table. Briefly, in each experiment an initially water saturated soil column was first drained with air under an applied suction to create an initial vadose zone condition. After the water saturation stabilized, an organic phase was flooded into the column, simulating the infiltration of organic pollutants through the vadose zone. After the fluid saturations had stabilized, the organic liquid was drained under an applied suction. Once the column re-stabilized, the residual organic liquid saturation was measured.

The ultimate organic liquid saturation left behind in the vadose zone is not independent of saturation history. In our column studies, we chose one simple but realistic saturation history to directly compare residual organic liquids found trapped in the saturated zone to those found trapped in the vadose zone. Owing to the saturation history dependence of residual saturation, the following **operational definition** for residual saturation in the vadose zone was used:

> *vadose zone residual saturation* — The organic liquid saturation obtained by injecting organic liquid into a water- and air-filled porous medium — in which water is already at its residual saturation — until the fluid saturations stabilize, followed by drainage of the organic liquid with air until the organic liquid becomes immobile and can be reduced no further.

It was hypothesized that residual saturations in the vadose zone would be substantially less than those measured for the saturated zone. It was anticipated that the presence of a third and non-wetting phase, air, along with the increased buoyancy forces and decreased capillary forces operating in the vadose zone, would be the causes for this lower residual saturation. The following discussion offers an explanation of the reasoning behind the hypothesis (expanded from Conrad and Wilson, 1988; Wilson et al., 1988b).

In the subsurface, capillary forces often dominate over viscous and buoyancy forces which oppose trapping. However, in instances where either viscous, or buoyancy, or a combination of these forces are large enough to overcome capillary forces, the residual organic liquid saturation may be reduced (Morrow and Songkran, 1981). Figure 85 illustrates this process. In two curves — one in which a wetting fluid displaces a non-wetting fluid, and the other in which a non-wetting fluid displaces a wetting fluid — the residual saturation is plotted as a function of the ratio of viscous plus buoyancy forces to capillary forces, $\dfrac{F_v + F_b}{F_c}$. First consider the case when the organic phase is non-wetting (such as when water displaces organic liquid in the saturated zone). Beneath a critical value of $\dfrac{F_v + F_b}{F_c}$, viscous and buoyancy forces are small compared to capillary forces and residual saturations are maximum, at a value of S_{or}^* . Once the critical value is exceeded, the combination of viscous and buoyancy forces overcome capillary forces at some locations and the residual organic liquid saturation is reduced. Amaulfule and Handy (1982) suggest that when displacing a wetting fluid (such as organic liquid being drained by air in the vadose zone),any increase in the capillary number (analogous to our ratio, $\dfrac{F_v + F_b}{F_c}$) will bring about a reduction in trapping. No critical value need be exceeded for a reduction in residual saturation to occur. The difference in displacement behavior for wetting and non-wetting fluids may be attributable to the fact that a wetting fluid is able to remain connected as it is being displaced while a non-wetting fluid breaks into discontinuous blobs. Although it is the intermediate-wetting fluid in the vadose zone, organic liquid will usually remain as a continuous
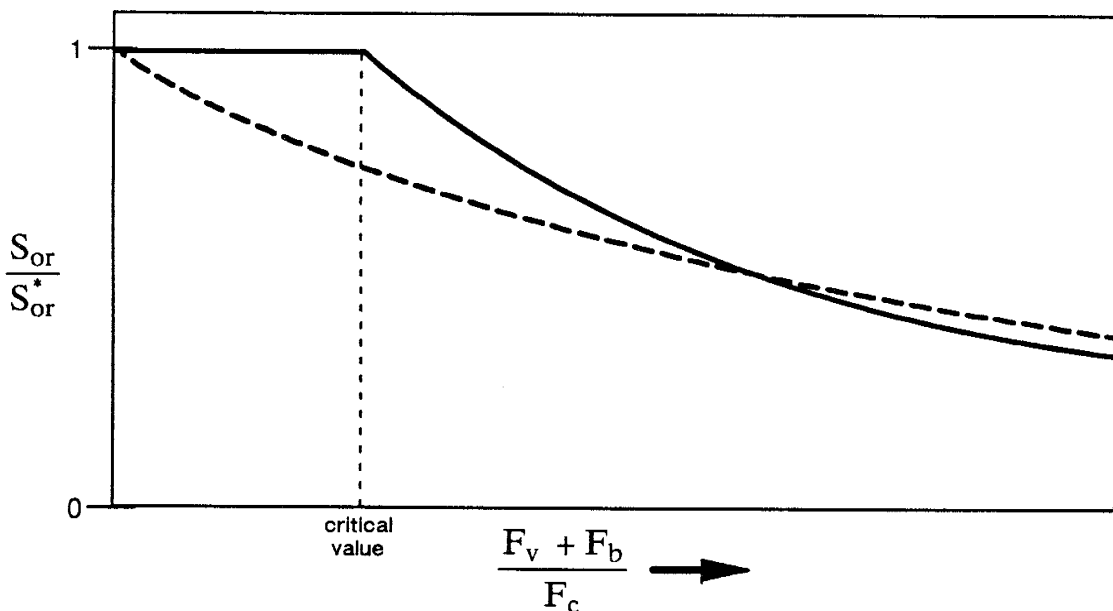
Figure 85.   A theoretical plot of trapped organic liquid as dependent upon the ratio of viscous and buoyancy forces over capillary forces when the organic phase is non-wetting (solid line), and when it is the wetting fluid (dashed line).

Zone	fluid pair	density difference (g/cm3)	Interfacial tension (dyne/cm)
Vadose	Soltrol/air	0.75	19.2
Saturated	Soltrol/water	0.25	48.7

Table 16. Relative density differences and interfacial tensions in the vadose zone and saturated zone.

phase, at least through films on the water phase. In this sense it acts as a wetting phase as it is drained by air in the vadose zone.

Residual saturation decreases as the ratio, $\dfrac{F_v + F_b}{F_c}$, is increased. Significantly, most organic pollutants immiscible with water have a much greater buoyancy force in the vadose zone (larger F_b), due to the large fluid density difference with air. The interfacial tension between air and organic liquid in the vadose zone is usually smaller than the tension between the organic liquid and water in the saturated zone (smaller F_c). For example, Soltrol-130, the organic liquid used in the micromodel experiments and column studies, has three times the buoyancy forces and 2.5 times less capillary forces in the vadose zone than in the saturated zone (see Table 16).

Under equivalent conditions (i.e., same soil and packing), $\dfrac{F_v + F_b}{F_c}$ will be a much larger in the vadose zone compared to the saturated zone. It is speculated that in the vadose zone buoyancy forces are sufficient to at least partially overcome capillary forces and thereby reduce the residual saturation. Conversely, in the saturated zone, the combined buoyancy and viscous forces are not great enough to overcome the capillary forces and the residual saturation is maximum.

Measured Residual Saturations

A summary of the vadose zone results is presented in Table 17. (These results were also reported in Hagan et al., 1989). All experiments were conducted with Sevilleta soil and Soltrol-130. In the first step of the experiment, an initially water-saturated column was drained to created unsaturated conditions. The column was drained under sufficient suction to reach the asymptotic portion of the capillary retention curve where the sand was almost completely drained and the water saturation became relatively insensitive to changes in capillary pressure. Water saturations in this region of the retention curve approached the residual water saturation, S_{wr} . The water saturation established in this drainage step remained constant throughout the duration of the experiment. The air saturation after this initial drainage step was: 100% − S_w . The

Trial	Suction * ($\pm$ 1 cm)	Temp. Range (°C)	Water Saturation (%)	Maximum Organic Liquid Saturation (%)	Residual Organic Liquid Saturation (%)
1	60	4.0	18.1 $\pm$ 1.9	62.1 $\pm$ 1.6	8.3 $\pm$ 0.4
2	68	3.6	19.8 $\pm$ 1.9	65.5 $\pm$ 1.8	12.0 $\pm$ 0.5
3	59	5.0	22.8 $\pm$ 2.3	63.9 $\pm$ 2.1	9.7 $\pm$ 0.6
4	61	4.3	21.6 $\pm$ 2.1	78.3 $\pm$ 2.2	11.3 $\pm$ 0.5
5	66	2.3	18.5 $\pm$ 2.1	64.5 $\pm$ 1.9	7.7 $\pm$ 0.4
6	71	4.3	20.3 $\pm$ 2.2	66.2 $\pm$ 2.0	7.9 $\pm$ 0.5
7	70	2.1	23.2 $\pm$ 2.2	56.9 $\pm$ 1.8	12.2 $\pm$ 0.6
8	69	1.9	18.3 $\pm$ 2.4	65.2 $\pm$ 2.1	7.1 $\pm$ 0.4
9	71	2.6	19.8 $\pm$ 3.7	66.1 $\pm$ 3.2	9.1 $\pm$ 0.7
10	75	2.0	15.8 $\pm$ 2.4	71.4 $\pm$ 2.2	5.5 $\pm$ 0.4
Avg.	–	–	19.8	66.0	9.1
σ_{n-1}	–	–	2.3	5.6	2.2

* cm of water were used during water drainage, cm
of Soltrol were used during organic liquid drainage.

Table 17.   Results from the vadose zone column experiments. Soltrol-130 was used as the organic liquid and Sevilleta sand served as the soil.

average water saturation over the ten experimental trials was 19.8%, thus the average air saturation was 80.2%.

Next, Soltrol was injected into the column simulating the movement of organic liquid percolating through the vadose zone toward the water table. Advancing Soltrol displaced only air from the column. Again, because the water saturation was so low (at or near its residual saturation), the water was essentially immobile and none was displaced from the column. At the conclusion of this step the organic phase had reached its maximum saturation (listed in Table 17). The maximum organic saturation reached in these vadose zone experiments was significantly lower than the maximum saturation reached in the saturated zone column experiments (66.0% versus 85.1% on average) due to to the presence of a third phase — that is, entrapped air occupied pore space that otherwise would have been occupied by Soltrol in a two-phase (saturated zone) system.

The entrapped air saturation at the conclusion of the Soltrol injection was calculated as: 100% – S_o – S_w . The mean entrapped air saturation over the ten experimental trials was 14.2%. Since the water saturation was unchanging, it might be reasonable to think of organic liquid displacing air as being analogous to the final displacement step of the saturated zone

experiments where water displaced organic liquid leaving behind a residual saturation — in each case a more wetting fluid displaced a less wetting one and some entrapped non-wetting phase was left behind. However, the entrapped air saturation in the three-phase experiments was found to be only about one half the residual organic saturation of the saturated zone experiments (14.2% versus 27.1%). Some of the air may have dissolved into the displacing organic phase, but more likely the displacement was more efficient for some reason. Perhaps, due to the very low viscosity of the air phase, the air was less likely to become by-passed. One could think of this phenomena as the effect of an extremely favorable mobility ratio operating on a pore scale. At any rate, it appears that entrapped air saturations are consistently smaller than residual organic saturations. Two-phase organic/air and water/air retention curves yield similar entrapped air saturations (see Appendix A).

In the final step of the three-phase experiment, organic liquid was drained from the column and replaced by air. Sufficient suction was applied to reduce the organic liquid saturation as low as possible by purely hydraulic means. **The average measurement of residual organic liquid saturation in the vadose zone was found to be 9.1 ± 2.2% — less than one third of the value measured in the saturated zone, confirming the hypothesis.** As will be seen in the flow visualization experiments, the residual organic phase in the vadose zone remains interconnected (unlike in the saturated zone where the residual becomes trapped as discontinuous blobs), but the permeability at this saturation has been reduced so low as to be negligible. This vadose zone residual saturation has been referred to by other researchers as the organic phase 'retention' for a soil.

Comparison with Other Studies

The organic phase retention from these three-phase experiments were not significantly different from the minimum organic saturations obtained from air/organic drainage curves (compare with the results in Appendix A). These findings are somewhat inconsistent with those of other researchers reporting results from column studies. Eckberg and Sunada (1984) reported slightly higher organic liquid retentions in two-phase (organic/air) systems than for three-phase (water/organic/air) systems. Convery (1979) reported two-phase retentions to be between 10% and 25% higher than three-phase systems, while Hoag and Marley (1986) reported retentions between 20% and 30% higher.

Eckberg and Sunada measured fluid saturations at points along their long column, but both Convery, and Hoag and Marley reported saturations that were integrated over the length of their long soil columns. Such an approach gives an 'averaged' saturation as opposed to a vadose zone retention because the fluid saturations were not uniform over the length of the columns. Due to the boundary conditions at the bottom of their columns ($P_c = 0$, an open-air boundary), they had a capillary fringe (a capillary end effect) at the bottom. This lower boundary caused fluid saturations to vary from the bottom of a column (high wetting phase saturation) to the top (much lower wetting phase saturation). Not surprisingly, Hoag and Marley found that their measured saturations varied with the length of column they used in their experiments.

Failure to account for capillary end effects resulted in artificially high organic phase retentions. This result was especially true for the two-phase system in which the organic liquid

acted as the wetting phase and assuredly was present in high saturations at the bottom of the column, in the capillary fringe. In Eckberg and Sunada's study, the problem of capillary end effects was avoided by taking point measurements. In the current study, the problem was avoided by using a short column (in which the saturations can vary only slightly over the length of the column), and by applying a suction at the bottom boundary $(P_c \gg 0)$.

In summary, the organic phase retentions measured in this study were similar to those of Eckberg and Sunada (1984) in that the organic liquid retentions measured for three-phase (water/organic/air) systems were not much different than retentions measured for two-phase (organic/air) systems. Although Convery (1979) and Hoag and Marley (1986) reported higher organic liquid retentions for two-phase systems than for three-phase systems, these results may be attributable to an artifact of their experimental design. They measured one 'averaged' organic liquid retention over the length of a long column, but didn't account for capillary end effects at the bottom boundary of their columns.

ORGANIC LIQUID IN AN UNSATURATED HOMOGENEOUS MICROMODEL

Micromodel flow visualization techniques in homogeneous media were used to illustrate the scenario of a large slug of organic liquid percolating vertically downward into the vadose zone (Mason et al., 1989a,b). This scenario was simulated by first saturating a micromodel with water. Then, a vadose zone condition was created by draining the water with air to a low water saturation. An organic liquid was advanced downward into the experimental apparatus, representing the advance of the slug of organic liquid. And finally, the organic liquid itself was drained by air, representing the trailing end of the slug and the residual saturation left behind. The organic phase left behind in the vadose zone was observed visually. By creating a saturation history similar to the three-phase column experiments, we can get an inkling of what the residual saturation in those soil columns must have looked like.

Creating the Initial Vadose Zone Condition

The homogeneous micromodel with the capillary barrier (see Figures 33 and 41) was used in this three-phase experiment. The model, oriented vertically with the barrier at the bottom, was imbibed with water from the bottom and then drained from the top with air to achieve the initial vadose zone condition. The water was introduced and drained from a buret. The water was drained under a suction of about 15 cm H_2O, just under the air entry pressure of the capillary barrier. The steady-state condition of the entire model, at the end of drainage, is shown in Figure 86. In these photos the water was dyed blue; the air was colorless. This steady-state condition represented the vadose zone above the transition zone, where the water approached residual wetting-phase saturation. Because the model had fairly large pores and a relatively uniform pore size distribution, not much suction was needed to achieve a fairly complete drainage. Unlike the results obtained from other micromodels, the presence of the capillary barrier at the bottom of the model prevented a capillary end effect.

Figure 86. Initial vadose zone condition, with water drained by air to residual (irreducible) water saturation. The water was dyed blue, and the air was not dyed.

Organic Liquid Advance

Red-dyed Soltrol was advanced downward into the drained micromodel at a relatively slow rate of 0.096 ml/min. Air and perhaps some water was pushed ahead of the advancing front of organic liquid. At the bottom of the model sufficient pressure was achieved to exceed the air entry pressure of the capillary barrier, thus allowing air to escape.

Often during this displacement, some organic liquid was observed ahead of the main front of advancing organic liquid. At first glance, it was difficult to understand where this fluid had come from, but closer examination revealed that it had traveled through thin films of organic phase formed between the air and water phases. McBride et al. (1990) argue that the spreading pressure that leads to the formation of these films is not implicitly incorporated into the capillary pressure, and that this spreading force needs to be explicitly incorporated into the calculation of the driving forces for three-phase flow models.

The steady-state condition for the entire model, at the end of the organic liquid advancement, is shown in Figure 87 and a more detailed photo is shown in Figure 88. Notice in the detailed photo that the Soltrol has formed a number of thin films between the air and the water. Many organics have relatively little internal cohesion and therefore tend to spread in this fashion, resulting in a reduction of the surface energy of the system. As will be discussed in more detail later, these films are quite often the thread of continuity that keep all the little pockets of organic liquid in hydraulic connection.

Notice also that the saturation and distribution of the water phase remained almost entirely unchanged when compared to the initial vadose zone condition, and that the air phase has been reduced to an entrapped residual non-wetting phase saturation similar to that seen for the organic phase in two-phase micromodel experiments (refer back for instance to Figure 55b). Because of the presence of air in the vadose zone, the maximum organic liquid saturation achieved was not as great as in the saturated-zone case. Compare the organic liquid saturation in Figure 87 to that of Figure 55a.

Drainage of Organic Liquid by Air

In the final step of the experiment, Soltrol was drained from the model by air, representing the continued percolation of the organic phase downward toward the water table. The Soltrol was drained from the model under a small applied suction. This suction is believed to have been insufficient to completely drain the organic phase to its lowest possible saturation, but because Soltrol has a much lower surface tension than water, higher applied suctions would have resulted in air breaking through the capillary barrier.

The final distribution of fluids within the entire model is shown in Figure 89, while the close-up photos in Figure 90 illustrate the more complex distribution of organic liquids left behind in the vadose zone. Compare Figure 89 to Figure 55b and note that the amount of organic phase retained in the vadose zone is much less than the residual saturation left behind in the saturated zone — just as was the case in the column experiments.
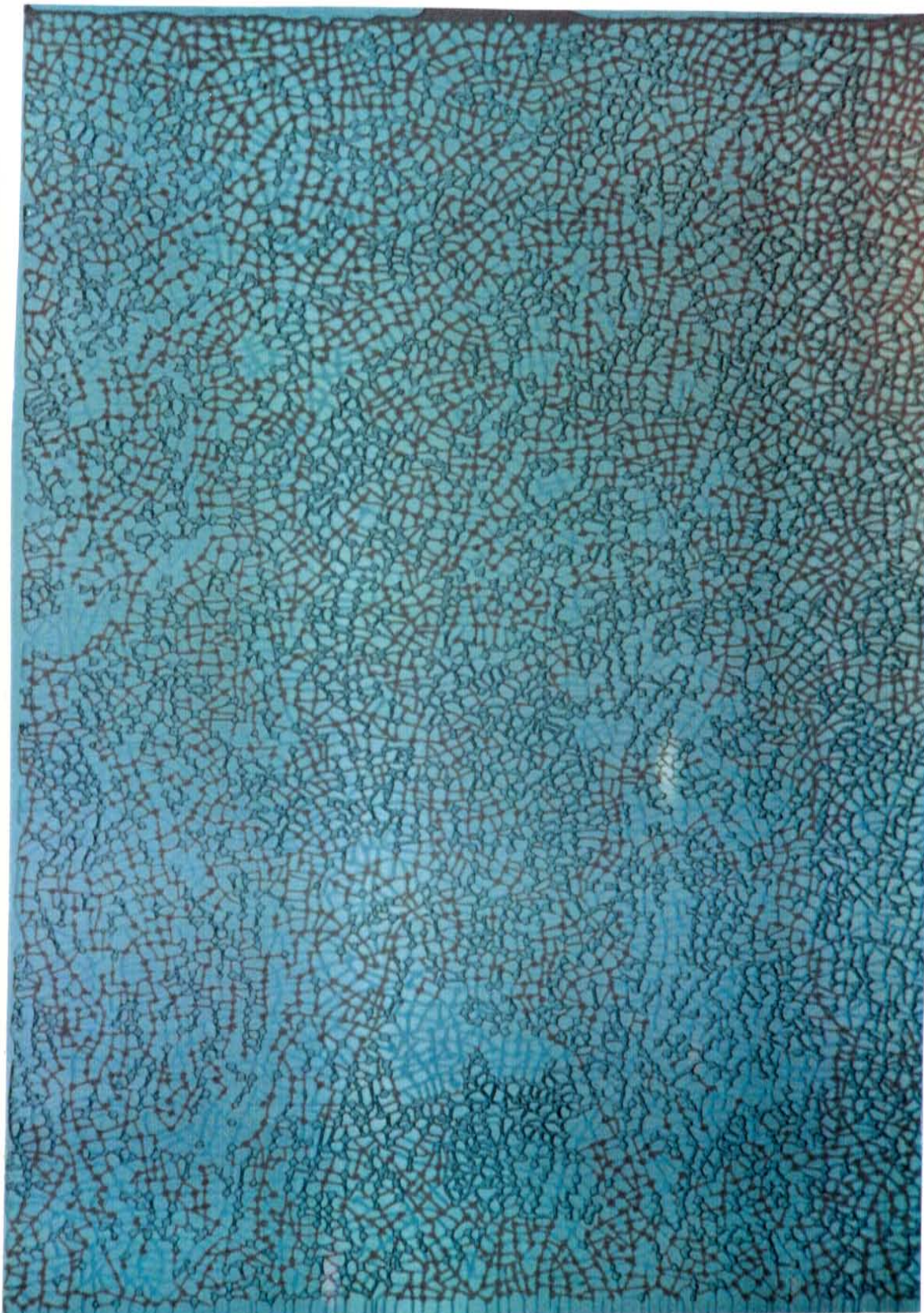
Figure 87. Steady state conditions after the Soltrol invasion into the vadose zone model. Soltrol was dyed red, water was dyed blue, and the air was not dyed.
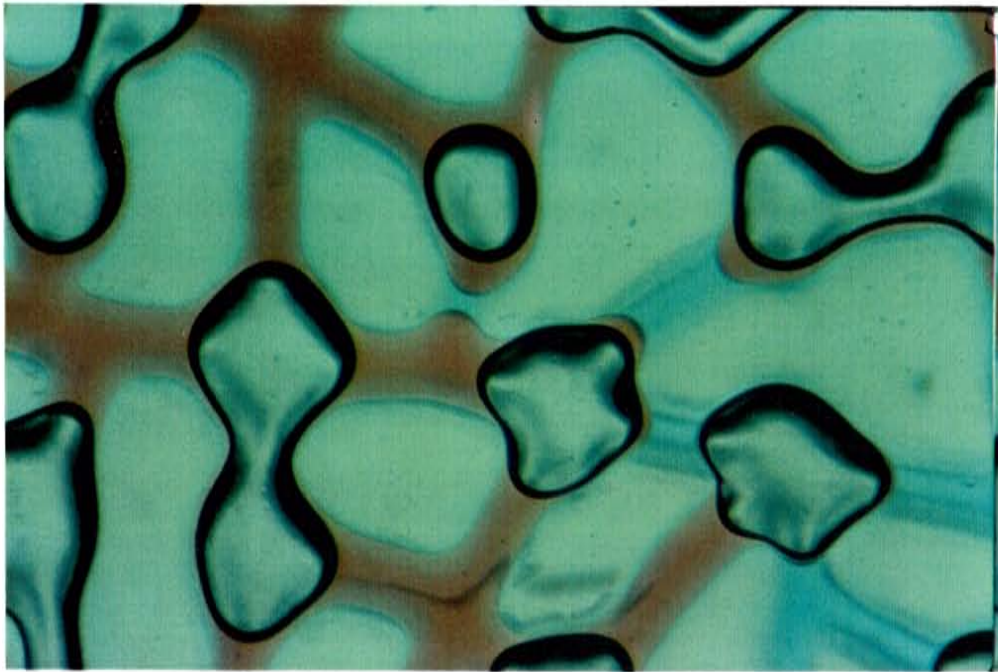
Figure 88. Detail of steady state conditions after the Soltrol invasion into the vadose zone model. Soltrol was dyed red, water was dyed blue, and the air was not dyed.

Organic liquid can be trapped in several different ways in the vadose zone. In particularly dry areas, it can be trapped in pore throats, in small pores, and as films entirely within the air phase. Occasionally, organic liquid can be trapped — as in a two-phase case — as blobs within the water phase, although this kind of trapping is more likely to occur when the initial water content is relatively high or when infiltrating water follows the organic liquid (e.g., rainfall following a spill event). However, due to its intermediate wetting properties and its tendency to spread, organic liquid in the vadose zone is most commonly retained in between the water and air phases. Notice in the detailed photo that although the saturation of the organic phase had been reduced by drainage, the thin films of organic liquid between the air and the water were still present.

In contrast to blobs trapped in the saturated zone, the organic phase trapped in the vadose zone remains more or less continuous. The final distribution of Soltrol in this micromodel — although complicated by the presence of water — was not dissimilar to drained wetting phase distributions described by Hillel (1980), Gvirtzman et al. (1987) and others. In this particular experiment, because of the relatively low initial water saturation and because the organic phase readily spread on the water/air interface, the organic phase acted much like a wetting phase both in its character of migration and its final distribution within the pore space. Based on this observation, unsaturated (water/air) flow models could serve as a good approximation to organic liquid movement for spills in arid soils.

Implications for flow modelling

Some of the insights gained from these pore-level and bench-scale vadose zone experiments may be used to refine our present conceptions about multi-phase fluid flow and the

– 158 –
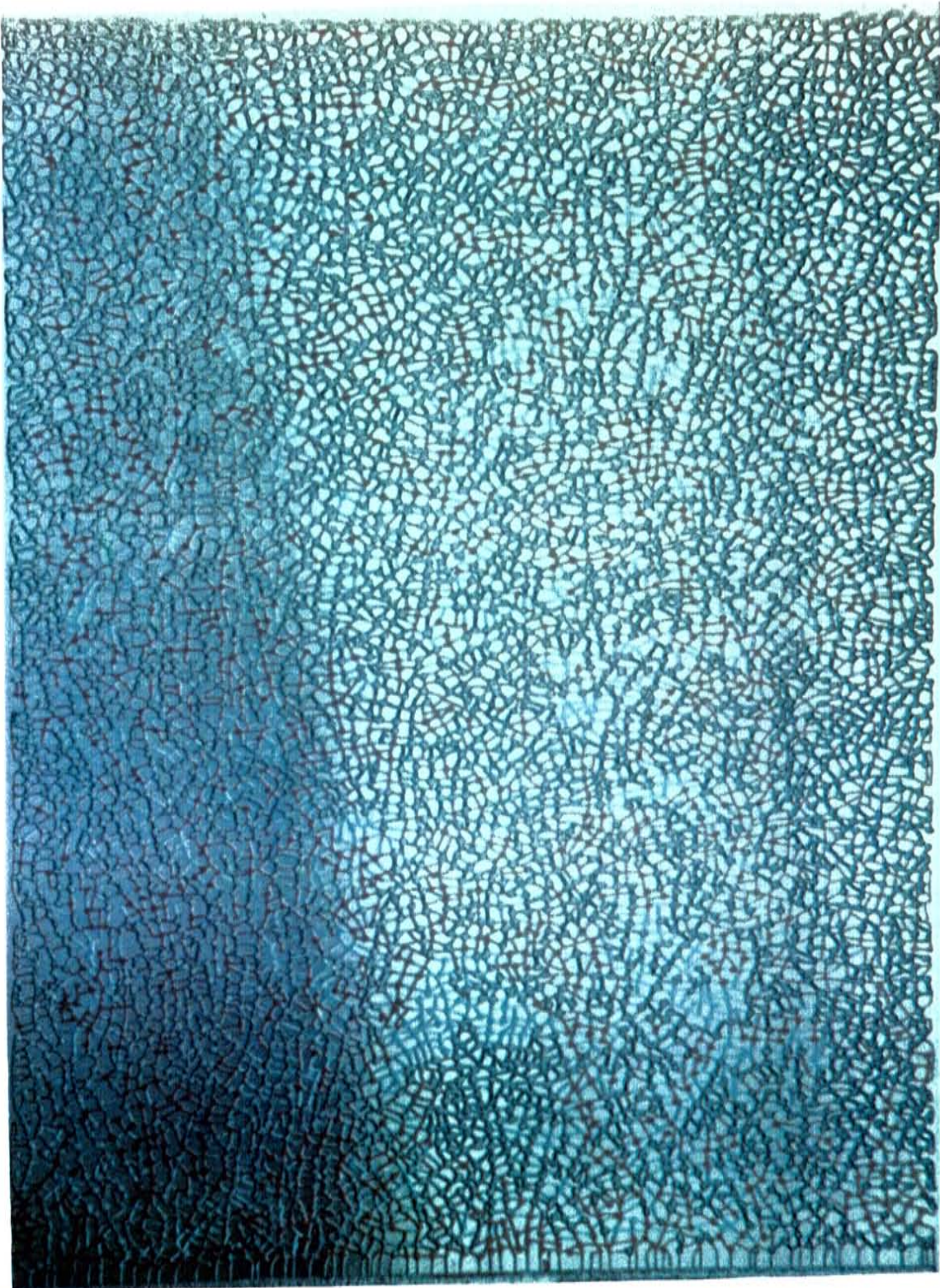
Figure 89.   Steady state conditions after the Soltrol had been drained by air from the vadose zone model. Soltrol was dyed red, water was dyed blue, and the air was not dyed.
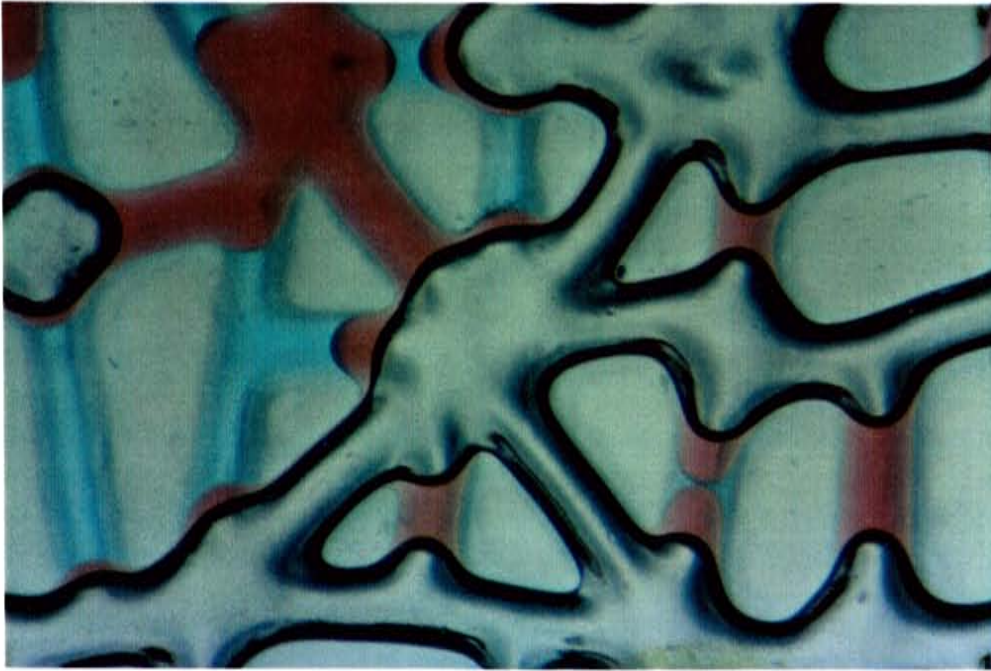
Figure 90.   Detail of steady state conditions after the Soltrol has been drained by air from the vadose zone model. Soltrol was dyed red, water was dyed blue, and the air was not dyed.

partitioning of organic components between phases. The pore-scale observations in some cases also can be useful in evaluating the reasonableness of multi-phase flow and transport models.

As a quick example of how these results can be applied to evaluating multi-phase flow models, let's look at one assumption of Parker and Lenhard's (1987) hysteretic model of multi-phase flow. In this model, entrapment of one fluid phase within another fluid phase of lesser wettability is assumed not to occur (e.g. organic liquid within air). This assumption, while being computationally advantageous, may not always be reasonable as demonstrated in the three-phase micromodel and column displacement experiments of this study. Figure 90 shows trapped organic liquid in a three-phase system. In this photo, almost all of the organic liquid is trapped between the air and water phases — contrary to the assumption of the Parker/Lenhard model which allows for trapping of organic liquid only within the water phase.

Our three-phase flow visualization experiments have shown that the organic liquid can be trapped in several different ways in the vadose zone, not just as discontinuous blobs within the water phase. Three-phase soil column experiments provide additional evidence. The Parker/Lenhard model would predict no trapping of the organic liquid in our column experiments, but results show that a significant amount of organic liquid is indeed trapped (9%). As a practical matter however, when the organic liquid saturation gets low enough, the Parker/Lenhard model drops the organic liquid permeability so low that organic liquid flow essentially ceases. So in this case, even though the assumptions of the Parker/Lenhard model are not in agreement with

experimental observations, the model would appear to be able to reproduce similar 'residual' organic liquid saturations in the vadose zone to those observed experimentally.

On the other hand, another assumption of the Parker/Lenhard model — that three-phase capillary pressure/saturation relationships can be approximated by two two-phase relationships — appears to be a valid one. This assumption, first proposed by Leverett (1941), maintains that water saturations in a three-phase system are a function of the two-phase water/organic retention curve, while the total fluid saturations (water + organic) are functions of the organic/air curve. Implicitly, this assumption does not allow water/air interfaces to exist. And indeed, in our flow visualization experiments we see comparatively few water/air interfaces. So for the majority of common organic pollutants which tend to spread between the air and water phases in the vadose zone, approximation of three-phase capillary pressure/saturation relationships using two two-phase retention curves seems to be an appropriate assumption to invoke because it preserves the physics and surface chemistry of the three-phase flow system (in addition to being computationally advantageous).

Network or percolation models have been used to model multi-phase displacements on a pore scale. Recently, attempts have been made to extend percolation theory to three-phase systems (e.g. Soll and Celia, 1988). These models operate on an either/or principle, meaning each pore is either contains one fluid or another. Two fluids are not permitted to occupy the same pore simultaneously. In our micromodel experiments however, we have commonly observed two and three phases simultaneously occupying a single pore. Because the wetting and intermediate-wetting phases remain self connected through films, they maintain continuity to drain or imbibe in a manner that cannot be captured using a traditional network approach.

Implications for phase partitioning

As discussed earlier in the saturated zone chapter, the pore-scale distribution of the organic phase influences the partitioning of organic liquid components. Because the organic phase is almost always less wetting than water but more wetting than air, it remains in direct contact with both the air and water allowing for both dissolution into the water phase and volatilization into the air phase. And importantly, the formation of thin organic liquid films between the water and air increases the surface area of the organic phase, enhancing the propensity for inter-phase partitioning of organic components. Soil venting of organics in the vadose zone has become an attractive remediation strategy because volatile organics partition easily to the air phase. Figure 91 provides a good example of the large organic/air and organic/water interfaces generated by the organic phase's tendency to spread.

Non-spreading Organics

As stated previously, in the vadose zone most organic liquids tend to spread along the air-water interface. However, not all organic liquids spread. For pure fluids, whether or not a liquid will spontaneously spread or form a lens can be predicted from the spreading coefficient, S. The spreading coefficient is calculated as the air-water interfacial tension, σ_{aw}, minus the sum of the air-organic interfacial tension, σ_{ao}, and the organic-water interfacial tension, σ_{ow}:

$$S = \sigma_{aw} - \sigma_{ao} - \sigma_{ow}$$

Spreading will not occur for $S < 0$, but will occur for $S > 0$. Of the fluids used in this study, PCE has a negative spreading coefficient and thus would be expected to behave somewhat differently than a spreading fluid in a vadose-zone micromodel experiment.

To observe the behavior of a non-spreading organic liquid, a vadose-zone micromodel experiment was run under identical procedures to that described previously except that PCE was used as the organic phase (Mason et al., 1989a). Qualitatively, the displacements of this experiment appeared not to be terribly dissimilar to those of the Soltrol (spreading fluid) experiment, except that the PCE was far less likely to travel through films ahead of the main front of advancing organic liquid.

Of greater interest was the final pore-scale distribution of the PCE. A photograph of the distribution of the three fluid phases within the lower right quadrant of a single pore is shown in Figure 92. Because addition of dyes to the liquids was found to change the spreading behavior of the PCE, no dyes were added to the fluids for this experiment. Consequently, all three phases are colorless making it more difficult to distinguish between the phases. The interfaces between the fluids are distinguishable however, and that is sufficient to allow us to see what's going on. At the far right of the photograph, the dark film is the water phase outlining the pore wall. The light feature against the water film to the left is PCE, the organic phase. Air occupies the interior of the

Figure 91. Detail a thin organic liquid film located between the gas and water. The photo represents steady state conditions after the Soltrol has been drained by air from the vadose zone model.

Figure 92. The distribution of three fluid phases (air, non-spreading PCE, and water) within a single pore in a micromodel.

pore, inside of the organic phase. The circular shapes seen within the air phase which look like dimples on a golf ball (or the craters of the moon) are actually lenses of PCE on the pore wall. Remember that the micromodel pores are truly three-dimensional. Although it cannot be seen, it must be presumed that a water film covers the entire pore surface. Between that water film and the air phase sits lenses of PCE. Because PCE does not spread, lenses of organic liquid — instead of a thin organic film — are found between the water and air phases. The PCE, because it is of intermediate wettability, continues to preferentially reside between the water and air phases, but because it is non-spreading, does not maximize its surface area between water and air as would a spreading fluid.

There are three important implications to be derived from the observation of non-spreading organics. First, with less surface area per unit volume, perhaps less interphase transfer will occur. Under the high air-flow rates associated with soil gas venting, it is possible that the less volatile constituents of the organic phase may not reach equilibrium with the passing air. Currently, gas venting models presume local equilibrium is reached between the organic phase and the soil gas. (e.g. Johnson et al., 1990). Second, since the organic liquid tends to break up into disconnected lenses instead of maintaining continuity through thin films, there is perhaps a potential for greater organic retention in the vadose zone. And finally, continuum three-phase flow models routinely invoke the hypothesis of Leverett (1941) in which organic liquid is presumed to be present between the air and water. The only interfaces which need to be considered are the water/organic and organic/air interfaces. This assumption is clearly not met

for non-spreading organics. For non-spreading organics, the complicating effect of a water/air interface will probably need to be explicitly taken into account.

THREE-PHASE PORE CASTS

As has been seen in the micromodels, the distribution of the trapped fluids in the vadose zone is markedly different from the distribution found below the water table. The three-phase distribution of fluids in a soil, as presented in Figure 93, shows similar patterns of fluid distributions to those seen in the micromodels. This photomicrograph shows a pore cast surface of a three-phase experiment which was performed using the Sevilleta sand. In the photo, the fluids occupy a channel between two quartz grains. The wetting phase (light pink) appears in the narrow portion of the channel. The intermediate-wetting phase epoxy — the colorless crescent between the pink and blue colored fluids — occurred between the wetting and non-wetting phases in a fashion similar to that observed in the three-phase micromodel experiments. The blue epoxy, introduced to fill the pore space occupied by air at the conclusion of the experiment, appears in the broadest part of the channel.

Unlike the micromodel experiments, the intermediate-wetting phase remained undrained from a substantial number of pores. The large number of undrained pores were an artifact of the rapid draining procedure (Peplinski et al., 1989). The relatively high viscosity (50-60 cps) and
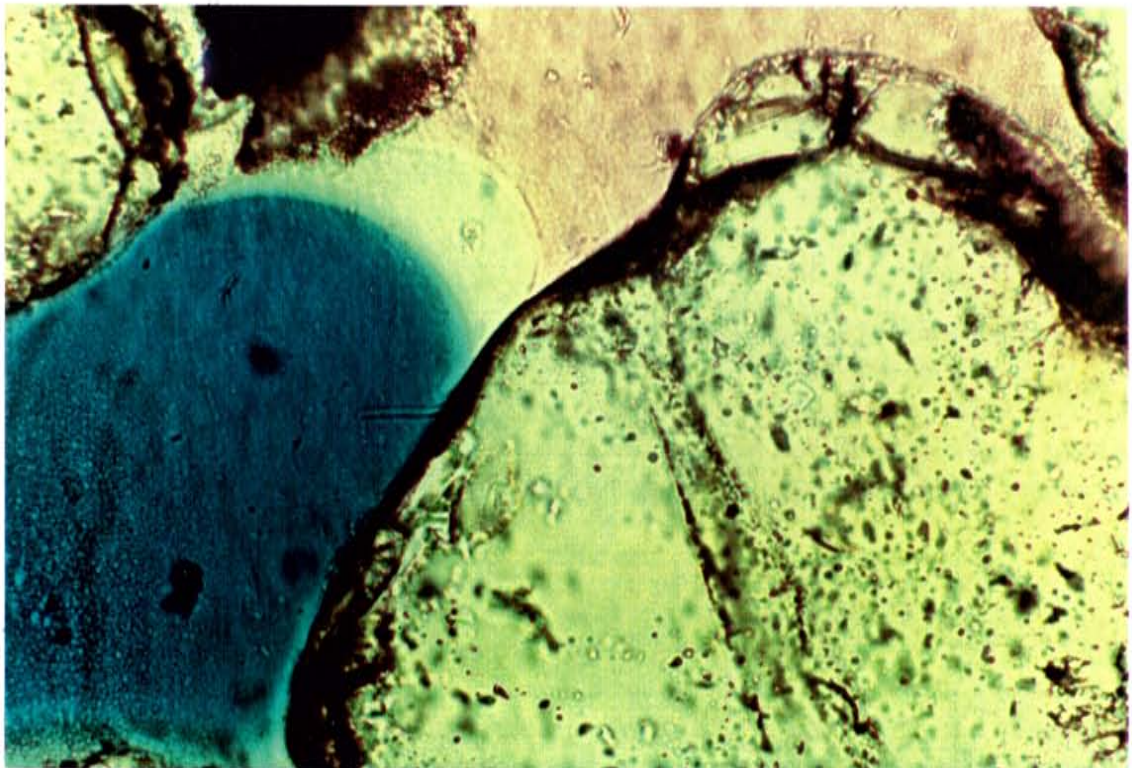
Figure 93. A photomicrograph of three phases in the Sevilleta sand. In the photo, the wetting phase, (styrene) is pink, the epoxy representing the air phase is blue, and in between the intermediate-wetting phase (epoxy) is colorless. Shown at 100X magnification.

rapid setup of the Tra-Bond epoxy required greater flow rates and higher pressures in the column. Higher pressures caused air to break through the capillary barrier at the bottom of the column, effectively stopping the epoxy drainage. The filter failed when the intermediate-wetting epoxy saturation had been reduced to about 35%, still far larger than the residual saturation expected for this soil under unsaturated conditions. What was actually observed in this experiment, then, was the distribution of fluids while the intermediate-wetting phase was still in the process of draining. In an attempt to improve the epoxy drainage of the sand pack another low viscosity epoxy, Polysciences' Ultralow® (μ = 10 cP), was tried but the epoxy proved to be incompatible with the already hardened styrene. The Ultralow leached the 9,10-diphenylanthracene dye out of the styrene and made it impossible to distinguish between the two phases.

Experimental difficulties — troubles with dyes, surrogate fluids, high viscosities, et cetera — make polymerization techniques less appealing than micromodels for observing multi-phase fluid flow. But the fact that, despite problems, these experiments show similar flow behavior (as observed through fluid distributions) to the that observed in the micromodel experiments again gives confidence that micromodels can serve as a reasonable representation of the pore networks found in soils. This result provides confirmation that additional three-phase micromodel experiments are worth persuing.

CHAPTER SUMMARY

Organic liquid movement and capillary trapping in the vadose zone were investigated through the use of soil columns, micromodels, and pore casts. The implications from the results of these experiments were discussed including a comparison with saturated zone results.

Soil Columns

It was hypothesized that residual saturations in the vadose zone would be significantly lower than those measured in the saturated zone because of a substantially different balance of forces — namely smaller capillary forces and greater buoyancy forces. The results of the soil column experiments confirmed that hypothesis. Experiments run using Soltrol as the organic liquid and Sevilleta sand as the soil yielded residual saturations on the order of 9% in the vadose zone versus about 27% in the saturated zone.

Micromodels

Most notable from observations of the micromodel experiments was the formation of thin films of organic liquid between the air and water phases. As suggested by other researchers, the spreading force which leads to the formation of films may be a significant driving force for organic liquid movement in the vadose zone.

In confirmation of the soil column results, residual saturations in the three-phase micromodel experiments were significantly lower than those observed in two-phase (organic/water)

micromodel displacements. The high degree of continuity maintained within the organic phase due to the presence of interconnecting films almost certainly plays a part in achieving low residual saturations in the vadose zone.

Photographs of final fluid distributions showed that organic liquid residual saturations in the vadose zone were profoundly different from the blobs seen in the saturated zone. In the saturated zone, surface area of the organic phase is minimized whereas in the vadose zone the surface area is maximized — at least for spreading organics. This spreading, film-forming behavior has important implications for maximizing interphase transfer in the vadose zone.

Non-spreading organics showed somewhat different final fluid distributions. PCE used as the organic phase in a three-phase micromodel experiment showed a tendency to form small lenses instead of films in between the water and air phases. Through the formation of lenses, less surface area of the organic phase was created as compared to spreading organics, but certainly a much greater surface area was created as compared to the minimized surface areas observed for blobs in the saturated zone. Implications of non-spreading behavior may include: the possibility of reduced interphase transfer; higher residual saturations; and for flow modellers, the inability to invoke Leverett's (1941) simplification for three-phase capillary pressure versus saturation relationships.

Pore Casts

The three-phase pore casts suffered from some experimental difficulties, but still showed similar three-phase fluid distributions to those seen in the micromodel experiments.

Model Validation

Again, as suggested in the previous chapter, these experimental results can be useful as tools for model validation. They can be useful in two ways: first, they can be used as a check to assure the assumptions of flow and transport models conform to experimental observations; and secondly, the results can be used as benchmarks to test the models. The models should be able to reasonably reproduce the experimental results.

CHAPTER 10

CONCLUSIONS AND RECOMMENDATIONS

The intent of this study has been to better understand the basic physical mechanisms controlling the movement, and especially the capillary trapping, of organic liquid pollutants spilled into soils and groundwater. This goal was pursued by observing the flow behavior of organic liquids in a multi-phase system in laboratory soil columns and through etched glass micromodels built to represent various conditions in the subsurface. Fluid movement could be explained in terms of three basic forces acting on the fluid phases — capillary forces, viscous forces associated with flow, and the effect of gravity.

The most interesting series of observations in this study has illustrated how the interplay between capillarity and soil heterogeneities profoundly influence the the migration and trapping of an organic phase in a multi-phase system. These findings for immiscible displacements extend the recent work on heterogeneity-induced fingering or 'macrodisdersion' for miscible displacements as well as the work on moisture-dependent anisotropy for water movement in the vadose zone.

Not unlike many scientific studies, the results of this research seem to have raised as many questions as they have answered. Recommendations for future work logically stem from the conclusions, and therefore many of the recommendations are interspersed amongst the conclusions.

This chapter is divided into five parts. The first three parts present conclusions and recommendations corresponding to the three results chapters. It is recommended that the reader peruse the photographs in Chapters 7, 8, and 9 to fully appreciate many of the conclusions. The fourth part presents some conclusions and recommendations concerning the experimental procedures, and in the final part, some additional recommendations for future research are presented.

SATURATED ZONE CONCLUSIONS — HOMOGENEOUS MEDIA

A series of column studies were performed to measure residual organic liquid saturations in soils. A general conclusion from that work was:

- **As organic liquid moves through the saturated zone, a significant portion is left behind, trapped by capillary forces.** Residual saturations were measured that ranged from 14% to 30% in unconsolidated sands. If these estimates are at all typical for organic liquids in sandy soils, then there is a tremendous storage capacity for organic liquid pollutants in the saturated zone. Even under optimal conditions, hydraulic removal of organic liquids will leave behind a substantial portion of the total spilled volume. Any unrecovered organics constitute a continual source of contamination to the aquifer as constituents of the organic phase slowly dissolve into the water phase.

Residual saturations were measured in the Sevilleta sand for a suite of organic liquids. The fluids were selected as examples of (or surrogates for) commonly spilled organics, and to cover a fairly wide range of fluid properties between them. It was concluded that:

- **Residual saturation in a given soil was found to be independent of organic liquid composition.** Residual saturations were measured for a variety of multi-component and single component organic liquids: Soltrol-130, gasoline, kerosene, p-xylene, n-decane, and tetrachloroethylene (PCE). In repeated quantitative short column experiments, no correlation was found between residual saturation, and viscosity, density, or interfacial tension for the six organic liquids tested. The residual saturation was virtually identical for all of the organic liquids.

  Recommendation — Since residual saturation has been shown to be independent of fluid properties, it is probably best to **chose an ideal organic liquid when measuring residual saturations in the lab**. Such a surrogate for the organic liquid of interest would have the following attributes: low solubility in water, low volatility, low toxicity, and (for gravimetric measurement of residual saturations) a sufficient density difference with water.

- **The interfacial tension must be reduced significantly to allow hydraulic schemes to mobilize residual saturations.** Quantitative analyses of pore-scale trapping mechanisms showed that trapping could not be averted unless interfacial tensions were dramatically reduced. Surfactant floods hold promise of perhaps reducing interfacial tensions sufficiently to allow some mobilization of the residual saturation.

  Recommendation — **Investigate mobilization via surfactant floods.** Surfactant floods can be used in an attempt to mobilize residual organic liquid saturations by reducing interfacial tensions and capillary numbers, or simply by emulsifying the organic liquid. Both of these mechanisms should be explored in micromodel and column experiments for typical combinations of organic liquids, surfactants, and soils.

Residual saturations were also measured over several soils. From this suite of experiments it was concluded that:

- **A priori prediction of residual saturations for a given soil is uncertain.** A large number of residual organic liquid saturation measurements were made on the Sevilleta sand, an unconsolidated, aeolian sand. Its texture is much more like glass beads than sandstone, both of which had been previously investigated by petroleum engineers. We examined the hypothesis that, because of its similar texture, the Sevilleta sand should behave more like the glass beads. Uniform glass beads exhibit a residual saturation of 14-16%. The Sevilleta mean residual saturation was 27.1%, almost 10% greater than expected. Singlet blobs are common in glass beads. Photomicrographs of Sevilleta blob and pore casts revealed a much larger population of complex, branching blobs. Residual saturations in the Sevilleta sand did not behave as expected. However, residual saturations measured in two other

sandy soils, the Llano coarse sand and the Traverse City sand, yielded saturations of 17.2% and 17.6% respectively. These residual saturations were much closer to results reported for glass beads than to the Sevilleta sand results.

● **Residual saturations appear to be very sensitive to soil properties, but any correlation between residual saturation and soil texture may not be straightforward.** Residual saturations were measured in several sandy soils. Two soils of very similar texture and grain size (the Sevilleta sand and the Traverse City sand) yielded significantly different residual saturations (27.1% and 17.6%, respectively). Two soils with somewhat different textures and grain sizes (the Traverse City sand and the coarser, less uniform Llano sand) had very similar residual saturations (17.6% and 15.8%, respectively).

Recommendation — **Study 2-phase residual saturations for more soils.** What had originally been thought of as a 'beefhead' study has suddenly become more interesting in light of surprising residual saturation results. A combination of quantitative experiments, pore casts, and blob casts could be employed to develop an explanation for these inscrutable preliminary results.

● **Even minor amounts of clay or silt in a soil may play a significant role in the observed residual saturation.** The Sevilleta sand had about 2% clay and silt, by weight. The Traverse City and Llano sands were essentially clay and silt free. It is hypothesized that the clay and silt content of the Sevilleta was responsible for the high residual saturation and complex, branching blobs that were observed. One possible explanation is that the fine material may have settled into microlayers during the column packing procedure. This type of heterogeneity could lead to increased water by-passing of the coarser material. If this is true, then the residual saturations measured for the Sevilleta sand demonstrate that even minimal soil structure and heterogeneity can have a dramatic influence on the degree of capillary trapping.

Recommendation — **Determine the role of clay and silt on residual organic liquid saturations.** This issue must be resolved. The large and unexplained variation in residual saturations between soils (17% to 27%) has enormous practical implications. A careful investigation of the role of the fine fraction with an emphasis on possible packing induced heterogeneities is recommended.

● **Fine-grained, water-wet soils (which do not shrink in the presence of organics) can serve as an effective barrier to organic liquid movement in the subsurface.** This conclusion was indirectly demonstrated by our inability to inject an organic phase into the Palouse loam.

Two types of flow visualization experiments — micromodels and organic-phase polymerization — permitted the observation of the pore-scale distribution of organic liquid and water resulting from immiscible displacements. The pore-scale distribution of the residual organic phase may have important implications for dissolution and biodegradation. More specifically, it was concluded that:

- **The 'irreducible' water saturation is continuous and is composed of an interconnected network of films, pendular rings, and wedges.** Photographs of pore-scale fluid distributions following organic liquid advance into a previously water-filled micromodel show the residual wetting-phase saturation located in by-passed pores and pore clusters and as films, rings, and wedges within individual pores.

- **The residual organic liquid saturation is trapped as discontinuous 'blobs'.** Photographs of trapped organic liquid in micromodels, pore casts, and blob casts show that the residual saturation is trapped as disconnected blobs of varying size and shape — ranging from spherical shaped singlets occupying one pore to complex, branching, multi-pore blobs. Although no quantitative analysis was performed on the distribution of blob sizes, direct observations of the residual organic liquid saturation from both the micromodel and the blob polymerization experiments corroborate earlier studies which showed that even in homogeneous media, the majority of the residual saturation is held in large, branched blobs.

- **The size and shape distribution of the trapped blobs can influence interphase transfer.** For large, branched blobs, in which perhaps only the ends of the ganglia are exposed to the bulk flow of water, the dissolution rates may depend as much upon diffusion and advection of organic constituents through thin water films as upon organic-to-water partition kinetics. From review of photomicrographs, it has been concluded that:

  - Mass transfer may or may not be governed by local equilibrium. When groundwater velocities are high enough or the dissolution kinetics are slow enough, the local equilibrium assumption no longer holds. In this sense the rate of mass transfer between phases strongly depends upon the distribution of the residual saturation. For large, single-component, branched blobs, mass transfer can be limited by a diffusional process. Substantial portions of these blobs are only in contact with thin water films along the walls of pores. Diffusion through the films to the main body of passing groundwater can be the rate-limiting step in dissolving organic liquid into the water phase.

  - Appropriate mass transfer coefficients have yet to be developed. Mass transfer coefficients used in the mathematical models of partitioning often employ the analogy of an equivalent spherical blob (e.g., Pfannkuch, 1984). Certainly singlets fit this model, but an appropriate definition of equivalent sphere size has yet to be proposed for the population of branched blobs.

  - Dissolution from a multi-component organic phase is more complex. For large branched blobs or by-passed regions of multi-component liquids, the mass transfer rate for a given component can become limited by rate of diffusion of that component within the organic phase to the organic/water interface. Since the major portion of the transfer may be occurring at the ends of these tortuous blobs, intra-blob diffusion may be the rate-limiting step.

Recommendation — **Investigate the dissolution of residual saturations.** The position of a capillary trapped blob within the pore space has a strong influence on mass transfer

between phases. Additional micromodel experiments using a fluorescent dye or fluorescent microspheres are suggested. The flow of water could then be observed on a pore scale, especially through the water films and wedges surrounding the blobs.

● **The size and shape distribution of the trapped blobs can influence microorganisms.** From the review of photomicrographs, it has been concluded that:

○ Microorganisms that degrade organic contaminants experience an environment that depends on their location. In the thin water films found between blobs and pore walls, the organisms have ready access to organic components that partition into the aqueous phase from the nearby blob surface. However, these organisms may not have a ready supply of other substrates, which can only diffuse (or flow) slowly through the thin water film. In the other pores, occupied by flowing water, wall-attached microorganisms are readily exposed to available dissolved substrates, subject only to upstream substrate re-supply.

○ Migration of microorganisms is probably influenced by the spatial distribution of blobs. It should be difficult for a seed population to find its way into regions with thin aqueous films because of their low flow rates and tortuous diffusion paths. In any event, most organisms would probably not thrive in these stagnant regions because of the substrate re-supply problem and the possibility of toxicity due to locally high concentrations of dissolved organics.

○ Not only might the pore-scale distribution of organics affect the rate of biodegradation, but microbial growth may in turn affect how water flows through the blob-filled pore network.

Recommendation — **Employ micromodels to observe bacterial transport and colonization.** Micromodels with fluorescent bacteria could be used to study bacterial motility and colonization.

Micromodel experiments were used to examine the influence of flow rate on organic/water displacements. It was concluded that:

● **The 'irreducible' water saturation is somewhat dependent upon flow rate.** Higher flow velocities of organic liquid displacing water resulted in a small reduction of the residual water saturations.

● **The residual saturation is relatively insensitive to the maximum organic saturation attained during organic liquid advance.** This result was found for both the homogeneous soil columns and the homogeneous micromodels.

● **The residual organic liquid saturation is independent of flow rate.** The results suggest that for the pumping rates attainable in homogeneous aquifers, a higher pumping rate will not result in increased recovery of free product, but it may change the pore-scale distribution of the residual organics.

- **The groundwater velocities and capillary numbers needed for mobilization make hydraulic remediation of contamination unrealistic in the saturated zone.** Several schemes have been published in the literature and implemented in the field for hydraulically sweeping organic liquids from polluted aquifers. These schemes are presumably meant to sweep out the continuous organic liquid, knowingly leaving behind the residual. Sometimes however, it seems that naivete prevails and designers assume that as long as ground water is flowing toward a collection system, eventually all of the organic liquid will make it. No matter how long one waits, unless gradients are increased above the critical level, none of the residual will be hydraulically removed.

SATURATED ZONE CONCLUSIONS — HETEROGENEOUS MEDIA

Laboratory experiments were conducted to examine two-phase (organic/water) displacements and capillary trapping in heterogeneous porous media. Three types of heterogeneities were studied. In the aggregated system, strings of interconnected macropores separated clumps of micropores. This dual porosity arrangement served as an analog to fractured media. In the coarse lenses system, coarse lenses were imbedded into a finer matrix. In the layered system, coarser and finer layers were arranged perpendicular to flow. A general conclusion from this work was that:

- **Porous media heterogeneities dominate displacement and trapping mechanisms.** The interplay between soil heterogeneities and capillarity control the movement and trapping of fluids. Advancing organic liquid selectively travels through the coarser (and more permeable) portions of heterogeneous aquifers by-passing finer-grained regions. And correspondingly for water displacing organic liquid, capillary forces can relegate the flow of water to finer-grained regions, by-passing the coarser organic-filled regions. The character of these displacements were compared with homogeneous displacements.

In organic/water displacements conducted in the aggregated micromodel, it was concluded that:

- **Organic liquid selectively travels through interconnected macropores, by-passing finer-grained regions.** As a result of this by-passing, spilled organic liquids can be expected to move quickly through aquifers which have interconnected coarse layers or fractures.

- Due to by-passing, the maximum organic liquid saturation attained was much lower than that attained in the homogeneous micromodel. And as a consequence, **the residual saturations attained following displacement by water were much lower than that attained in the homogeneous micromodel.** The amount of organic liquid that is ultimately trapped is strongly dependent on the nature of original emplacement. Aquifers which have interconnected coarse layers or fractures can be expected to leave behind residual saturations that are comparatively low, but these residual saturations can be expected to extend over a much larger portion of aquifer.

- **The rate of initial invasion of a non-wetting organic liquid may influence 'irreducible' water saturations and, later, organic residual saturations.** Again, the amount of organic liquid that is ultimately trapped is strongly dependent on the nature of original emplacement. Higher flow rates during organic liquid advance led to organic liquid intrusion into some of the microporosity. Correspondingly, higher maximum organic liquid saturations led to elevated residual saturations.

Of the three types of heterogeneities examined, the 'coarse lenses' heterogeneity was the most extensively studied. A mathematical model that used capillarity and average flux to predict two-phase flow through two media aligned in parallel was developed. The model was demonstrated for the case of water displacing organic liquid from coarse lenses. Results from micromodel and sand column experiments were compared with the model predictions. The model showed that:

- **The force exerted by capillarity was sufficient to cause by-passing of organic liquid in the coarse lenses even though these lenses were more permeable.**

- **At higher flow rates water can be forced into the coarse lenses, resulting in displacement of additional organic liquid and improved recovery.** The critical flow rate at which water enters the coarse lenses is a function of: the permeabilities of each of the media, the proportion of cross-sectional area occupied by the lenses, the length of the flow domain (for this example, the length of the lenses), and the interfacial tension and the relative wetting of the fluids.

- The capillarity of the system does not change with flux rate. **At still higher flux rates, capillarity becomes relatively unimportant and the flow regime approximates a single-phase system in which water preferentially flows through the higher permeability regions.** At high average flux rates, the flux rates between regions approach the ratio of the permeabilities — just as would be the case for one-phase flow.

- In the absence of mobility-induced fingering, **improved recovery of organic liquid is attained when the ratio of fluxes through coarse and fine regions becomes greater than zero, and maximum recovery is attained when the ratio of fluxes approaches unity.** Increasing the average flux rate beyond a critical value results in improved recovery.

- **Improved recovery can be achieved within the realm of attainable field pumping rates.** A hypothetical example was used to show this principle.

Observations of flow behavior from displacements conducted in micromodels and in sand columns compared favorably with the flow behavior to that predicted by the dual-media model. These laboratory experiments showed that:

- **The residual saturation left behind in a heterogeneous medium containing disconnected coarse lenses is larger than residual left behind in a homogeneous medium.**

- **At low flux rates the organic liquid in the lenses was completely by-passed.** At typical aquifer flow velocities, capillary forces can relegate the flow of water to finer-grained regions, by-passing the coarser regions filled with organic liquid.

- **At higher rates, some displacement of the organic liquid in the lenses was attained, resulting in improved recovery and a reduced residual saturation.** Increased recovery of organic liquids from coarse lenses may be attained by increasing the pumping rate.

  Recommendation — **Continue experiments and theoretical modeling of residual saturations caused by heterogeneities.** The effects of heterogeneities were shown to have a dramatic impact on water/organic displacements, and consequently, on the magnitude and distribution of the residual saturation. Further laboratory and theoretical research is needed on this issue. Additional micromodel experiments are suggested in which quantitative measurements of the saturations are made (using image analysis) over a wide variety of heterogeneities. Heterogeneities could be explicitly incorporated into currently available multi-phase flow models to further examine the interplay between heterogeneities and capillarity without the restrictions imposed by the simplifying assumptions of the simple dual-media model used in this study. Finally, field experiments on organic liquid movement should pay special attention to the complications imposed by heterogeneities.

The layered media experiments were conducted in micromodels. Observations of water displacing organic liquid from a micromodel with layering perpendicular to flow showed that:

- **By-passing of the organic phase occurred as the water front progressed from a coarse layer to a fine layer.** This particular form of the by-passing mechanism is identical to the capillary end effect, and can result in significantly higher residual saturations — especially if the layers are not thick and the process repeats often. It is hypothesized that this is the operative mechanism leading to the high residual saturations measured for the Sevilleta sand.

A micromodel experiment illustrating the movement of a dense organic liquid through a layered media showed that:

- **The presence of layering may be fortuitous in the case of dense organics migrating downward through the saturated zone.** Halogenated solvents may tend to finger beneath the water table because these organic liquids tend to be more dense, less viscous, and non-wetting relative to water. In layered media, the tendency for a non-wetting phase to migrate into coarser layers results in a lateral component to the flow which slows the growth of fingers.

  Recommendation — **Determine the conditions required for the onset of fingering as dense organics move downward through the saturated zone.** Many halogenated solvents are more dense and less viscous than water — attributes which promote flow instabilities (gravity fingering) as an organic phase percolates downward through an aquifer. Of

special interest in this problem are the roles of capillarity and heterogeneity. In the case of a non-wetting phase displacing a wetting phase, capillary forces appear to promote fingering, while layering in the soil transverse to flow appears to promote stability. Further micromodel, sandbox, and mathematical models of these issues are needed.

VADOSE ZONE CONCLUSIONS

Organic liquid movement and capillary trapping in the vadose zone were investigated through the use of soil columns, micromodels, and pore casts. Results from soil column and micromodel experiments confirmed the hypothesis that:

● **Residual saturations are much lower in the vadose zone than they are in the saturated zone.** In the Sevilleta soil the vadose zone residual saturation was measured to be 9.1%, compared to 27.1% for saturated zone conditions. The lower residual is explained by:

  ○ continuity of the films during drainage;

  ○ presence of a third, non-wetting gas phase;

  ○ additional buoyancy forces due to the greater density contrast of the organic liquid to air, than to water; and

  ○ less capillarity due to the lower interfacial tensions between the organic liquid and gas, than between the organic liquid and water.

  Recommendation — **Investigate the behavior of organic liquids in the transition zone between the vadose and saturated zones. Determine the equilibrium saturation.** Particularly for organic liquids lighter than water, the low suction range in and just above the capillary fringe is where all the action, occurs as light organics reach the water table and begin to migrate laterally to form a lens. Unfortunately, this is where the balance of forces governing movement for the three fluid phases becomes much more complicated (and perhaps the least understood). Three possible approaches for additional experiments are suggested: (1) Run pressure controlled (instead of flux controlled) vadose zone experiments in micromodels; (2) Build a better short column apparatus to look at equilibrium saturations near the water table; and, (3) Devise a method of measuring saturations in a 2-D sand box model constructed in a fashion that allows the lateral redistribution of the organic phase.

Most notable from observations of the flow visualization experiments was the formation of thin films of organic liquid between the air and water phases. The spreading force which leads to the formation of films may be a significant driving force for organic liquid movement in the vadose zone. From the flow visualization experiments it was concluded that:

● **The movement of organic liquid through the vadose zone is more complex than organic liquid movement in the saturated zone, especially because of the tendency for**

many organics to spread. The organic liquid is commonly of intermediate wettability between water, the wetting phase, and the non-wetting gas phase. The propensity for a given organic liquid to spread between water and gas can be predicted from the spreading coefficient, $S = \sigma_{aw} - (\sigma_{ow} + \sigma_{ao})$. Positive spreading coefficients lead to the formation of organic liquid films along the water/gas interface.

- **Films appear to be an important mechanism of organic liquid invasion into the vadose zone.** The organic liquid usually advances by displacing gas, and sometimes water, from pore throats and bodies. But it also advances through film flow, most easily seen in micromodel experiments when pockets of organic liquid began to accumulate deeper in the model, with no obvious connection to sources of organic liquid above.

- **Films of a spreading organic liquid maintain continuity of the organic phase.** These films are the thread of continuity that keep all the little pockets of residual organic liquid in hydraulic communication.

- **Residual saturations in the vadose zone are profoundly different from the blobs seen in the saturated zone.** In the saturated zone, surface area of the organic phase is minimized whereas in the vadose zone the surface area is maximized — at least for spreading organics. This spreading, film-forming behavior has important implications for maximizing interphase transfer in the vadose zone.

- **The films expose a large organic liquid surface area to the gas phase, making soil venting of organics in the vadose zone an attractive remediation strategy.**

- **The formation of films also exposes a large organic liquid surface area to the water phase, increasing the rate of dissolution.** The effectiveness of this mass transfer mechanism can be severely limited by the water flow rate.

Non-spreading organics showed somewhat different flow behavior. From a three-phase micromodel experiment using PCE, a non-spreading organic liquid, it was concluded that:

- **Non-spreading organic liquids do not form films, but rather coalesce into small lenses that float at the water/gas interface.** There is no interconnecting film between all the little pockets of residual organic liquid.

- Because of the tendency of a non-spreading organic liquid break into small lenses instead of maintaining films in between the water and air phases, **less surface area of the residual organic phase was created as compared to spreading organics.** Certainly however, a much greater surface area was created as compared to the minimized surface areas observed for blobs in the saturated zone. Implications of non-spreading behavior may include (1) the possibility of reduced interphase transfer, (2) higher residual saturations, and (3) for flow modellers, the inability to invoke Leverett's (1941) simplification for three-phase capillary pressure versus saturation relationships.

Recommendation — **Study the movement and ultimate distribution of non-spreading organic liquids; compare to spreading organic liquids.** In three-phase

(air/organic/water) systems in which the organic liquid is of intermediate wettability, some organics spread between the water and air phases while others, such as some halogenated solvents, do not. Preliminary micromodel experiments indicate that the spreading coefficient can have a profound influence on how the organic phase moves and where (especially on a pore scale) it ends up. This can be particularly important to remediation via soil venting. Additional quantitative and visualization experiments are suggested.

CONCLUSIONS ABOUT THE EXPERIMENTAL APPROACH

The experimental apparatus and procedures used to measure residual saturations in laboratory soil columns offered several advantages:

- **The short column method used relatively simple experimental procedures to provide fairly precise measurements of two- and three-phase fluid saturations in soils.** Gravimetric measurements (which exploit the density difference between the fluids to measure saturations) gave precise measurements of residual organic liquid saturations. In the saturated zone, residual saturation measurements for most of the fluids were precise to within ± 2%. Measurements of residual saturation for Soltrol in the vadose zone were also precise to about ± 2%.

- **A short column with a semi-permeable membrane yielded relatively constant saturations over the length of the column with no capillary end effect.** These features are especially important for the vadose zone measurements, because measurements of organic liquid saturation in the vadose zone can be strongly biased by failure to account for capillary end effects.

In addition it was observed that:

- **Temperature control was important for obtaining consistent results.**

- **The residual saturations were independent of the variability in packing from one experimental trial to the next.**

- **The residual saturations were relatively insensitive to the maximum organic liquid saturation attained.**

Two recommendations for improving the soil column apparatus are made:

- **Redesign the apparatus to handle low permeability soils.** It was not possible to measure residual saturations in fine-grained soils because it was difficult to supply sufficient pressure to force organic liquid into the soil. This problem can be circumvented with a high-pressure system, including a high-pressure fluid delivery pump, a column built to withstand high pressures, and a bottom membrane with a very high non-wetting phase entry pressure.

- **Redesign the apparatus and procedure to permit observation of conditions in the transition zone between the vadose and saturated zones.** Results from the transition

zone experiments gave what are believed to be unreasonably high equilibrium organic liquid saturations. During organic liquid drainage, water was unable to re-imbibe into the soil. Under low applied suctions representing the capillary fringe and just above, re-imbibing water would have displaced organic liquid resulting in lower equilibrium organic saturations than the values that were measured. The largest change in forces acting on the organic liquid occurs in the capillary fringe and just above, where the transition from vadose zone to saturated zone conditions is most pronounced.

Blob polymerization techniques make it possible to observe the distribution of the different fluid phases within the pore space. Like with the micromodels, the fluid distributions may be observed in both a bulk sense and within individual pores. Because the fluids eventually become solidified, one can only see a 'snapshot' of the flow behavior using polymerization techniques. However, the advantage over micromodels is that the fluid distributions can be observed in a real soil. Such a soil has three-dimensional pore interconnections, irregularly shaped pores, and rough surfaces which are not found in micromodels.

Difficulties in attaining complete drainage of the organic liquid surrogate in the three-phase experiment presented a problem. Also there is some question as to whether solidifying the wetting phase prior to introduction of the intermediate-wetting phase gives realistic fluid distributions.

Still, the pore and blob casts give important information about the distribution of residual organic liquids within the pore space. The distribution of fluids within the pore space has implications to dissolution, volatilization, and biodegradation of residual organic liquid contaminants.

Based on the experience gained from using blob polymerization, it is recommended that the usefulness of the technique be extended by;

- **Observing fluid distributions for other saturations.** The *in situ* visualization work with pore and blob casts focused on residual non-wetting phase saturations. These techniques should be applied to the visualization of fluid distributions at other saturations.

- **Improving thin sectioning of pore casts.** It was difficult to make thin sections of the pore casts because the combination of an unconsolidated soil and an infill of various plastics made it difficult to cut and polish the sections without plucking or cracking the mineral grains. Improvements in this technology would certainly aid in the production of better photomicrographs.

- **Investigating other monomers, initiators, epoxies, and techniques for for making pore and blob casts.** Several problems with fluids used in these experiments were experienced, principally relating to the changing viscosities of the fluids and the miscibility of one epoxy with another. This was especially a problem with the epoxy representing the intermediate wetting phase in the vadose zone experiment. These problems affected fluid distributions and interfaces in the pore casts. Additional efforts could be directed toward finding a better combination of porous media, fluids, and dyes to minimize these problems.

- **Reducing blob cast breakage.** Size and shape analysis on the produced blob casts were not performed, partly because of breakage. New materials and handling procedures that will reduce the incidence of breakage need to be investigated.

- **Quantifying the blob polymerization saturations using image processing techniques.** Without access to image analysis equipment, the blob polymerization techniques were not quantitative. Quantification would take much of the conjecture out of the interpretation of results.

The attractiveness of performing multi-phase flow experiments in glass micromodels is that we can actually see the fluids displace one another. Micromodels provide an excellent method with which to study multi-phase flow behavior because the structure of the pore network and the wettability of the system can be closely controlled.

As with the blob polymerization technique, the biggest limitation of using micromodels is the lack of quantitativeness. Micromodels can be made more quantitative in three ways:

- **Use image processing techniques to measure fluid saturations.** Saturations can be measured using a high resolution video camera, a frame grabber and image processing software. These quantitative measurements could be combined with mathematical models at the pore and network level (e.g., Soll and Celia, 1988) to help explain observations and validate the models.

- **Improve the micromodel end reservoirs.** Incorporate oil- or water-wet etched channel porous membranes (as shown in Figure 41) to provide a mechanism for controlling capillary end effects. Pressures could be controlled and measured through these reservoirs.

- **Improve the micromodel construction techniques to allow greater control of the pore size distribution.** Presently, it is difficult to measure media properties such as hydraulic conductivities, characteristic curves, or on a smaller scale, the dimensions of individual pores. And of course, the pores are too big. Improved construction techniques (perhaps drawing on the methods developed to etch integrated circuits into silicon wafers) would provide much greater control for micromodel properties and much greater control between one micromodel and the next.

ADDITIONAL RECOMMENDATIONS

Some additional recommendations for future research include:

- **Exploring the effect of heterogeneities on behavior in the vadose zone.** Three-phase flow through heterogeneous media is a logical extension of this study, which has examined two-phase flow through heterogeneous media and three-phase flow through homogeneous media.

- **Using the laboratory experiments of this study to validate multi-phase flow models.** In addition to whatever these experiments have illustrated about the nature of immiscible flow of organic liquid, they also make excellent tests against which to attempt to validate flow models. They can be useful in two ways: first, they can be used as a check to assure the assumptions of flow and transport models conform to experimental observations; and secondly, the experimental results can be used as benchmarks to test the models.

- **Comparing 2- and 3-phase flow in micromodels to results from cellular automata (CA).** Cellular automata has recently been used to mathematically model multiphase fluid flow on a pore scale. This molecular-scale modelling technique uses rules that satisfy the conservation laws of mass and momentum along with other rules describing the relative affinity of one particle for another. Together these rules control the manner in which particles interact, allowing CA models to simulate interfacial tensions. With this technique, multi-phase flow can be simulated on a pore scale. Well-controlled micromodel experiments would be ideal for validating CA models. It is believed that CA can be extended to three fluid phases. By changing the interfacial tension rules it may be possible to accurately describe the movement of a spreading or non-spreading intermediate wetting phase (organic liquid) on a pore scale in the vadose zone. Again, modelling results could be compared to three-phase flow experiments conducted in micromodels.

- **Investigating wetting phase relative permeability as a function of reduced residual saturation.** Compositional models are numerical codes which simulate multi-phase flows with interphase transfers such as dissolution. 'Black oil' models focus on more sophisticated representation of the multi-phase flow, but at the expense of neglecting compositional behavior. The two approaches are being integrated by various researchers, allowing better predictions of the migration of organic pollutants. These models need estimates of relative permeabilities to each of the fluids. In particular they need the wetting phase relative permeability at residual saturation. When residual non-wetting phase saturations are reduced by mobilization, volatilization, or dissolution, the wetting phase relative permeability increases. Increases in permeability result in either increased water flow under constant head boundary conditions, or increased residence time under constant flux conditions. In either case an accelerated rate of dissolution is the ultimate result. It is expected that the distribution of organic liquid, after having undergone significant dissolution, will be much different than the distribution of an organic phase subjected only to hydraulic forces. Hence, it is hypothesized that two systems, each having the same fluid saturations, will not have the same fluid permeabilities due to different distributions of the fluids — because in each case the saturations are achieved by a different process. Accurate measures of relative permeabilities at reduced residual saturations may be as important as good estimates of mass transfer coefficients for predicting pollutant migration.

- **Investigating the conditions under which surface wetting properties can be altered.** Surface wetting on can have a profound influence on multi-phase flow behavior and the movement and capillary trapping of organic liquids. Typically, it is assumed that soils are water wet, but this assumption has not been tested. It is possible that some of the

compounds present in organic waste solutions, or even in gasoline, can alter wettability. It is also possible that wettability could be altered through microbial activity.

- **Determining the conditions required for the onset of gravity fingering as liquid organics move downward through the vadose zone.** All liquid organics are more dense and viscous than the gas phase in the vadose zone. The greater density promotes flow instabilities (gravity fingering) as an organic phase percolates downward toward the water table. Capillarity and heterogeneity play a significant role in this process. There is significant literature on the two phase flow instability issue. There is little on three-phase flow instability.

- **Conducting field experiments to confirm laboratory observations.** Well-controlled field experiments should be conducted to 'up-scale' many of the conclusions reached in this laboratory study.

REFERENCES

Ababou, R., L. W. Gelhar, and D. McLaughlin. 1988. Three-dimensional flow in random porous media. Ralph M. Parsons Laboratory Report 318, Massachusetts Institute of Technology Department of Civil Engineering, 833 p.

Abriola, L. M., and G. F. Pinder. 1985a. A multiphase approach to the modeling of porous media contaminated by organic compounds 1. Equation development. Water Resources Research, vol.21, no.1, pp.11-8.

Abriola, L. M. , and G. F. Pinder. 1985b. A multiphase approach to the modeling of porous media contaminated by organic compounds 2. Numerical Simulation. Water Resources Research, vol.21, no.1, pp.19-26.

Adamson, A. W. 1982. *Physical Chemistry of Surfaces*, 4th edition. Wiley, New York.

Amaufule J. O., and L. L. Handy. 1982. The effect of interfacial tensions on relative oil/water permeabilities of consolidated porous media. SPE Journal, vol.22, no.3, pp.371-81.

ASTM. 1986. *Annual Book of ASTM Standards.* American Society for Testing and Materials, Philadelphia, PA.

Amott, E. 1959. Observations relating to the wettability of porous rock. AIME Transactions, vol.216, pp.156-62.

Anderson, W. G. 1986a. Wettability literature survey — part 1: rock-oil-brine interactions and the effects of core handling on wettability. Journal of Petroleum Technology, v.38, no.10, pp.1125-49.

Anderson, W. G. 1986b. Wettability literature survey — part 2: wettability measurement. Journal of Petroleum Technology, v.38, no.11, pp.1246-62.

Anderson, W. G. 1987a. Wettability literature survey — part 4: the effects of wettability on capillary pressure. Journal of Petroleum Technology, vol.39, no.10, pp.1283-300.

Anderson, W. G. 1987b. Wettability literature survey — part 5: the effects of wettability on relative permeability. Journal of Petroleum Technology, vol.39, no.11, pp.1453-68.

Araktingi, U. G., D. C. Brock, and F. M. Orr. 1988. Viscous fingering in heterogeneous porous media. presented at the Fall 1988 AGU meeting, abstract in EOS, vol.69, no.44, pp.1204-5.

Baehr, A. L. 1987. Selective transport of hydrocarbons in the unsaturated zone due to aqueous and vapor phase partitioning. Water Resources Research, vol.23, no.10, pp.1926-38.

Baehr, A. L., and M. Y. Corapcioglu. 1984. A predictive model for pollution from gasoline in soils and ground water. in proceedings of *Petroleum Hydrocarbons and Organic Chemicals in Ground Water*, NWWA, Houston, TX, pp.144-56.

Baehr, A. L., and M. Y. Corapcioglu. 1987. A compositional multiphase model for groundwater contamination by petroleum products 2. numerical solution. Water Resources Research, vol.23, no.1, pp.201-13.

Bowman, R. S., M. E. Essington, and G. A. O'Conner. 1981. Soil sorption of nickel: influence of solution composition. SSSAJ, v.45, no.5, pp.680-5.

Boyer, R. F., ed. 1970. Styrene Polymer, in Bikales, N. M., ed., *Encyclopedia of Polymer Science and Technology,* vol.13, Interscience Publishers, New York, pp.128-447.

Burmaster, D. E., and R. H. Harris. 1982. Groundwater contamination: an emerging threat. Technology Revue, vol.84, no.7, pp.50-62.

Burris, D. R., and W. A. MacIntyre. 1986. Solution of hydrocarbons in a hydrocarbon-water system with changing phase composition due to evaporation. Environmental Science and Technology, vol.20, no.3, pp.296-9.

Byer, H. G., W. Blankenship, and R. Allen. 1981. Ground-water contamination by chlorinated hydrocarbons: causes and prevention. Civil Engineering, ASCE, March, pp.54-55.

Carman, P. C. 1937. Fluid flow through granular beds. Transactions: Institute of Chemical Engineers (London), v.15, pp.150-66.

Cary, J. W., J. F. McBride, and C. S. Simmons. 1989. Observation of water and oil infiltration into soil: some simulation challenges. Water Resources Research, vol.25, no.1, pp.73-80.

Chatzis, I., and F. A. L. Dullien. 1983. Dynamic immiscible displacement mechanisms in pore doublets: theory versus experiment. Journal of Colloid and Interface Science, vol.91, no.1, pp.199-222.

Chatzis, I., N. R. Morrow, and H. T. Lim. 1983. Magnitude and detailed structure of residual oil saturation. SPE Journal, vol.23, no.2, pp.311-25.

Chatzis, I., M. S. Kuntamukkula, and N. R. Morrow. 1984. Blob-size distribution as a function of capillary number in sandstones. paper SPE 13213, presented at 1984 SPE Annual Technical Conference and Exhibition, Houston, TX.

Chatzis, I., and N. R. Morrow. 1984. Correlation of capillary number relationships for sandstones. SPE Journal, vol.24, no.5, pp.555-62.

Chatzis, I., M. S. Kuntamukkula, and N. R. Morrow. 1988. Effect of capillary number on the microstructure of residual oil in strongly water-wet sandstones. SPE Reservoir Engineering, vol.3, no.3, pp.902-12.

Chuoke, R. I., P. van Meurs, and C. van der Poel. 1959. The instability of slow, immiscible, viscous liquid-liquid displacements in permeable media. Trans. AIME, vol.216, pp.188-94.

Conrad, S. H., and J. L. Wilson. 1988. Residual saturations of organic liquids: vadose vs. saturated zones. presented at Spring 1988 AGU meeting, Abstract in EOS, vol.69, no.16, p.370.

Conrad, S. H., W. R. Mason, W. J. Peplinski, E. F. Hagan, and J. L. Wilson. 1988. The combined effects of soil heterogeneities and flow rate on the advance and ultimate recovery of spilled organic liquids. presented at Fall 1988 AGU meeting, Abstract in EOS, vol.69, no.44 p.1205.

Conrad, S. H., J. L. Wilson, W. R. Mason, and W. J. Peplinski. 1989. Observing the transport and fate of petroleum hydrocarbons in soils and in ground water using flow visualization techniques, in proceedings, *Symposium on Environmental Concerns in the Petroleum Industry*, AAPG, Palm Springs, CA, May 10, 1989, pp.1-13.

Convery, M. P. 1979. The Behavior and Movement of Petroleum Products in Unconsolidated Surficial Deposits. M.S. Thesis, University of Minnesota.

Corapcioglu, M. Y., and A. L. Baehr. 1987. A compositional multiphase model for groundwater contamination by petroleum products 1. theoretical considerations. Water Resources Research, vol.23, no.1, pp.191-200.

Corapcioglu, M. Y., and M. A. Hossain. 1989. Ground-water contamination by high-density immiscible hydrocarbon slugs in gravity-driven gravel aquifers. Ground Water, vol.28, no.3, pp.403-12.

Craig, F. F. 1971. *Reservoir Engineering Aspects of Waterflooding.* SPE Monograph Series, no.3, Dallas, TX.

Dagan, G. 1986. Statistical theory of groundwater flow and transport: pore to laboratory, laboratory to formation, and formation to regional scale. Water Resources Research, vol.22, no.9, pp.120S-34S.

de Pastrovich, T. L., Y. Baradat, R. Barthel, A. Chiarelli, and D. R. Fussell. 1979. Protection of Groundwater from Oil Pollution. Report 3/79, CONCAWE, Den Haag, the Netherlands.

Donaldson, E. C., R. D. Thomas, and P. B. Lorenz. 1969. Wettability determination and its effects on recovery efficiency. SPE Journal, v.9, no.1, pp.13-20.

Dullien, F. A. L., F. S. Y. Lai, and I. F. MacDonald. 1986. Hydraulic continuity of residual wetting phase in porous media. Journal of Colloid and Interface Science, vol. 109, no. 1, pp.201-18.

Eames, V. 1981. Influence of Water Saturation on Oil Retention Under Field and Laboratory Conditions. University of Minnesota M.S. Thesis.

Eastman Kodak Company. 1975. Decorating Glass Using Kodak Photosensitive Resists. Kodak Publication No. P-245, 4 p.

Eastman Kodak Company. 1979. Photofabrication Methods with Kodak Photoresists. Kodak Publication No. G-184, 32 p.

Eckberg, D. K., and D. K. Sunada. 1984. Nonsteady three-phase immiscible fluid distribution in porous media. Water Resources Research, vol.20, no.12, pp.1891-7.

EPA. 1980. Proposed Groundwater Protection Strategy. Office of Drinking Water, Washington, D.C.

Ewing, R. E., T. F. Russel, and L. C. Young. 1989. An anisotropic coarse-grid dispersion model of heterogeneity and viscous fingering in five-spot miscible displacement that matches experiments and fine-grid models, in proceedings, *Tenth Annual SPE Symposium on Reservoir Simulation*, February 6-8, Houston, TX, pp.447-65.

Faust, C. R. 1985. Transport of immiscible fluids within and below the unsaturated zone: a numerical model. Water Resources Research, vol.21, no.4, pp.587-96.

Feenstra, S., and J. Coburn. 1986. Subsurface contamination from spills of denser than water chlorinated solvents. Bulletin of the California Water Pollution Control Association, vol.23, no.4, pp.26-34.

Ferrand, L. A., P. C. D. Milly, and G. F. Pinder. 1986. Dual-gamma attenuation for the determination of porous medium saturation with respect to three fluids. Water Resources Research, vol.22, no.12, pp.1657-63.

Gelhar, L. W. 1986. Stochastic subsurface hydrology from theory to applications. Water Resources Research, vol.22, no.9, pp.135S-45S.

Girifalco, L. A., and R. J. Good. 1957. A theory for the estimation of surface and interfacial energies, I: derivation and application to interfacial tension. Journal of Physical Chemistry, vol.61, p.904.

Gvirtzman, H., M. Magaritz, E. Klein, and A. Nader. 1987. A scanning electron microscopy study of water in soil. Transport In Porous Media, no.2(1987), pp.83-93.

Hagan, E. F., S. H. Conrad, and J. L. Wilson. 1989. A quantitative experimental investigation of the physical processes responsible for determining residual organic liquid saturations in porous media. Open file report 89-4, New Mexico Tech Hydrology Program, 170p.

Hillel, D. 1980. *Fundamentals of Soil Physics.* Academic Press, New York, NY, 413p.

Hoag, G. E. and M. C. Marley. 1986. Gasoline residual saturation in unsaturated uniform aquifer materials. Journal of Environmental Engineering, vol.112, no.3, pp.586-604.

Hornof, V. and N. R. Morrow. 1987. Gravity effects in the displacement of oil by surfactant solutions. SPE Reservoir Engineering, Nov., pp.627-33.

Jercinovic, D. E. 1984. Petroleum-Product Contamination of Soil and Water in New Mexico. Ground Water/Hazardous Waste Bureau, New Mexico Environmental Improvement Division, EID/GWH-84/4.

Johnson, P. C., M. W. Kemblowski, and J. D. Colthart. 1990. Quantitative analysis for the cleanup of hydrocarbon-contaminated siols by in-situ soil venting. Ground Water, v.28, no.3, pp.413-29.

Kuppusamy, T., J. Sheng, J. C. Parker, and R. J. Lenhard. 1987. Finite element analysis of multiphase immiscible flow through soils. Water Resources Research, vol.23, pp.625-31.

Kyte, J. R., R. J. Stanclift Jr., S. C. Stephan Jr., and L. A. Rapoport. 1956. Mechanism of water flooding in the presence of free gas. Trans. AIME, vol.207, pp.215-21.

Lake, L. W., and H. B. Carroll, Jr. - eds. 1986. *Reservoir Characterization.* Harcourt Brace Jovanovich, Publishers, Orlando, FL., 659p.

Lenhard, R. J., and J. C. Parker. 1987a. A model for hysteretic constitutive relations governing multiphase flow, 2. permeability – saturation relations. Water Resources Research, vol.23, no.12, pp.2197-206?.

Lenhard, R. J., and J. C. Parker. 1987b. Measurement and prediction of saturation – pressure relationships in three phase porous media systems. Journal of Contaminant Hydrology, vol.1, pp.407-24.

Lenhard, R. J., and J. C. Parker. 1988a. Experimental validation of the theory for extending two phase saturation – pressure relationships to three phase systems for momotonic drainage paths. Water Resources Research, vol.24, pp.373-80.

Lenhard, R. J., and J. C. Parker. 1988b. Estimation of oil volumes in soils from observed fluid levels in monitoring wells. presented at the Fall 1988 AGU meeting, abstract in EOS, vol.69, no.44, pp.1212-13.

Lenhard, R. J., J. H. Dane, and J. C. Parker. 1988. Measurement and simulation of one-dimensional transient three phase flow for monotonic liquid drainage. Water Resources Research, vol.24, pp.853-63.

Lenhard, R. J., and J. C. Parker. 1989. A model for hysteretic constitutive relations governing multiphase flow, 3. refinements and numerical simulations. Water Resources Research, vol.25, pp.1727-36.

Leverett, M. C. 1941. Capillary behavior in porous solids. Trans. AIME, vol.142, pp.152-69.

Lyman, W. J., W. F. Reehl, and D. H. Rosenblatt (eds.). 1982. *Handbook of Chemical Property Estimation Methods.* McGraw-Hill, New York.

Mantoglou, A., and L. W. Gelhar. 1987. Stochastic modeling of large-scale transient unsaturated flow in stratified soils. Water Resources Research, vol.23, no.1, pp.57-68.

Mason, W. R., S. H. Conrad, and J. L. Wilson. 1988. Micromodel study of organic liquid advance into a soil. presented at Spring 1988 AGU meeting, abstract in EOS, vol.69, no.16, p.370.

Mason, W. R., W. J. Peplinski, J. L. Wilson and S. H. Conrad. 1989a. Visualization of three phase flow on a pore scale. presented at Spring 1989 AGU meeting, abstract in EOS, vol. 70, no.15, p.337.

Mason, W. R., S. H. Conrad, and J. L. Wilson. 1989b. An investigation of the transport and fate of petroleum hydrocarbons in homogeneous and heterogeneous pore networks using flow visualization techniques. Open file report, New Mexico Tech Hydrology Program, 53p.

Mattson, E. D., A. M. Parsons, D. B. Stephens, K. Black, and K. Flanigan. 1988. Field simulation of waste impoundment seepage in the vadose zone. in proceedings of *FOCUS on Southwestern Ground Water Issues Conference*, NWWA, March 23-25.

Maugh II, T. H. 1979. Toxic waste disposal a growing problem. Science, vol.204, pp.819-23.

McBride, J. F., J. W. Cary, and C. S. Simmons. 1990. The effect of spreading coefficient on the advance of an organic liquid front in water-wet porous media. presented at Spring 1990 AGU meeting, abstract in EOS, vol.71, no.17, p.497.

McCarty, P. L., M. Reinhard, and B. E. Rittmann. 1981. Trace organics in groundwater. Environmental Science and Technology, vol.15, no.1, pp.40-51.

McCord, J. T., D. B. Stephens, J. L. Wilson. 1988a. Field-scale variably saturated flow and transport in a sloping uniform porous media: field experiments and numerical simulations, in proceedings of *International Workshop on Validation of Flow and Transport Models for the Unsaturated Zone,* May 23-26, Ruidoso, NM, New Mexico State University.

McCord, J. T., D. B. Stephens, and J. L. Wilson. 1988b. Field-scale variably saturated flow and transport: the roles of hysteresis and state-dependent anisotropy, in proceedings of NATO Advanced Study Institute on *Recent Advances in Modeling Hydrologic Systems*, July 9-22, Sintra, Portugal.

McKellar, M., and N. C. Wardlaw. 1988. A Method of Viewing "Water" and "Oil" Distribution in Native-State and Restored-State Reservoir Core. AAPG Bulletin, vol.72, no.6, pp.765-71.

Melrose, J. C., and C. F. Brandner. 1974. Role of capillary forces in determining microscopic displacement efficiency for oil recovery by waterflooding. Journal of Canadian Petroleum Technology, vol.13, no.4, pp.54-62.

Mohanty, K. K., H. T. Davis, and L. E. Scriven. 1980. Physics of oil entrapment in water-wet rock. paper SPE 9406, presented at 1980 SPE Annual Technical Conference and Exhibition, Dallas, TX.

Moissis, D. E., C. A. Miller, and M. F. Wheeler. 1989. Simulation of miscible viscous fingering using a modified method of characteristics: effects of gravity and heterogeneity, in proceedings of *Tenth Annual SPE Symposium on Reservoir Simulation*, February 6-8, Houston, TX, pp.431-46.

Moore, T. F., and R. L. Slobod. 1956. The effect of viscosity and capillarity on the displacement of oil by water. Producers Monthly, vol.20, pp.20-30.

Morrow, N. R. 1970. Physics and thermodynamics of capillary action in porous media. Industrial Engineering Chem., vol.62, no.6, pp.32-56.

Morrow, N. R. 1979. Interplay of capillary, viscous and buoyancy forces in the mobilization of residual oil. Journal of Canadian Petroleum Geology, vol.18, no.3, pp.35-46.

Morrow, N. R., and B. Songkran. 1981. Effect of trapping and buoyancy forces on non-wetting phase trapping in porous media. in *Surface Phenomena in Enhanced Oil Recovery*, D.O.Shah (ed.), Plenum Publishing Corporation.

Morrow, N. R., and I. Chatzis. 1982. Measurement and Correlation of Conditions for Entrapment and Mobilization of Residual Oil. Report DOE/BC/10310-20, Department of Energy.

Morrow, N. R., I. Chatzis, and J. J. Taber. 1988. Entrapment and mobilization of residual oil in bead packs. SPE Reservoir Engineering, vol.3, no.3, pp.927-34.

Ng, K. M., H. T. Davis, and L. E. Scriven. 1978. Visualization of blob mechanics in flow through porous media. Chemical Engineering Science, vol.33, pp.1009-17.

Oh, S. G. and J. C. Slattery. 1979. Interfacial tension required for significant displacement of residual oil. SPE Journal, vol.19, pp.83-96.

Osborne, M., and J. Sykes. 1986. Numerical modelling of immiscible organic transport at the Hyde Park. Water Resources Research, vol.22, no.1, pp.25-33.

Parker, J. C., and R. J. Lenhard. 1987. A model for hysteretic constitutive relations governing multiphase flow, 1. saturation – pressure relations. Water Resources Research, vol.23, no.12, pp.2187-96.

Parker, J. C., R. J. Lenhard and T. Kuppusamy. 1987. A parametric model for constitutive properties governing multiphase flow in porous media. Water Resources Research, vol.23, pp.618-24.

Pathak, P., H. T. Davis, and L. E. Scriven. 1982. Dependence of residual non-wetting liquid on pore topology. paper SPE 11016, presented at 1982 SPE Annual Technical Conference and Exhibition, New Orleans.

Peplinski, W. J., S. H. Conrad, and J. L. Wilson. 1989. Simulation of organic liquid saturations using styrene monomer and epoxy resin. Open file report 89-1, New Mexico Tech Hydrology Program, 35p.

Pfannkuch, H. O. 1984. Determination of the contaminant source strength from mass exchange processes at the petroleum–ground–water interface in shallow aquifer systems. in proceedings of *Fourth National Symposium on Aquifer Restoration and Groundwater Monitoring*, NWWA, Columbus, OH.

Pinder, G. F., and L. M. Abriola. 1986. On the simulation of nonaqueous phase compounds in the subsurface. Water Resources Research, vol.22, no.9, pp.109S-19S.

Powers, S. E., Y. M. Chen, L. M. Abriola, and W. J. Weber. 1988. The significance of non-equilibrium effects on interphase partitioning of organic contaminants in multiphase systems. presented at Fall 1988 AGU meeting, abstract in Eos, vol.69, no.44, p.1201.

Roberts, J. R., J. A. Cherry, and F. W. Schwartz. 1982. A case study of a chemical spill: polychlorinated biphenyls (PCBs) 1. history, distribution, and surface translocation. Water Resources Research, vol.18, no.3, pp.523-34.

Roberts, P.V., M. Reinhard, and A. J. Valocchi. 1982. Movement of organic contaminants in groundwater: implications for water supply. Journal of the American Water Works Association, vol.74, pp.408-13.

Schwille, F. 1967. Petroleum contamination of the subsoil — a hydrological problem. in *The Joint Problems of the Oil and Water Industries* (P.Hepple — ed.), Elsevier, Amsterdam, pp.23-53.

Schwille, F. 1981. Groundwater pollution in porous media by fluids immiscible with water. in *Quality of Groundwater* (W. van Duijvenbooden et al. — eds.), Elsevier, Amsterdam, pp.451-63.

Schwille, F. 1984. Migration of organic fluids immiscible with water in the unsaturated zone. in *Pollutants in Porous Media: The Unsaturated Zone Between Soil Surface and Groundwater* (B.Yaron, G.Dagan, and T.Goldschmid — eds.), Springer-Verlag, New York, pp.27-48.

Schwille, F. 1988. Dense Chlorinated Solvents in Porous and Fractured Media. Lewis Publishers, Chelsea, MI. 146p.

Saez, A. E., C. J. Otero, and I. Rusinek. 1989. The effective homogeneous behavior of heterogeneous porous media. Transport in Porous Media, vol.4, pp.213-38.

Soll, W. E. and M. A. Celia. 1988. A pore-scale model of three-phase immiscible fluid flow. poster presented at Fall 1988 AGU meeting, abstract in Eos, vol.69, no.44, pp.1189-90.

Stephens, D. B., and S. Heermann. 1988. Dependence of anisotropy on saturation in a stratified sand. Water Resources Research, vol.24, no.5, pp.770-778.

Taber, J. J. 1981. Research on enhanced oil recovery: past, present, and future. in *Surface Phenomena in Enhanced Oil Recovery* (D.O.Shah ed.), Plenum, New York, pp.13-52.

Treiber, L. E., D. L. Archer, and W. W. Owens. 1972. A laboratory evaluation of the wettability of fifty oil producing reservoirs. SPE Journal, vol.12, pp.531-40.

Twenter, F. R., T. R. Cummings, and N. G. Grannemann. 1985. Ground water contamination in East Bay Township, Michigan. USGS Water Resources Investigation Report 85-4064.

van Dam, J. 1967. The migration of hydrocarbons in water-bearing stratum. in: *The Joint Problems of the Oil and Water Industries* (P.Hepple — ed.), Elsevier, Amsterdam, pp.55-88.

Vomocil, J. A. 1965. Porosity. in *Methods of Soil Analysis,* Part 1, C. A. Black (Ed.), American Society of Agronomy, Madison, WI, pp.299-314.

Wardlaw, N. C., and R. P. Taylor. 1976. Mercury capillary pressure curves and the interpretation of pore structure and capillary behavior in reservoir rocks. Bulletin of Canadian Petroleum Geology, vol.24, no.2, pp.225-62.

Wardlaw, N. C. 1982. The effect of geometry, wettability, viscosity, and interfacial tension on trapping in single pore-throat pairs. Journal of Canadian Petroleum Technology, vol.21, no.3, pp.21-7.

Weast, R. C. (ed.). 1981. *Handbook of Chemistry and Physics.* CRC Press, Boca Raton, Fla.

Welty, C. and L.W. Gelhar, 1987. Stochastic analysisof the effects of viscosity variability on macrodispersion in heterogeneous porous media. presented at Fall 1987 AGU meeting, abstract in EOS, vol.68, no.44, pp.1189-90.

Welty, C. and L. W. Gelhar, 1989. Stochastic analysis of the effects of density variability on macrodispersion in heterogeneous porous media. presented at Spring 1989 AGU meeting, abstract in EOS, vol.70, no.15, p.340.

Wilson, J. L. 1984. Double-cell hydraulic containment of pollutant plumes. in proceedings of *Fourth National Symposium on Aquifer Restoration and Groundwater Monitoring*, NWWA, Columbus, OH.

Wilson, J. L., and S. H. Conrad. 1984. Is physical displacement of residual hydrocarbons a realistic possibility in aquifer restoration? in proceedings of *Petroleum Hydrocarbons and Organic Chemicals in Ground Water*, NWWA, Houston, TX, pp.274-98.

Wilson, J. L., W. Cox and W. R. Mason. 1988a. Flow visualization of two–phase flow in a fracture. presented at Spring 1988 AGU meeting, Abstract in EOS, vol. 69, no.16, p.353.

Wilson, J. L., S. H. Conrad, E. F. Hagan, W. R. Mason, and W. J. Peplinski. 1988b. The pore level spatial distribution and saturation of organic liquids in porous media. in proceedings of *Petroleum Hydrocarbons and Organic Chemicals in Ground Water*, NWWA, Houston, TX, pp.107-33.

Wilson, J. L., and R. Mace. 1989. Role of the clay fraction in capillary trapping of organic liquids in soils. presented at the Fall 1989 AGU meeting, abstract in EOS, vol.70, no.43, p.1092.

Wilson, J. L., S. H. Conrad, W. R. Mason, W. J. Peplinski, and E. F. Hagan. 1989. Laboratory investigation of residual liquid organics from spills, leaks, and the disposal of hazardous wastes in groundwater. EPA/600/6-90/004, 267p.

Yadav, G. D., F. A. L. Dullien, I. Chatzis, and I. F. Macdonald. 1987. Microscopic Distribution of Wetting and Nonwetting Phases in Sandstones During Immiscible Displacements. SPE Reservoir Engineering, vol.2, pp.137-47.

Yeh, T.-C. Jim, L. W. Gelhar, A. L. Gutjahr. 1985a. Stochastic analysis of unsaturated flow in heterogeneous soils, 1, statistically isotropic medium. Water Resources Research, vol.21, no.4, pp.447-56.

Yeh, T.-C. Jim, L. W. Gelhar, A. L. Gutjahr. 1985b. Stochastic analysis of unsaturated flow in heterogeneous soils, 2, statistically anisotropic media with variable α. Water Resources Research, vol.21, no.4, pp.457-64.

Yeh, T.-C. Jim, L. W. Gelhar, A. L. Gutjahr. 1985c. Stochastic analysis of unsaturated flow in heterogeneous soils, 3, observations and applications. Water Resources Research, vol.21, no.4, pp.465-72.

APPENDIX A:

SATURATION CURVES AND PROCESSED DATA FOR THE

SHORT COLUMN SEVILLETA SAND EXPERIMENTS

The following pages contain capillary pressure-saturation curves for the two-phase fluid pair combinations tested with the Sevilleta soil. These include air-water, air-organic, and organic-water curves. Soltrol-130 was used as the organic liquid phase in all trials. Following the curves, Table A-1 tabulates the numerical values of saturation and capillary pressure for each curve, and the temperature of the experiment at the time of the measurement. Results from 12 experimental trials are presented.

Seven Soltrol-Water (SW) Capillary Pressure Curves. Figures A-1 through A-8

Two of these curves have drainage, imbibition, and secondary drainage cycles, three curves have drainage and imbibition cycles, and two curves have the main drainage branch only. Figure A-8 plots all but one of the primary drainage curves together, illustrating the repeatability of the experiments. Trial 8 (Figure A-2) shows a similar behavior, but is not as consistent as the other curves. The SW trial numbers corresponds to the numbers in Table 9-2.

Two Soltrol-Air (SA) Capillary Pressure Curves. Figures A-9 through A-11

The first curve has the main drainage branch only, while the second curve has drainage, imbibition, and secondary drainage cycles. The primary drainage curves are compared in Figure A-11.

Three Air-water Capillary Pressure Curves. Figures A-12 through A-15

Two curves have the main drainage and imbibition cycles, while the third curve has the main drainage branch only. The primary drainage curves are compared in Figure A-15.

Figure A-1. Soltrol-water saturation curve for SW trial 7.

Figure A-2. Soltrol-water saturation curve for SW trial 8.

Figure A-3.   Soltrol-water saturation curve for SW trial 9.
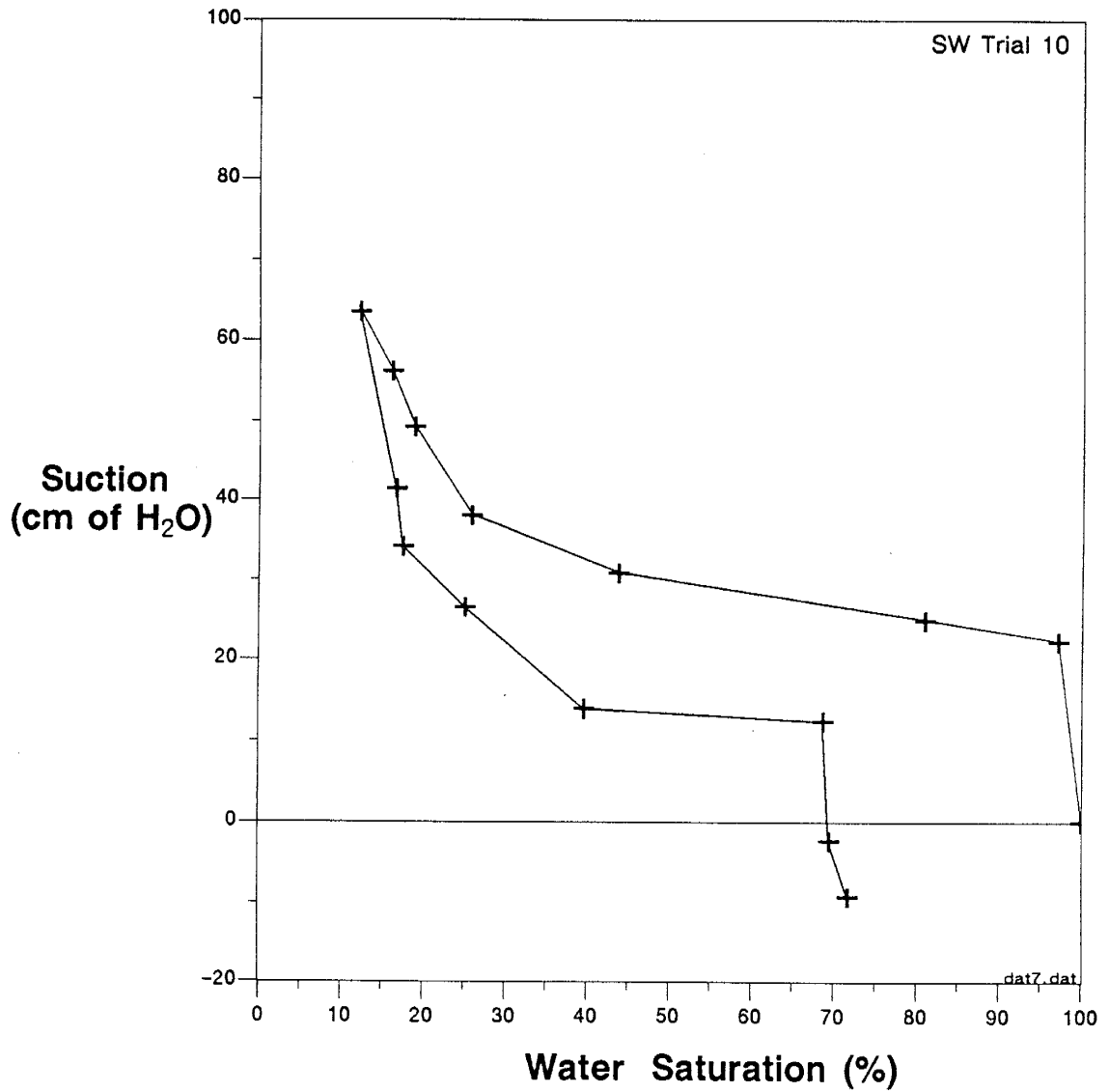
Figure A-4. Soltrol-water saturation curve for SW trial 10.

Soltrol-Water Saturation Curve (Drainage-Imbibition)

Figure A-5.   Soltrol-water saturation curve for SW trial 11.
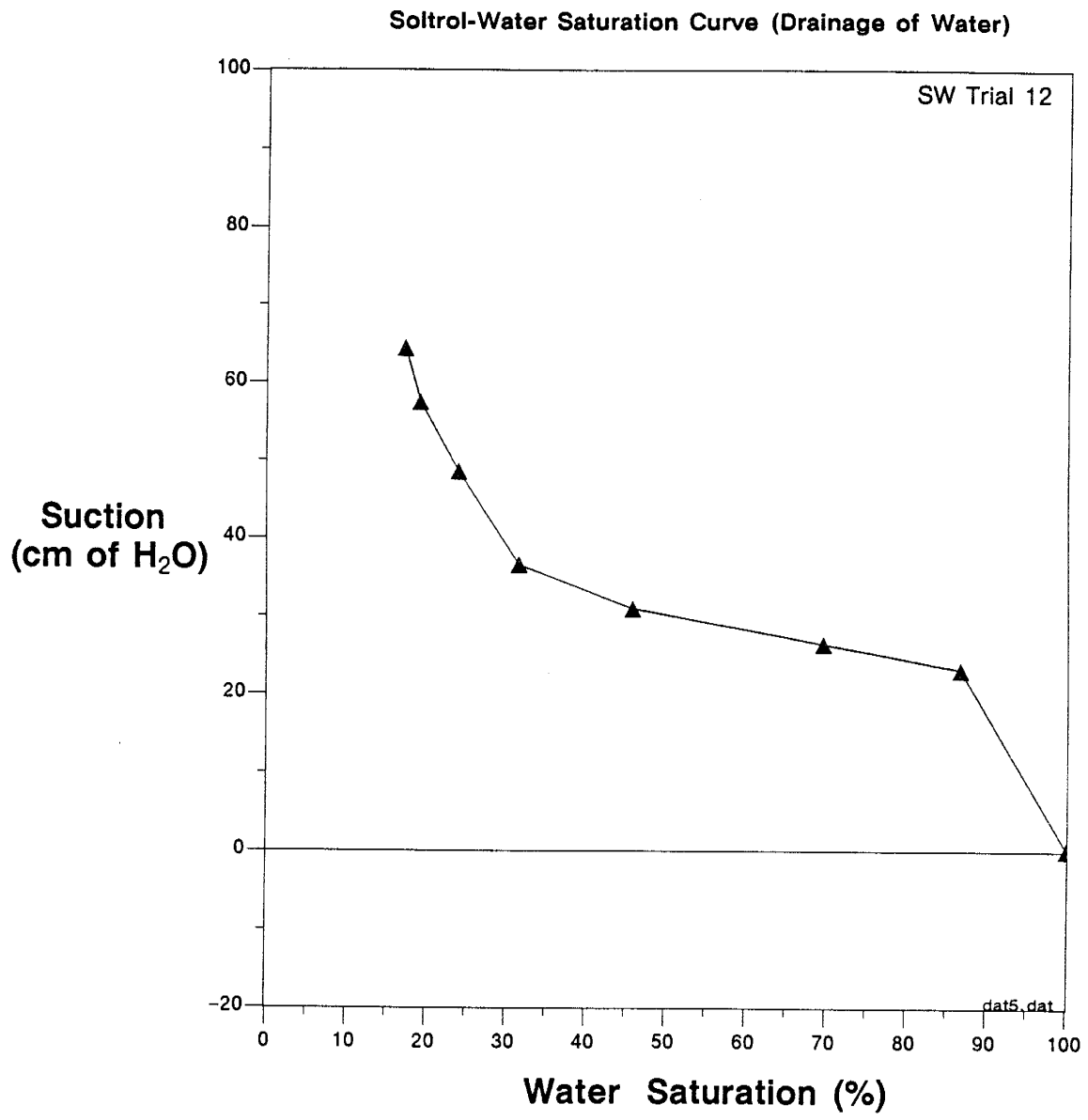
Figure A-6.   Soltrol-water saturation curve for SW trial 12.

Soltrol-Water Saturation Curve (Drainage of Water)
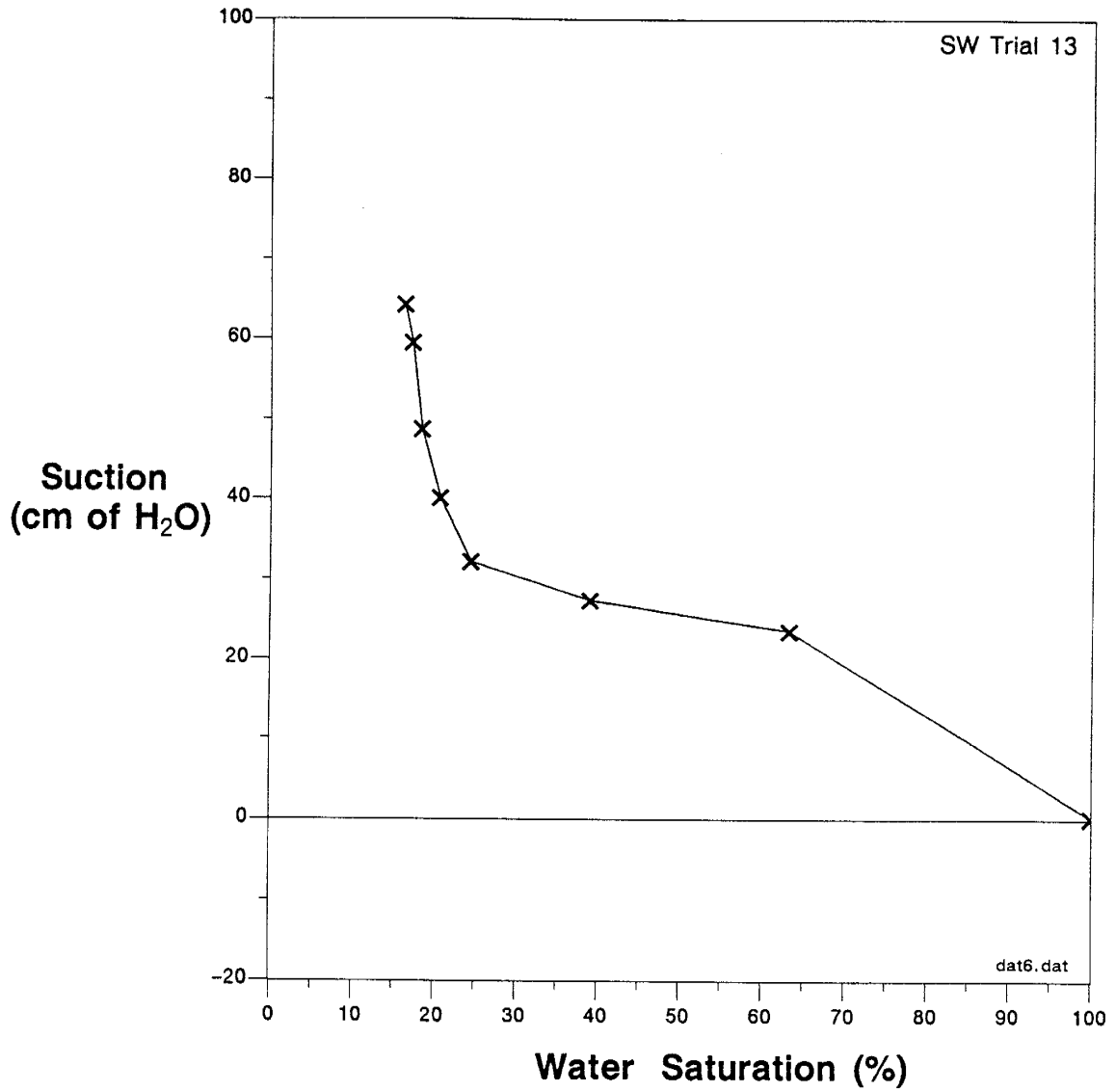
Figure A-7.   Soltrol-water saturation curve for SW trial 13.
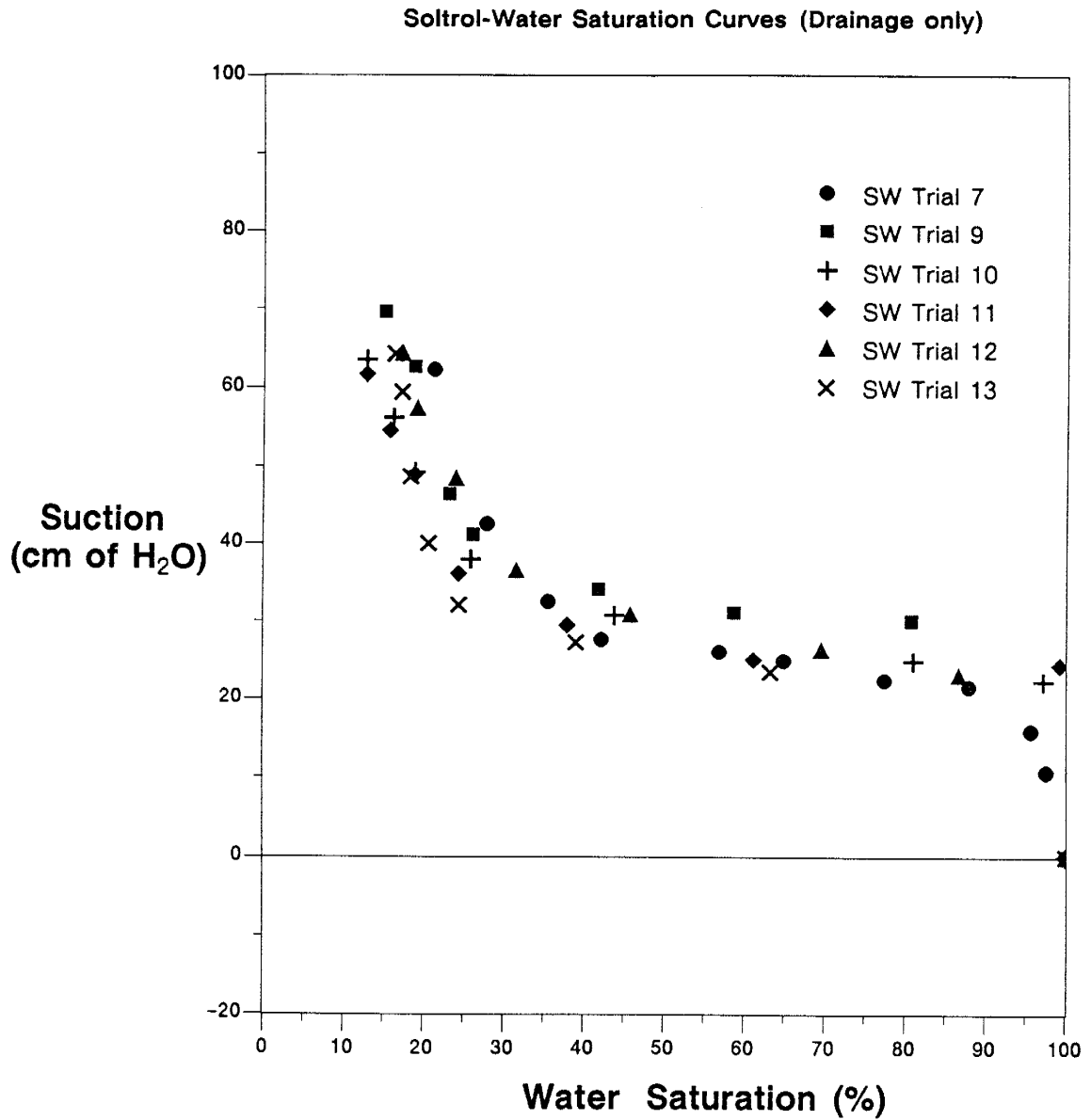
Figure A-8.   Soltrol-water primary drainage curves for SW trials 7-13, minus trial 8.
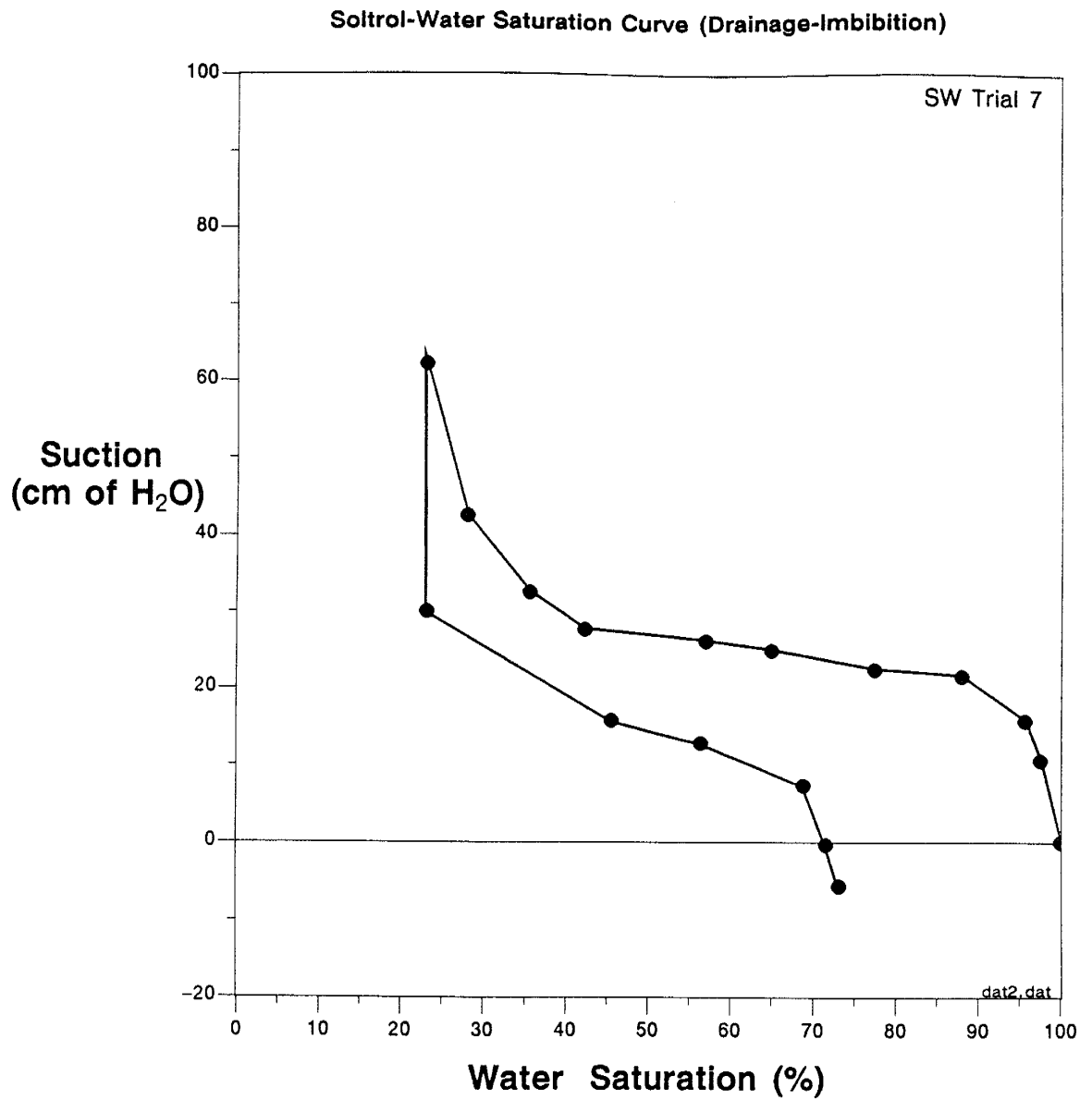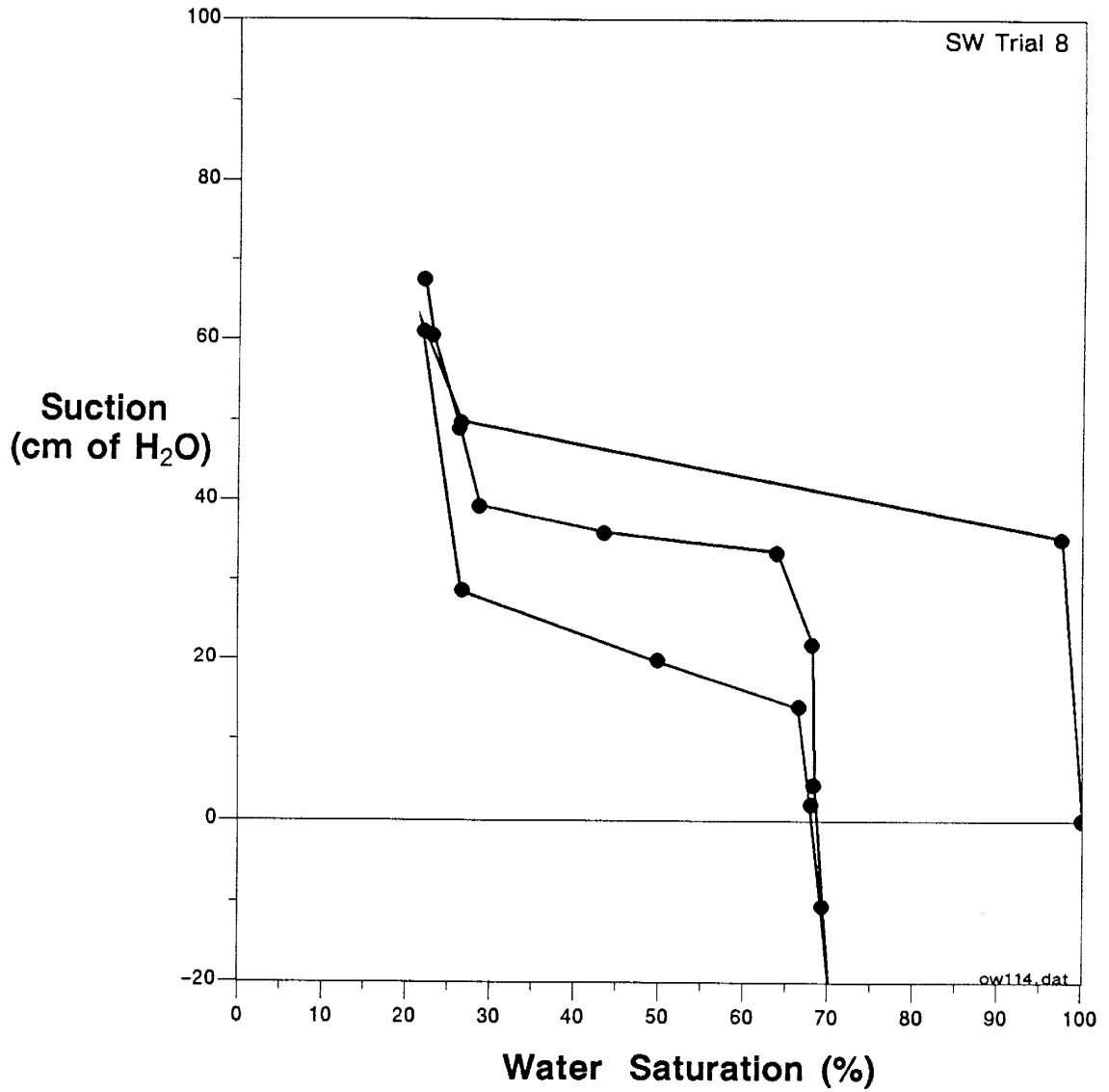
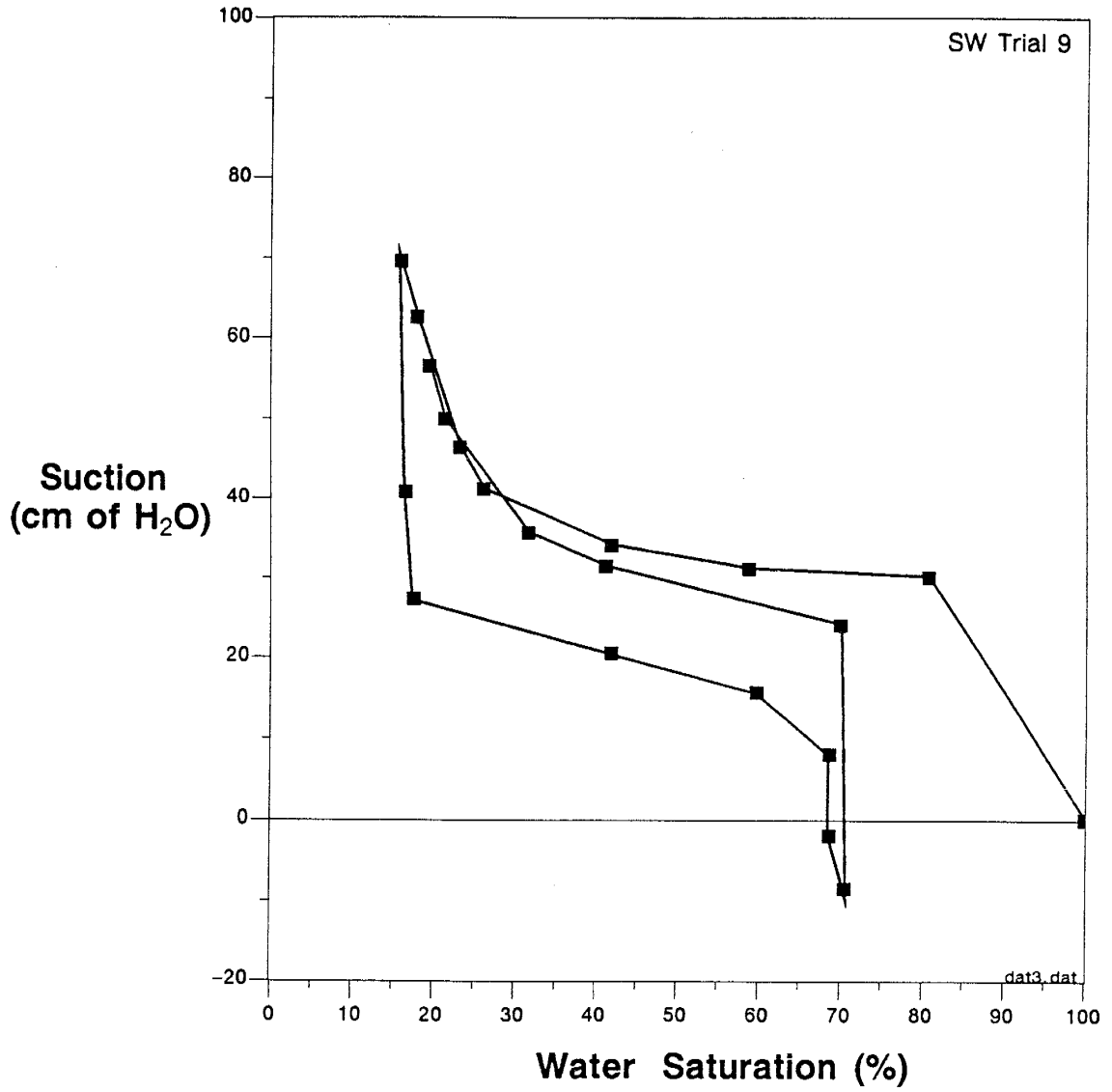**Soltrol-Air Saturation Curve (Drainage)**
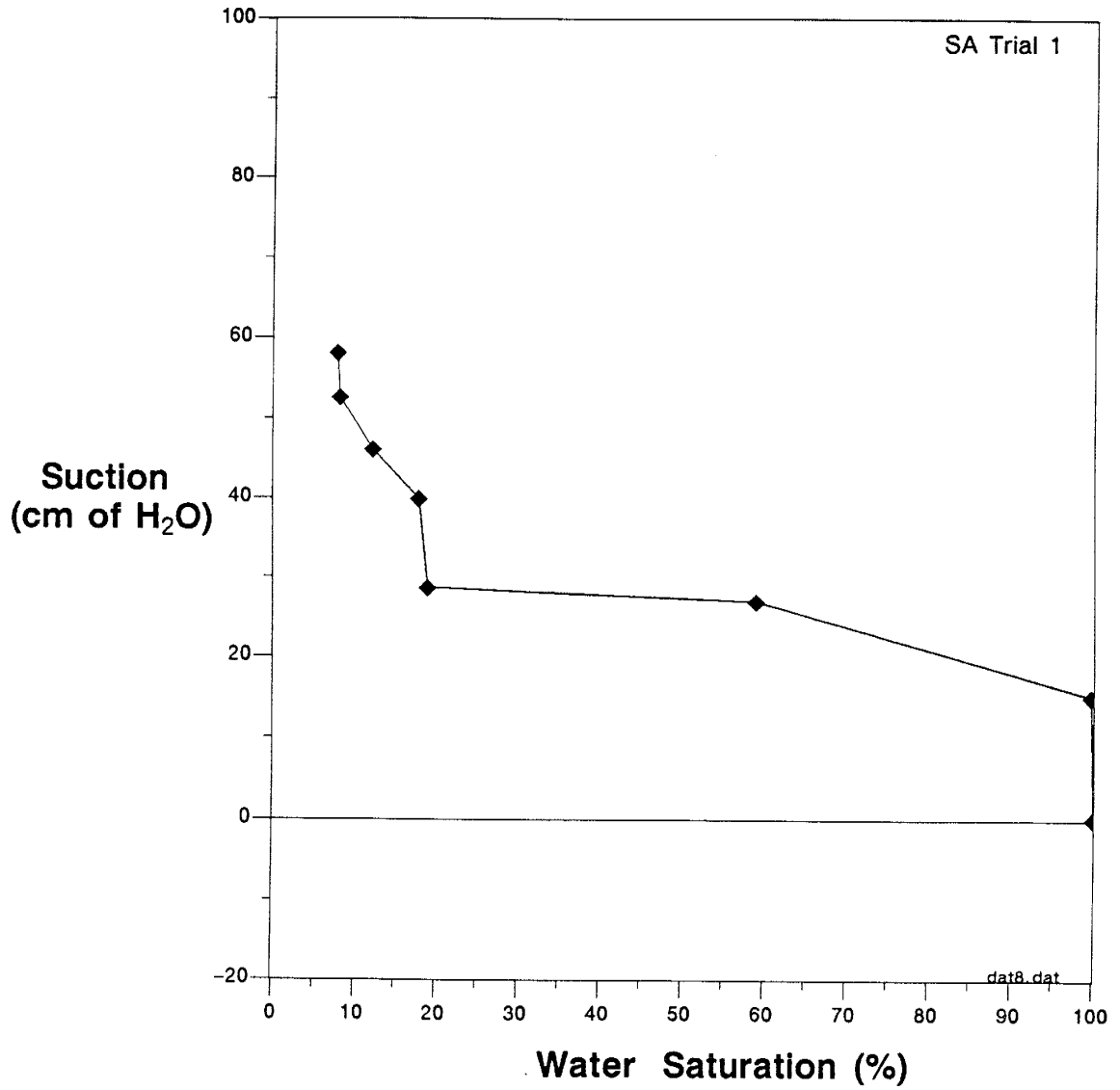
Figure A-9.   Soltrol-air saturation curve for SA trial 1.

Soltrol-Air Saturation Curve (Drainage-Imbibition-Drainage)
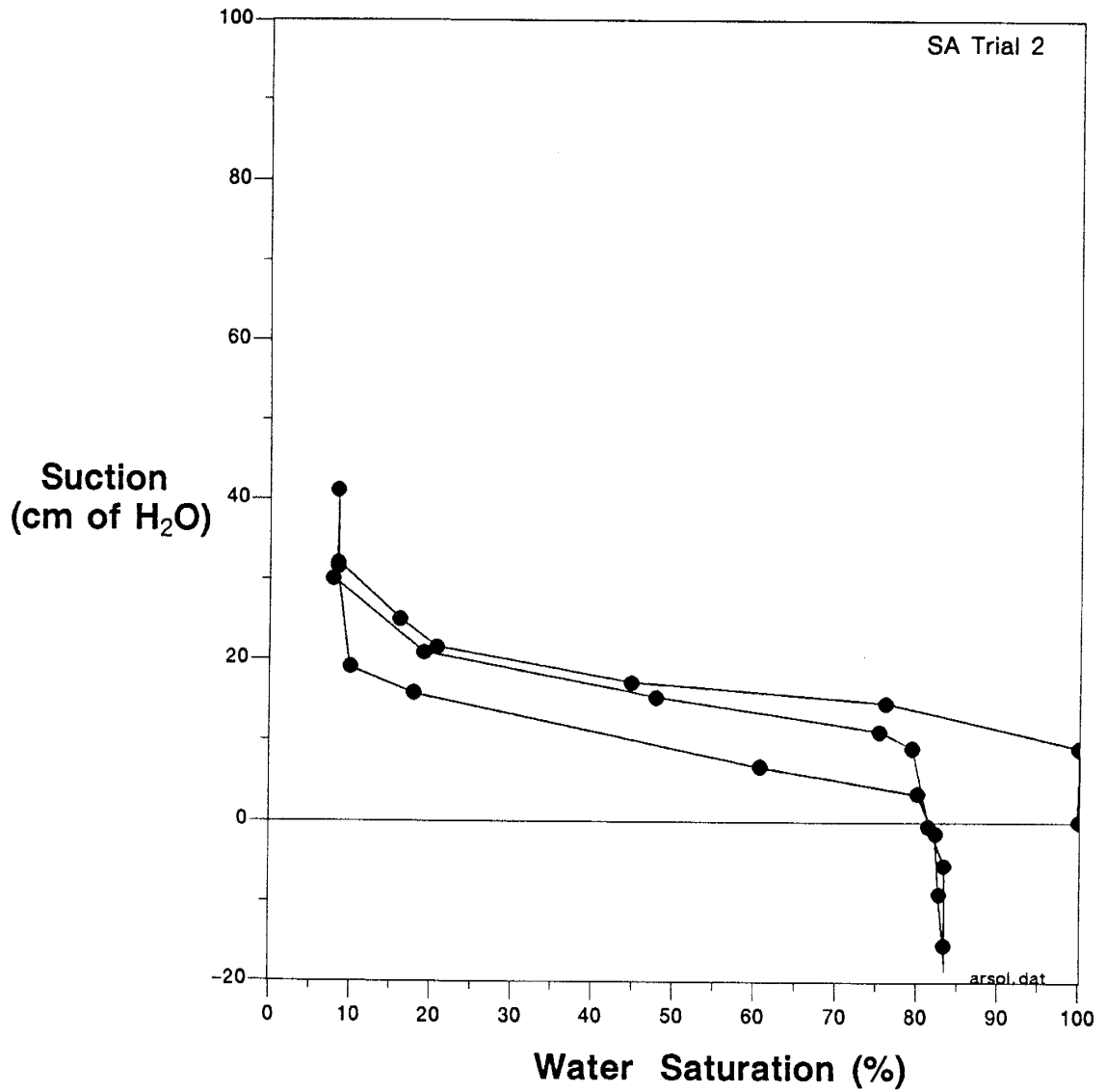
Figure A-10. Soltrol-air saturation curve for SA trial 2.

Soltrol-Air Saturation Data (Drainage)
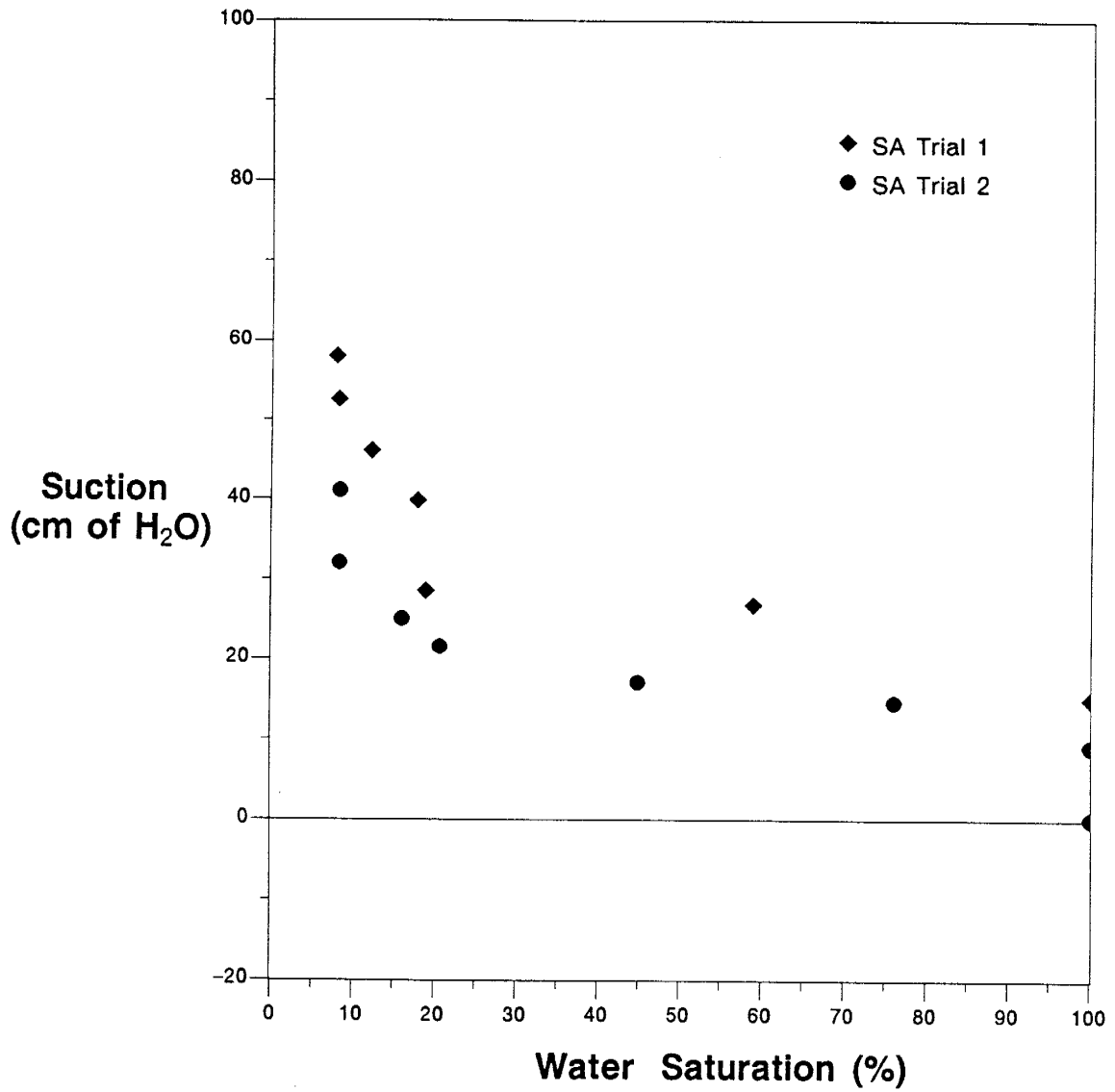
Figure A-11. Comparison of Soltrol-air primary drainage curves for SA trials 1 & 2.

Air-Water Saturation Curve (Drainage-Imbibition)

AW Trial 1

Suction (cm of H₂O) — *Suction (cm of H_2O)*

Water Saturation (%)

arwat.dat
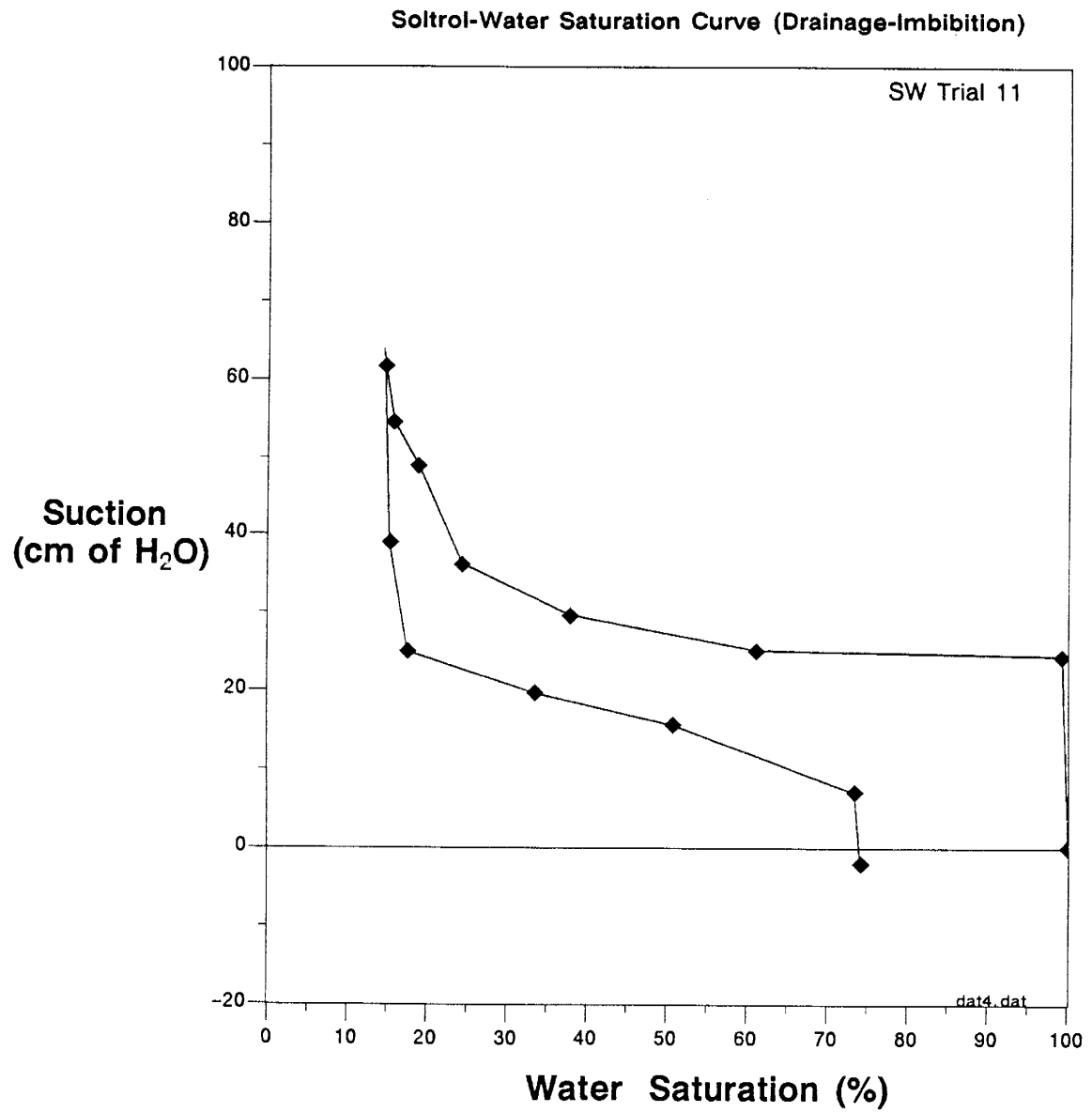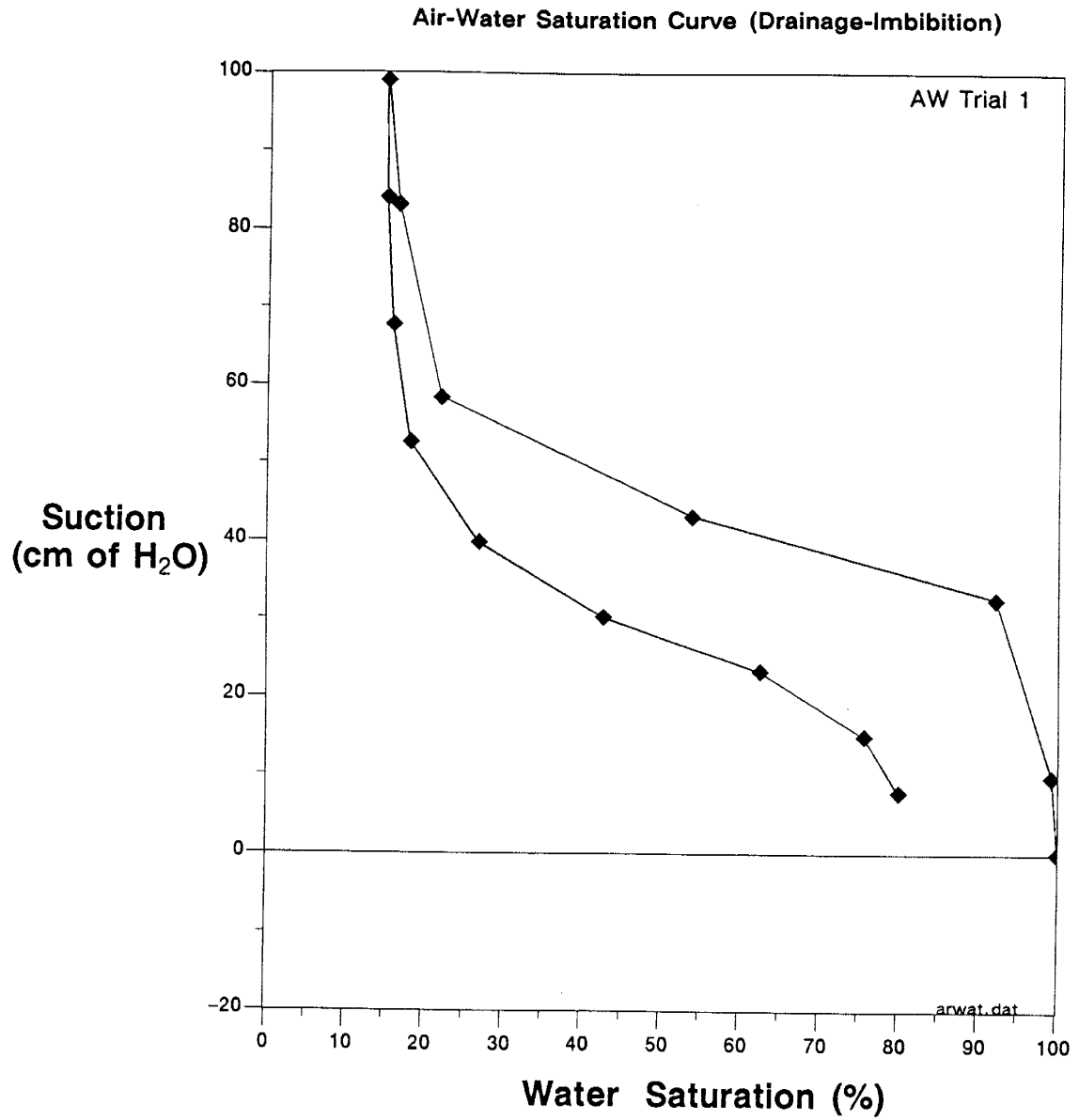
Figure A-12. Air-water saturation curve for AW trial 1.
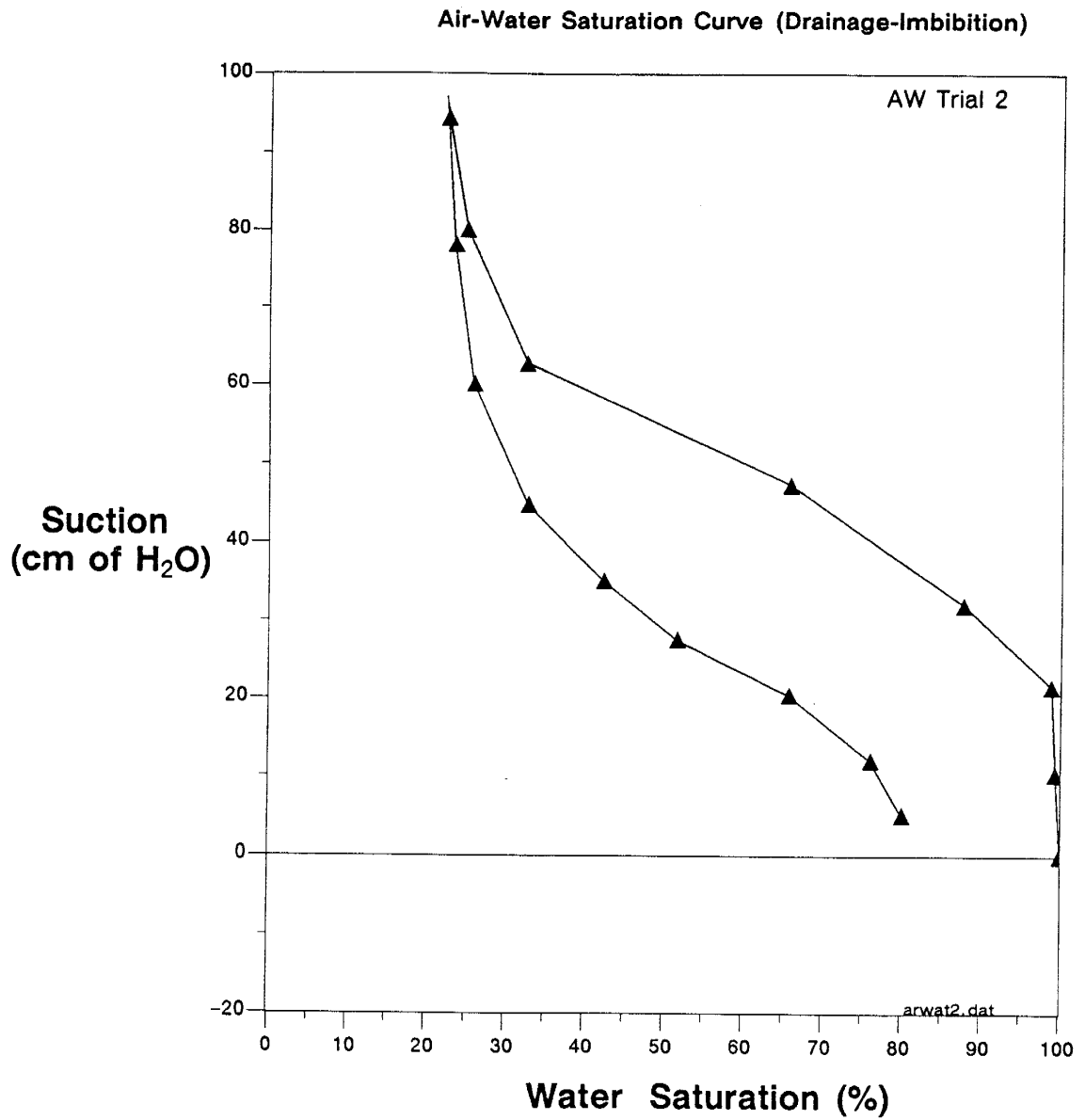
Figure A-13. Air-water saturation curve for AW trial 2.

Air-Water Saturation Curve (Drainage)

AW Trial 3

Suction (cm of H₂O) vs Water Saturation (%)

arwat3.dat
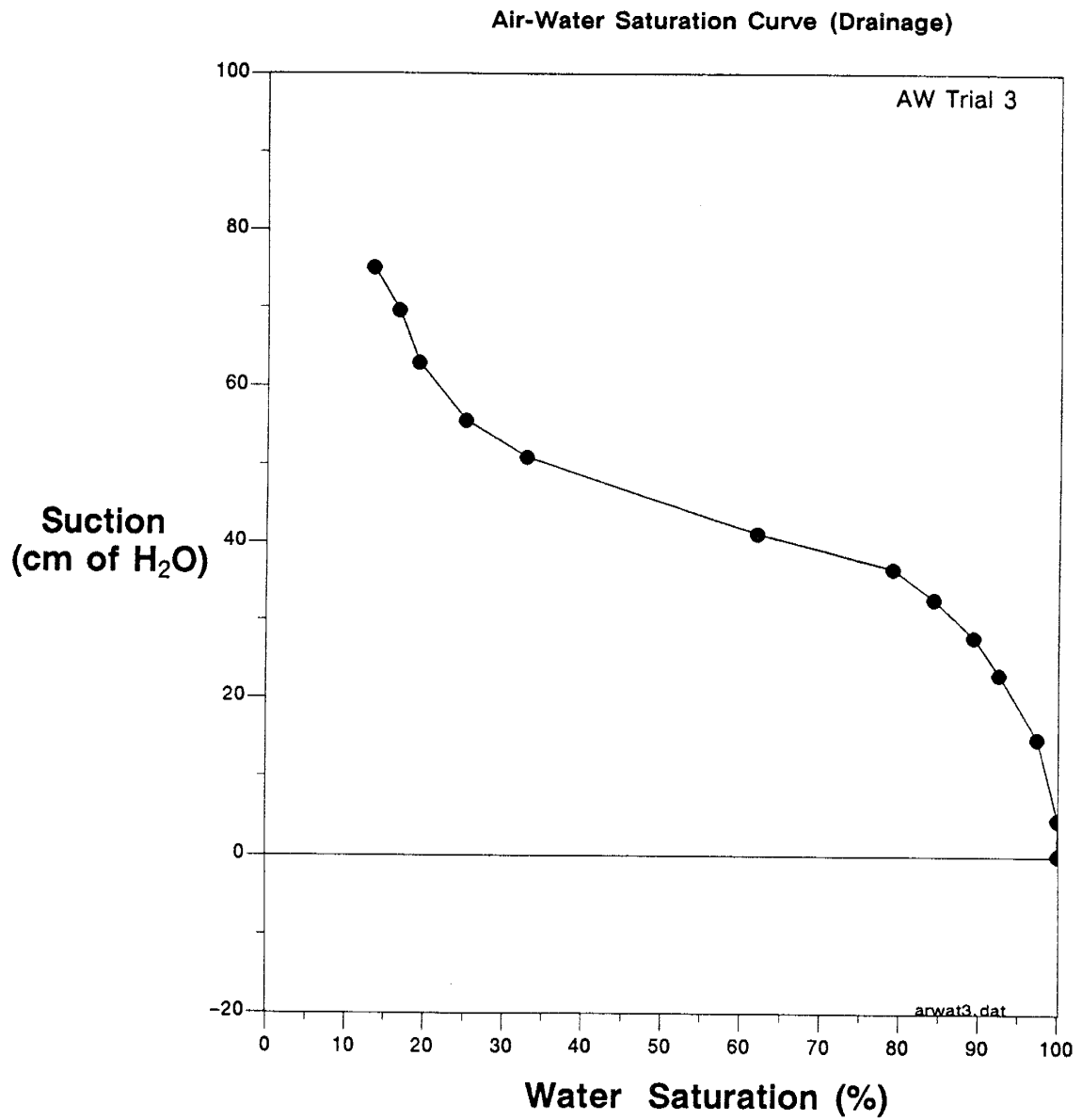
Figure A-14. Air-water saturation curve for AW trial 3.
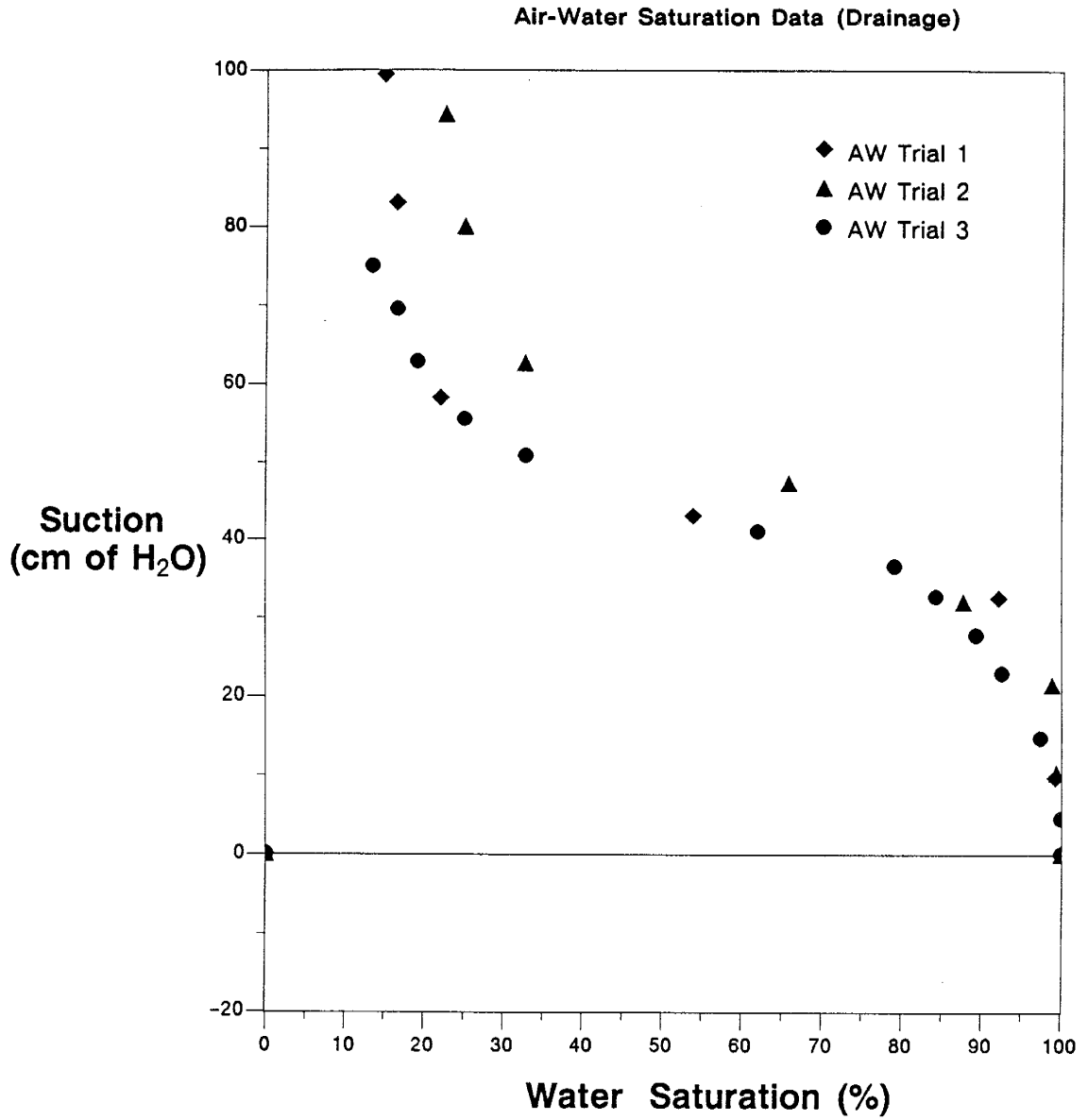
Figure A-15. Comparison of air-water primary drainage curves for SA trials 1 through 3.

Table A-1. Numerical values of measured saturations, pressures, and temperatures. (continued on next four pages)

SW Trial 7			SW Trial 8		
sat.	**P$_c$**	**temp.**	**sat.**	**P$_c$**	**temp.**
	— Primary Drainage —			— Primary Drainage —	
100	0	26.5	100	0	22
97.6	10.5	26	97.6	35.1	24
95.7	15.7	25	26.5	49.6	24.5
88	21.5	24	22	60.9	24
77.5	22.3	23		— Primary Imbibition —	
65	24.8	24	26.7	28.6	24.5
57	26	24.5	49.9	19.8	23
42.3	27.6	25	66.6	14	27
35.6	32.5	27	68	1.9	28
28	42.5	28.5	69.3	−10.6	26
23	62.1	31		— Secondary Drainage —	
	— Primary Imbibition —		68.3	4.3	21.5
23.1	30	31	68.1	21.8	20.5
45.6	15.7	31	63.9	33.3	20
56.4	12.7	28.5	43.5	35.8	20
68.9	7.2	18.5	28.7	39.1	18.3
71.6	−0.4	19	26.3	28.8	20
73.2	−5.7	20	23	60.4	23
			22	67.4	21.5

Note: the saturations are given in percent, capillary presures are given in equivalent cm of water (at 20°C), and the temperature is the room/cabinet temperature in °C, measured at the same time.

Note: The S designates Soltrol, W is water and A is air. Therefore SA is a Soltrol-air experiment.

Table A-1. Numerical values of measured saturations, pressures, and temperatures. (continued)

SW Trial 9   SW Trial 10

sat.	P_c	temp.	sat.	P_c	temp.
— Primary Drainage —				— Primary Drainage —	
100	0	24	100	0	23
80.8	30	24.5	97.2	22.2	23.2
58.8	31.1	25.5	81	24.8	20.5
41.9	34.1	24	43.9	30.8	21.5
26.2	41.1	24.5	25.9	38	20.5
23.3	46.3	20	19	49.1	21.8
18	62.5	24	16.2	56.1	21.3
16	69.5	24.5	12.3	63.4	21.8
— Primary Imbibition —				— Primary Imbibition —	
16.6	40.8	25.5	16.8	41.3	21.8
17.6	27.3	23	17.6	34.1	20.8
41.9	20.5	27	25.2	26.4	23
59.8	15.6	28	39.7	13.9	20
68.7	8	22	68.8	12.4	22
68.7	-2	22.5	69.5	-2.4	22.5
70.6	-8.6	21.5	71.8	-9.3	19.5
— Secondary Drainage —					
70	24	20.5			
41.2	31.4	20			
31.7	35.6	20			
21.4	49.8	18			
19.5	56.4	20			
15.7	66.5	20.5			

Table A-1. Numerical values of measured saturations, pressures, and temperatures. (continued)

SW Trial 11

SW Trial 12

sat.	P_c	temp.	sat.	P_c	temp.
— Primary Drainage —				— Primary Drainage —	
100	0	23.2	100	0	24.5
99.3	24.3	21.6	86.7	23	24.5
61.2	25	20.5	69.6	26.3	26.8
38	29.5	21.5	45.8	30.9	25.8
24.4	36.1	20.5	31.6	36.5	26.4
18.9	48.8	21.8	24	48.4	24.8
15.8	54.5	21.3	19.2	57.3	27.6
14.7	61.6	21.7	17.3	64.3	25.6
— Primary Imbibition —					
15.4	38.9	21.8			
17.7	24.9	20.8			
33.6	19.6	23			
50.8	15.6	20			
73.5	7	22			
74.2	−2.1	22.5			

SW Trial 13

SA Trial 1

sat.	P_c	temp.	sat.	P_c	temp.
— Primary Drainage —				— Primary Drainage —	
100	0	24.5	100	0	23
63.3	23.4	26.8	99.7	15	21.5
39.1	27.2	25.8	59	26.8	22.4
24.5	32	26.4	19	28.5	22.8
20.7	40	24.8	17.9	39.8	22
18.4	48.5	27.6	12.2	46	22
17.3	59.3	25.6	8.1	52.5	22.6
16.4	64.1	28.2	7.8	58	22

Table A-1. Numerical values of measured saturations, pressures, and temperatures. (continued)

SA Trial 2

AW Trial 1

sat.	P$_c$	temp.	sat.	P$_c$	temp.
	— Primary Drainage —			— Primary Drainage —	
100	0	21.3	100	0	26.9
100	9	21.8	99.3	9.7	23.3
76.1	14.5	21.2	92.2	32.5	25
44.9	17	22	53.9	43.1	25
20.7	21.5	22.2	22	58.2	24
16.1	25	22.2	16.4	83.1	18.4
8.4	32	22	14.9	99	16.8
8.4	41	22		— Primary Imbibition —	
	— Primary Imbibition —		15	84	15.6
8.4	31.5	22	15.9	67.6	18.6
10	19	22	18.2	52.5	24.2
17.9	15.7	22	26.9	39.7	24.6
60.7	6.7	22	42.7	30.2	26.2
80.1	3.4	22	62.6	23.2	26.8
82.3	−1.5	22.6	75.7	14.9	22.2
82.8	−9.1	22	80	7.7	21
83.4	−15.5	22.5			
	— Secondary Drainage —				
83.4	−5.5	22.8			
81.4	−0.6	22.9			
79.4	9	22.7			
75.4	11	23			
47.9	15.2	23			
19.1	20.8	23.5			
7.8	30	22.5			

Table A-1. Numerical values of measured saturations, pressures, and temperatures. (continued)

AW Trial 2

AW Trial 3

sat.	P_c	temp.	sat.	P_c	temp.
	— Primary Drainage —			— Primary Drainage —	
100	0	27	100	0	24.9
99.4	10.2	23.3	100	4.5	24.3
98.9	21.5	24	97.4	14.7	24
87.8	31.9	25	92.6	22.9	25.1
65.9	47.3	25	89.4	27.7	24.6
32.7	62.7	18.4	84.3	32.6	24
25	80	16.8	79.1	36.5	27
22.6	94.4	15.6	62	41	24.6
	— Primary Imbibition —		32.8	50.8	24.4
23.6	78.1	18.6	25.1	55.5	24.4
26	60.1	24.2	19.1	62.8	26.1
32.8	44.8	24.6	16.6	69.5	26
42.4	35.1	26.2	13.4	75	22.9
51.7	27.5	26.8			
65.8	20.4	22.2			
76.1	11.9	21			
80.1	5	20			

APPENDIX B:

QUANTITATIVE TWO-PHASE RESIDUAL

SATURATION RESULTS, WITH STYRENE AS THE

ORGANIC PHASE

The pore and blob cast experiments described in Chapter 5 produced quantitative results, as well as results pertaining to flow visualization. Unfortunately, the experimental methods made these quantitative results too inaccurate to be included with the main body of two-phase residual saturation data presented in Chapter 7. There were several reasons for the inaccuracies, as reviewed in Chapter 5.

Perhaps the largest source of error in the styrene experiments was the mass of the TFE column itself. Another factor contributing to the lower accuracy in the results was the density of the styrene. In comparison to Soltrol-130, styrene is the denser — 0.90 versus 0.75 g/cm³. The column was weighed, during the gravimetric determinations of saturation, on the high capacity Mettler PM 11 balance, which has an accuracy of only 0.1 grams. As a result of these problems the styrene experiments had saturation errors of ±6-8%, while the short-column experiments had errors of only ±2-3%. When we considered that 6-8% was sometimes up to 50% of the residual saturation measurement, it seemed prudent to consider these less accurate results separately.

Another reason for excluding the styrene data from the other quantitative data was that the residual saturations obtained were consistently lower than those obtained with the short-columns. In Chapter 5, we hypothesize that time constraints put on the experiment by styrene's ever increasing viscosity, did not allow enough time for the column to come to equilibrium. The wettability of the column walls was also found to affect the amount of time required to reach an equilibrium during the organic liquid flood, and may have influenced the residual styrene saturations.

EXPERIMENTAL RESULTS

The first column in the Table B-1 describes the experimental column, and the experimental run performed in it. There were three TFE columns constructed, two of which are represented here. For example, experiment 0-6 was the sixth experiment performed in TFE column 0, and experiment 2-1 was the first experiment performed in column 2. Column 1 was used exclusively for three-phase experiments, which were non-quantitative, so it is not represented in this table. Porosity values in column 2, maximum organic liquid saturations, S_o , in column 3, and residual organic saturations, S_{or} , in column 4, were calculated as described in Chapter 5.

Experiments 0-1 through 0-4 and 2-1 were homogeneous two-phase runs using the Sevilleta soil and styrene. The S_{or} data set has an average value of 0.16 and a standard deviation of 0.04. In comparison to the glass short column results (see Chapter 7), they are uniformly lower.

Column	Porosity (%)	S_o	S_{or}
0-1 homogeneous	32.3	0.710 ± .091	0.170 ± .065
0-2 homogeneous	33.5	0.667 ± .087	0.108 ± .059
0-3 homogeneous	33.5	0.713 ± .094	0.192 ± .065
0-4 homogeneous	31.7	0.722 ± .101	0.157 ± .071
2-1 homogeneous	34.6	0.700 ± .086	0.200 ± .060
0-5 soltrol-130	33.4	0.764 ± .039	0.265 ± .027
0-6 soltrol-130	34.1	0.745 ± .038	0.186 ± .025
2-2 crushed tuff	38.7	0.918 ± .116	0.295 ± .082
0-8 heterogeneous	34.5	0.936 ± .107	0.263 ± .072
2-3 heterogeneous	37.1	0.896 ± .133	0.407 ± .105

Table B-1. Two-phase TFE column residual saturation results; styrene was used unless otherwise noted.

In experiment 0-6, Soltrol-130 was flooded into, and drained out of, a TFE column following procedures dictated by the viscosity related time constraints of the styrene procedure. The residual saturation obtained matched those commonly found when performing experiments with styrene in the TFE column (19%). In experiment 0-5 Soltrol was again flooded into the TFE column but without time constraints, following the glass short column procedures of Chapter 4. Since sufficient time was allowed for the system to come to equilibrium, a value of residual saturation was obtained (27%) which closely matched those found when using Soltrol-130 in a glass column. These results suggest that the differences in residual saturation values were related not to differences in fluid characteristics, but to the amount of time the liquid/soil system had in which to equilibrate.

Experiment 2-2 was a homogeneous two-phase run done with a crushed and sieved tuff. This was an attempt to obtain blob casts that would photograph well on black and white film. The black tuff would stand out from the hardened fluid phases. Other methods of creating black and white photographs were successful so these casts were never used.

Experiments 0-8 and 2-3 were heterogeneous two-phase runs using Sevilleta soil split into two fractions, as described in Chapter 5. High organic saturations, as seen in these experiments, indicated that the organic liquid displaced the aqueous phase from the larger pores found in the stringers. This was expected, as a non-wetting fluid will move preferentially to larger pores in order to decrease its surface to volume ratio, and therefore decrease the surface energy of the system. So with the larger pores available, more non-wetting liquid can enter the system for a given energy level, or head. The fact that the columns were packed dry may have also contributed to the higher S_o values. The dry soil may have settled and compacted during the water saturation process, creating a large pore at one end of the column. This one 'macro' pore could have filled with styrene and contributed to a high organic saturation.

The S_{or} values presented represent 'bulk' residual saturations in that they are averaged over the whole heterogeneous column. Observations of the core, after it had been cut on a rock saw indicate however, that most of the residual styrene was trapped in the coarse stringers. A lesser amount, approximately the same as that observed in the earlier homogeneous experiments (16%), was trapped in the finer matrix. The measured 'bulk' residual saturation can be compared with a theoretical value (see Chapter 8):

Estimated bulk residual styrene saturation =

$$= (normalized\ lens\ volume) \times S_o + (normalized\ matrix\ volume) \times S_{or}$$
$$= (0.40 \times 0.90) + (0.60 \times 0.16) = (0.36 + 0.09) = 0.45 = 45\%$$

Column 2-3's value of residual saturation, 41%, comes close to the theoretical value, while column 0-8 is nowhere near the predicted value. This suggests that by-pass trapping may not totally exclude water from the coarse stringers (refer to Chapter 8).

The differing S_{or} values of experiments 0-8 and 2-3 are explained by the flow rate of the water flood. Experiment 0-8 was flooded with water as described in Chapter 4. That is to say, it was flooded exactly as if it were a homogeneous two-phase experiment. The residual saturation value, 26%, reflects the relatively larger volume of styrene trapped in the coarser sand stringers. Column experiment 2-3, in contrast, was water-flooded at a much lower rate, approximately 1 ml/minute. This flow rate was controlled by pushing water through the column with a syringe pump. The low flow rate led to a situation where almost 45% of the styrene in the column was bypassed and trapped. In this case, the combination of viscous and buoyancy forces were not strong enough to overcome the capillary forces holding the styrene in place. Although some $CaCl_2$ did flow through the stringers, the majority of the stringer's pore space remained filled with styrene. For photographs of the styrene filled stringers, see Chapter 8.